UNIVERSITY OF LIVERPOOL

Investigation of the roles of Ebola virus RNA-dependent RNA polymerase and its co-factor VP35 with the host

Thesis submitted in accordance with the requirements of the University of Liverpool for the degree of Doctor in Philosophy

by

Jordana Muñoz-Basagoiti

May 2019

AUTHOR'S DECLARATION

Apart from the help and advice acknowledged, this thesis represents the unaided work of the author

……..

Jordana Muñoz-Basagoiti

May 2019

This research was carried out in the Department of Infection Biology, Institute of Global health, University of Liverpool.

Acknowledgments

First of all, I would like to thank my supervisors, Prof. Julian Hiscox and Prof. Miles Carroll, for having given me the opportunity of doing my PhD at the University of Liverpool and taken me to conferences in amazing places such as Crete and Singapore. Specially, thanks Julian for having guided me through the journey during these 3 years.

Not less important, I would also like to thank my postdoc, my colleague and good friend Dr. Isabel García-Dorival, for her wisdom, her patience and her belief I would go through it and make it. You embraced me from the first day I arrived at Liverpool and have been my mentor in the lab and one of my pillars through my journey.

Many thanks to Dr. Stuart Armstrong for his help with mass spectrometry and scientific knowledge, and to the rest of the Hiscox group and IC2 colleagues, wonderful people with whom I have shared loads of good moments in and out of work.

Not related to my work, I want to thank Alessandra for being the perfect flatmate (cleaning-obsessed and a good cook who would always feed me!), and for making me laugh even in the worst of the days.

Last but not least, I wanted to thank my family and friends in Catalunya.
Mama, papa, Clàudia i tieta Nuri, gràcies per fer-me sentir encara part del vostre dia a dia tot i estar a 1400 km de distància. Les visites anuals, les trucades setmanals i els whatsapps diaris m'han donat força i han fet que l'anyorança no se'm mengés, sobretot a l'inici d'aquesta aventura.
Ari, Eli, Tere, Brian, Alba i Carlota, gràcies per compartir les vostres vivències doctorals, pel suport des de que vem sortir de la carrera pensant que ens menjariem el món i l'amistat que n'ha sortit d'ella.

I per acabar, no menys important, gràcies Judith per compartir gairebé tot aquest viatge al meu costat. Gràcies per confiar en mi, seguir al meu costat fins i tot a tants quilòmetres de distància i per recordar-me que sóc forta dia sí i dia també.
Gràcies a tots!

Abstract

Ebola virus (EBOV) was first identified in 1976 and, since then, small outbreaks have been occurring in central and West African countries. The largest EBOV outbreak until now, taking place from year 2013 to 2016, left more than 28.000 cases and 11.000 deaths. EBOV is a highly contagious and virulent pathogen with no FDA-licensed therapeutic available yet. Huge efforts are currently being made for the development of effective antiviral therapeutics and the investigation of viral evolution dynamics in correlation with its virulence. Viruses are obliged parasites of the host cell in order to accomplish every stage of their biological life cycle. For viral RNA synthesis, occurring in the cell cytoplasm, Ebola virus must interact with host proteins, which at the same time can be exploited as potential antiviral targets. In this study, co-immunoprecipitation and high-throughput label-free proteomics are used to elucidate novel protein associations between EBOV VP35, L and host factors. Biological importance of the host proteins DYNLL1 and CALM on Ebola virus life cycle is assessed by using small molecule inhibitors in an EBOV minigenome system in cellular culture, resulting in a significant decrease of viral replication when either of the cellular factors is antagonised. The study of VP35 is taken further and the phenotypic changes on the protein functionality during the early beginning of the 2013-2016 West African outbreak are characterised, demonstrating slight differences on the viral protein performance that could help understand better Ebola virus virulence. Overall, this thesis provides a better understanding of the interactions that Ebola virus establishes with its host, the implications that single mutations can have on viral proteins functionality and the EBOV pathogenesis.

Table of contents

List of figures

List of tables

List of abbreviations

Ad5	Adenovirus type 5
APS	Ammonium persulphate
ATP5I	ATP synthase subunit e
BAG2	BAG family molecular chaperone regulator 2
BCA	Bicinchoninic acid
BDBV	*Bundibugyo ebolavirus*
BOMV	*Bombali ebolavirus*
BSL	Biosafety level
BHK	Baby hamster cells
C-terminal	Carboxyl-terminal
CALM	Calmodulin
CAT	Chloramphenicol acetyl transferase
CCD	Coiled-coil domain
CDC	Centers for Disease Control and Prevention
cDNA	Complementary DNA
CHE	Switzerland
CIRBP	Cold-inducible RNA-binding protein
COD/CDR	Democratic Republic of Congo
coIP	Co-immunoprecipitation
CP	Convalescent plasma
CRS	Calmodulin recruitment signalling
CTLA-4	Cytotoxic T-lymphocyte-associated protein 4
CWB	Convalescent whole blood
DAPI	4',6'-diamino-2-phenylinidole
DC	Dendritic cell
DC-SIGN	Dendritic cell-specific ICAM-grabbing non-integrin
ddH_2O	Double distilled H_2O
DENV	Dengue virus
DIP	Defective interfering particle

DLA	Dual luciferase assay
DMEM	Dulbecco's modified Eagles medium
DMSO	Dimethyl sulfoxide
DNA	Deoxyribonucleotide
DRBP76	Double-stranded RNA-binding nuclear protein
dsRNA	Double stranded DNA
DYNLL1	Dynein light chain 1
EBOV	*Zaire ebolavirus*
ECACC	European Collection of Authenticated Cell Cultures
ECL	Enhanced chemiluminescence
EDTA	Ethylenediaminetetraacetic acid
EGFP	Enhanced GFP
EHF	Ebolavirus haemorrhagic fever
EMCV	Encephalomyocarditis virus
EVD	Ebolavirus disease
FBS	Foetal bovine serum
FC	Fold change
FDA	Food and drug administration
FDR	False-discovery rate
GAB	Gabon
GAPDH	Glyceraldehyde-3-phosphate
GFP	Green fluorescent protein
GIN	Guinea
GP	Glycoprotein
HBS	HEPES buffered saline
HCV	Hepatitis C virus
HEK293T	Human embryonic kidney 293T cells
HEPES	4-(2-hydroxyethyl)-1-piperazineethanesulfonic acid
HSPA8	Heat-shock protein 8
IC_{50}	Half maximal inhibitory concentration
ICAM3	Intercellular adhesion molecule 3

ICTV	International committee on the taxonomy of viruses
IFN	Interferon
IgG	Immunoglobulin G
IID	IFN inhibitory domain
IRES	Internal ribosome entry site
IRF	Interferon regulatory factor
L	Large protein
L-SIGN	Liver/lymph node-specific intercellular adhesion molecule-3-grabbing integrin
LB	Luria-Bertani broth
LBR	Liberia
LC-MS/MS	Liquid chromatography tandem-mass spectrometry
LC8	Light chain 8
LFQ	Label-free quantification
LUC	*Firefly* luciferase
M	Matrix protein
mAb	Monoclonal antibody
MARV	Marburg virus
MDA5	Melanoma differentiation-associated protein 5
MG	Minigenome system
MHC	Major histocompatibility complex
mRNA	Messenger RNA
MTT	Methylthiazolyldiphenyl-tetrazolium bromide
N-terminal	Amino-terminal
NC	Nucleocapsid
NCBI	National Center for Biotechnology Information
NGA	Nigeria
NP	Nucleoprotein
NPC1	Niemann-Pick type C1 receptor
NS	Negative sense
NS5A	Non-structural protein 5A

nsNS	Non-segmented negative sense
ORF	Open reading frame
P	Phosphoprotein
PAI1	Plasminogen activator inhibitor 1
PAMP	Pathogen-associated molecular pattern
PBS	Phosphate buffered saline
PD-1	Programmed cell-death 1
PFA	Paraformaldehyde
PKR	Protein kinase-R
PLB	Passive lysis buffer
Poly(I:C)	Polyinosinic:polycytidylic acid
PPI	Protein-protein interaction
PRRSV	Porcine reproductive and respiratory syndrome virus
PTM	Post-translation modification
PVDF	Poly-vinylidene difluoride
RdRp	RNA-dependent RNA polymerase
RESTV	*Reston ebolavirus*
RFP	Red fluorescent protein
RIG-1	Retinoic acid inducible gene 1 protein
RIPA	Radioimmunoprecipitation buffer
RLTK	*Renilla* luciferase-encoding plasmid
RNA	Ribonucleic acid
RNase A	Ribonuclease A
RNP	Ribonucleoprotein
RPS21	Ribosomal protein S21
RT-PCR	Retrotranscriptase polymerase chain reaction
rVSV	recombinant vesicular stomatitis virus
SD	Standard deviation
SDS-PAGE	Sodium dodecyl-sulphate polyacrylamide gel electrophoresis
SeV	Sendai virus
sGP	soluble GP

siRNA	Short interfering RNA
SLE	Sierra Leone
SNP	Single nucleotide polymorphism
ssGP	Small soluble GP
ssRNA	Single-stranded RNA
STAT1	Signal transducer and activator of transcription 1
SUDV	*Sudan ebolavirus*
TAFV	*Tai Forest ebolavirus*
TBE	Tris/Borat/EDTA buffer
TBS-T	Tris-buffered saline-Tween 20 buffer
TLR	Toll-like receptor
TEMED	Tetramethylethylenediamine
TnT	Transcription and translation system
TOP1	DNA topoisomerase 1
TPC2	Two pore segment channel 2
UTR	Untranslated region
VLP	Viral-like particle
VP24	Viral protein 24
VP30	Viral protein 30
VP35	Viral protein 35
VP40	Viral protein 40
vRNA	Viral ribonucleic acid
W-7	N-(6-aminohexyl)-5-chloro-1-naphthalenesulfonamide
WHO	World Health Organization
WR	Working reagent
YBX1	Y-box binding protein 1
YMH	Yumbuku Mission Hospital

Chapter 1: Introduction to Ebola virus

1.1. Introduction to the Ebola virus biology

1.1.1. Taxonomy and classification

1.1.1.1. Order *Mononegavirales*

The genus *Ebolavirus* belongs to the order *Mononegavirales*. The name is derived from the Greek adjective *μόνος* (monos; alluding to the monopartite and single-stranded genome), the latin verb *negare* (alluding the negative polarity of the genome) and the suffix –*virales* (denoting a viral order). The order *Mononegavirales* was first established in 1991, comprising related viruses with non-segmented, linear, single-stranded negative-sense RNA genomes. In 2017, the taxonomy of *Mononegavirales* was extended and accepted by the Committee on Taxonomy of Viruses (ICTV). The update comprised 8 families; *Bornaviridae, Filoviridae, Mymonaviridae, Nyamiviridae, Paramyxoviridae, Pneumoviridae, Rhabdoviridae,* and *Sunviridae* (Amarasinghe et al., 2017).

The order *Mononegavirales* include the viruses that share the following characteristics (Amarasinghe et al., 2017):

- Linear genome, non-segmented, single-stranded non-infectious RNA of negative polarity. The genome has inverse-complementary 3’ and 5’ termini and is not covalently linked to a protein.
- The genome has a specific and characteristic gene order *3’-UTR Leader → core protein genes → envelope protein genes → RNA-dependent RNA polymerase gene → Trailer 5’-UTR*.
- The genome has a single promoter located at the 3’ end and produces monocistronic mRNAs via polar sequential transcription, following a stop-start mechanism between genes.
- The genome replicates by synthesising complete antigenomes.
- The viral genome synthesis forms infectious helical ribonucleocapsids as the templates for the production of mRNAs and for replication.

- The RNA-dependent RNA polymerase encoded in the viral genome is highly homologous among mononegaviruses.

1.1.1.2. Family *Filoviridae*

The terminology of the family *Filoviridae* comes from the Latin *filo* (thread-like), referring to their filamentous rod-like shape. The family currently comprises of 3 genera and 7 species (Table 1.1). Comparison of filoviral genomes with other families within the order *Mononegavirales* demonstrates similar genome structure and suggests comparable mechanisms of transcription and replication. However, comparative sequence analyses of single genes indicate that filoviruses are phylogenetically distinct from other members of the same order. The different members of the order *Mononegavirales* share five proteins in common. These are the nucleoprotein (NP), the viral proteins 35 and 40 (VP35 and VP40), the glycoprotein (GP) and the RNA-dependent RNA polymerase (L). Only the viral protein 24 (VP24) appears to be unique to filoviruses (Mühlberger, 2007).

Within the family *Filoviridae*, all of the genes show conservation in gene organisation but only cuevaviruses and ebolaviruses present significant amino acid sequence similarity with a cut-off of 50% minimum sequence identity over at least 50% of the sequence length (Jun et al., 2015). Ebola virus and Marburg virus differ by approximately 67% at the amino acid level and 55% at the genomic level (Elshabrawy et al., 2015).

There are five known and broadly accepted *Ebolavirus* species. Four of them cause Ebolavirus haemorrhagic fever. These are Ebola virus (EBOV), with the highest case-fatality rate in humans (57-90%), followed by Sudan virus (SUDV) (41-65%), Bundibugyo virus (BDBV) (40%) and Taï Forest virus (TAFV), with only two known non-fatal human infections. To date, Reston virus (RESTV) is the only Ebola virus species that causes an asymptomatic infection to humans (Moghadam et al., 2015). Between the five species, they differ by 37-40% at the nucleotide level and by 34-43% by the amino acid level (Elshabrawy et al., 2015). Late in 2018, the genome of a new putative

Ebolavirus species was sampled from 4 bats in Sierra Leone. *Bombali ebolavirus* (BOMV) was named after the location where bats were sampled. Its nucleotide and amino acid identities to other Ebola viruses was 55-59% and 64-72%, respectively (Goldstein et al., 2018).

Table 1.1. ICTV-accepted taxonomy of the family Filoviridae as of 2017.

Genus	Species	Virus (Abbreviations)
Cuevavirus	*Lloviu cuevavirus*	Lloviu virus (LLOV)
Ebolavirus	*Bundibugyo ebolavirus*	Bundibugyo virus (BDBV)
	Reston ebolavirus	Reston virus (RESTV)
	Sudan ebolavirus	Sudan virus (SUDV)
	Taï Forest ebolavirus	Taï Forest virus (TAFV)
	Zaire ebolavirus	Ebola virus (EBOV)
	**Bombali ebolavirus*	*Bombali virus (BOMV)
Marburgvirus	*Marburg marburgvirus*	Marburg virus (MARV)
		Ravn virus (RAVV)

**Putative new species discovered in 2018* (Goldstein et al., 2018)*, not included in the updated ICTV-accepted taxonomy as of 2017.*

1.1.2. Genome organisation and Ebola virus genetics

The genome of Ebola virus consists of a non-segmented single stranded, negative-sense RNA molecule of about 19kb in length, consisting of seven genes, which encode 9 proteins in the following order: *NP* (Nucleoprotein) – *VP35* (viral protein 35) – *VP40* (viral protein 40) – *GP* (Glycoprotein). It also encodes the small glycoprotein and the soluble small glycoprotein (sGP and ssGP, respectively) – *VP30* (viral protein 30) – *VP24* (viral protein 24) – *L* (RNA-dependent RNA polymerase) (Sanchez et al., 1993) (Figure 1.1). Each gene contains the respective open reading frame (ORF) and are flanked by highly conserved transcriptional gene start (GS) and gene end (GE) signals (Brauburger et al., 2016). Transcription stop and start signals in *Ebolavirus* genes are separated by intergenic regions (IGRs) that differ in length. They overlap in three gene boundaries, which share the nucleotide sequence ATTAA and are found between genes *VP35-VP40, GP-VP30* and *VP24-L* (Sanchez et al., 1993). The *leader* and *trailer* sequences are extragenic regions located at the ends of the genome and contain the promoters required for transcription and replication (Neumann et al., 2009). The end of the genome consists of short non-transcribed regions containing cis-acting signals important for replication, transcription initiation and encapsidation of the genomic RNA (Mühlberger, 2007).

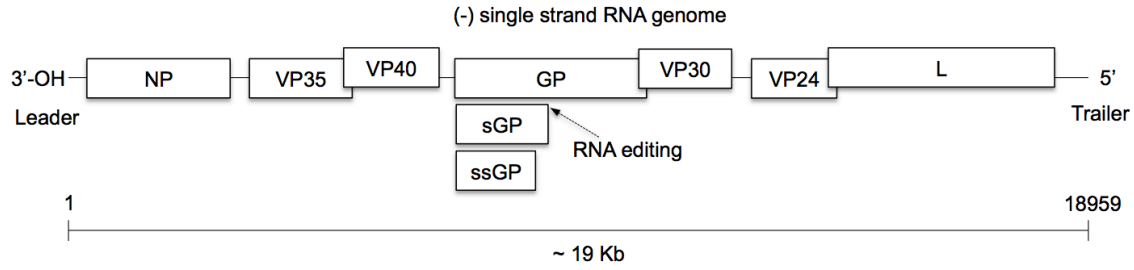

Figure 1.1. Schematic representation of the genomic organisation of Zaire ebolavirus (EBOV). *Boxes represent the open-reading frames (ORF) that encode each viral protein. Intergenic regions overlap between VP35-VP40, GP-VP30 and VP24-L genes. Post-translational modifications (PTMs) of GP result in the subunits sGP and ssGP by host cell furin cleavage. Image representation based on Cantoni and Rossman, 2018.*

1.1.3. Mutation rate and defecting interfering particles (DIPs)

In RNA viruses, the evolution rate is estimated to be between 10^{-5} and 10^{-2} substitutions per year (Jenkins et al., 2002; Hanada et al., 2004). According to sequences analysed from the 2013-2016 Ebola virus West African Outbreak, which is also the largest to date, the evolution rate of *Zaire ebolavirus* was estimated to be 1.42×10^{-3} substitutions per site per year (Carroll et al., 2015). The activity of the error-prone viral replicase is thought to be the reason why defective interfering particles (DIPs) have been seen in nearly all RNA viruses like Ebola virus, vesicular stomatitis virus or influenza virus (Calain et al., 1999; Galet et al., 1976; von Magnus, 1954). DIPs are defined as infectious truncated viral genomes derived from the parental RNA genome that require the presence of a full-length non-defective helper virus for their replication and propagation. DIPs are created spontaneously during viral replication and contain all the cis-acting replication elements but lack the capacity to encode all the viral proteins necessary for independent transcription and replication. These fusion events are maintained in natural viral infections and compete with the helper virus for viral and host factors (reviewed in Pathak and Nagy, 2009). Due to this property, DIPs are considered interesting alternatives for potential antiviral therapies (Dimmock and Easton, 2014).

1.1.4. Ebolavirus replication cycle

Filoviruses replicate in the cytoplasm. The negative-sense single stranded RNA is first transcribed, producing seven monocistronic mRNA, which will be translated into the viral proteins. Replication and secondary transcription take place when the viral RNA polymerase switches to replication mode with the increase of translated viral proteins. There is a transcription gradient in EBOV, with transcripts whose genes are located closer to the 3' end being more abundant than the transcripts whose genes are closer to the 5' end of the template (Shabman et al., 2013; Albariño et al., 2018). A balance between replication, secondary transcription and translation leads towards the assembly and release of the viral progeny (Figure 1.2).

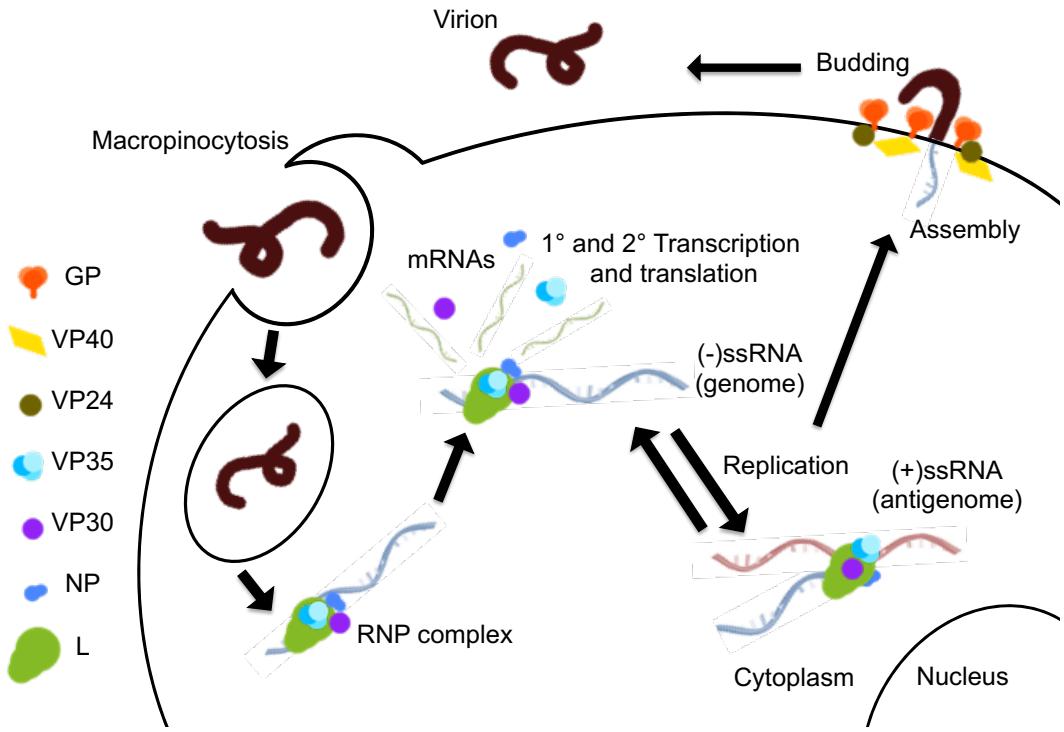

Figure 1.2. Schematic representation of the Ebola virus life cycle.

1.1.5. Attachment and entry

EBOV particles attachment to the cell membrane is mediated by the *N*-and *O*-glycans on the viral protein GP and is dependent on C-type lectin receptors, including dendritic cell-specific ICAM3-grabbing non-integrin (DC-SIGN) and liver and lymph node SIGN (L-SIGN), and glycosaminoglycans (Simmons et al., 2003). The viral particles also interact with other entry-mediators cell surface proteins, such as integrins, mucin-domain-containing (TIM) proteins, tyrosine protein kinase receptor 3 (TYRO3) family members, and T cell immunoglobulin (Wang et al., 2016). Virions are then internalised through macropinocytosis (Saeed et al., 2010). In the endosome, cleavage of GP and other unknown factors trigger the uncoating of the nucleocapsid. The interaction between cleaved GP with Niemann-Pick C1 (NPC1) transporter protein and two-pore channel 2 (TPC2) induces EBOV and cellular membrane fusion, allowing the release of the core to the cytoplasm (Wang et al., 2016; Sakurai et al., 2015).

1.1.6. Transcription and replication

Replication and transcription are conserved among the nsNS RNA viruses. Both processes require the ribonucleoprotein (RNP) complex as a template. Due to the negative polarity of NS virus genomes, transcription is mandatory the first step in the virus gene expression process. Therefore, naked genomic RNA is not infectious. For Ebola virus, minigenome systems have demonstrated that the protein requirements for viral replication lay in the RNP complex, composed of RNA, NP, VP30, VP35 and L (Mühlberger et al., 1998; Muhlberger et al., 1999; Conzelmann, 2004). The replication promoters of the filoviruses are located at the 3' end of both the viral genome and antigenome. Therefore, the viral RdRp can only access the RNA template at the 3' end. The minimal length for the genome and antigenome promoters are 155 and 176 nucleotides, respectively (Calain et al., 1999). The viral polymerase is thought to stop and resume transcription at each gene boundary. Ebola virus messenger RNAs (mRNAs) are presumed to be modified with a 5'-7-methylguanosine cap and a 3' poly(A) tail by the viral RNA polymerase (Weik et al., 2002). After primary transcription, where the negative stranded RNA is used as a template for sequential transcription of mRNA for translation of viral proteins, the viral RNA polymerase switches to a replicative mode and generates positive-sense RNA genomes, the above-mentioned antigenomes. These serve as templates for the generation of new viral genomes.

1.1.7. Virion assembly and release

Nucleocapsid formation occurs in inclusion bodies in regions close to the nucleus and are transported to the budding sites (Dolnik et al., 2015). Transport of the nucleocapsid relies on NP, VP35 and VP40, which are essential and sufficient to form transport-competent nucleocapsid-like (NC-like) structures. VP40 is the most abundant protein found under the viral envelope and enhances the efficiency of nucleocapsid recruitment into filopodia for EBOV budding (Takamatsu et al., 2018). A model for virion release has been proposed where NP self-assembles into helical tubes (Noda et al., 2006). VP35 and VP24 interact with NP, constituting NC structures. VP40 mediates the transport of NC-like particles via microtubules towards the cell

surface. Finally, NC-like particles are incorporated into virions and bud from the cell membrane (Noda et al., 2006; Wan et al., 2017).

1.1.8. Viral proteins

Ebolavirus particles are filamentous and are surrounded by an envelope, which is acquired during the budding process from the plasma membrane of the host cell. The glycoprotein is the only viral protein on the surface of the viral particle and it is essential for host membrane fusion and viral release. The viral matrix proteins VP24 and VP40 are found in the inner side of the envelope and provide structural support to the virion. Inside the viral particle, the genomic RNA is associated with the viral RNA-dependent RNA polymerase L, NP, VP30 and 35, forming the RNP complex (Figure 1.3).

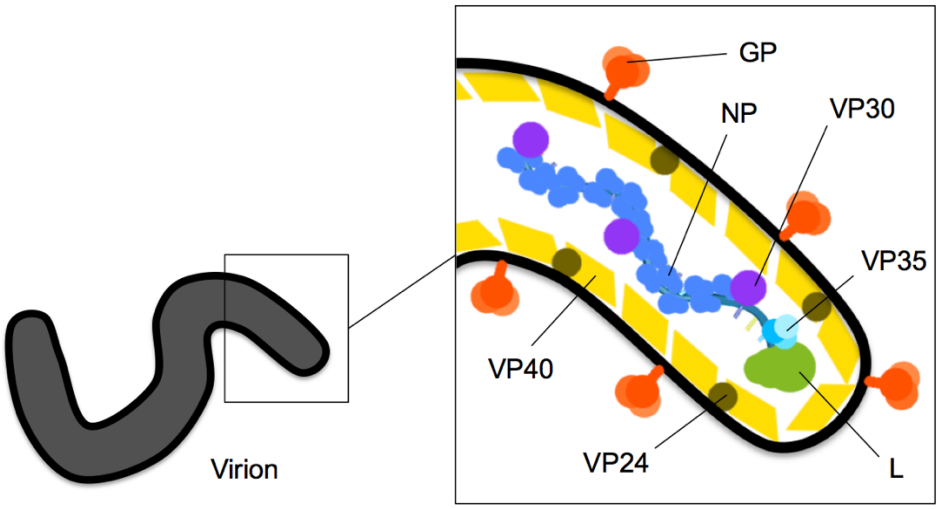

Figure 1.3. Schematic representation of the Ebola virus virion protein composition.

1.1.1.3. Nucleoprotein (NP)

NP is one of the RNP complex components and coats the viral genome (Mühlberger et al., 1999). Together with VP24 and VP35, they build a helical nucleocapsid of ~50nm in diameter and 1000nm of length. As part of the RNP complex, it has a critical role in protecting viral RNA (vRNA) from degradation.

1.1.1.4. Viral protein 35 (VP35)

VP35, the viral RNA dependent RNA polymerase cofactor, is the functional equivalent of the phosphoprotein P of other nsNS RNA viruses, such as paramyxoviruses and rhabdoviruses (Mühlberger et al., 1999; Brzózka et al., 2005; Fuentes et al., 2010). VP35 is also an antagonist of the host IFN type I response. It is able to inhibit the phosphorylation of IRF-3 and thus blocking a pathway that leads to the type I IFN gene expression (Basler et al., 2003), the activation of the dsRNA-dependent protein kinase PKR (Schumann et al., 2009) and supresses RNA silencing (Haasnoot et al., 2007). VP35 forms homotrimers mediated by a coiled-coil domain, facilitating the antagonism of IFN-α/β (Reid et al., 2005). VP35 functions as a structural bridge between L and NP, leading to the formation of trimeric complexes (Groseth et al., 2009). VP35 also dissociates RNA-NP oligomers, allowing the release of the genomic RNA for replication (Kirchdoerfer et al., 2015).

1.1.1.5. Viral protein 40 (VP40)

VP40 is a multifunctional protein with different roles in the EBOV life cycle depending on the structural rearrangements it presents. EBOV VP40 exists in three different structural forms; the dimeric conformation associates with the plasma membrane and oligomerises into hexamers. The hexametric structure of the protein forms filaments, which makes up the viral matrix, provides support to the new EBOV virion particles. Hence, it has a role in the budding process (Ruigrok et al., 2000; Bornholdt et al., 2013; Gerstman and Chapagain, 2017). The third structure the viral protein can

be rearranged in is an octamer, which has a role on the viral genome replication and RNA binding (Timmins et al., 2003).

1.1.1.6. Glycoprotein (GP)

GP is the only surface capsid protein of Ebola virus and plays an important role in interacting with host cell receptors in order to activate viral attachment and entry. The GP gene encodes three different forms of GP. GP_1 is the full-length protein and has a receptor binding function. It is located on the virion surface and it is responsible for the cell attachment and membrane fusion (Lee and Saphire, 2009). GP_2 subunits are involved in the viral fusion. The soluble GP (sGP) lacks the transmembrane domain. The small soluble GP (ssGP), also called Δ-peptide, is a smaller fragment product of the furin cleavage of sGP. These different products are due to the transcriptional editing performed by the viral RNA polymerase L (Mehedi et al., 2011). Overexpression of GP results toxic for the infected cell (Sullivan et al., 2005). Its expression is restricted by the gene transcriptional editing and conversion into recombinant GP (Volchkov et al., 2001).

1.1.1.7. Viral protein 30 (VP30)

VP30 is a phosphoprotein and the minor component of the RNP. It has an important role in viral transcription initiation and reinitiation (Martínez et al., 2008) and it is also involved in nucleocapsid assembly as it has the capacity of interacting with NP. Its phosphorylation state negatively regulates transcription, enabling binding to NP (Modrof et al., 2002). VP30 can also interfere with RNA silencing due to its interaction with the protein Dicer and potentially prevents this antiviral mechanism in the host (Li et al., 2013). VP30 has a zinc-binding motif, which facilitates RNA binding and enhances viral genome transcription (Modrof et al., 2003; Schlereth et al., 2016). The C-terminal domain of VP30 is homologous in structure to the respiratory syncytial virus (RSV) protein M2-1, giving more evidence in the transcriptional regulation strategies shared by nsNS viruses (Blondot et al., 2012).

1.1.1.8. Viral protein 24 (VP24)

VP24 is a minor component of virions, a secondary matrix protein and has a direct role in genome packaging and nucleocapsid condensation. The viral protein presents a strong association with lipid membranes (Han et al., 2003). The function of the viral protein is dependent on the interaction with NP (Banadyga et al., 2017). VP24 also has a critical role on the viral evasion of IFNs by binding transporter molecules to prevent STAT1 translocation (Reid et al., 2006). Another described function of VP24 is the regulation of viral replication, as it has a key role in the nucleocapsid assembly and the silencing of the expression of this viral protein prevents the release of EBOV (Mateo et al., 2011).

1.1.1.9. RNA-dependent RNA polymerase (L)

The L protein is 2212 amino acids in length and has an estimated size of 253 kDa (Volchkov et al., 1999). It has catalytic activity and is responsible for mRNA synthesis and modification, and generation of progeny genomes (Ortín and Martín-Benito, 2015). The viral polymerase binds to the genomic RNA at the 3' leader promoter and transcribes the viral genes with a decreasing efficiency towards the 5' end (Albariño et al., 2018). EBOV L protein displays conserved sequence blocks, which are separated by more variable regions. This suggests it has a structural organisation in three functional domains called motifs A-C, conserved among the order *Mononegavidae*. Motif A (aa 553-571) comprises an RNA binding element; motif B (aa 738-744) represents a putative RNA template recognition and/or phosphodiester bond formation domain; and motif C (aa 1815-1841) is an ATP and-or purine ribonucleotide triphosphate binding domain (Poch et al., 1990; Volchkov et al., 1999a).

1.2. Reverse genetics

Reverse genetics is the term used to define the generation, replication and transcription of full or truncated recombinant RNA genome viruses *de novo* from cloned complementary DNA (cDNA). Reverse genetics enable the study of different aspects of the virus life cycle, the development of targeted antiviral therapies, the functionality of host factors for the virus biology, specific properties of clonal subpopulations and also represent attractive biotechnological tools for the development of live attenuated vaccines. When reverse genetics apply to cDNA that encodes a truncated genome analogue, these systems are useful to model the replication of the virus life cycle. Included in this category are minigenome (or minireplicon) systems, and transcription and replication competent virus-like particle (trVLP) systems. These systems revolutionised the study of nsNS RNA viruses and have also been used in this thesis to provide functional information.

1.2.1. History of reverse genetics and replicon systems

The beginning of reverse genetics took place in positive sense single stranded RNA viruses when in 1978 Taniguchi et al. made a full-length cDNA of bacteriophage Qβ RNA capable of forming plaques after transfection in *E. coli* (Taniguchi et al., 1978). Following this, in 1981, Racaniello and Baltimore generated poliovirus type I clones from cDNA of the virus genome (Racaniello and Baltimore, 1981). The first reverse genetics were accomplished on positive-sense RNA viruses since transfection of its full deproteinated genome in eukaryotic cells allows direct viral transcription and subsequent translation of the viral proteins. In contrast, the RNP complex is required for the initiation of viral transcription and replication of negative-sense RNA viruses. These need their own RNA polymerase to mediate the synthesis of *de novo* proteins. Therefore, their genome alone is not infectious in permissive cells unless the RNP complex is supplied *in trans*. It was not until 1989 that Palese and colleagues established the first reverse genetic system in a negative-single stranded RNA virus, influenza A virus (Luytjes et al., 1989). In 1991, Park et al. used synthetic defective

interfering particles (DIPs) derived from the 5' or 3' end of Sendai virus (SeV) fused to chloramphenicol acetyl transferase (CAT) gene and achieved CAT activity in transfected cells after helper virus infection (Park et al., 1991). That same year, Pattnaik and Wertz established the first plasmid-based minigenome system by co-transfecting vesicular stomatitis virus (VSV) DIPs together with M, G, N, NS and L viral proteins-encoding plasmids (Pattnaik and Wertz, 1991). Two years after, Collins et al. achieved recovery of DIPs derived of RSV (Collins et al., 1993). In 1994, Schnell et al. rescued the first member of the *Mononegavirales*, Rabies virus, from its anti-genomic strand (Schnell et al., 1994). EBOV Mayinga strain virus was first rescued from cDNA by using the positive-sense antigenomic RNA (Volchkov et al., 2001) and one year later, the negative-sense genomic RNA (Neumann et al., 2002). All these studies demonstrated that the viral polymerase complex is required for the amplification of negative single stranded RNA genome viruses.

1.2.2. EBOV replicon system

Ebola virus is classified as a Biosafety level 4 (BSL-4) pathogen, requiring high containment facilities for the study of its biology. Minigenome systems allow researchers to study EBOV replication aspects under less restrictive facilities - BSL-2 laboratories - and without the risk of workers being exposed to virions. Minigenomes are monocistronic truncated genome cDNA analogues were the viral genes have been replaced with a reporter gene. They contain all the necessary cis-acting signals for EBOV polymerase to lead minigenome replication and reporter gene transcription (Jasenosky et al., 2010). Four separated support plasmids encode the four viral proteins that are constituents of the RNP complex. These are NP, VP30, VP35 and L. The first minireplicon system for EBOV was made in 1999 (Mühlberger et al., 1999), one year after the creation of the minireplicon system of another member of the family *Filoviridae*, Marburg virus (MBGV) (Mühlberger et al., 1998). While replication of MARV minigenome only required three of the nucleoproteins – NP, VP35 and L -, EBOV minigenome transcription was observed to be dependent on VP30 as well.

In the piece of work described in this thesis, BSR-T7 cells constitutively expressing the phage T7 RNA polymerase are co-transfected with the minigenome encoding plasmid, the four supporting plasmids encoding the RNP complex proteins under the control of a T7 RNA polymerase promoter (Figure 1.4) (García-Dorival et al., 2016). The T7 polymerase produces transcripts from the cDNA encoding the supportive proteins for its translation. The T7 promoter/terminator system has the advantage of being high in expression levels in a cellular environment whereas the T7 polymerase is not used for the cellular cytoplasmic production of RNAs. As for the minigenome cDNA plasmid, the reporter gene *Firefly* luciferase is surrounded by the leader and trailer sequences of the EBOV genome and the whole construct is comprised between the T7 promoter and a hepatitis D virus (HDV) ribozyme. These features allow an exactly defined 3' end by the self-cleavage of the HDV ribozyme, and an exact 5' end corresponding to the very end of the EBOV genome (Pattnaik et al., 1992; Mühlberger et al., 1999). The translated supportive EBOV proteins lead to transcription, replication and eventually translation of the minigenome system. The transcription and replication rate can be measured by the luciferase activity. Luciferase reporter assays have a high sensitivity and are semi-quantitative methods to assess gene expression. *Firefly* luciferase (*Photinus pyralis*) gene encodes a 61kDa protein that can oxidate D-luciferin in the presence of ATP, magnesium and oxygen, producing light. This reporter activity is proportional to the steady-state level of mRNA (Greer and Szalay, 2002).

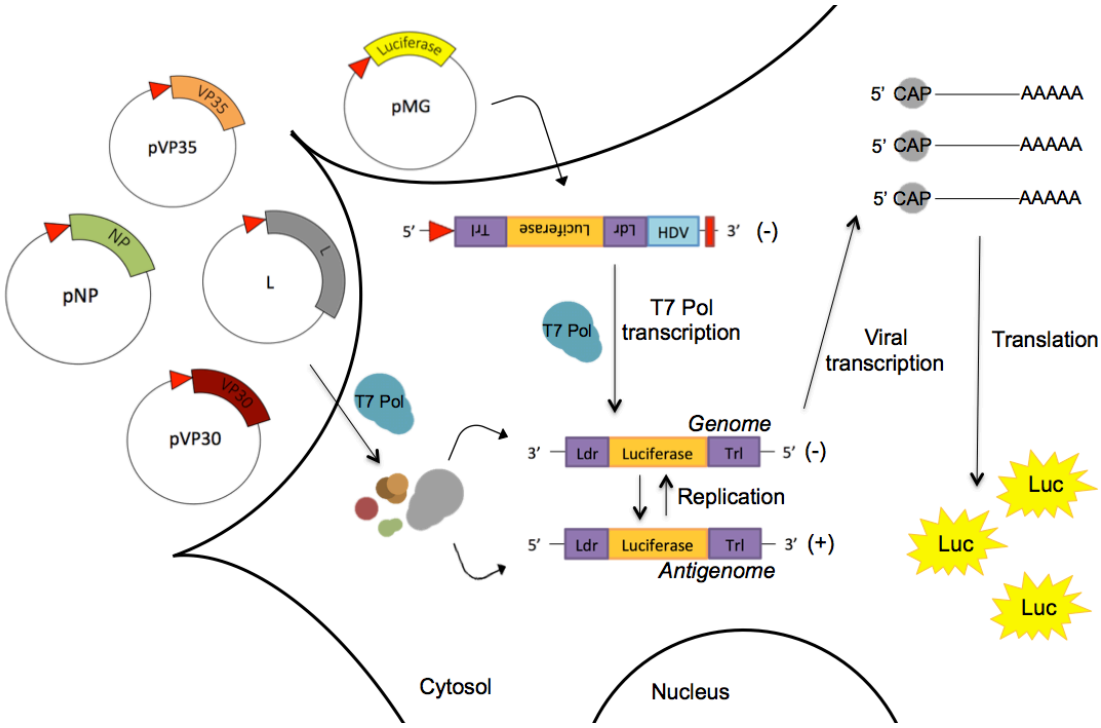

Figure 1.4. Schematic representation of the EBOV minigenome system.

1.3. EBOV virus-like particles (VLP)

Minigenome systems are only suitable to study viral transcription and replication. To overcome this limitation, VLP systems were developed (Warfield et al., 2003; Watanabe et al., 2004). In these systems, the minigenome plasmid is co-transfected together with plasmids encoding the seven EBOV proteins. Virions are created but cannot make new virions, as they don't contain the viral genome but the minigenome. Also, the maintenance of VLPs requires the constant transfection of plasmids encoding the RNP complex proteins.

1.4. Ebola Virus Disease

Ebola virus disease (EVD) or Ebola virus haemorrhagic fever (EHF) is a zoonotic and acute disease affecting humans and non-human primates. It is characterised by a multi-organ shock caused by an imbalance of the immune system, disordered coagulation and tissue damage, leading to severe bleeding (Baseler et al., 2017).

Although EVD is known for its haemorrhagic feature, it is not the major cause of death. EVD is also associated to a high case-fatality rate with an average of 50% and a range between 20-90%.

1.4.1. EBOV discovery, epidemiology, economic and social impact

1.4.1.1. EBOV discovery

On the 22nd of August of 1976, a 42-year old man from Yadongi Village (Democratic Republic of Congo), returned from an excursion to northern Zaire, where he had consumed antelope and smoked monkey meat. Four days after, he was treated at Yambuku Mission Hospital (YMH) for malaria as he was suffering chills and fever. He died on the 6th of September from a haemorrhagic symptom of unknown cause. In early September, several patients and those who received injections at YMH and their contacts presented a similar haemorrhagic febrile syndrome and died in about one week (reviewed in Breman et al., 2016). The cases in that first outbreak were 318, with 280 deaths (case-fatality rate 88%) (Burke et al., 1978). Shortly after the first outbreak in Zaire, that same year, another outbreak took place in southern Sudan, which caused 284 cases and 151 deaths (case-fatality rate 53%). Virologic investigations were taken to elucidate the unknown etiological pathogen, finding that it was a virus similar to the previously described Marburg virus (MARV) and was dubbed Ebola virus by Peter Piot, from the Institute of Tropical Medicine in Antwerp, Belgium (Johnson et al., 1977).

1.4.1.2. Epidemiology

According to the Centers for Disease Control and Prevention (CDC), since EBOV discovery in 1976, there have been at least 31,000 cases of EBOV infected individuals and 12,900 deaths, giving a case-fatality rate of ~42%. The EBOV species that produce disease in humans are *Zaire ebolavirus, Sudan ebolavirus* and *Bundibugyo ebolavirus,* although one EVD case was reported to be caused by *Taï Forest ebolavirus* in 1994 in Côte d'Ivoire.

EBOV outbreaks have occurred across the Equatorial belt of Africa, being it more prevalent in western Central and West Africa, and SUDV and BDBV being most common in eastern Central Africa (Pigott et al., 2016). A total of 20 confirmed outbreaks and 17 minor or single cases have occurred from 1976 in 19 countries as of October 2018 ("Ebola Virus Disease Distribution Map: Cases of Ebola Virus Disease in Africa Since 1976 | 2014-2016 Outbreak West Africa | History | Ebola (Ebola Virus Disease) | CDC," 2018).

1.4.1.3. Economic and social impact

The 2013-2016 EBOV West African outbreak in Liberia, Guinea and Sierra Leone had an estimated cost of $2.2 billion in the gross domestic product. The outbreak provoked a substantial loss in the private sector growth, the cross-border trade, and the agricultural production. Also, among healthcare workers, those at the higher risk of contracting the disease, there were a total of 881 confirmed infected and 513 deaths between Liberia, Guinea and Sierra Leone, according to the World Health Organisation ("Ebola Situation Report - 4 November 2015 | Ebola", 2015). By December 2015, the cost of the response was more than $3.6 billion for technical expertise resources and emergency operations centres, being the top donators the United States of America, the United Kingdom and Germany (Evans et al., 2015).

Ignorance, lack of preparedness of the health systems and population fear and distrust contributed to the spread of EVD. Women were more affected by the virus than men, probably by their role within the family as caregivers. Moreover, they were giving birth outside the health facilities, making them even more vulnerable. The increasing number of orphans will represent a long-term human development impact in the countries affected by EBOV outbreaks. Also, due to the impact of EVD, poverty in countries affected by the disease show a very strong increase in poverty and undernourishment (UN, 2015).

1.4.2. Reservoirs, transmission and persistence

The reservoir of EBOV is currently unknown, although EBOV-specific IgG antibodies and viral nucleotide sequences have been found in three species of fruit bats: *Hypsignathus monstrosus, Epomops franqueti* and *Myonycteris torquata* (Leroy et al., 2005). EBOV-specific antibodies only have been found in other fruit bat species, like *Eidolon helvum* in Ghana and Gabon (Olival and Hayman, 2014; Weyer et al., 2015). The role of vectors is not known, and spillover epidemics have been observed in small mammals, duikers, primates and humans.

Transmission of EBOV occurs through contact with skin and secretions of an infected individual suffering from active infection. The virus can be transmitted through urine, sweat, saliva, semen, faeces, blood, vomitus, breast milk and virus-contaminated objects. The infection of EBOV needs a relatively low viral dose, with 10 or fewer viral particles to infect a human being (Osterholm et al., 2015). Transmission is not likely to occur before the onset of symptoms (Elshabrawy, et al., 2015). The major route between humans requires direct contact with blood, body fluids or injured skin. There is no known connection of virus spread with any vector. There is virologic evidence that EBOV can persist for months and without causing cytopathic effects in immune-privileged tissues and their fluids, such as semen, breast milk, cerebrospinal fluid and aqueous humour (Vetter et al., 2016).

1.4.3. Pathogenesis and host immune response

Ebola virus disease (EVD) remains not completely understood due to the many different cell targets and manifestations of the systemic disease. The clinical outcome depends not only on the virus strain but the host immune system and genetics (Liu et al., 2017). Entry into a host occurs through exposure of infected body fluids to mucosal surfaces, wounds or through parental transmission. The first targets of infection are the dendritic cells (DCs) and the macrophages, where the viral proteins directly trigger unbalanced proinflammatory responses (e.g. IL-6, IP-10) and supress induction of antiviral host cell functions. Additional susceptible antigen-presenting

cells are recruited to the site of infection by this unregulated secretion of proinflammatory cytokines and chemokines, becoming subsequently infected. This proinflammatory gene expression occurs very early in infection and appears to be induced by EBOV GP during entry to the cell (Wahl-jensen et al., 2005). Infected macrophages and DCs will both spread the virus to secondary lymph nodes, where more susceptible myeloid antigen-presenting cells will be infected and induce apoptosis in lymphocytes. Adaptive immunity drives viral clearance. Early production of IgM and isotype switch to IgG was observed to be correlated with positive outcome in EVD, while diminished IgM and IgG responses have been associated with fatal cases (Baize et al., 2002; Ksiazek et al., 1999). Antibody responses play many roles during EVD, including antibody-dependent killing of infected cells, complement activation and neutralization. $CD8^+$ and $CD4^+$ T cells are essential for virus clearance and can only be activated by DCs. In both fatal and surviving cases and unrelated to treatment, EVD is characterised by a robust T cell activation. Nevertheless, a lack of T cell effectiveness is thought to be related to high expression of T cell co-inhibitor molecules, programmed cell death-1 (PD-1) and cytotoxic T-lymphocyte-associated protein 4 (CTLA-4) in T cells, which leads to T cell exhaustion (Mohamadzadeh et al., 2007; Ruibal et al., 2016). High viremia occurs due to the increasing number of infected DCs and macrophages, giving rise to the infection of hepatocytes and Kupffer cells in the liver, accompanied by progressive acute hepatitis (Bradfute et al., 2010). In late stages of infection, endothelial cells lining the blood vessels become infected and activated, resulting in an increase of the cardiovascular barrier permeability, vascular leakage, bleeding and impaired coagulation (Geisbert et al., 2003) (Figure 1.5).

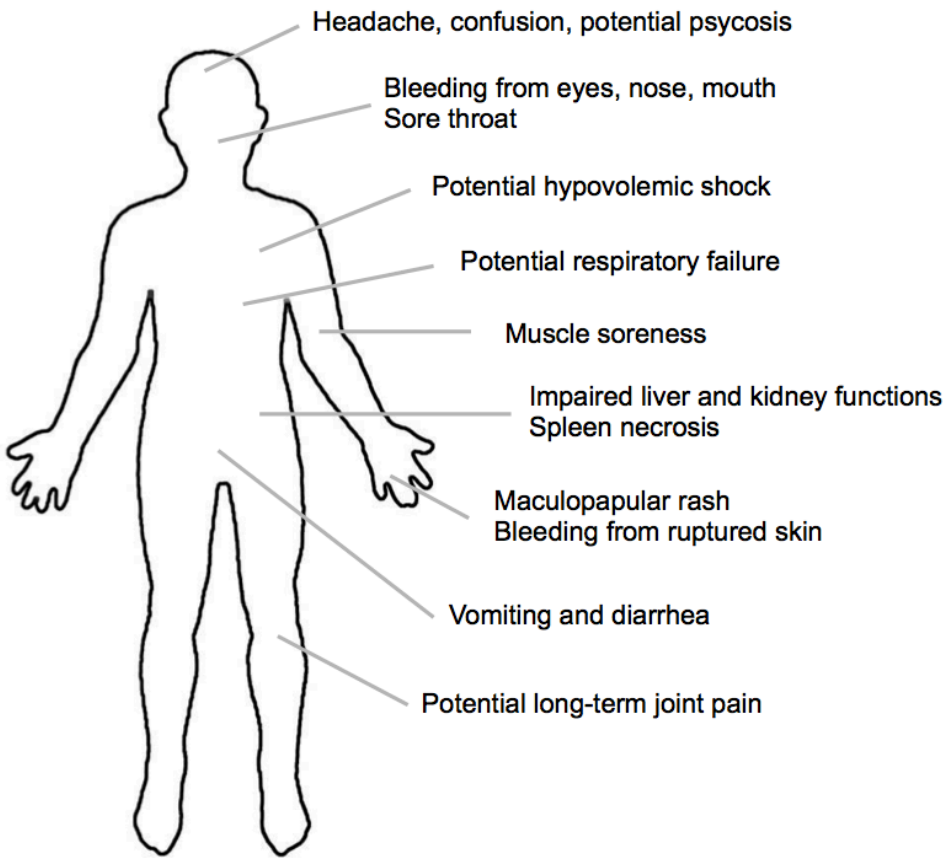

Figure 1.5. Observed symptoms associated to EVD. *Schematic representation based on Mendoza et al. observations (Mendoza et al., 2016).*

1.4.4. EBOV suppression of host antiviral responses

EBOV interferes with the immune response by blocking the interferon (IFN) production signalling by the VP35 and VP24 proteins and by the GP/sGP-based immune diversion. VP35 functions as a type-I IFN antagonist by blocking the activation of IFN regulatory factor 3 (IRF-3), possibly by preventing transcription of IFN-β and by impeding the detection of the dsRNA stage of viral replication/transcription (Feldmann and Geisbert, 2011), while VP24 blocks a number of IFN signalling pathways. Together, VP35 and VP24 ensure the poor production of IFN and therefore the infected cell is unable to respond (Audet and Kobinger, 2015). Moreover, maturation of DCs is inhibited by VP35, which interferes with RIG-I signalling pathway. It prevents the up-regulation of co-stimulatory molecules CD40, CD80 and CD86, MHC-1 and MHC-2. Therefore, antigen presentation to $CD8^+$ and

$CD4^+$ T cells gets impaired as well as B cell activation (Baseler et al., 2017). VP40 plays a role in EBOV immune evasion by suppressing RNAi and via exosome-bystander cell death (García et al., 2012). Ebola virus GP also contributes to escape the host immune detection by hiding MHC-1 on the surface of the cells (Francica et al., 2010) and by preventing Fas-mediated apoptosis of EBOV infected cells (Noyori et al., 2013). It also counteracts tetherin (Kaletsky et al., 2009). sGP neutralises the humoral immune response by adsorbing anti-GP antibodies (Mohan et al., 2012).

1.5. Therapeutics for EVD

Although Ebola virus was first described more than 40 years ago, neither vaccine nor treatment has been approved for use in humans. The impact on West African population of the largest ever EBOV outbreak, occurring between 2013-2016, highlighted the urgent need to find effective therapeutics against EVD and gave the chance to evaluate several vaccine candidates. Nevertheless, EBOV-infected patients received supportive care, which remains the mainstay of treatment due to non-licensed therapy for humans against EVD (as of April 2019).

1.5.1. Current state of vaccine development

There is currently no FDA-licensed vaccine to prevent EVD (as of April 2019). As an emergency response to the 2013-2016 Ebola virus epidemic in West Africa, several candidate vector-based vaccines have been tested in trials. During 2015, a phase-2 clinical trial was performed in Sierra Leone to test the efficacy of a recombinant adenovirus type-5 vector-based Ebola (Ad5-EBOV) vaccine expressing the viral glycoprotein of the Makona strain. Non-human primates were used for a preclinical challenge trial with the Ad5-EBOV vaccine and showed 77% protection against death. Nevertheless, durability of the vaccine-elicited GP-specific antibodies was not sufficiently long lasting and robust (Zhu et al., 2017). Moreover, a large proportion of adults worldwide have immunity against adenoviral vectors, which compromises the efficacy of this vaccination platform.

The effect of the recombinant, replication-competent vesicular stomatitis virus-based trial vaccine expressing Zaire Ebola virus Mayinga strain surface GP protein (rVSV-ZEBOV) was tested during the 2013-2016 in Guinea. No cases among vaccinated people from day 10 post-vaccination demonstrated substantial protection against EVD, showing 100% efficacy (CI 74.7-100%) in 7651 individuals enrolled in the ring vaccination trial (Henao-Restrepo et al., 2017).

1.5.2. Current state of treatment development

Small molecule inhibitors comprise repurposed drugs, newly developed nucleic acid-based products (small interfering RNA; siRNA) and immune-based therapeutics, including plasma transfusions, interferons and monoclonal antibodies (mAbs) against EBOV.

1.5.2.1. Small molecule inhibitors

Many small molecules have shown protection in cellular culture but the one that stands out is Favipiravir (6-fluoro-3-hydroxy-2-pyrazinecarboxamide), which is a broad spectrum inhibitor of viral RNA polymerase activity of RNA viruses (Furuta, et al., 2017). Favipiravir has shown increased survival rates in individuals suffering from EVD and a significant reduction in viral RNA load (>100 fold difference) determined by (q)RT-PCR (Bai et al., 2016). Nevertheless, monotherapy with Flavipiravir is unlikely to be effective in patients with very high viral loads (Ct value < 20) (Sissoko et al., 2016).

1.5.2.1. Immune-based therapeutics

ZMapp is a cocktail composed of three chimeric, humanised, monoclonal antibodies that target different sites of the Mayinga EBOV-GP. The three antibodies that compose the ZMapp cocktail were sourced from MB003 and ZMab, which are previous anti-EBOV GP antibody collections (Tran et al., 2016). ZMapp was used as a complementary therapy to treat EBOV-infected patients during the West African

EBOV outbreak and showed an increased chance of survival. However, its effectiveness could not be assessed as this therapeutic was administered with other treatments such convalescent plasma transfusion (Davey et al., 2016; Mendoza et al., 2016). Convalescent whole blood (CWB) and convalescent plasma (CP) from those patients who have recovered from EVD carry specific antibodies. CP and CWB have been used to treat EBOV-infected patients but its effectiveness remains inconclusive. Interferons (IFNs) have also been used in combination with CP as treatment. IFNs have been used as broad-spectrum antivirals as they have a pivotal role in the innate immunity against viral infections. IFNs treatments may be beneficial for the patient but they are not fully protective by themselves (Smith et al., 2013).

1.6. Research aims and objectives

The general aim of this PhD was to give insight into the roles of Ebola virus VP35 and L proteins within the host cell. In order to achieve so, label-free proteomics were used to elucidate host-virus protein associations. Besides, a minigenome system enabled the study of selected protein-protein interaction functionalities on EBOV RNA synthesis in BSL-2 facilities. The work comprised in this thesis was organised in three chapters.

The first part aimed to elucidate the EBOV VP35 cellular interactome by using a co-immunoprecipitation approach coupled to LC-MS/MS. Several novel and potential VP35-host protein-protein interactions were identified. Two of the most significant hits were DYNLL1 and CIRBP. The anti-viral activity of the DYNLL1 antagonist Ciliobrevin D on EBOV RNA synthesis were evaluated in this chapter.

The second chapter of results focused on the investigation of relevant EBOV L-host protein interactions by also using a co-immunoprecipitation approach coupled to LC-MS/MS. To overcome the hindrance that a relatively big protein entails in terms of cellular stability and levels of expression in cell culture, a cell-free rabbit reticulocyte coupled transcription and translation system was used to express L and investigate potential host interactions. The observed interaction between EBOV L and the host protein CALM and also the role of free intracellular calcium ions on the viral RNA synthesis were further investigated in this chapter.

The third part of this thesis studied the potential significance on the viral RNA synthesis and IFN-β antagonism performance of three EBOV VP35 non-synonymous mutations observed to occur in the start of the 2013-2016 West African outbreak.

Chapter 2: Materials and Methods

2.1. Recombinant protein constructs

2.1.1. Fluorescent fusion vector cloning

2.1.1.1. EBOV EGFP-VP35 and VP35-EGFP, mutated VP35-encoding vectors and pL-mCherry

A codon-optimised for human cell expression cDNA sequence encoding viral protein VP35 was cloned into pEGFP-C1 (Figure 2.1A) and pEGFP-N1 (Figure 2.1B) vectors for the expression of *Zaire ebolavirus* Makona strain VP35 [NCBI sequence reference number KJ660347.2] with either a C-terminal EGFP tag and an N-terminal EGFP tag, respectively. The same codon-optimised for human cell expression EBOV VP35 sequence was used for the introduction of non-synonymous mutations. The mutated genes were inserted in a pUC57 vector (Figure 2.1C) and under the control of a T7-Pol promoter. Three constructs encoding mutated Makona strain EBOV VP35 proteins were pVP35$_{M68T}$, pVP35$_{L249F}$ and pVP35$_{L330F}$, encoding residue substitutions M68T, L249F and L330F, respectively.

A codon-optimised for human cell expression cDNA sequence encoding the reporter protein mCherry [NCBI sequence reference number AY678264] was introduced in the second hinge (H2) region of the EBOV RNA-dependant RNA polymerase of *Zaire ebolavirus* Makona strain [NCBI sequence reference number KJ660347.2], between nucleotides 5527 and 5528 (amino acids G162 and S163). The insert was cloned in a pUC57 vector (Figure 2.1C), under the control of a T7 polymerase promoter.

The Invitrogen GenArt Gene Synthesis (Thermo Fisher Scientific) service was used for plasmid design, cloning and codon optimisation of the coding sequences.

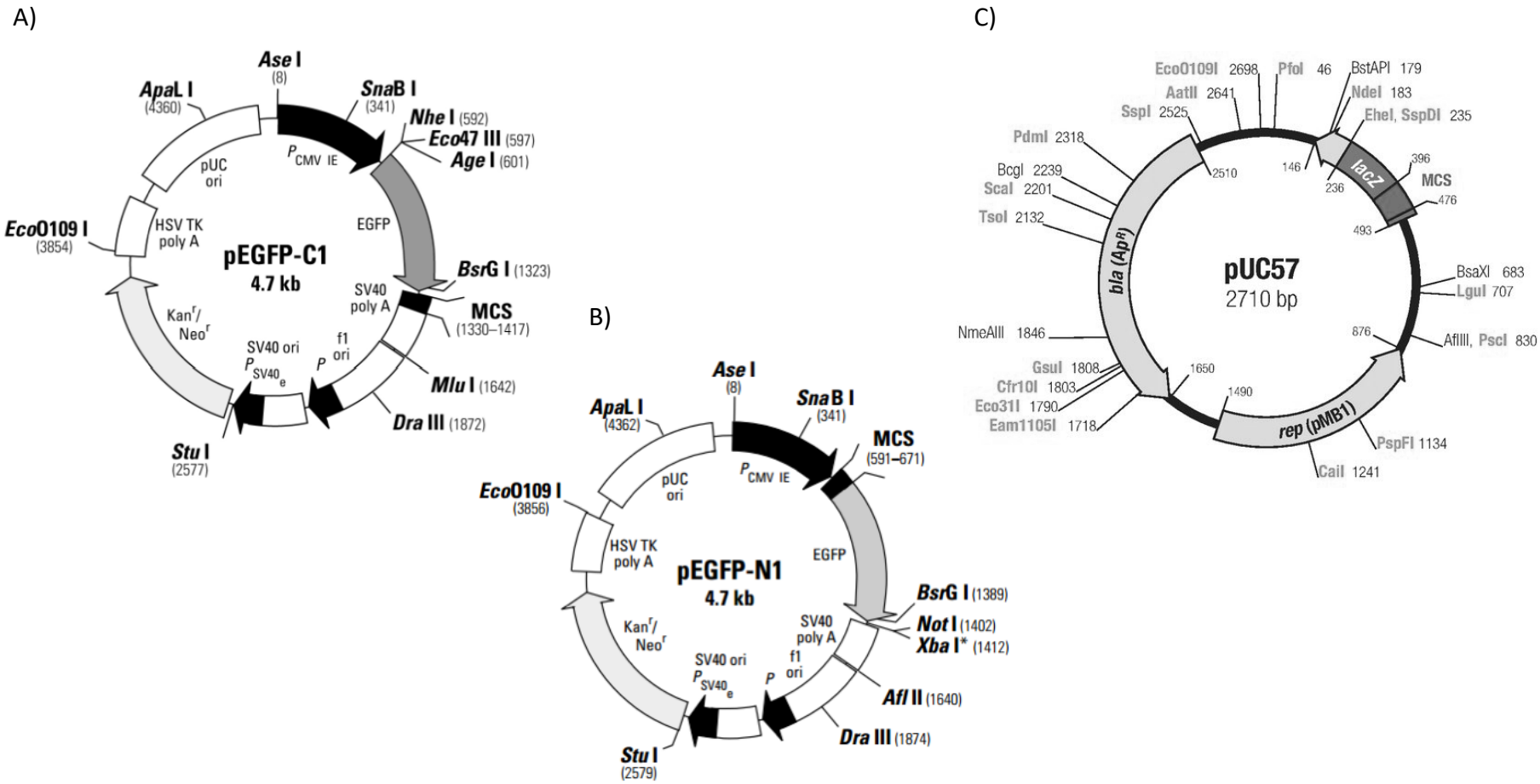

Figure 2.1. Map of the expression vectors used in this thesis. *(A) pEGFP-C1 and (B) pEGFP-N1 for the expression of EBOV VP35 with an EGFP tag at either the C-terminal or the N-terminal end. (C) A pUC57 vector was used for the expression of the minigenome system proteins, the EBOV minigenome, the mutated VP35 protein variants and the recombinant protein L-mCherry.*

2.2. Analysis of 2014-2015 EBOV VP35 sequences

On the 6th of March 2017, 968 *Zaire ebolavirus* (EBOV) VP35 protein sequences were downloaded from GenBank (NCBI). Sequences that were not completed had been withdrawn from the analysis previously. All of the analysed sequences were 340 amino acids in length. The sequences were aligned, and the analysis of the non-synonymous amino acid mutations was performed through MEGA (Version 6.06). All sequences were compared to a Makona strain reference sequence from 2014 [KJ660347.2] and to a *Zaire ebolavirus* Mayinga strain [NCBI ref. num. AGB56837.1] sampled in 1976 in the Democratic Republic of Congo during the first known outbreak ever.

2.3. DNA methods

2.3.1. Transformation of cells

2.3.1.1. DH5α competent cells

Subcloning Efficiency DH5α Competent Cells (Invitrogen) were used for transforming pEGFP C1, pEGFP-VP35 C1 and pVP35-EGFP N1. Aliquots of 50µl of competent cells were used for each plasmid DNA and transformations were performed according to the manufacturer's instructions. For each transformation, 10ng of plasmid DNA were used. LB-Kanamicin agar dishes were used to plate transformed cells, with a kanamycin concentration of 50µg/ml.

2.3.1.2. SURE competent cells

SURE competent cells (Agilent) were used for the production of pMG, pL, pVP30, pVP35, pNP, pL-mCherry, pIFNβ_GL3, pRLTK, $pVP35_{M68T}$, $VP35_{L249F}$, $pVP35_{L330F}$ and pT7-Pol stocks. Each plasmid transformation was performed in 100µl of competent cells and according the manufacturer's instructions. 10ng of plasmid were used per

transformations. LB-Ampicillin agar dishes were used to plate transformed cells, with an ampicillin concentration of 50µg/ml.

2.3.2. Preparation of plasmid DNA: Minipreps and Maxipreps

For the preparation of plasmids, a QIAGEN® Plasmid Mini and Maxi kits (QIAGEN) were used according to the manufacturer's instructions. For each Miniprep and Maxiprep, 12ml or 0.5L, respectively, of turbid overnight culture of plasmid DNA-containing bacteria with the correspondent selective antibiotic were used as input and 20µl and 300µl of nuclease-free water, respectively, were added to each eluted DNA pellet, left overnight at 4°C and resuspended and stored at 80°C the following day.

2.3.3. Measurement of DNA concentration and purity

DNA plasmid stock concentrations were measured by using a NanoDrop ONE spectrophotometer (Thermo Scientific) according to the manufacturer's instructions. To blank, 1µl of nuclease-free water was used and for each measurement, 1µl of sample. Measurements of each sample were taken twice.

2.3.4. Restriction endonuclease digestion

Endonuclease digestion was performed on plasmid DNA to obtain linear fragments and determine their size by electrophoresis for screening purposes. The endonucleases used in this study were SacI-HF, SalI-HF, and BsgII-HF, from New England Biolabs. The amount of restriction endonuclease was 1 unit/50µl reaction, and time, temperature of incubation and buffer used for each enzyme was in accordance with the manufacturer's instructions.

2.3.5. Agarose gel electrophoresis

Agarose gel electrophoresis (0.5-1% w/v) was used to achieve visualisation, separation and size determination of DNA. HI-Res standard agarose (AGCT Bioproducts) was added to the appropriate volume of TBE 1X (Tris-borate-EDTA) buffer (89mM Tris, 89mM boric acid, and 2mM EDTA, pH 8.3) and heated until molten. To prepare warm agarose solution, 0.1µl/ml of SYBR Safe DNA Gel stain (Thermo Scientific) was added. The molten agarose was mixed, poured into a gel-casting tray, left to cool down and submerged in TBE 1X buffer. DNA samples were mixed with DNA loading buffer (5% glycerol, 1mM EDTA, 0.2% bromophenol blue (w/v)) in a ratio 4:1 and loaded into the gel. Hyperladder™ 1kb (Bioline) or Quick-Load 1kb Extend DNA Ladder (New England Biolabs) were used according to manufacturer's instructions to determine the DNA fragments size. Electrophoresis was then carried out at 90-100v until dye migrated 80% of the gel approximately.

2.4. Tissue culture methods

In this thesis, two cell lines were used. Human Embryonic Kidney 293T cells (HEK293T), obtained from the European Collection of Authenticated Cell Cultures (ECACC), and BHK-21, a cell line stably expressing T7 polymerase (BRS-T7 cells). BSR-T7 cells were kindly provided by John Barr's group, from the University of Leeds.

2.4.1. Cell culture

293T cells were grown with Dulbecco's Modified Eagle's Medium (DMEM; Sigma-Aldrich) supplemented with 10% foetal bovine serum (FBS; Sigma-Aldrich), 1% Glutamax (Thermo Fisher Scientific) and 1% Penicillin-Streptomycin (Sigma-Aldrich) at 37°C with 5% CO_2. BRS-T7 cells were cultured in Dulbecco's Modified Eagle's Medium supplemented with 10% FBS, 1% Glutamax, 1% Penicillin-Streptomycin and 0.6% Geneticin® G418 (Thermo Fisher) (100µg/ml stock) at 37°C with 5% CO_2. For cell passage, cells were washed with phosphate buffered saline (PBS; Sigma-Aldrich), trypsinised with Trypsin solution 1X (Sigma-Aldrich) and mixed with fresh pre-warm supplemented DMEM with the appropriate antibiotic.

2.4.2. Freezing and thawing cells

To freeze cells, media was removed from T-175 flasks containing grown cells. Monolayers were washed with 10ml PBS, decanted, and washed again with 3ml of pre-warmed trypsin, following trypsination with 3ml of pre-warmed trypsin at 37°C for 5 minutes. Flasks were tapped for the cell monolayer detachment and 10ml of the appropriate pre-warmed media were added and mixed with cells to neutralise trypsin. Cells were trespassed into a 15ml Falcon tube and centrifuged for 5 minutes at 400rfc. Supernatant was discarded, following resuspension of pellet in 10ml of ice-cold freezing medium (DMEM 80%, FBS 10%, 10% dimethyl sulfoxide (DMSO; Sigma-Aldrich)). Cell suspension was aliquoted in cryovials, left at -80°C for 24 hours and stored into liquid nitrogen until requested.

To thaw cells, frozen cell cryovial aliquots were warmed up at 37°C and trespassed into 15ml Falcon tubes containing 9ml of cold PBS. Suspended cells were centrifuged for 5 minutes at 1000rpm. Supernatant was discarded, and cell pellets were washed two more times with PBS followed by spinning down and supernatant removal. Cell pellets were resuspended with 10ml of pre-warm media, transferred into T-25 cell culture flasks and incubated at 37°C with 5% CO_2 for 24 to 48 hours for the correct cell attachment to the flask surface.

2.4.3. Transfection of cells

2.4.3.1. Lipofectamine™ 2000 and Lipofectamine™ 3000

The minigenome system plasmids in BSR-T7 cells were transfected with Lipofectamine™ 2000 (Invitrogen). For transfections in a 24-well dish format, cells were seeded at 10^5 cells/well and plasmid transfections were carried out according to the manufacturer's instructions. For transfection of IFN-β assay plasmids in 293T cells, they were seeded at $1.6x10^5$ cells/well in a 24-well dish and transfection were performed with Lipofectamine 3000® (Invitrogen) according to the manufacturer's instructions.

2.4.3.2. Calcium phosphate

Calcium phosphate co-precipitation was used as the transfection method in chapter 3 for the expression of recombinant proteins EGFP-VP35 C1 and VP35-EGFP N1 in 293T cells. Filtered double distilled H_2O (ddH_2O) was used to resuspend $CaCl_2$. Plasmid DNA was added in a tube containing 2M $CaCl_2$ and ddH_2O was used to complete the volume. The mix was added into another tube containing 2X HEPES buffered saline (HBS) in a drop wise manner and left incubating for 30 minutes at room temperature. The solution was then added onto cells. Number of cells seeded, quantity of chemical compounds, plasmid DNA amount and transfection media volume depended on the dish format used (Table 2.1.).

Table 2.1. Calcium phosphate transfection solution recipes for 293T cells.

Format	24-well	12-well	6-well	10-cm^2	50-cm^2
Relative area	0.25x	0.5x	1.2x	7x	60x
Cell number	$6x10^4$	$1x10^5$	$2x10^5$	$1.25x10^6$	$8x10^6$
Culture media	500µl	1ml	2ml	10ml	100ml
Transfection media	280µl	570µl	1.4ml	8ml	68ml
2X HBS	18µl	36µl	86µl	500µl	4.28ml
2M $CaCl_2$	2.18µl	4.36µl	10.5µl	61µl	523µl
DNA	0.36µg	0.71µg	1.71µg	10µg	86µg
Volume/well	36µl	72µl	172µl	1ml	8.56ml

2.5. Protein techniques

2.5.1. Cell-free protein expression

TnT® Quick Coupled Transcription/Translation System (Promega) was used to express the fused protein EBOV L-mCherry *in vitro*. 2µg of the plasmid encoding L-mCherry were incubated together with 40µl of TnT® T7 Quick Master Mix, 1µl of methionine 1mM, 1µl of T7 TnT Enhancer and 4µl of nuclease-free water (Table 2.2). A positive and a negative control for the protein expression reaction were also included. The total volume per reaction was 50µl. Reactions were incubated at 30°C for 90 minutes.

Table 2.2. Components and quantities used per reaction.

Components	Positive reaction	Negative reaction	L-mCherry expression
TnT® Quick Master Mix	40µl	40µl	40µl
Methionine, 1mM	1µl	1µl	1µl
T7 TnT® PCR Enhancer	-	-	1µl
L-mCherry plasmid	-	-	2µg
Firefly luciferase plasmid	0.5µg	-	-
Nuclease-free Water	8µl	9µl	4µl

2.5.2. GFP and RFP co-immunoprecipitation of proteins

2.5.2.1. RNAse A treatment

For each ml of diluted cell lysate, 2µl (15 units) of RNase A (Qiagen) were added and the mix was incubated in a rotor for 1 hour at 4°C.

2.5.2.2. Forward co-Immunoprecipitations

EGFP, VP35-EGFP and EGFP-VP35 proteins co-immunoprecipitations (coIPs) were performed with GFP-Trap (Chromotech). Harvested cell pellets were lysed in 200µl of lysis buffer (10mM Tris/HCl pH 7.5, 150mM NaCl, 0.5mM EDTA, 0.5% NP-40 supplemented with 1X Halt protease Inhibitor Cocktail EDTA-Free (Thermo Scientific)). After an incubation of 30 minutes on ice, cell lysates were cleared by centrifugation at 14,000G and the supernatants were diluted five-fold with dilution/wash buffer (10mM Tris/Cl pH 7.5; 150mM NaCl; 0.5mM EDTA supplemented with 1X Halt protease Inhibitor Cocktail EDTA-Free (Thermo Scientific)). The GFP agarose beads were equilibrated with ice-cold dilution/wash buffer and incubated with the diluted cell lysates on a rotary mixer at 4°C overnight, and then centrifuged at 2500G for 2 minutes. The pellet was washed two times with dilution/wash buffer. After removal of the dilution/wash buffer, the beads were resuspended with 25µl of glycine-elution buffer (200mM glycine pH 2.5), incubated for 10 minutes at 300rpm at room temperature, collected by centrifugation at 2,500G for 2 minutes at 4°C and transferred to another Eppendorf tube together with 2.5µl of 1M tris-base (pH 10.4) to neutralise the eluted bound-proteins. This step was repeated 4 times. Samples were then analysed by mass spectrometry.

2.5.2.3. Reverse co-Immunoprecipitations

Reverse coIPs was performed utilising the immobilised recombinant protein G resin (Generon). Harvested cell pellets previously lysed with 200µl of lysis buffer were clarified by centrifugation and diluted five-fold with dilution/wash buffer. Diluted cell lysates were incubated with 3µg of specific antibodies against host proteins of interest for 2 hours at 4°C on a rotor. Recombinant protein G sepharose beads were equilibrated as previously described in the forward co-immunoprecipitations section (section 2.5.2.2). Cell lysates containing the antibody were incubated with the protein G sepharose beads overnight at 4°C on a rotor.

2.5.3. Harvest and lysis of culture cells

Cell lysis for western blot was performed with RIPA buffer (50mM Tris-HCl (pH 7.4), 1% (v/v) NP40, 0.55 (w/v) sodium deoxycholate, 150mM NaCl, 100mM sodium dodecyl-sulphate, 1x EDTA-free complete protease inhibitor (Roche)). Media from the wells containing the grown and transfected cells was removed. For a 24-well dish format, wells were washed with 1ml of PBS and following its removal, 50µl of ice-cold RIPA buffer were added in each well. Dishes were incubated on ice for 30 minutes and cell monolayers were scrapped and transferred into Eppendorf tubes. Cell lysates were centrifuged for 10 minutes at 14000rfc at 4°C. Supernatants were put into Eppendorf tubes and stored at -80°C until required for western blot.

2.5.4. Protein concentration determination

The Pierce™ BCA Protein Assay Kit (Thermo Scientific) was used for the colorimetric detection and quantification of total protein in cell lysates to equal the protein concentration loaded in the SDS-PAGE gels for immunoblotting. The microplate (96-well dish format) procedure was used according to the manufacturer's instructions. The calibration curve was constructed by using bovine serum albumin (BSA) standards. The diluent for the standards was the same as used for the samples, ddH_2O. For each sample, 10µl were pipetted into a well together with 200µl of Working Reagent (WR). Plates were incubated at 37°C for 30 minutes, and subsequently read on an Infinite® F50 absorbance microplate reader (Tecan Trading AG) at 560nm.

2.5.5. SDS-PAGE (Sodium-dodecyl sulphate polyacrylamide gel electrophoresis)

Protein samples were resolved by using a Mini-PROTEAN tetra cell (Bio-Rad). Gel recipes are described in Table 2.3. Throughout this thesis, 10% resolving gels are used unless otherwise indicated. Two ethanol-cleaned glass plates were held in a stand and resolving gel solution was poured in between. To provide a flat and air bubble-free surface, 1ml of water-saturated butanol was added at the top of the resolving

gel. Following the polymerisation of the gel and water-saturated butanol removal, the stacking gel solution was poured on top of the resolving gel and a comb of either 10 or 15 wells was added. Upon polymerisation of the stacking gel, the comb was removed, and the gels were inserted in an electrophoresis tank with 1X SDS-PAGE running buffer (25mM Tris-HCl [pH 8.3], 250mM glycine, o.1% [w/v] SDS). Protein samples were boiled and denaturalised for 10 min at 95°C with 5X SDS loading buffer (120 mM Tris-Cl, pH 6.8, 20% glycerol, 4% SDS, 0.04% bromophenol blue, 10% β-mercaptoethanol). As a reference marker for molecular weight, 7.5µl of ColorPlus™ pre-stained protein ladder, broad range (10-230 kDa) (New England Biolabs) or Spectra™ MultiColor High Range Protein Ladder (40-300kDa) (Thermo Scientific) were loaded. SDS-PAGE gels were run at 100-120v, 400mA for approximately 1 hour or until optimum resolution of the protein ladder was achieved.

Table 2.3. SDS-PAGE resolving and stacking gels recipes. *Amounts and volumes given to make 2 mini gels. APS refers to ammonium persulphate. SDS refers to sodium dodecyl sulphate. TEMED refers to tetraacetylethylenediamine.*

Resolving Gel (10ml)					**Stacking Gel (5ml)**	
% Gel	15%	12%	10%	7.5%	**% Gel**	5%
30% Acrylamide	5ml	4ml	3.3ml	2.5ml	**30% Acrylamide**	0.83ml
1.5M tris-HCl pH 8.8	2.5ml	2.5ml	2.5ml	2.5ml	**1M Tris-HCl pH 6.8**	0.63ml
dH_2O	2.3ml	3.3ml	4ml	4.8ml	**dH_2O**	3.4ml
10% (w/v) SDS	100µl	100µl	100µl	100µl	**10% (w/v) SDS**	50µl
10%(w/v) APS	100µl	100µl	100µl	100µl	**10%(w/v) APS**	50µl
TEMED	10µl	10µl	10µl	10µl	**TEMED**	5µl
Resolution (kDa)	10-40	20-100	30-100	25-200		

2.5.6. Western blot analysis

Poly-vinylidene fluoride (PVDF) membranes (Millipore) were activated in 100% methanol and equilibrated by immersion in Towbin buffer (25mM Tris-base [pH8.1-8.5], 192mM Glycine, 20% v/v methanol). SDS-PAGE gels were placed on over PVDF membranes and sandwiches between sheets of thick filter paper previously soaked in Towbin buffer. Transfer was performed using a Bio-Rad semi-dry apparatus at 25V for 45 minutes. After transfer, membranes were blocked in 10% (w/v) skimmed milk powder (Marvel) made up in Tris-buffered saline (0.25M Tris-base [pH 7.4], 1.5M NaCl) containing 10% (v/v) Tween-20 (TBS-T) and incubated on a rocker for one hour at room temperature. Blocking solution was then discarded and the membrane washed three times in TBS-T. Primary antibody in TBS-T or 5% (w/v) skimmer milk powder TBS-T was added to the membrane and incubated overnight (ON) at 4°C on a rocker. Antibodies used for the primary incubation are listed in Table 2.4. Following the incubation, unbound antibody was removed by washing the membrane three times with TBS-T. Horse radish peroxidase-conjugated secondary antibody in TBS-T 5% (w/v) skimmed milk was added to the membrane and incubated for one hour at room temperature on a rocker. Unbound secondary antibody was washed off as for primary antibody. The antibodies used for the protein detection are listed in Table 2.5. Protein-antibody complexes were visualized using the Clarity™ Western ECL Blotting Substrates (Bio-Rad) according to the manufacturer's instructions. A ChemiDoc touch gel imaging system (Bio-Rad) was utilised to obtain pictures of the developed membranes. PVDF membranes could be restored and reused by stripping them off with a Blot restore and rejuvenation kit (Millipore) according to the manufacturer's instructions.

2.5.7. Functional assays

2.5.7.1. Cell viability assay

Cell viability was determined by using a colorimetric (3-(4,5-dimethylthiazol-2-yl)-2,5-diphenyltetrazolium bromide) MTT assay. BSR-T7 cells were seeded in triplicate in 96-well plates at a density of 7.5×10^3 cells/well to ensure 70-90% confluence at 24 h. Ciliobrevin D (Merck) BAPTA-AM (Abcam) or W-7 (N-(6-Aminohexyl)-5-chloro-1-naphthalenesulfonamide hydrochloride; Sigma-Aldrich) were then added to wells at different concentrations (low to high) and incubated for 24h at 37°C. Dimethyl sulfoxide (DMSO; Sigma-Aldrich) was used as the vehicle control. After the small molecule inhibitor incubations, wells were washed once with 1X PBS. 0.024g MTT (Sigma) were dissolved in 10 ml of pre-warmed medium (DMEM 10% FBS, 1% Glutamax). The MTT was filtered and a volume of 100µl was added to each well. Plates were incubated for 45 minutes at 37°C, MTT was removed. 100µl of DMSO were added and mixed by pipetting. Absorbance was measured at 450nm by using an Infinite® F50 absorbance microplate reader (Tecan Trading AG).

2.5.7.2. Small molecule inhibitors

Ciliobrevin D ($C_{17}H_8Cl_3N_3O_2$) (Merck) is an inhibitor of dynein ATPase activity, which prevents the retrograde and anterograde transport of organelles and vesicles by disrupting spindle pole focusing and kinetochore-microtubule attachment. For the functional assays, 10mg of Ciliobrevin D were dissolved in 5ml of DMSO (2.5mg/ml) according to the manufacturer's instructions.

W-7 (N-(6-Aminohexyl)-5-chloro-1-naphthalenesulfonamide hydrochloride; $C_{16}H_{21}ClN_2O_2S{\cdot}HCl$) (Santa Cruz), a Ca^{2+}-calmodulin dependent phosphodiesterase and myosin light chain kinase inhibitor, was used to antagonise calmodulin in BSR-T7. For the functional assays, 25mg of W-7 were dissolved in 1ml of DMSO according to manufacturer's instructions.

BAPTA-AM (1,2-Bis(2-aminophenoxy)ethane-N,N,N′,N′-tetraacetic acid (acetoxymethyl ester); $C_{34}H_{40}N_2O_{18}$) (Abcam), a membrane permeable selective chelator of intracellular calcium, was used to reduce the levels of free Ca^{2+} ions in BSR-T7 cells. For the functional assays, 25mg of BAPTA-AM were dissolved in 327µl of DMSO according to the manufacturer's instructions.

2.5.7.3. EBOV Minigenome system

The EBOV minigenome system used in this thesis was the same used by García-Dorival et al. in our lab (García-Dorival et al., 2016) (Figure 2.2). BSR-T7 cells were seeded at a cell number for 10^5 cells/well in 24-well plates for an 80-90% confluence the next day. The minigenome system was transfected with Lipofectamine™ 2000 24 hours after seeding with the following plasmid amounts per well; 500ng pMG, 250ng pNP, 125ng pVP30, 125ng pVP35 and 125ng pL or pUC57, together with 50ng of the control plasmid pRLTK, encoding *Renilla* luciferase. 24 hours post-transfection, cells were washed with PBS and lysed with 100µl of passive lysis buffer (PLB; Promega) five-fold diluted with H_2O. After a 15-minute incubation, cells were harvested into Eppendorf tubes and stored at -20°C until further use.

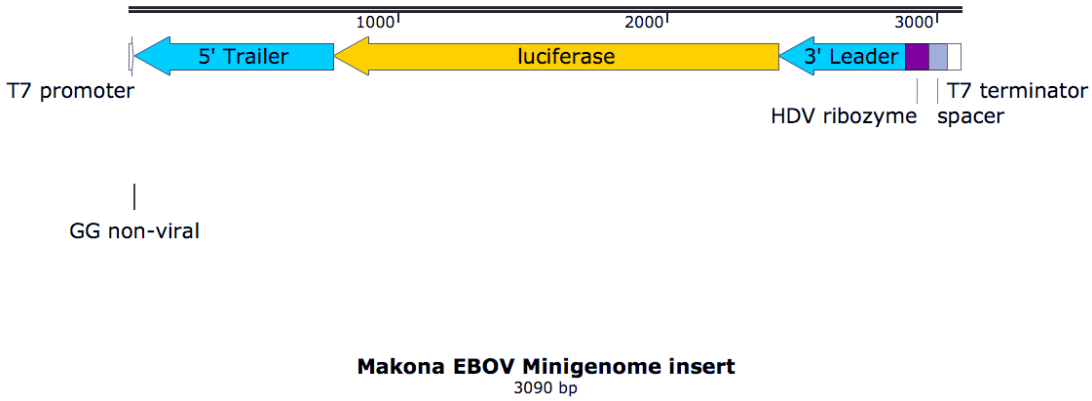

Figure 2.2. Map of the EBOV minigenome insert used for the minigenome system. *The minigenome insert and the RNP genes are encoded individually in the backbone pUC57, and their transcription is under the control of a phage T7 RNA polymerase promoter. For the construction of the EBOV minigenome plasmid, 5' end trailer (nucleotides 18220 to 18959 of the EBOV genome) and 3' end leader (the first 469 nucleotides of the 3' end of the EBOV genome including the translational NP gene START codon) sequences were placed flanking the reporter Firefly luciferase gene in the negative direction (3' to 5'). A non-viral GG motif was introduced between the T7 polymerase promoter and the 5' end trailer EBOV sequence for a higher efficient transcription by the T7 polymerase. Attached to the 3'end of the minigenome there is a hepatitis delta virus (HDV) ribozyme, which self-cleavage activity provides a precise 3'end, a prerequisite for the replication activity of the minigenome system. SalI and SacI restriction sites flanked the minigenome insert, as well as the RNP genes individually inserted in pUC57. The EBOV strain used for the construction of the minigenome and the support plasmids was Makona [NCBI sequence reference number KJ660347.2].*

2.5.7.4. IFN-β assay

293T cells were seeded on a 24-well plate format at a density of $1.6x10^5$ cells per well. After 24 hours, pIFN-β_GL3 (Figure 2.3), pVP35 (or mutated variants $pVP35_{M68T}$, $pVP35_{L249F}$, $pVP35_{L330F}$), pUC57, pT7 Pol and pRLTK were transfected with Lipofectamine™ 3000 according to the manufacturer's instructions and left incubating for 24 hours. DMEM media was replaced by fresh warmed media and low molecular polynosinic-polycytidylic acid (Poly(I:C), InvivoGen) was transfected with Lipofectamine™ 2000 according to the manufacturer's instructions. After 24 hours, cells were washed once with PBS, lysed with 1X PLB and extracted proteins were collected and stored to be used in DLA analyses and western blotting.

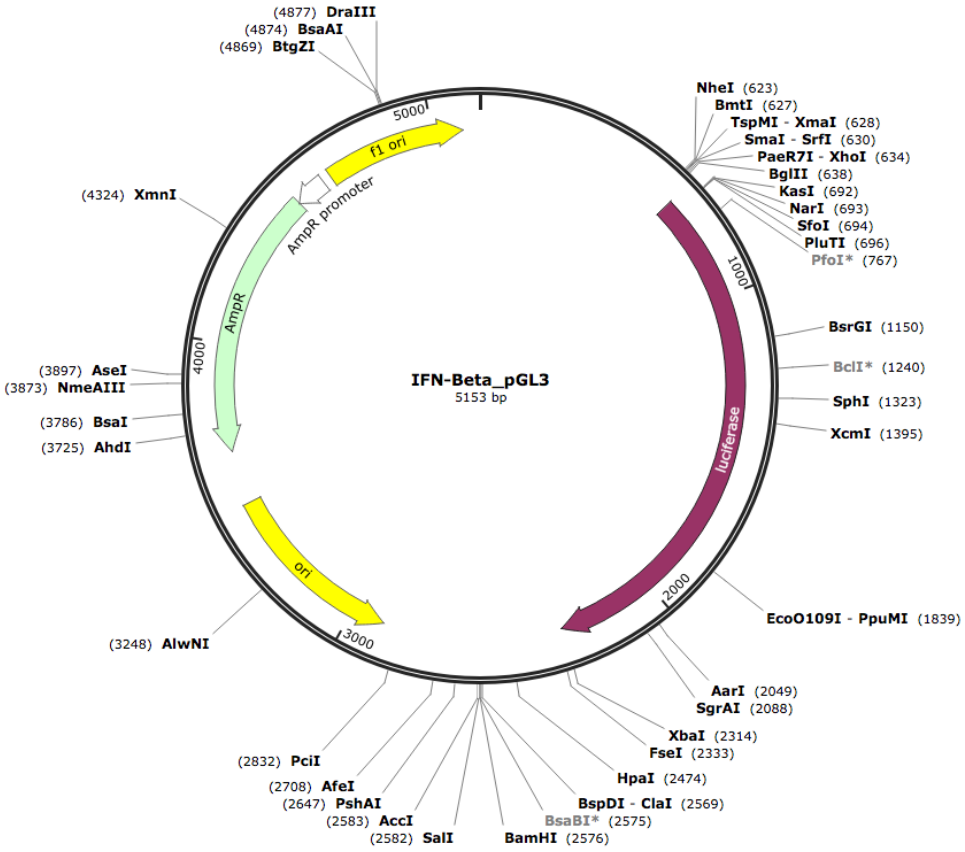

Figure 2.3. Map of the luciferase reporter plasmid under the control of an IFN-β promoter*. IFN-β promoter drives the expression of Firefly luciferase. The plasmid was used in the IFN-β assay. IFN-Beta_pGL3 was a gift from Nicolas Manel (Addgene plasmid # 102597) (Gentili et al., 2015).*

2.5.7.5. Dual luciferase assay

Cells transfected in a 24-well dish format were washed once with PBS 24 hours post-transfection. Passive Lysis 5X Buffer (PBL) (Promega) was diluted 5-fold with nuclease-free water and 100µl of PLB 1X were dispensed in each well. Plates were incubated at room temperature for 15 minutes with agitation and cell lysates were transferred to Eppendorf tubes. 100µl of Luciferase Assay Reagent II (LARII) and 100µl of Stop&Glo® reagent (Promega) were used per 20µl of supernatant of cell lysate in a 96-well white plate. Firefly luciferase and *Renilla* luciferase activities were read in a GloMax Explorer plate reader (Promega) with a Dual-Luciferase® Reporter Assay System (Promega) according to the manufacturer's instructions. The *Renilla* luciferase activity measurements were used to normalise the firefly luciferase activity of the samples. Each condition was done in triplicate for the statistical analysis.

2.6. Imaging techniques

2.6.1. Preparation of the coverslips and cell fixation

Coverslips (19mm Ø) were soaked into ethanol 70% and let dry before soaking them again with phosphate buffered saline (PBS; Sigma-Aldrich) and put in wells in a 12-well dish format. Wells with coverslips in were washed twice with PBS and once with Dulbecco's Modified Eagle's Medium (DMEM; Sigma-Aldrich) supplemented with 10% Foetal Bovine Serum (FBS; Sigma-Aldrich). 293T cells were seeded at $1x10^5$ cells per well and incubated at 37°C with 5% CO_2. After 24 hours, they were transfected with pGFP C1, pVP35-EGFP, pEGFP-VP35, pmCherry or pL-mCherry together with pT7-Pol by using the calcium phosphate transfection (section 2.4.3.2.). After 24 hours, cell monolayers were fixed with 4% paraformaldehyde (PFA) diluted in 1x phosphate-buffered saline (PBS) for 10 minutes at room temperature and washed three times with PBS.

2.6.2. Cell permeabilization and immunofluorescence staining

Cells were permeabilised with a 10-minute incubation of PBS with 0.1% Triton X-100 at room temperature. Following aspiration of the fixation solution, cells were washed 3 times with PBS with 0.5% Tween-20. Primary and secondary antibodies were prepared in PBS containing 2% FBS and 0.5% Tween with the indicated dilution in Table 2.4. and Table 2.6. A final volume of 100µl of primary antibody master mix was added to each well and left for 1 hour at room temperature in darkness, followed by three washes with PBS with 0.5% Tween. A final volume of 100µl of master mix with the appropriate secondary antibody was added to each well and incubated for one hour at room temperature in darkness. Wells were washed three times with PBS with 0.5% Tween to remove unbound antibodies.

2.6.3. Mounting of fixed cell samples

Coverslips with fixed cells were picked up from wells with forceps, inverted and put on glass microscope slides spotted with ProLong® Gold Antifade Reagent with DAPI (4',6-diamidino-2-phenylindole) (Invitrogen).

2.6.4. Fluorescent imaging

Slides were imaged on a Zeiss Axio Imager M2 fluorescence microscope (Carl Zeiss Microscopy). All images were captured by using a 63x/1.4 oil objective lens with the Zen 2 Pro software.

2.7. Mass Spectrometry

Sample preparation and LC-MS/MS analyses (sections 2.7.1. to 2.7.2.) were performed by Dr. Stuart Armstrong (Infection Biology, Institute of Infection and Global Health, University of Liverpool).

2.7.1. Proteomics analysis

Eluted samples were diluted two-fold with 25mM ammonium bicarbonate. Proteins were reduced with 3 mM dithiothreitol (Sigma) at 60°C for 10 minutes then alkylated with 9 mM iodoacetimide (Sigma) at room temperature for 30 minutes in the dark. Proteomic grade trypsin (Sigma) was added (0.2 µg) and samples were incubated at 37°C overnight. The resulting peptide samples were then acidified with trifluoroacetic acid (1% (v/v) final). Peptides were concentrated and desalted using C18 Stage tips (Thermo Fisher Scientific) and then samples dried using a centrifugal vacuum concentrator (Eppendorf). Peptides were re-suspended in 0.1% (v/v) trifluoroacetic acid and 5% (v/v) acetonitrile.

Mass spectrometry analysis was essentially as described in Dong et al. (Dong et al., 2017). Peptides were analysed by on-line nanoflow LC using the Thermo EASY-nLC 1000 LC system (Thermo Fisher Scientific) coupled with Q-Exactive mass spectrometer (Thermo Fisher Scientific). Samples were loaded on a 50cm Easy-Spray column with an internal diameter of 75 µm, packed with 2 µm C_{18} particles, fused to a silica nano-electrospray emitter (Thermo Fisher Scientific). The column was operated at a constant temperature of 35°C. Chromatography was performed with a buffer system consisting of 0.1 % formic acid (buffer A) and 80 % acetonitrile in 0.1 % formic acid (buffer B). The peptides were separated by a linear gradient of 3.8 – 50 % buffer B over 30 min at a flow rate of 300 nl/min. The Q-Exactive was operated in data-dependent mode with survey scans acquired at a resolution of 70,000. Up to the top 10 most abundant isotope patterns with charge states +2, +3 and/or +4 from the survey scan were selected with an isolation window of 2.0 Th and fragmented by higher energy collisional dissociation with normalised collision energies of 30. The maximum ion injection times for the survey scan and the MS/MS scans were 250 and 100ms, respectively, and the ion target value was set to 1E6 for survey scans and 1E4 for the MS/MS scans. Repetitive sequencing of peptides was minimised through dynamic exclusion of the sequenced peptides for 20s.

2.7.2. Label-free analysis

Label-free quantitation was performed using MaxQuant (MQ) software (version 1.6.1.0) with its internal search engine Andromeda as described in García-Dorival et al. (García-Dorival et al., 2014). Precursor mass and fragment mass were searched with mass tolerance of 4.5 and 20 ppm respectively (default settings). All other settings were default. The search included variable modifications of methionine oxidation and N-terminal acetylation, and fixed modification of carbamidomethyl cysteine. Enzyme specificity was set to trypsin, minimal peptide length was set to 7 amino acids and a maximum of two mis-cleavages were permitted. The false discovery rate (FDR) was set to 0.01 for peptide and protein identifications. The Andromeda search engine was configured for a database containing human proteins (Uniprot release-2017_11). The MQ software further includes a decoy database as well as common contaminants database to determine the false discovery rate and to exclude false positive hits due to contamination by proteins from different species. For LFQ analysis, “multiplicity” was set to one. Feature matching between raw files was enabled; using a retention time window of 2 min. “Discard unmodified counterpart peptides” was unchecked. Only unmodified and unique peptides were utilised. Averaged LFQ intensity values were used to calculate protein ratios.

2.7.3. Bioinformatics analysis

Label-free mass spectrometry results were processed and analysed using the Perseus software (version 1.6.1.1); this software was used to perform statistical analysis and to help differentiate background proteins (e.g. those cellular proteins that interacted with EGFP alone) from interacting proteins (those cellular proteins that interacted with viral protein bait). LFQ intensity value differences were compared using a t-test. A volcano plot graphic and table were generated showing the statistically significant proteins, those proteins that had a high probability of interacting with the viral bait.

2.8. Antibodies

The antibodies used for western blotting, immunostaining and ci-immunoprecipitation of proteins of interest in this piece of work are the following.

2.8.1. Primary antibodies

Table 2.4. Primary antibodies used for western blotting (Wb), immunofluorescence (IF) and co-immunoprecipitation (co-IP) experiments.

Target	Vendor	Cat. Number	Wb dilution	IF dilution	coIP dilution
RPS21	Abcam	ab90874	1/1000	1/1000	N/A
ATP5I	Abcam	ab122241	1/1000	1/400	3µg
DYNLL1	Abcam	ab51603	1/1000	1/200	3µg
PAI1	Abcam	ab187263	1/1000	1/500	N/A
CIRBP	Abcam	ab191885	1/1000	1/1000	N/A
GFP	Santa Cruz	sc-8334	1/2000	N/A	N/A
GAPDH	Abcam	ab8245	1/5000	N/A	N/A
***Firefly* Luc**	Abcam	ab185923	1/1000	N/A	N/A
***Renilla* Luc**	Abcam	ab185926	1/10000	N/A	N/A
EBOV NP	IBT Bioservices	0301-012	1/3000	N/A	N/A
EBOV L	IBT Bioservices	0301-045	1/1000	N/A	N/A
EBOV VP35	IBT Bioservices	0301-040	1/1000	N/A	N/A
mCherry	Abcam	ab167453	1/2000	N/A	4µg
BAG2	Abcam	ab47106	1/1000	N/A	3µg
YBX1	Abcam	ab225706	1/2000	1/200	4µg
CALM	Millipore	05-173	1/2000	1/400	3µg

2.8.2. Secondary antibodies

2.8.2.1. For western blot

Table 2.5. Secondary antibodies used for western blotting.

Target	Vendor	Cat. Number	Dilution
Goat anti-Rabbit IgG	Sigma	A6154	1/2000
Goat anti-Mouse	Sigma	A4416	1/2000

2.8.2.2. For immunofluorescence

Table 2.6. Secondary antibodies used for immunofluorescence.

Target	Vendor	Cat. Number	Dilution
Donkey anti-Rabbit IgG Alexa Fluor® 488	Life technologies	A-21206	1/50
Donkey anti-Rabbit IgG Alexa Fluor® 546	Life technologies	A-100040	1/50
Rabbit anti-Mouse IgG Alexa Fluor® 488	Life technologies	A-11059	1/50
Rabbit anti-Mouse IgG Alexa Fluor® 568	Life technologies	A-11061	1/50

Chapter 3: Elucidation of the cellular interactome of EBOV VP35 and effect of the DYNLL1 antagonist Ciliobrevin D on the synthesis of viral RNA

3.1. Introduction

Ebolavirus is a highly contagious and virulent pathogen with no FDA-licensed therapeutic available yet. The case-fatality rates and magnitude of the 2013-2016 West African outbreak and the open-ended Democratic Republic of Congo EBOV outbreak highlight the need for effective therapeutics against Ebola virus disease (EVD) (Espeland et al., 2018). Huge efforts are currently being made in the development and implementation of an EBOV preventive vaccine (Henao-Restrepo et al., 2017; Lévy et al., 2018). However, equally important is the investigation of antiviral treatments to diminish the viral load in EBOV infected patients, thus increasing the chance of survival and prevent EVD spread among population. The elucidation of specific host-oriented molecules instead of viral-target drug candidates has arisen as an alternative to be investigated as antiviral treatment because (i) viruses are obligate parasites of the host cell machinery and (ii) RNA viruses have a high mutation rate due to the error-prone viral RNA-dependent RNA polymerase (Rdrp or L) and its low fidelity (Hoenen et al., 2015; Sanjuán and Domingo-Calap, 2016). Small molecule inhibitors directed against cellular proteins or signalling pathways potentially have a much broader spectrum of antiviral activity, as different viruses may need similar cellular factors for transcription and replication and host proteins are less likely to mutate and acquire drug resistance (Ma-Lauer et al., 2012; Baillie and Digard, 2013). For instance, the host protein viperin (virus inhibitory protein endoplasmic reticulum-associated, interferon-inducible) can interact and inhibit replication of many RNA viruses such as Influenza virus, dengue virus, hepatitis C virus, HIV-I and Chikungunya (Reviewed in Ng and Hiscox, 2018). Therefore, the better understanding of all the viral processes involved in EBOV replication inside cells will improve the guidance towards the finding of a therapy to treat EVD. The interactome is the totality of protein-protein interactions that take place in an organism, in a cell or in a specific biological context. Finding the interaction partners for a protein can reveal its function and its relevance in a certain condition and period of time.

EBOV has a 19Kb genome that encodes at least nine proteins encoded in seven genes (Cantoni and Rossman, 2018). EBOV viral proteins carry out several functions but still require the interaction, modulation or hijacking of the host cell machinery in order to accomplish each stage of the viral life cycle. As observed in the 2013-2016 West African outbreak, the lower the viral load in patients infected with EBOV, the higher the chance they will survive (de La Vega et al., 2015; Fitzpatrick et al., 2015; Kerber et al., 2016), making the viral RNA synthesis process an antiviral target to be taken into account. Some host proteins have already been recognised as having a role in these processes. For instance, the down-regulation of TOP1, a nuclear protein that unwinds the dsDNA helices for transcription and replication in the host cell (Takahashi et al., 2013), the inhibition of Hsp90, a cytosolic chaperone (Smith et al., 2010), or the disruption of ATP1A1 and HSP70 (García-Dorival et al., 2016, 2014) have been proven to diminish EBOV replication as well. The viral component that sustains EBOV transcription and replication is the ribonucleoprotein (RNP), a macromolecular complex composed of viral RNA, the viral RNA-dependent RNA polymerase, the nucleoprotein (NP) the non-catalytic phosphoprotein (VP30) and the viral polymerase co-factor (VP35). Viral transcription and replication of EBOV RNA takes place in the cytoplasm of infected cells, and is dependent on VP35 (Mühlberger et al., 1999).

VP35 is a multifunctional protein with diverse roles in the viral lifecycle and essential for the viral transcription and replication processes (Mühlberger et al., 1999; Mühlberger, 2007). The protein also plays an important role in the ribonucleocapsid assembly by its interaction with NP and VP30 (Huang et al., 2002), functions as a type-I interferon (IFN) antagonist by blocking both the activation of IFN regulatory factor 3 (IRF-3) and the detection of the dsRNA stage of viral transcription/replication and by upregulating the SUMOylation of IRF-7 (Basler et al., 2003; Elshabrawy et al., 2015; Chang et al., 2009; Binning et al., 2013). Together with VP24, VP35 ensures the poor production of IFN and therefore the infected cell is unable to produce a sufficient response to counteract the virus activity (Audet and Kobinger, 2015). VP35 can also inhibit antiviral effects by blocking protein kinase R and impairs the dendritic cell maturation (Schumann et al., 2009; Yenet al., 2014). It regulates the RNA synthesis

by modulating NP-RNA interactions (Groseth et al., 2009) and by associating with other cellular factors, such as the cytoplasmic dynein light chain 1 (LC8/DYNLL1) and the double stranded RNA binding protein 76 (DRBP76/NFAR-1/NF90) (Luthra et al., 2015; Shabman et al., 2011). These cellular factors could only represent a small part of all the cellular associations that take place between VP35 and the infected host cell, and these cellular factors could also be potential candidates for antiviral-directed targets.

In this chapter, a label-free liquid chromatography coupled with tandem mass spectrometry (LC-MS/MS) based approach was used to elucidate protein-protein interactions between EBOV VP35 and the host cell in human embryonic kidney 293T cells. Novel interactions with the viral protein were discovered and validated with forward and reverse pulldowns followed by the detection of these associations with specific antibodies by western blotting. An EBOV minigenome system was utilised to measure the effect on viral RNA synthesis that the small molecule inhibitor Ciliobrevin D has when antagonising the VP35 cellular partner DYNLL1 and the potential this host factor has as an antiviral-target candidate.

3.1.1. Objectives

Since viruses require the host protein machinery to accomplish their life cycle, this study aims to elucidate novel cellular partners of EBOV VP35 by using high-affinity purification coupled to a label-free mass spectrometry approach to give further insight into virus biology. By determining the viral RNA polymerase co-factor cellular interactome, novel host partners of EBOV VP35 could be further examined as anti-viral targets and their functional roles in the virus life cycle.

One of the top hits identified was the cytoplasmic dynein light chain 1 (DYNLL1), a host factor previously observed to interact with VP35 and to have a role in EBOV genome synthesis (Kubota et al., 2009; Luthra et al., 2015). The second aim of this chapter was to test the antiviral effect of the repurposed drug Ciliobrevin D, a cell permeable small molecule inhibitor that reversely and specifically blocks the cytoplasmic dynein motors, on the EBOV viral RNA synthesis.

NOTE: The sample preparation for LC-MS/MS and the raw data analyses obtained were performed by Dr. Stuart Armstrong (Infection Biology, Institute of infection and Global Health, University of Liverpool).

3.2. Results

3.2.1. Construction of EGFP, EGFP-VP35 and VP35-EGFP in 293T cells

In order to determine the cellular associations between Makona EBOV VP35 and the host, an enhanced green fluorescent protein (EGFP)-tagged co-immunoprecipitation strategy coupled to a label-free proteomic approach was used in HEK293T (293T) cells. Therefore, a codon-optimised complementary DNA (cDNA) sequence encoding EBOV VP35 was cloned into either the pEGFP-C1 or the pEGFP-N1 vectors for the expression of the viral protein together with an EGFP tag at either the N-terminal or C-terminal ends. The sequence used belonged to a *Zaire ebolavirus* Makona strain [NCBI sequence reference number KJ660347.2]. The constructs were designed by using the online tool GeneArt Gene Synthesis Services (https://www.thermofisher.com/order/geneartgenes/projectmgmt) and production and validation of the cloned insertions inside backbone vectors were performed by Invitrogen (Figure 3.1A and 3.1B). The vector EGFP-C1, referred in this chapter as pEGFP, was used for the expression of EGFP. pEGFP-V35 C1, pVP35-EGFP N1 and pEGFP were transformed into competent cells and grown for plasmid production. After plasmid extraction and purification, plasmids were digested once and twice, and size was checked by electrophoresis agarose gels (Figure 3.1C).

In order to confirm cellular expression of the above-mentioned fusion proteins, 0.36μg of either pEGFP, pEGFP-VP35 C1 or pVP35-EGFP N1 were calcium phosphate-transfected into 293T cells in a 24-well format at a density of $6x10^4$ cells per well. Cells were examined 24 hours after transfection by fluorescence microscopy to confirm recombinant EGFP-tagged VP35 variants expression in the cytoplasm (Figure 3.1D).

A

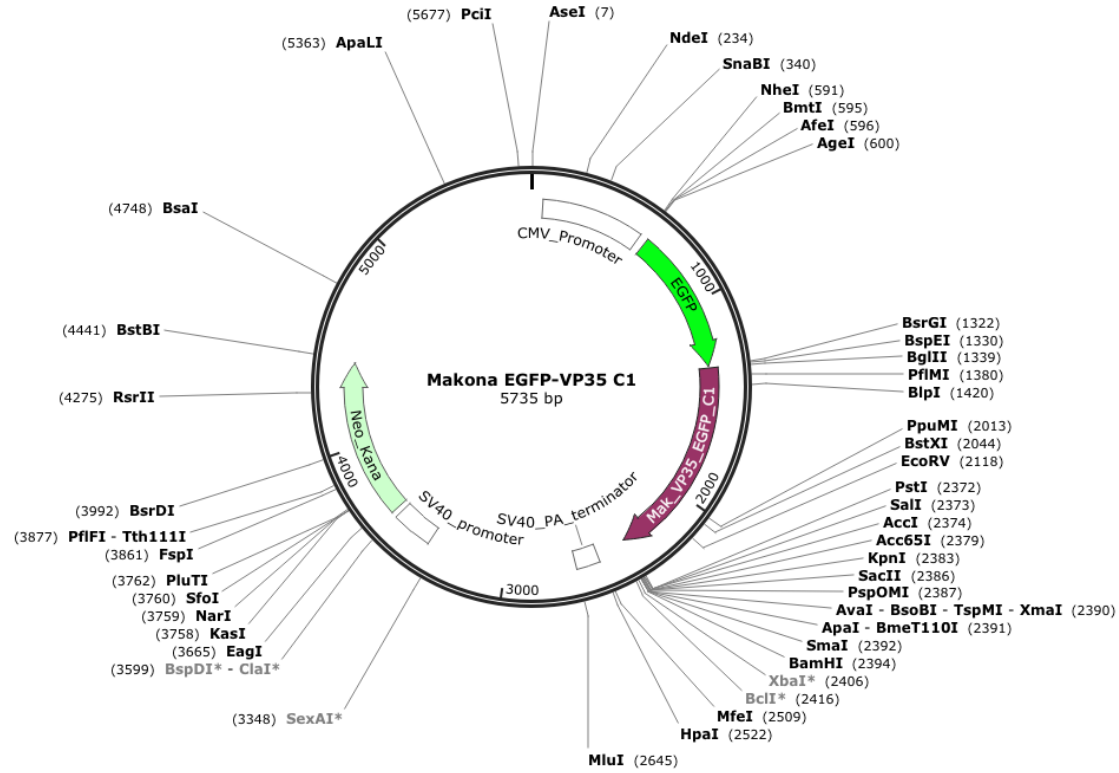
(5677) PciI
AseI (7)
(5363) ApaLI
NdeI (234)
SnaBI (340)
NheI (591)
BmtI (595)
AfeI (596)
AgeI (600)
(4748) BsaI
5000
CMV_Promoter
EGFP
1000
BsrGI (1322)
BspEI (1330)
BglII (1339)
PflMI (1380)
BlpI (1420)
(4441) BstBI
Makona EGFP-VP35 C1
5735 bp
(4275) RsrII
Neo_Kana
4000
Mak_VP35_EGFP_C1
2000
PpuMI (2013)
BstXI (2044)
EcoRV (2118)
PstI (2372)
SalI (2373)
AccI (2374)
Acc65I (2379)
KpnI (2383)
SacII (2386)
PspOMI (2387)
AvaI - BsoBI - TspMI - XmaI (2390)
ApaI - BmeT110I (2391)
SmaI (2392)
BamHI (2394)
XbaI* (2406)
BclI* (2416)
MfeI (2509)
HpaI (2522)
MluI (2645)
(3992) BsrDI
(3877) PflFI - Tth111I
(3861) FspI
(3762) PluTI
(3760) SfoI
(3759) NarI
(3758) KasI
(3665) EagI
(3599) BspDI* - ClaI*
(3348) SexAI*
SV40_promoter
SV40_PA_terminator
3000

B

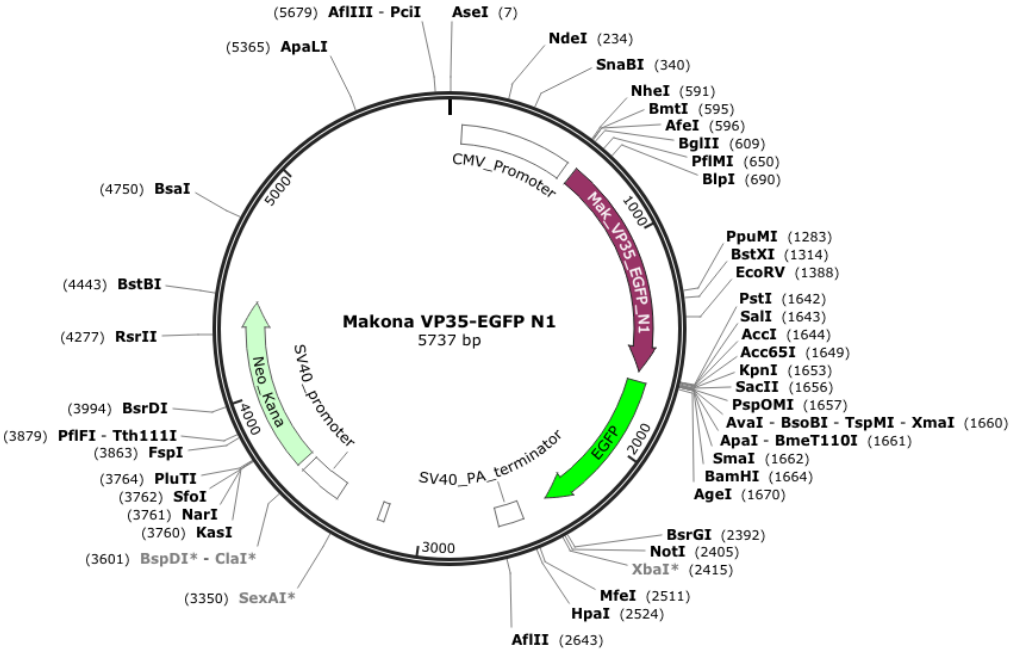
(5679) AflIII - PciI
AseI (7)
(5365) ApaLI
NdeI (234)
SnaBI (340)
NheI (591)
BmtI (595)
AfeI (596)
BglII (609)
PflMI (650)
BlpI (690)
(4750) BsaI
5000
CMV_Promoter
Mak_VP35_EGFP_N1
1000
PpuMI (1283)
BstXI (1314)
EcoRV (1388)
(4443) BstBI
Makona VP35-EGFP N1
5737 bp
PstI (1642)
SalI (1643)
AccI (1644)
Acc65I (1649)
KpnI (1653)
SacII (1656)
PspOMI (1657)
AvaI - BsoBI - TspMI - XmaI (1660)
ApaI - BmeT110I (1661)
SmaI (1662)
BamHI (1664)
AgeI (1670)
(4277) RsrII
SV40_promoter
Neo_Kana
4000
(3994) BsrDI
(3879) PflFI - Tth111I
(3863) FspI
(3764) PluTI
(3762) SfoI
(3761) NarI
(3760) KasI
(3601) BspDI* - ClaI*
(3350) SexAI*
SV40_PA_terminator
EGFP
2000
3000
BsrGI (2392)
NotI (2405)
XbaI* (2415)
MfeI (2511)
HpaI (2524)
AflIII (2643)

C)

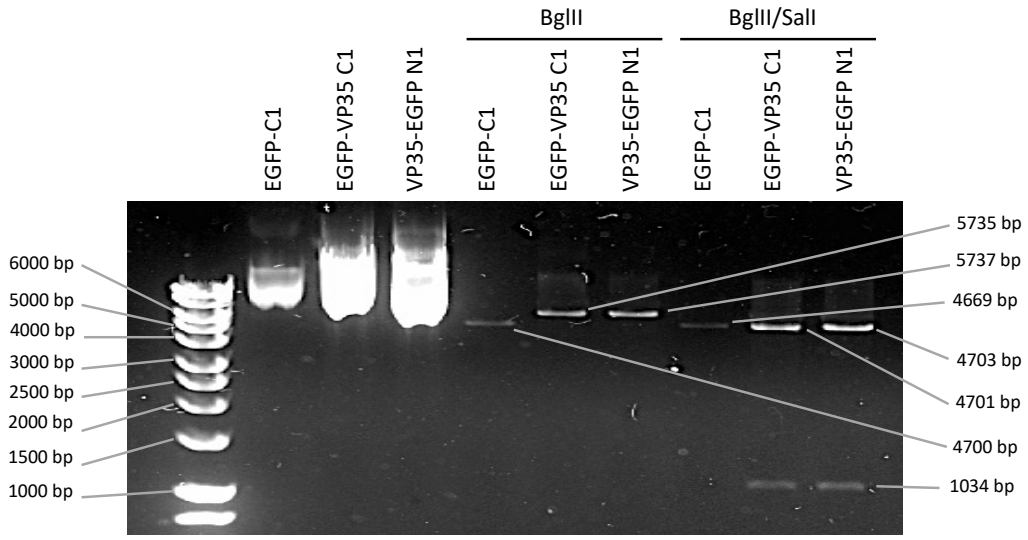
BglII
BglII/SalI
EGFP-C1
EGFP-VP35 C1
VP35-EGFP N1
EGFP-C1
EGFP-VP35 C1
VP35-EGFP N1
EGFP-C1
EGFP-VP35 C1
VP35-EGFP N1
6000 bp
5000 bp
4000 bp
3000 bp
2500 bp
2000 bp
1500 bp
1000 bp
5735 bp
5737 bp
4669 bp
4703 bp
4701 bp
4700 bp
1034 bp

D)

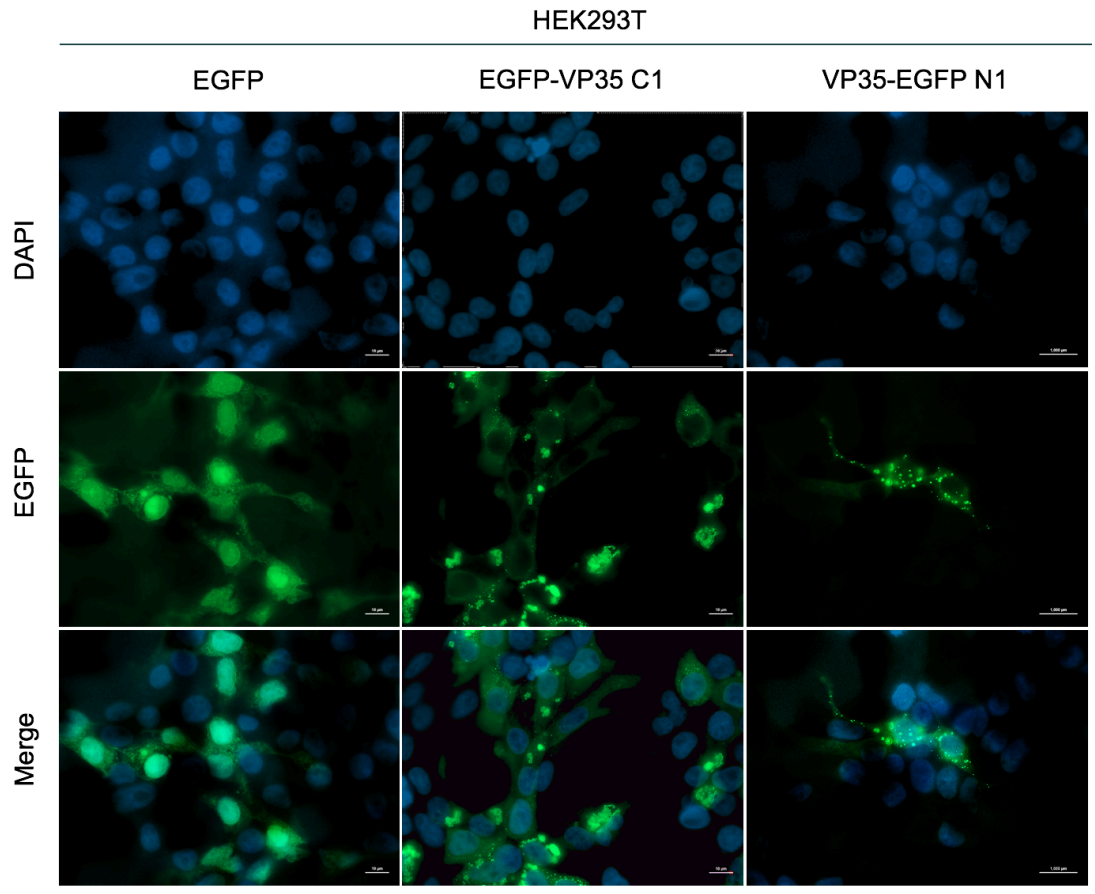
HEK293T
EGFP
EGFP-VP35 C1
VP35-EGFP N1
DAPI
EGFP
Merge

Figure 3.1. Construction, design and expression of the vectors encoding EGFP and recombinant proteins EGFP-VP35 C1 and VP35-EGFP N1. *Maps of the vectors encoding cDNA of EBOV VP35 tagged to the reporter gene EGFP. (A) cDNA of EBOV VP35 with EGFP tagged at the N-terminal end of the gene; (B) cDNA of EBOV VP35 with EGFP tagged at the C-terminal end of the gene. (C) Endonuclease digestion of pEGFP, pEGFP-VP35 C1 and pVP35-EGFP N1. Vectors were cut once by BglII, and twice by BglII and SalI. Uncut plasmid and digestion products were run in a 1% agarose gel electrophoresis to confirm product lengths. (D) Fluorescence microscope visualisation of transfected 293T cells expressing EGFP, EGFP-VP35 C1 and VP35-EGFP N1 24 hours post-transfection. Scale bar, 10μm.*

3.2.2. Co-immunoprecipitation of EGFP-VP35 C1 and VP35-EGFP N1 and determination of VP35-host protein interactions by label-free LC-MS/MS

Following visual confirmation of EGFP-fused VP35, the viral recombinant proteins were overexpressed in 293T cells to obtain enough amounts for their co-immunoprecipitation (coIP) wiith GFP-Trap® beads for further analyses on virus-host protein interactions (Figure 3.2A).

Cells were seeded in triplicate in two 145cm^2 dishes per condition and calcium phosphate-transfected either with pEGFP, pEGFP-VP35 C1 or pVP35-EGFP N1. Cells were harvested, lysed and EGFP-tagged VP35 proteins and host protein interactors were co-immunoprecipitated with GFP-Trap®. To assess the abundance and presence of the recombinant proteins in the pulled-down protein complexes, co-IP products were run in SDS-PAGE and a blotting was performed with a specific antibody anti-EGFP (Figure 3.2B). EGFP (27 kDa) was detected in the input and eluted samples of HEK293T transfected with pEGFP. EGFP-VP35 C1 and VP35-EGFP N1 (62 kDa) were detected in the input and eluted samples of 293T transfected with the vectors encoding either of the two fused viral proteins, confirming that the recombinant viral proteins had been pulled-down for the following analysis on their host interactors by mass spectrometry.

A label-free proteomics approach was used to identify and quantify cellular proteins that potentially associate with EBOV VP35. Co-immunoprecipitation of each condition was done in triplicate to maximise the identification of positive interactions and help identify non-specific interactions between the cellular factors and the binding matrix. LC-MS/MS was used to determine VP35-host PPIs and the data obtained was statistically analysed by Perseus software (1.5.6.0. version). Contaminants and proteins identified by only one unique peptide were removed from the list. The false discovery rate (FDR) was set at 1% or below, meaning that theoretically 99% of the proteins would be identified correctly. LFQ intensity values of the identified proteins were analysed using a t-test for statistical significance. In

order to identify changes in the replicate data set, volcano plots were generated, showing the logarithmic p-values for confidence in peptide identification vs. fold change difference in binding protein between VP35 fusion proteins and EGFP. Therefore, data points appearing at the top right side of the plot represent identified proteins that have lower p-values and larger fold change between conditions. Between the EGFP-VP35 C1 and the VP35-EGFP N1 cellular interactor data sets, 28 significant proteins with a fold change difference equal or higher than 2 were identified (Figure 3.3A and Figure 3.3B, Table 3.1 and Table 3.2).

In order to have a further insight into the relation among the potential EBOV VP35 cellular interactions, the 28 proteins potentially interacting with EBOV VP35 were uploaded into the STRING software (version 10.5). Clusters of cellular proteins predicted to interact with each other were identified as ribosomal proteins (in green), motility and structural proteins (in blue), TIMM family proteins (in red). Proteins shown in yellow were not associated to a cluster (Figure 3.3A). To identify the potential functionality of the data set of proteins in Table 3.1 and Table 3.2, the 28 significant proteins found between the two data sets were uploaded to the PANTHER bioinformatics algorithm (version 12.0), resulting in 26 protein function hits. Data was displayed as a pie chart, showing the category of protein and the number of proteins in each group. Four main groups of proteins were separated according to their molecular function, indicating that the identified EBOV VP35 potential interactors had binding, catalytic, structural molecule and transporter activities (Figure 3.3B).

A)

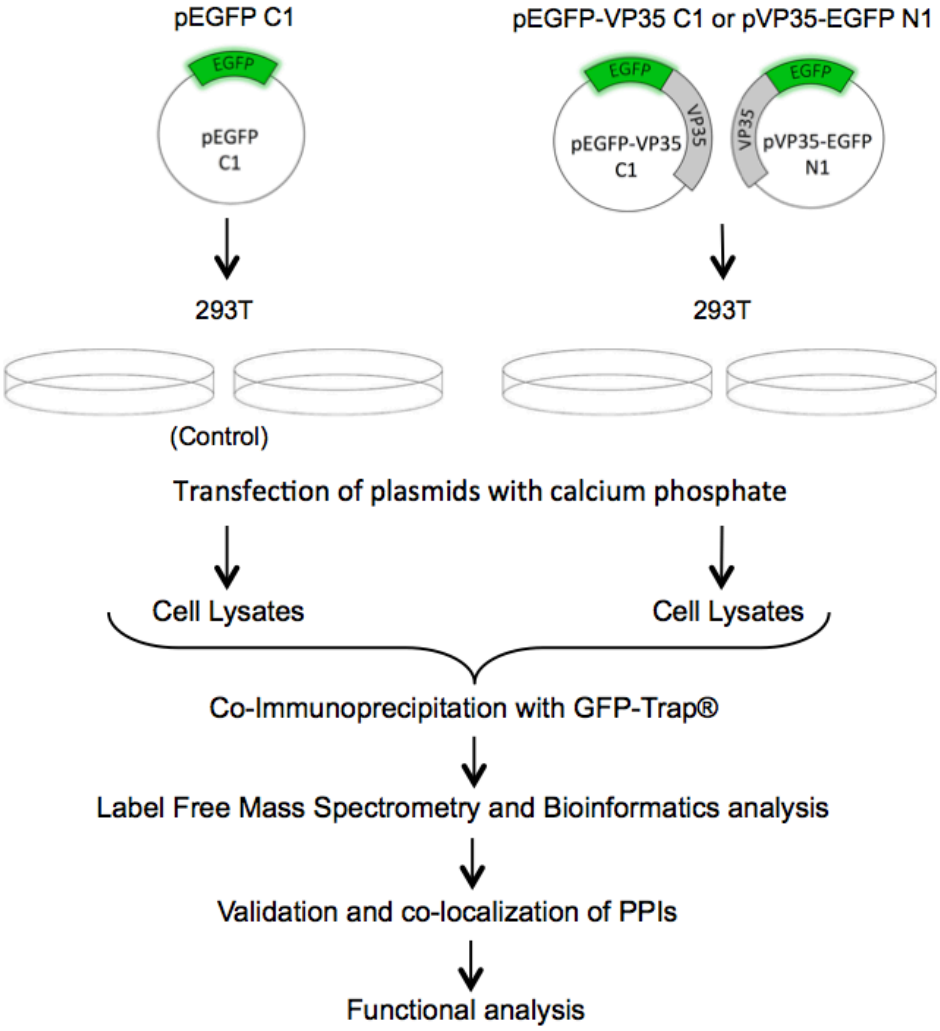
pEGFP C1
pEGFP-VP35 C1 or pVP35-EGFP N1
EGFP
pEGFP C1
EGFP
VP35
pEGFP-VP35 C1
VP35
EGFP
pVP35-EGFP N1
293T
293T
(Control)
Transfection of plasmids with calcium phosphate
Cell Lysates
Cell Lysates
Co-Immunoprecipitation with GFP-Trap®
Label Free Mass Spectrometry and Bioinformatics analysis
Validation and co-localization of PPIs
Functional analysis

B)

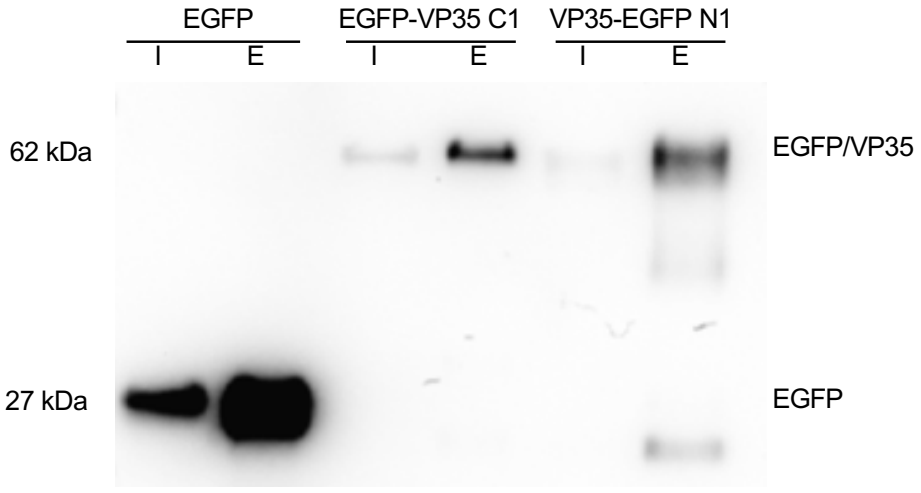
EGFP
EGFP-VP35 C1
VP35-EGFP N1
I
E
I
E
I
E
62 kDa
27 kDa
EGFP/VP35
EGFP

Figure 3.2. Co-immunoprecipitation of EGFP/VP35 and EGFP in 293T cells. *(A) Schematic representation of the method used for the transfection, co-IP and LC-MS/MS analysis of EGFP/VP35 transfected cells. (B) Identification by western blot of the co-immunoprecipitated EGFP-fused EBOV VP35 proteins. Cell lysates were diluted and incubated overnight with GFP-Trap® beads. Beads and protein complexes attached were washed and eluted by boiling with 2X SDS buffer. Input [I] and eluted [E] samples were run in an SDS-PAGE, proteins were transferred onto a PVDF membrane and blocked. Monoclonal mouse anti-EGFP was used as the primary antibody, and goat anti-mouse was used as the secondary antibody.*

A)

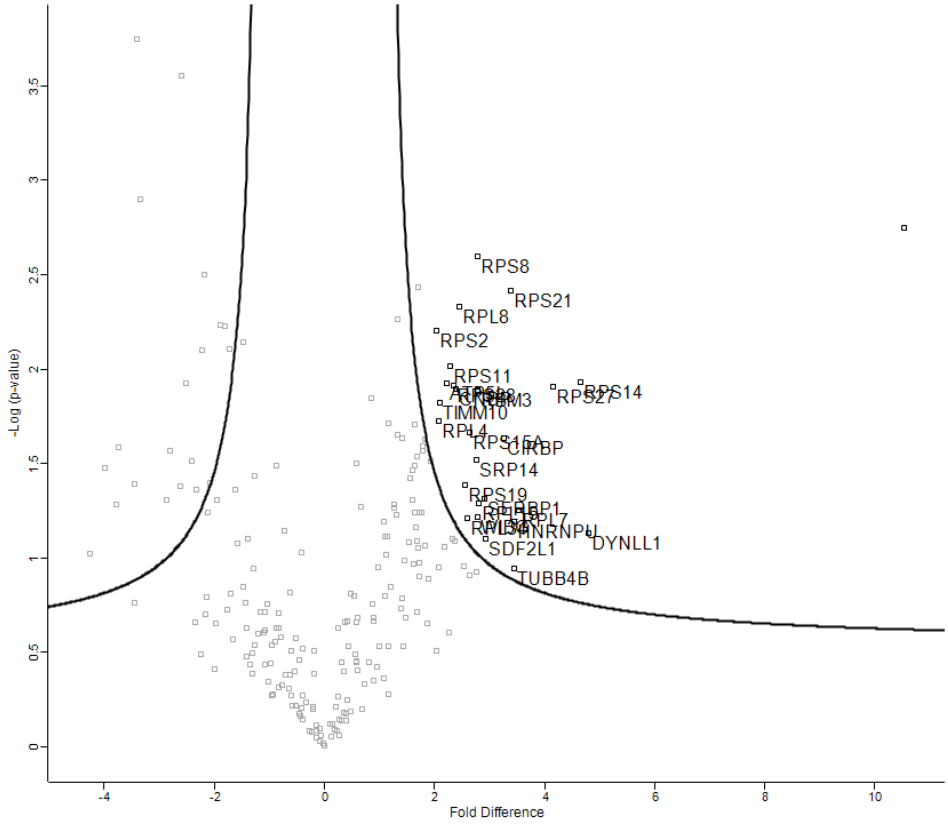
-Log (p-value)
Fold Difference
RPS8
RPS21
RPL8
RPS2
RPS11
RPS27
RPS14
TIMM10
RPL4
SRP14
RPS19
DYNLL1
SDF2L1
TUBB4B

B)

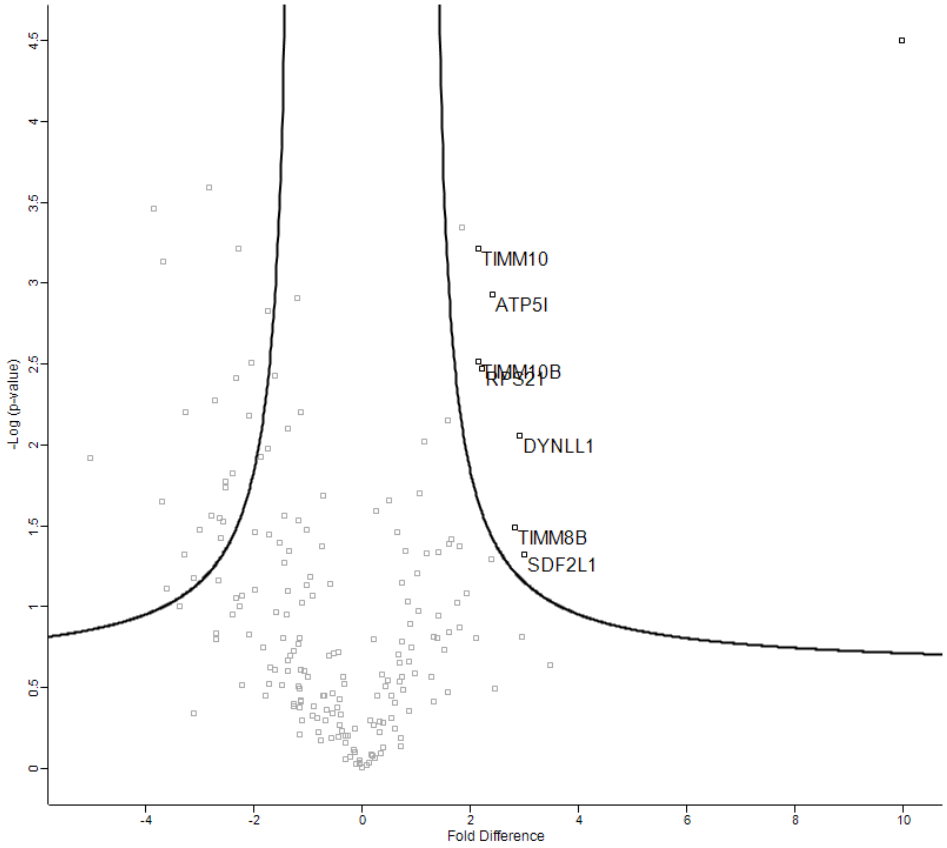
-Log (p-value)
Fold Difference
TIMM10
ATP5I
DYNLL1
TIMM8B
SDF2L1

Figure 3.3.1. Analysis of the potentially significant cellular proteins that interact with EBOV VP35. *Statistical analysis of the cellular proteins found to potentially interact with (A) EGFP VP35 C1 and (B) VP35-EGFP N1 using a volcano plot, with the names of the proteins of interest. The logarithmic p-value for confidence in peptide identification is plotted against the fold change difference in binding protein between EBOV VP35/EGFP and EGFP (≥ 2 FC). The isolated dot on both upper right corners represents EBOV VP35.*

A)

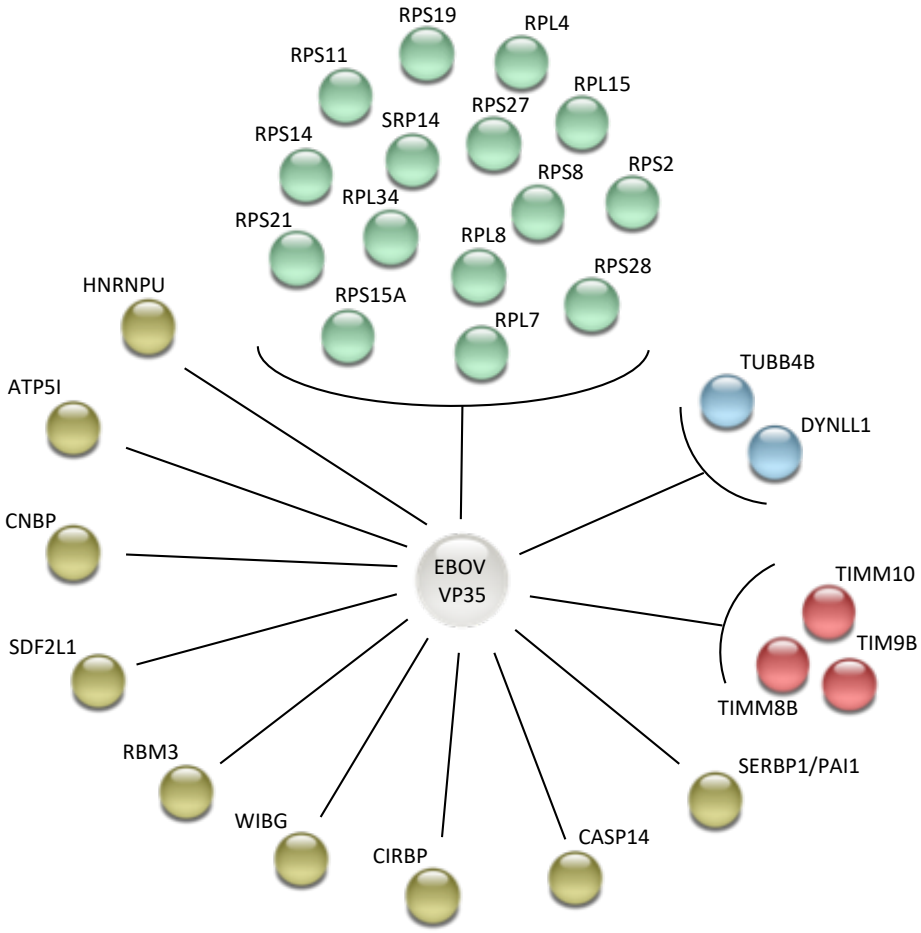
RPS19
RPL4
RPS11
RPL15
RPS27
SRP14
RPS14
RPS8
RPS2
RPL34
RPS21
RPL8
RPS28
HNRNPU
RPS15A
RPL7
TUBB4B
ATP5I
DYNLL1
CNBP
EBOV VP35
TIMM10
TIM9B
SDF2L1
TIMM8B
RBM3
SERBP1/PAI1
WIBG
CASP14
CIRBP

B)

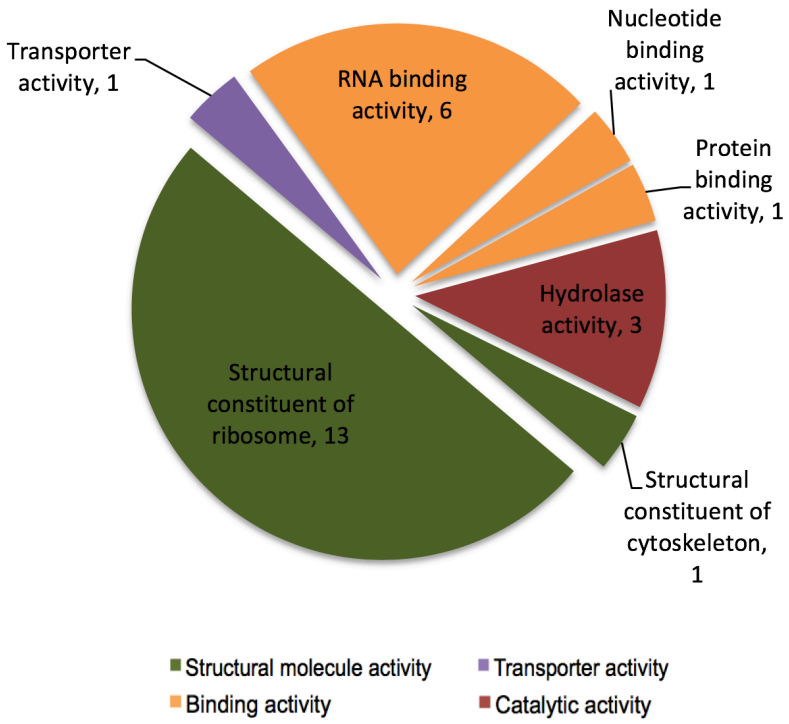
Transporter activity, 1
RNA binding activity, 6
Nucleotide binding activity, 1
Protein binding activity, 1
Hydrolase activity, 3
Structural constituent of ribosome, 13
Structural constituent of cytoskeleton, 1
Structural molecule activity
Transporter activity
Binding activity
Catalytic activity

Figure 3.3. Potential host protein interactors of EBOV VP35 and their molecular function classification. (A) *The significant cellular proteins potentially interacting with EBOV VP35 from the LC-MS/MS data sets were submitted to the STRING software (version 10.5) to show the currently known PPI networks. Associations are meant to be specific and meaningful, but they are not necessarily physically binding to each other. Clusters of cellular proteins were identified as ribosomal proteins (green), motility and structural proteins (blue), TIMM family proteins (red). Proteins in yellow were not associated in a cluster. (B) Molecular function classification of proteins identified with cut-off ratio of change ≥2 in abundance in both EGFP-VP35 C1 and VP35-EGFP N1 sets of data compared to the EGFP data set protein abundance. Twenty eight cellular proteins were submitted to the PANTHER online software (www.pantherdb.org).*

Table 3.1. List of statistically significant and potentially EBOV EGFP-VP35 C1 cellular interacting partners. *Contaminants and proteins identified by only one unique peptide were removed. The false discovery rate (FDR) was set at 1% or below, meaning that theoretically 99% of the proteins would be identified correctly. LFQ intensity values of the identified proteins were analysed using a t-test. The proteins that interact specifically with VP35 would be expected to show a higher binding ratio that the ones that interact with the control, which show a FC close to 1. The threshold was set to 2.*

Protein ID	Protein name	Gene Name	Peptides	Unique Peptides	SC (%)	LOG (p-value)	Fold Change	Function
P63167	Dynein light chain 1, cytoplasmic	DYNLL1	12	8	75.3	1.131	4.8	Cytoplasmic dynein 1 acts as a motor for the intracellular retrograde motility of vesicles and organelles along microtubules.
P62263	40S ribosomal protein S14	RPS14	9	9	43	1.929	4.7	Structural constituent of ribosome. It has a translation regulator activity.
P42677	40S ribosomal protein S27	RPS27	5	5	44	1.907	4.2	Structural constituent of ribosome. It has a translation regulator activity.
P18124	60S ribosomal protein L7	RPL7	4	4	21.4	1.251	3.5	Binds to G-rich structures in 28S rRNA and in mRNAs. Plays a regulatory role in the translation apparatus; inhibits cell-free translation of mRNAs.
Q00839	Heterogeneous nuclear ribonucleoprotein U	HNRNPU	13	13	22.7	1.189	3.5	Component of the CRD-mediated complex that promotes MYC mRNA stabilization. Binds to pre-mRNA. Has high affinity for scaffold-attached region (SAR) DNA. Binds to double- and single-stranded DNA and RNA. Plays a role in

								the circadian regulation of the core clock component ARNTL/BMAL1 transcription (By similarity).
P68371	Tubulin beta-4B chain;Tubulin beta-4A chain	TUBB4B	23	4	64.3	0.942	3.5	Major constituent of microtubules. It binds two molecules of GTP.
P63220	40S ribosomal protein S21	RPS21	6	6	57.8	2.415	3.4	Structural constituent of ribosome.
Q14011	Cold-inducible RNA-binding protein	CIRBP	6	6	50	1.636	3.3	Protective role in the genotoxic stress response by stabilizing transcripts of genes involved in cell survival. Translational activator and repressor. Seems to play an essential role in cold-induced suppression of cell proliferation. Binds to the 3-UTRs of stress-responsive transcripts RPA2 and TXN. Promotes assembly of stress granules, when overexpressed.
Q9HCN8	Stromal cell-derived factor 2-like protein 1	SDF2L1	4	4	23.5	1.104	2.9	Dolichyl-phosphate-mannose-protein mannosyltransferase activity.
Q8NC51	Plasminogen activator inhibitor 1 RNA-binding protein	SERBP1	6	6	13.7	1.311	2.9	May play a role in the regulation of mRNA stability. Binds to the 3-most 134 nt of the SERPINE1/PAI1 mRNA, a region which confers cyclic nucleotide regulation of message decay.

P61313	60S ribosomal protein L15	RPL15	2	2	7.8	1.291	2.8	Structural constituent of ribosome.
P62241	40S ribosomal protein S8	RPS8	7	7	33.2	2.596	2.8	Structural constituent of ribosome. It has a translation regulator activity.
Q9BRP8	Partner of Y14 and mago	WIBG	4	4	27.9	1.214	2.8	Key regulator of the exon junction complex (EJC).
P98179	RNA-binding protein 3	RBM3	2	2	15.9	1.889	2.8	Cold-inducible mRNA binding protein that enhances global protein synthesis at both physiological and mild hypothermic temperatures. Reduces the relative abundance of microRNAs, when overexpressed. Enhances phosphorylation of translation initiation factors and active polysome formation.
P37108	Signal recognition particle 14 kDa protein	SRP14	5	5	40.4	1.521	2.8	Crucial role in targeting secretory proteins to the rough endoplasmic reticulum membrane.
P62244	40S ribosomal protein S15a	RPS15A	4	4	20	1.664	2.6	Structural constituent of ribosome.
P49207	60S ribosomal protein L34	RPL34	10	10	44.4	1.209	2.6	Structural constituent of ribosome.
P39019	40S ribosomal protein S19	RPS19	15	15	69.7	1.387	2.6	Required for pre-rRNA processing and maturation of 40S ribosomal subunits.
P62917	60S ribosomal protein L8	RPL8	6	6	19.5	2.328	2.5	Structural constituent of ribosome.

P62633	Cellular nucleic acid-binding protein	CNBP	5	5	31.6	1.896	2.4	Single-stranded DNA-binding protein, with specificity to the sterol regulatory element (SRE). Involved in sterol-mediated repression.
P62857	40S ribosomal protein S28	RPS28	9	9	79.7	1.909	2.3	Structural constituent of ribosome.
P62280	40S ribosomal protein S11	RPS11	12	12	62.7	2.018	2.3	Structural constituent of ribosome.
P56385	ATP synthase subunit e, mitochondrial	ATP5I	2	2	18.8	1.927	2.2	Produces ATP from ADP in the presence of a proton gradient across the membrane.
P62072	Mitochondrial import inner membrane translocase subunit Tim10	TIMM10	2	2	31.1	1.818	2.1	Mitochondrial intermembrane chaperone that participates in the import and insertion of multi-pass transmembrane proteins into the mitochondrial inner membrane.
P36578	60S ribosomal protein L4	RPL4	8	8	16.2	1.724	2.1	Structural constituent of ribosome.
P15880	40S ribosomal protein S2	RPS2	9	9	25.3	2.200	2.0	Structural constituent of ribosome and fibroblast growth factor.

Table 3.2. List of statistically significant and potentially EBOV VP35-EGFP N1 cellular interacting partners*. Contaminants and proteins identified by only one unique peptide were removed. The false discovery rate (FDR) was set at 1% or below, meaning that theoretically 99% of the proteins would be identified correctly. LFQ intensity values of the identified proteins were analysed using a t-test. The proteins that interact specifically with VP35 would be expected to show a higher binding ratio that the ones that interact with the control, which show a FC close to 1. The threshold was set to 2.*

Protein ID	Protein name	Gene Name	Peptides	Unique Peptides	SC (%)	LOG (p-value)	Fold Change	Function
Q9HCN8	Stromal cell-derived factor 2-like protein 1	SDF2L1	4	4	23.5	1.325	3	Dolichyl-phosphate-mannose-protein mannosyltransferase activity.
P63167	Dynein light chain 1, cytoplasmic	DYNLL1	12	8	75.3	2.058	2.9	Cytoplasmic dynein 1 acts as a motor for the intracellular retrograde motility of vesicles and organelles along microtubules.
Q9Y5J9	Mitochondrial import inner membrane translocase subunit Tim8 B	TIMM8B	3	3	37.3	1.490	2.8	Probable mitochondrial intermembrane chaperone that participates in the import and insertion of multi-pass transmembrane proteins into the mitochondrial inner membrane. Required for the transfer of beta-barrel precursors from the TOM complex to the sorting and assembly machinery or the outer membrane.

P56385	ATP synthase subunit e, mitochondrial	ATP5I	2	2	18.8	2.932	2.4	Produces ATP from ADP in the presence of a proton gradient across the membrane.
P63220	40S ribosomal protein S21	RPS21	6	6	57.8	2.470	2.2	Structural constituent of ribosome.
Q9Y5J6	Mitochondrial import inner membrane translocase subunit Tim10 B	TIMM10 B	3	3	37.9	2.516	2.2	Component of the TIM22 complex, which mediates the import and insertion of multi-pass transmembrane proteins into the mitochondrial inner membrane.
P62072	Mitochondrial import inner membrane translocase subunit Tim10	TIMM10	2	2	31.1	3.215	2.2	Mitochondrial intermembrane chaperone that participates in the import and insertion of multi-pass transmembrane proteins into the mitochondrial inner membrane.

3.2.3. Validation of cellular interactions with EBOV VP35

To validate the interactions observed in the LC-MS/MS analysis GFP-Trap®, co-immunoprecipitations were performed again in cells expressing EGFP, EGFP-VP35 C1 or VP35-EGFP N1. The validated PPIs were selected according to their presence in both EGFP-VP35 C1 and VP35-EGFP N1 data sets, the relative high fold change difference on interaction intensity between the mock eluate and the EGFP/VP35 eluate, or to antibody availability. These were the dynein light chain 1 (DYNLL1/LC8), the ATP synthase subunit e (ATP5I), the 40S ribosomal protein S21 (RPS21), the cold inducible RNA-binding protein (CIRBP) and the plasminogen activator inhibitor 1 (PAI1/SERBP1). PPI detection by western blot showed consistency with LC-MS/MS analyses, as selected proteins were detected by specific antibodies in at least one of the EGFP-VP35 C1 or VP35-EGFP N1 eluates (Figure 3.4A). Among the identified protein-protein associations, detection of DYNLL1 in the eluate fraction of the pull-down was enriched compared to the input in both EGFP-VP35 C1 and VP35-EGFP N1 coIP sets of samples. The enrichment suggested that there is either a strong interaction between this cellular protein and VP35 or that their interaction is favoured by a high expression of this cellular protein. According to the "*PaxDb: Protein Abundance Database*", DYNLL1 is one of the top 5-25% most abundant proteins in human cell lines (https://pax-db.org/protein/1843632#). DYNLL1 had been previously described, strengthening the confidence in the VP35-host interactors identified by LC-MS/MS (Kubota et al., 2009). DYNLL1 is a subunit of the large cytoplasmic dynein complex, involved in intracellular transport and motility. CIRBP is a cold-induced RNA chaperone that influences transcription and translation under hypothermic conditions. ATP5I is a minor subunit in the mitochondrial membrane ATP synthase, which is involved in the production of ATP from ADP. RPS21 is a component of the 40S subunit of ribosomes. PAI1 is a serine protease that inhibits the tissue plasminogen activator, disrupting fibrinolysis. ATP5I and CIRBP were also detected in the eluate fractions of both EGFP-tagged VP35 proteins, while RPS21 and PAI1 were only present in enough amounts for detection in the eluate fractions of the pulled-down EGFP-VP35 C1 recombinant protein. This observation may suggest that the EGFP tag at the C-terminal end of VP35 affected the recombinant protein

configuration or disrupted the interactions between the viral protein and RSP21 or PAI1 (Snapp, 2005), perhaps via a mechanism of steric hindrance. GAPDH was used as a negative control as it was not expected to interact with EBOV VP35, according to the data generated by LC-MS/MS.

EBOV VP35 is known to interact with dsRNA, for instance, when the protein interferes in the cellular expression of type-I IFN (Cardenas et al., 2006; Prins et al., 2010; Zinzula et al., 2012). To assess whether the observed interactions between EBOV VP35 and cellular factors were potentially direct or due to an RNA intermediate, 293T cells where EGFP, EGFP-VP35 C1 or VP35-EGFP N1 had been expressed were treated with RNase A prior to co-immunoprecipitation. RNA presence in the lysates was then assessed by electrophoresis in an agarose gel (Figure 3.4B). VP35-host protein interactions in the RNase A treated lysates were validated again by western blot (Figure 3.4C). DYNLL1, ATP5I and RSP21 were detected in the eluted samples of RNase A treated VP35/EGFP transfected cell lysates, confirming that their interaction was not mediated by RNA. On the other hand, the detection of CIRBP and PAI1 in the RNAse A non-treated cell lysates was due only to binding to RNA. Reverse pull-downs of DYNLL1 and ATP5I were performed to further validate the PPI seen in the LC-MS/MS analysis (Figure 3.4D).

As an alternative way to gain confidence on protein-protein interactions, immunofluorescence staining and fluorescence visualisation were performed on EGFP-VP35 C1 and VP35-EGFP N1 transfected 293T cells to assess potential co-localisation of the expressed recombinant proteins with either DYNLL1 or CIRBP. Specific rabbit primary antibodies and a secondary antibody against rabbit (Alexa Fluor® 546) were used for the detection of DYNLL1 and CIRBP in pVP35/EGFP-transfected cells. As seen in Figure 3.5, recombinant proteins and selected cellular proteins were expressed in the same cell compartment, the cytoplasm, making it more likely to establish an interaction between them.

A)

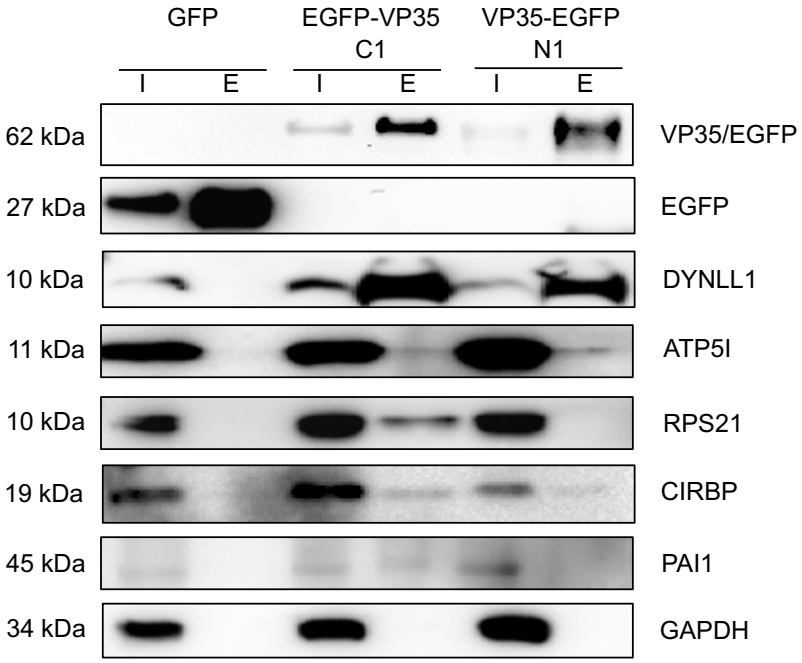
GFP
EGFP-VP35 C1
VP35-EGFP N1
I
E
I
E
I
E
62 kDa
VP35/EGFP
27 kDa
EGFP
10 kDa
DYNLL1
11 kDa
ATP5I
10 kDa
RPS21
19 kDa
CIRBP
45 kDa
PAI1
34 kDa
GAPDH

B)

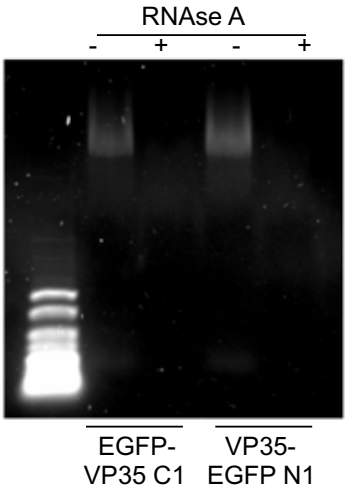
RNAse A
-
+
-
+
EGFP-VP35 C1
VP35-EGFP N1

C)

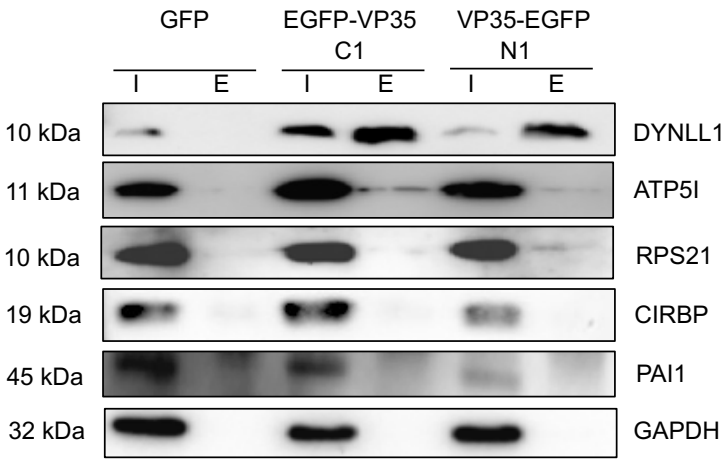
GFP
EGFP-VP35 C1
VP35-EGFP N1
I
E
I
E
I
E
10 kDa
DYNLL1
11 kDa
ATP5I
10 kDa
RPS21
19 kDa
CIRBP
45 kDa
PAI1
32 kDa
GAPDH

D)

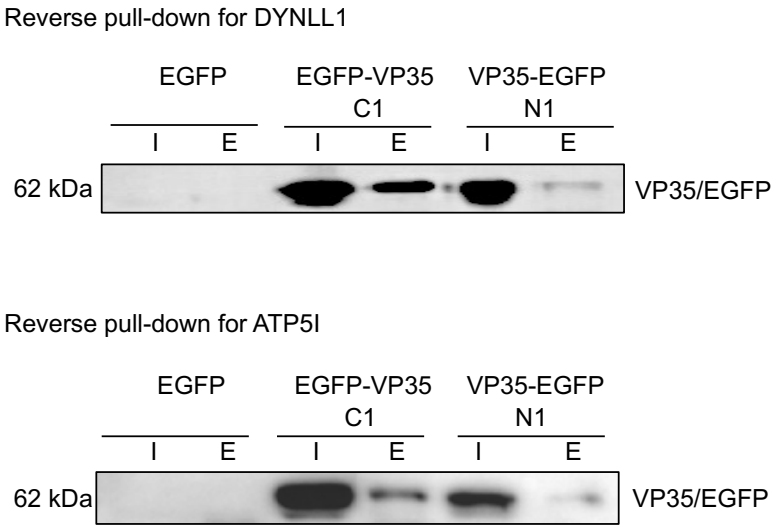

Figure 3.4. Validation of PPIs between 293T cellular proteins and VP35 by western blot. *(A) Detection of DYNLL1, ATP5I, RPS21, CIRBP and PAI1 in the cell lysates [input, I] and in the eluted fractions [eluate, E] of the pull-downs of the three constructs. (B) Agarose gel showing RNA presence in 293T cell lysates treated (+) and non-treated (-) with RNase A. (C) EGFP and EGFP-tagged VP35 expressing cell lysates were pre-treated with RNase A and co-immunoprecipitated by GFP-trap beads. A western blot was performed to assess the presence of selected host proteins potentially interacting with VP35 in the eluted fraction of the RNase A treated lysates. (D) Reverse co-immunoprecipitations for DYNLL1 and ATP5I and detection of EGFP-VP35 C1 and VP35-EGFP N1 with a specific antibody anti-EGFP. Cell lysates were incubated for 2 hours with specific antibodies against either DYNLL1 or ATP5I. Co-immunoprecipitations were performed by using protein G sepharose beads. Samples were eluted. A western blot assessed the presence of the EGFP-tagged VP35 proteins in the eluted samples.*

A)

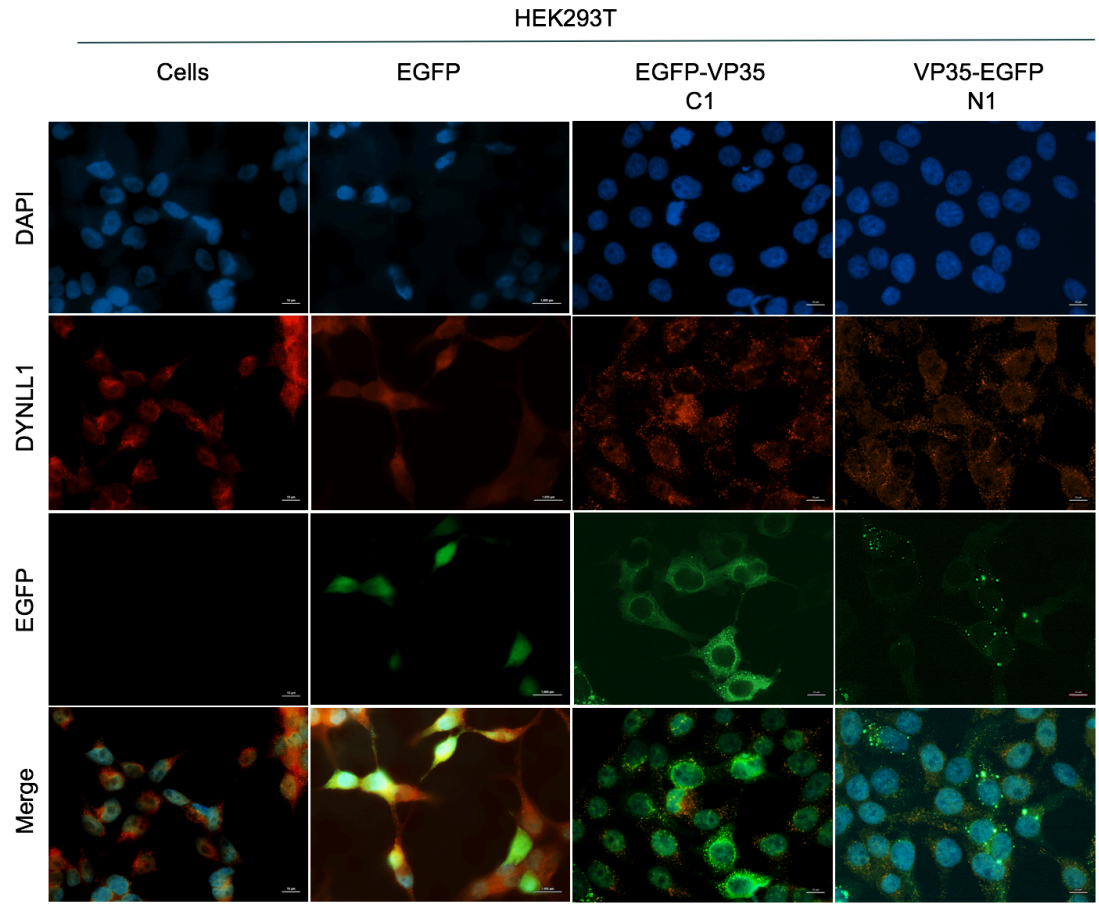
HEK293T
Cells
EGFP
EGFP-VP35 C1
VP35-EGFP N1
DAPI
DYNLL1
EGFP
Merge

B)

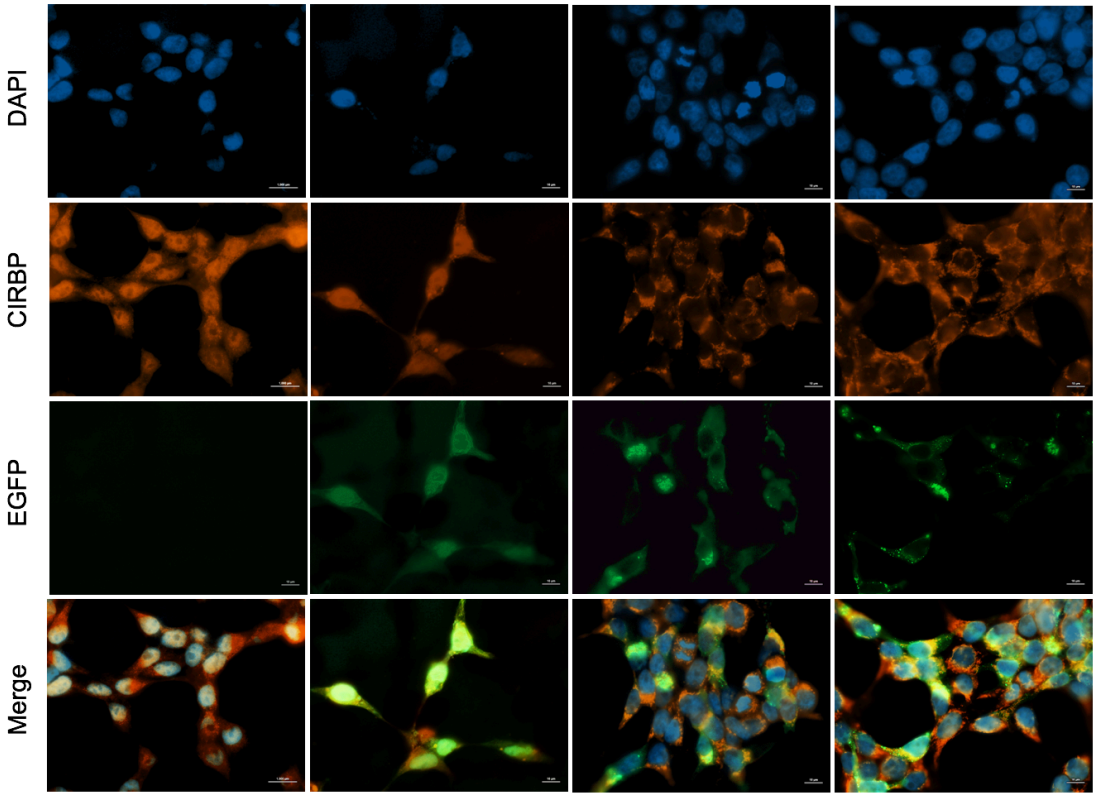
DAPI
CIRBP
EGFP
Merge

Figure 3.5. Immunofluorescent microscopy showing potential cytoplasmic co-localisation of expressed EGFP-VP35 C1 or VP35-EGFP N1 with host proteins. *(A) DYNLL1 and (B) CIRBP in red (Alexa Fluor® 546), auto-immunofluorescence of EGFP or EGFP tagged-VP35 recombinant proteins in green; DAPI-stained nuclei in blue. Bars, 10µm.*

3.2.4. Functionality of EGFP-tagged EBOV VP35 proteins

To assess EGFP-VP35 C1 and VP35-EGFP N1 functionalities, an EBOV minigenome system optimised in BSR-T7 cells was used. BSR-T7 cells are a widely used baby hamster kidney (BHK)-derived cell line that stably expresses the T7 RNA polymerase, allowing the expression of viral proteins required for RNA synthesis, whose transcription from corresponding genes was under the control of a T7 RNA polymerase promoter upstream (Mühlberger et al., 1998; García-Dorival et al., 2016; Jasenosky et al., 2010). Minigenome systems mimic viral transcription and replication of viruses in BSL-2 facilities by delivering the RNP complex proteins together with a minigenome plasmid in mammalian cells. They have been established for a number of negative strand RNA viruses, such as Marburg virus, Rift Valley fever virus and Nipah virus, for instance (Freiberg et al., 2008; Ikegami et al., 2005; Mühlberger et al., 1998). The minigenome plasmid encodes the EBOV genomic leader and trailer sequences flanking a reporter *Firefly* luciferase gene. L, NP, VP30 and VP35 conform the RNP complex, which recognises the viral genome leader and trailer sequences and transcribe the reporter gene. The reporter gene expression is an indicator of the transcription and replication activities of the system (Mühlberger et al., 1998).

The plasmids forming the EBOV minigenome system were pNP, pVP30, pVP35, pL and pMG, with a length of 5469 pb, 4116 pb, 4272 pb, 9888 pb and 5750 pb, respectively. The vector used to encode each of the viral proteins and also the EBOV minigenome was pUC57, and the inserts with the viral gene sequences were introduced between the restriction sites SalI and SacI. An agarose gel was run with the digested products of each plasmid to confirm their size (Figure 3.6). After plasmid size confirmation, BSR-T7 cells were seeded at a density of 10^5 cells/well in 24-well plate. After 24 hours, 500ng of pMG, 250ng of pNP, 125ng of pVP30, pVP35/pEGFP-VP35/pVP35-EGFP and pL/pUC57, and 50ng of pRLTK were transfected per well by using Lipofectamine™ 2000. Each condition was performed in triplicate for statistical significance. Cells were lysed 24 hours post-transfection. *Firefly* luciferase activities of the EGFP-tagged VP35-transfected minigenome system were measured and compared to the wild-type VP35 one by using a dual luciferase assay (DLA). Luciferase measurements of the

system were normalised with *Renilla* luciferase expression from the same lysates and significance was assessed by performing a t-test between groups (Table 3.3). Functionality of EGFP-VP35 C1 and VP35-EGFP N1 was 30.4% and 56.7%, respectively, compared to the reporter activity of the minigenome system. The EGFP tags may have affected somehow either the protein configuration and/or the interactions that VP35 stablishes with the RNP-RNA. Nevertheless, VP35 recombinant proteins still remained functional on their role as viral RNA polymerase co-factor (Figure 3.7).

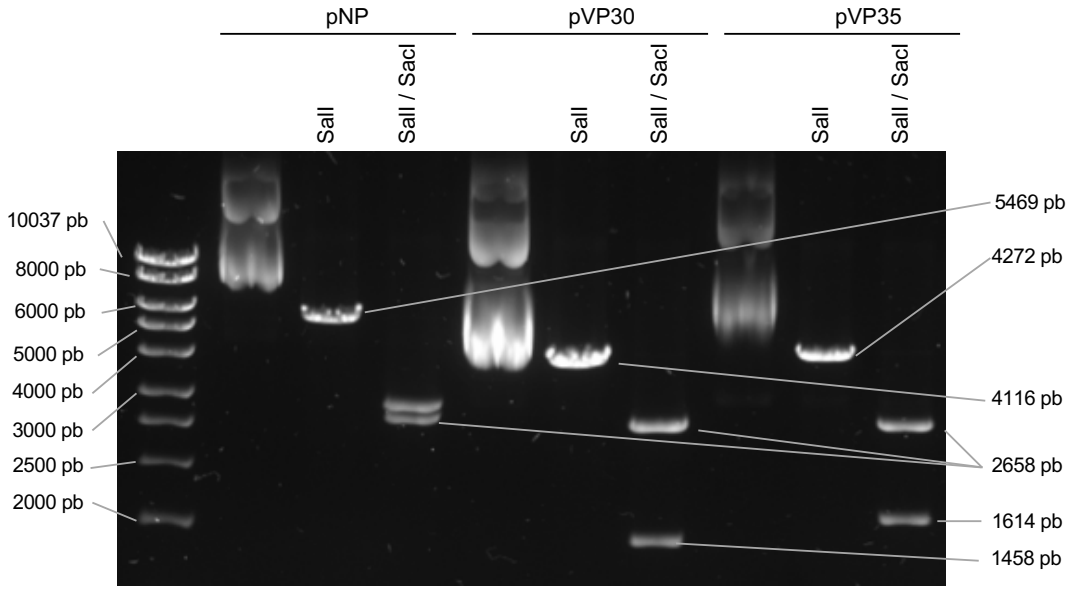

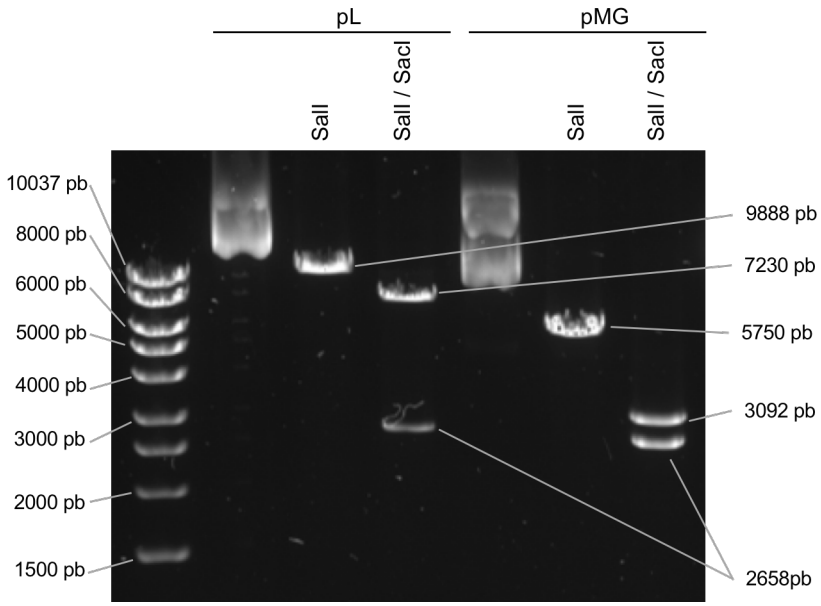

Figure 3.6. Endonuclease digestion of the EBOV minigenome system supportive plasmids pNP, pVP30, pVP35, pL and pMG. *Vector constructions were digested once using SalI, and twice using SalI and SacI. Uncut plasmid and digestion products were run in a 1% agarose gel electrophoresis to confirm product lengths.*

Table 3.3. Statistical analysis of luciferase activities in BSR-T7 cells transfected with EBOV minigenome system plasmids with either VP35, EGFP-VP35 C1 or VP35-EGFP N1. *A DLA was performed on BSR-T7 cell lysates. Each condition was carried out and measured in triplicate. Measurements of Firefly luciferase were normalised with Renilla luciferase values. A t-test between -L and the other conditions assessed significance. FC, fold change.*

Condition	Normalised FC difference over -L	Relative luciferase activity (%)	Standard deviation (SD)	t-test (p-value)
+ L	924.995	100	0.19	0.001
- L	1	1.08	0.00	1
EGFP-VP35 C1	280.9893	30.38	0.03	0.000
VP35-EGFP N1	524.476	56.70	0.15	0.003

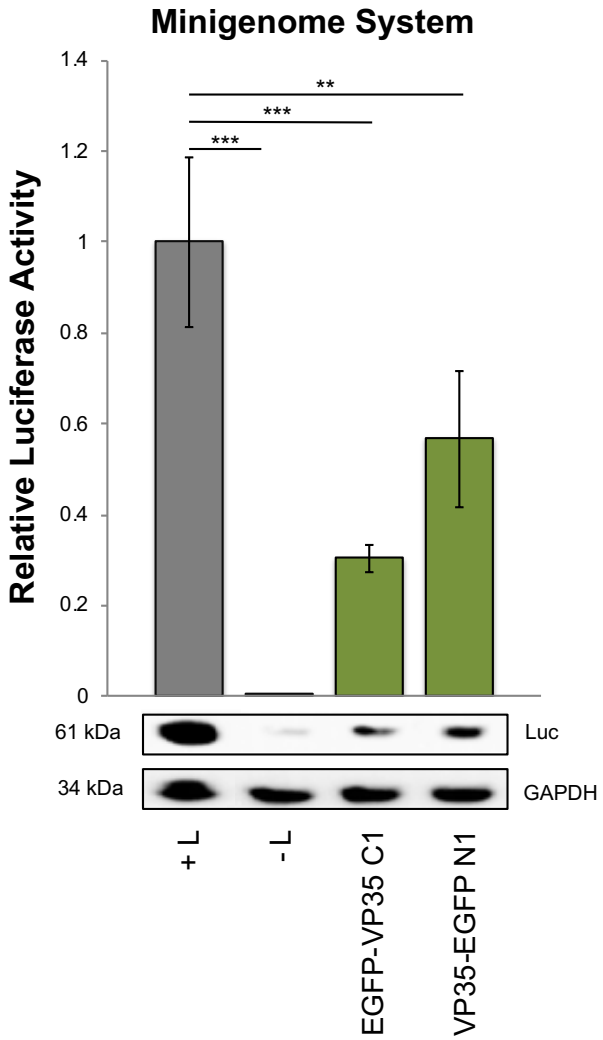

Figure 3.7. Relative functionality of recombinant EBOV EGFP-VP35 and VP35-EGFP proteins. *(A) An EBOV minigenome system assay assessed the functionality of the EGFP-tagged VP35 proteins compared to the wtVP35 in BSR-T7 cells. Firefly luciferase activities were normalised with Renilla luciferase values. A minigenome system lacking the support plasmid encoding L was used as the negative control. Each condition was performed in triplicate. A t-test between +L and the other conditions assessed significance (**p-value<0.01, ***p-value>0.001). A botting with 2.5µg of total protein per loaded sample, assessed by a bicinchonic acid protein (BCA) assay, was performed to confirm Firefly luciferase (Luc) expression. Detection of the housekeeping gene GAPDH was used as a loading control.*

3.2.5. Determining the potential antiviral activity of the DYNLL1 antagonist Ciliobrevin D in an EBOV minigenome system

DYNLL1/LC8, the cytoplasmic dynein light chain 1, has been observed to be implicated in the biological cycle of many viruses, such as rabies virus, human immunodeficiency virus 1, the African swine fever virus, hepatitis B virus or herpes simplex 1 virus, for instance (Bauer et al., 2015; Dodding and Way, 2011; García-Mayoral et al., 2011; Osseman et al., 2018). DYNLL1 was demonstrated to interact with EBOV VP35 (Kubota et al., 2009) and to enhance minigenome activity when the host protein is overexpressed in a dose-dependent manner (Luthra et al., 2015). These findings supported the LC-MS/MS analysis performed in this study as DYNLL1 was one of the top hits as an EBOV VP35 interactor. Nevertheless, in this piece of work the potential of DYNLL1 as an antiviral target and the effect of its antagonism on the EBOV genome RNA synthesis were assessed. The small molecule Ciliobrevin D is a cell permeable small molecule inhibitor that acutely, specifically and reversely blocks the AAA+ ATPase motor cytoplasmic dynein 1 and 2 in cells (Firestone et al., 2012). Ciliobrevin D affects the ATP function of the complex, disrupting the spindle pole focusing and kinetochore-microtubule attachments (Roossien et al., 2015).

A cell viability assay on BSR-T7 cells was performed to obtain the half maximal inhibitory concentration (IC_{50}) of Ciliobrevin D. Ciliobrevin D was dissolved in DMSO and a concentration range of 5 µM to 160 µM in DMEM was tested. Cells were seeded at $1.6x10^4$ in a 96-well dish format and incubated for 24 hours with the different Ciliobrevin D concentrations in triplicate. Following, an MTT ((3-(4,5-dimethylthiazol-2-yl)-2,5-diphenyltetrazolium bromide) tetrazolium reduction) assay was performed. IC_{50} of Ciliobrevin D in BSR-T7 cells was 40µM (Figure 3.8).

Cells were then seeded at $1x10^5$/well in a 24-well format to achieve ≥90% confluence the day after. Cells were transfected with the minigenome system plasmids by using Lipofectamine™ 2000. After 4 hours, media was replaced with fresh DMEM containing Ciliobrevin D at a concentration of 2.5 µM, 5 µM and 10 µM. Cells were harvested and lysed 24 hours post-transfection. In order to measure the *Firefly*

luciferase activity of the minigenome system under the different inhibitor concentrations, a DLA was performed on cell lysates. *Firefly* luciferase values were normalised by the *Renilla* luciferase activity of the transfected cells. Each condition was done in triplicate for statistical significance. Results indicated that 24 post-transfection and with a treatment period of 20 hours with Ciliobrevin D, minigenome system-transfected BSR-T7 cells presented an inverse dose-dependent response on *Firefly* luciferase expression. As seen in Figure 3.9 and Table 3.4, the reporter activity of the EBOV minigenome system significantly decreased to 27% relative expression when cells were treated with a concentration of 10 µM of Ciliobrevin D, being it not toxic to BSR-T7 cells according to the cytotoxicity assay. A dose-dependent manner decrease in *Firefly* luciferase expression was further confirmed by SDS-PAGE and western blot, whereas the detection of the housekeeping GAPDH did not show protein abundance variation between the conditions (Figure 3.9).

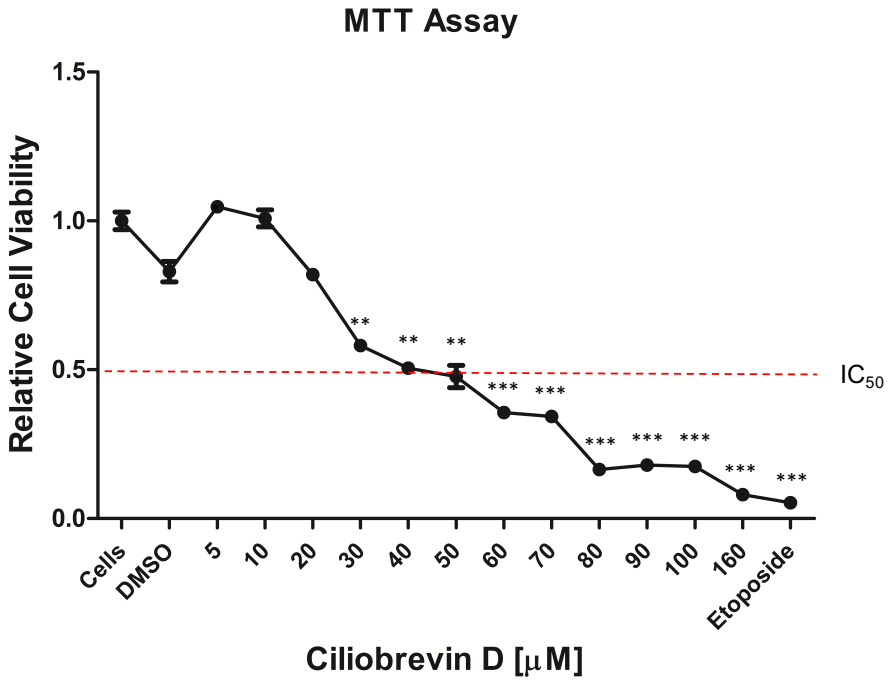

Figure 3.8. Cell viability assay (MTT) of BSR-T7 cells treated with the small molecule inhibitor Ciliobrevin D, a DYNLL1 antagonist. *A concentration range between 5 µM and 160 µM of Ciliobrevin D was diluted in DMEM and BSR-T7 cells were incubated for 24 hours. DMSO was used as vehicle control; Etoposide 10nM was used as a positive control for the induction of apoptosis. Dashed red line indicates the IC_{50}. A t-test between conditions assessed significance compared to non-treated cells (*p-value>0.05, **p-value>0.01, ***p-value>0.001).*

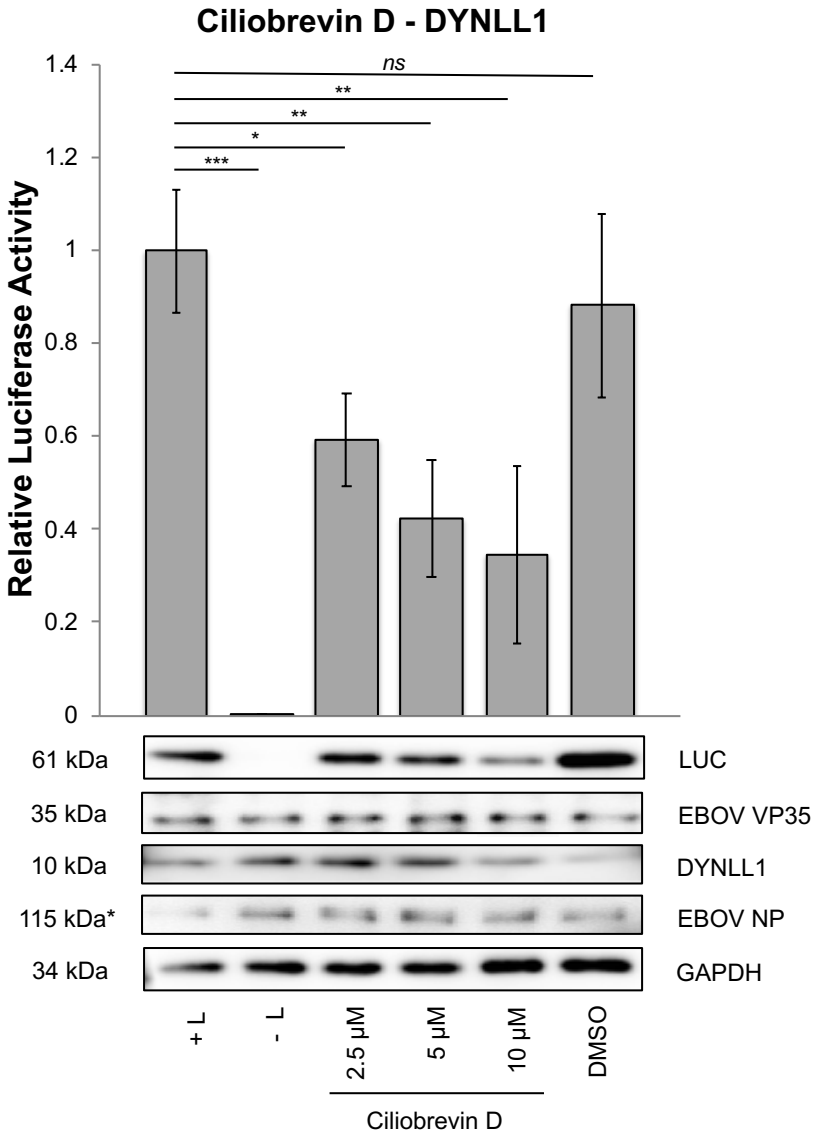

Figure 3.9. Effect of Ciliobrevin D 24 hours post-transfection on EBOV minigenome system transfected BSR-T7 cells. *Relative luciferase activity of EBOV minigenome system-transfected BSR-T7 cells treated with Ciliobrevin D for 20 hours and western blot of cell lysates. DMSO-treated cells were included as a vehicle control. Each condition was performed in triplicate. A t-test between conditions assessed significance (ns non-significant, *p-value > 0.05, **p-value < 0.01). +L as the positive control; - L as the negative control and DMSO as the vehicle control. Western blot showing abundance of Firefly luciferase (LUC), DYNLL1, NP (*actual protein size = 84 kDa; seen at 115 kDa due to protein phosphorylation). GAPDH abundance was used as the loading control, as 2.5 µg of total protein was loaded per sample.*

Table 3.4. Statistical analysis of luciferase activities in BSR-T7 cells transfected with EBOV minigenome system plasmids and treated with different concentrations of the DYNLL1 antagonist Ciliobrevin D*. A DLA was performed on BSR-T7 cell lysates treated with different concentrations of Ciliobrevin D. Each condition was performed in triplicate. Measurements of Firefly luciferase were normalised with Renilla luciferase values. A t-test between +L and the other conditions assessed significance. FC, fold change.*

Condition	Normalised FC difference over -L	Relative luciferase activity (%)	Standard deviation (SD)	t-test (p-value)
+ L	1358.41	100	0.1324	1
- L	1	0.74	0.0001	0.00019
Ciliobrevin D 2.5µM	803.34	55.64	0.0997	0.01293
Ciliobrevin D 5µM	573.31	42.23	0.1255	0.00536
Ciliobrevin D 10µM	803.34	27.00	0.1897	0.00805
DMSO	1067.71	88.22	0.1047	0.40621

3.3. Discussion

Proteins are essential components for most biological processes in a cell, such as cell growth, nutrient uptake, motility or intracellular communication among others. Viruses are characterised as obligate intracellular parasites since they do not possess the minimal protein machinery to ensure completing their replicative cycle and making viral progeny. Due to the low encoding capacity of its genome, Ebola virus proteins carry out diverse functions and bind to cellular partners or modify their function for their own benefit (reviewed in Yu et al., 2017). Several studies have used mass spectrometry to elucidate the cellular interactome of each viral protein, but the functional implications of these interactions within the virus biology remains little understood (Batra et al., 2018; García-Dorival et al., 2016, 2014; Shah et al., 2015; Takahashi et al., 2013).

This study presented the cellular interactome of Makona EBOV VP35 in 293T cells investigated by using GFP-Trap co-immunoprecipitation in combination with label-free LC-MS/MS. Results provided a comprehensive view on the interplay between EBOV VP35 and its specific host by giving insight into potential cellular partners of VP35. Findings suggested, for instance, that this viral protein may have a major role in modulating the translational machinery of the cell as at least 15 ribosomal constituent proteins showed to have a significant interaction with the viral protein. VP35 also has a potential interaction with RNA-binding proteins. CIRBP, a novel observed interactor, plays a protective role in the genotoxic stress response, stabilises transcripts of genes that are involved in cell survival and acts as a translational activator (Lleonart, 2010). According to the data obtained, the VP35-CIRBP interaction occurred through an RNA intermediate. Nevertheless, further work would need to be conducted to assess the importance of this interaction in viral RNA synthesis and the possible regulation of translation. PAI1/SERBP1, another novel VP35-host partner, is a serine protease inhibitor of tissue-type plasminogen activator responsible for the controlled degradation of blood clots and regulation of cell migration (Cesariet al., 2010). Cilloniz et al. observed that the upregulation of this acute phase signalling gene was associated with lethality in EBOV-infected mice

(Cilloniz et al., 2011). Whether VP35 modulates the function or hijacks PAI1 remains unknown but the study of its functionality could help understand the late clotting disorder symptoms observed in EVD patients and EBOV-infected animal models (Geisbert et al., 2003; Chang, 2017). VP35 also established a putative interaction with a small cluster of cellular proteins involved in motility and transport. These were TUBB4B, a major constituent of microtubules, and DYNLL1/LC8 a subunit of the cytoplasmic dynein 1 motor complex. Kubota et al. had previously discovered the VP35-DYNLL1 interaction, giving confidence to the protein-protein interactions (PPIs) elucidated by the label-free proteomic analysis performed in this study. Other significant and novel VP35 cellular partners with a greater than two-fold change abundance elucidated in this study were mitochondrial transmembrane chaperones TIMM8B, TIMM10 and TIMM10B; proteins with catalytic activity like ATP5I; and SDF2L1. Curiously, SDF2L1, a dolichyl-phosphate-mannose-protein with mannosyltransferase activity, had been observed to also associate with EBOV NP, suggesting it may have a role in the stabilisation of the viral RNP complex (García-Dorival et al., 2016). Nevertheless, interactomes do not only identify relevant cellular targets and functional validation of viral partners is often required (Meyniel-Schicklin et al., 2012). One of the main goals of this piece of work was to provide evidence that the cellular interactome of a viral protein can be used to examine the role of each cellular protein in the virus life cycle as well as to study the potential they have as targets of antiviral therapeutics.

Cytoplasmic dynein 1 motor is a multimeric complex responsible for the minus-end directed intracellular movement of various cargos and organelles along the microtubules. It is composed of two heavy chains, two intermediate chains, two light intermediate chains and several light chains (Hook and Vallee, 2006). Many different viruses use dyneins as facilitators of their direct movement across cells during the initial establishment of infection, including herpesvirus 1 (HSV1) (Dohner et al., 2002; Sodeiket al., 1997), papillomavirus (HPV) (Schneider et al., 2011) and the human immunodeficiency virus type 1 (HIV-1) (Jayappa et al., 2015). The cytoplasmic dynein light chain 1 (DYNLL1) is one of the several light chains that form part of the complex. DYNLL1 is the smallest light chain of the molecular motor dynein, being 10 kDa in

molecular weight (Mohan et al., 2006). It is involved in retrograde vesicular trafficking, ciliary/flagellar motility and cell division. DYNLL1 is the human homolog of LC8 and forms a dimer in a phosphorylation-dependent manner. DYNLL1 promotes dimerization of several enzymes, also including myosin V and apoptotic factors (King, 2008). Several studies have demonstrated this particular subunit to be an interactor partner and play a specific and essential role in the virus replication. For instance, hepatitis B capsids require binding to the cytoplasmic dynein light chain 1 for its translocation through the cytoplasm (Osseman et al., 2018). Rabies virus (RABV) L protein has a DYNLL1 motif that potentially mediates microtubules binding through the cytoplasmic dynein motors. DYNLL1, binding to both RABV L an P proteins, constitutes a viral primary transcription enhancer (Bauer et al., 2015; Jacob et al., 2000). African swine fever virus (ASFV) interacts with DYNLL1 through the viral protein p54, constituting a molecular mechanism for the virus transport along microtubules (Alonso et al., 2001). DYNLL1 also plays an important role in HIV-I proper uncoating process and efficient reverse transcription by interacting with the viral integrase (Jayappa et al., 2015). Luthra et al. demonstrated that the overexpression of DYNLL1 enhances the stability of the N-terminal domain of EBOV VP35 and also the reporter activity of an EBOV minigenome, suggesting that the cellular protein is involved in the viral genomic synthesis (Luthra et al., 2015).

The classification of EBOV as a biosafety level 4 (BSL-4) pathogen constitutes a huge limitation for the study of its biology. In order to overcome this hindrance, an EBOV minigenome system (García-Dorival et al., 2016) was used to allow the importance of selected host proteins in the viral RNA synthesis of the Makona variant of Ebola virus in a BSL-2 setting. This technology permitted the performance of functional assays on DYNLL1 with the dynein motor antagonist Ciliobrevin D to determine the use of it as a drug-target and its effect on viral transcription and replication. Results in this piece of work demonstrated that non-cytotoxic concentrations of Ciliobrevin D are able to significantly disrupt the reporter activity of an EBOV minigenome system. According to the blotting performed on cells transfected with the minigenome system and treated with Ciliobrevin D, abundance of VP35, NP and DYNLL1 did not differ from the non-treated cells. Therefore, these findings suggest that the mechanism of action

of Ciliobrevin D does not destabilise the RNP complex but focuses on the disruption of the ATPase activity of the dynein motor complex (Firestone et al., 2012), maybe making DYNLL1 less available for VP35 and having a negative effect on the viral transcription and replication.

One limitation of this study was the fact that the LC-MS/MS analysis was not performed with virus-infected cell lysates. Therefore, some of the interactions that possibly would be seen in a real infection were missed. For instance, Shabman et al. discovered that the interleukin enhancer binding factor 3 (ILF3) isoform DRBP76 associated with the interferon inhibitory domain (IID) of EBOV VP35 in the presence of the dsRNA analog and IFN-I inducer poly(I:C). Having VP35 a role as the RNA-dependent RNA polymerase co-factor, DRBP76 can inhibit the viral polymerase activity as well as disrupt the VP35-NP interaction, knocking down the EBOV replication (Shabman et al., 2011). Depending on the proteomic approach used, the type of cells transfected/infected and the treatment induced to them, the cellular interactomes of a viral protein can differ and give insight on the virus cellular partners in different environment conditions.

To conclude, every stage of the viral lifecycle is assumed to be dependent on the host proteins, which can be examined as potential antiviral targets. Traditionally, efforts to develop antiviral drugs are focused on viral enzymes because they are perceived as specific targets. Although host targets have been hampered by their potential on-target toxicity, there is a growing interest on exploring them because this strategy can provide broad coverage for different strains and possibly different viruses (Lin and Gallay, 2013). Furthermore, the current therapeutic arsenal against viral infections remains extremely limited, often with incomplete coverage and poor efficacy (Ma-Lauer et al., 2012). In this study, the cellular interactome of VP35 was provided, with multiple host-derived drug targeting candidates that were potential partners of the viral protein, and also demonstrated the efficacy of targeting DYNLL1 with the cytoplasmic antagonist Ciliobrevin D, which reduced the transcription and replication activities of EBOV in cellular culture.

Chapter 4: Characterisation of EBOV L – calmodulin interaction and influence of calmodulin/calcium on the synthesis of viral RNA

4.1. Introduction

Viruses are obligate intracellular parasites and utilise many aspects of host cell components and processes in order to accomplish their life cycle. For viral RNA synthesis, which occurs in the cell cytoplasm, Ebola virus must interact with host proteins. EBOV transcription and replication rely on the activity of the viral ribonucleoprotein (RNP) complex, composed of viral RNA and viral proteins NP, VP30, VP35 and L (Mühlberger et al., 1999). Nevertheless, EBOV transcription and replication remain still not completely understood, or the role of host factors that are involved in these two viral processes.

The viral RNA-dependent RNA polymerase (L for large) is the main player in EBOV transcription and replication. L is a multifunctional protein with a molecular weight of ~250 kDa and composed of 2210 amino acids. It is the catalytic subunit of the ribonucleoprotein RNP complex, and together with its co-factor, VP35, responsible for EBOV genome transcription and replication (Mühlberger et al., 1999). To date, non-segmented negative sense (nsNS) viruses are thought to encode conserved RNA dependent RNA polymerases believed to perform all of the RNA catalytic functions such as nucleotide polymerisation, mRNA capping, polyadenylation and cap methylation processes (Poch et al., 1990). Poch et al. and Volchkov et al. observed six conserved blocks shared among the amino acid sequence of the viral RNA polymerase of *Mononegavirales,* which were separated by more variable regions. Three polymerase motifs (A-C) were also identified for nsNS virus L proteins. Amino acid region 553 to 571 constitutes motif A, an RNA binding element. Motif B, which corresponds to amino acids 738 to 744, is a putative phosphodiester bond formation region and/or an RNA template recognition domain. Motif C is comprised between residues 1815 to 1841 and is an ATP and/or purine ribonucleotidetriphosphate binding domain (Figure 4.1) (Poch et al., 1990; Volchkov et al., 1999).

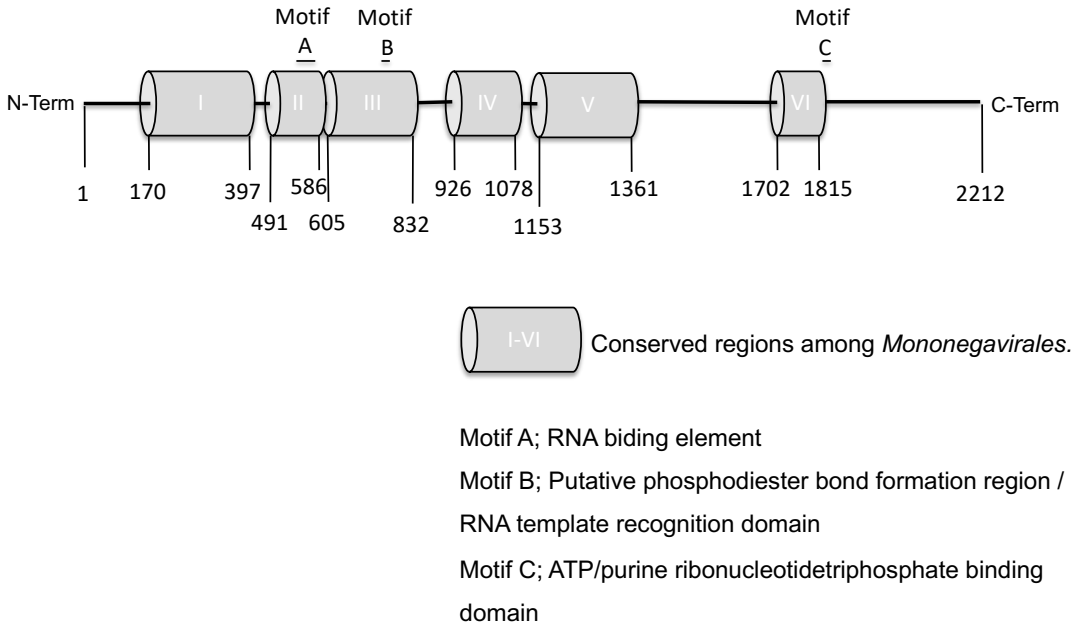

Figure 4.1. Schematic representation of Ebola virus L protein. *Conserved domains based on a model by Poch et al. (Poch et al., 1990).*

In nsNS RNA viruses, primary transcription is the first viral step after entry to the infected cell and uncoating. It originates from the 3' terminal end of the viral genomic RNA and polyadenylated, monocistronic mRNA of each gene is produced sequentially due to the presence of a single polymerase entry site (reviewed in Whelan et al., 2004). Attenuation of transcription occurs at every gene junction, triggering a progressive reduction in the production of mRNA of the genes proximal to the genomic 5' end. Therefore, viral genes whose products are needed in large amounts are located closer to the leader region, while those that are not, are more distal to the 3' terminus and proximal to the 5' end (Brauburger et al., 2016; Albariño et al., 2018). Members of the order *Mononegaviridae* have a highly conserved gene order, with core genes N (NP for EBOV), P (VP35 for EBOV) and M (VP40 for EBOV) always close to the 3' terminus and the viral RNA-dependent RNA polymerase (L for EBOV) being the most promoter distant and the lowest abundant in expression, reflecting a putative way for gene expression control (reviewed in Whelan et al., 2004). The host cellular machinery translates the viral mRNA and viral proteins accumulate in perinuclear regions before being transported to the budding sites at the plasma membrane. Phosphorylation of VP30 is thought to be related to the viral RNA

polymerase switch from transcription to replication mode, leading to the synthesis and encapsidation of genomic vRNA and its complementary sequence, the antigenome (Biedenkopf et al., 2016). Newly synthesised RNP complex proteins participate in what is called secondary transcription.

Levels of the viral RNA polymerase modulate the RNA synthesis activity. Shabman et al. demonstrated in an EBOV minigenome system where pL was added in increasing amounts that an excess of viral polymerase was detrimental for the virus replication. In their experiment, the replication of the system was barely functional when L amounts exceeded four times the optimal amount (Shabman et al., 2013). The large size of L and its complexity makes it the less studied of the EBOV proteins. Nevertheless, the RNP complex in general, and L in particular, represent very attractive antiviral targets due to the importance of the viral processes they carry out during Ebola virus infection. Although studies made on host protein associations with EBOV L are scarce, some host factors have been found to have a role in the EBOV transcription and replication. For instance, knockdown of DNA topoisomerase 1 (TOP1), a host protein that unwinds the helical structures of dsDNA to allow transcription and replication, has been seen to associate to L and reduce its viral replicase activity (Takahashi et al., 2013). Smith et al. also observed that heat-shock protein 90 (hsp90) is an important host factor for the replication of Ebola virus and its inhibition also affects negatively viral transcription and replication of EBOV (Smith et al., 2010), as well as its disruption impairs the RNA synthesis of other negative-stranded RNA viruses (Geller et al., 2012).

In this chapter, a label-free liquid chromatography coupled with tandem mass spectrometry (LC-MS/MS) was used to elucidate novel protein association between EBOV L and transcription, replication and translation host factors by using a cell-free transcription/translation system. Novel potential protein-protein interactions (PPIs) with the viral protein were discovered and validated. The role of the potential Ebola virus L cellular partner calmodulin (CALM) and the influence of calcium on viral replication were further investigated by using a minigenome system in cell culture where the CALM small molecule inhibitor W-7 or the calcium chelator BAPTA-AM

were added in non-cytotoxic amounts. Overall, this study examined the importance of free intracellular Ca^{2+} on viral biology and the potential of the host protein CALM as an antiviral target candidate to disrupt EBOV replication.

4.1.1. Objectives

The first aim of this piece of work is to examine novel interactions between the EBOV RNA-dependent RNA polymerase (EBOV L) and cellular factors to further test the hypothesis that cellular proteins play a putative role in the transcription and replication activity of the virus. Due to the large size and complexity of L, its expression in high amounts required for further analyses and stability was hindered in cell culture. Thus, a transcription/translation cell-free system was utilised instead for the production of the protein and examination of protein-protein interactions (PPIs). A liquid chromatography tandem-mass spectrometry approach was used for the analysis of the co-immunoprecipitated protein complexes and to identify potential cellular binding patterns. Finally, western blotting was used to further validate any interactions.

The second objective of the study was the investigation of potential EBOV L host partners as antiviral targets for the disruption of the viral RNA polymerase functionality. The importance of the host protein CALM and its substrate, calcium, on the viral transcription and replication was further studied in cell culture by using an EBOV minigenome system, and the CALM small molecule inhibitor W-7 and calcium chelator BAPTA-AM.

NOTE: The sample preparation for LC-MS/MS and the raw data analyses obtained were performed by Dr. Stuart Armstrong (Infection Biology, Institute of infection and Global Health, University of Liverpool).

4.2. Results

4.2.1. Construction and expression of a recombinant protein L-mCherry

In order to study potential cellular binding partners of EBOV L, label-free proteomics coupled to a co-immunoprecipitation strategy was used. An mCherry tag was inserted in EBOV L to selectively precipitate the viral protein and the cellular binding partners by utilising RFP-Trap® beads.

A pUC57 vector encoding a human codon-optimised cDNA sequence of the viral protein *Zaire ebolavirus* Makona strain RNA-dependent RNA polymerase (EBOV L) [NCBI sequence reference number KJ660347.2] was designed using the online tool Invitrogen GeneArt Gene Synthesis Plasmid Construction (https://www.thermofisher.com/uk/en/home/life-science/cloning/gene-synthesis/geneart-gene-synthesis.html) and constructed by Invitrogen (Thermo Fisher Scientific). The sequence coding for the reporter protein mCherry [NCBI ref. num. AY678264] was introduced between nucleotides 5555 and 5556 (amino acids M1852 and G1853) into the EBOV L sequence open reading frame (ORF) (Figure 4.2A). This variable region is located between conserved domains V and VI (Fix et al., 2011), a region called second hinge (H2), which constitutes a variable and non-conserved sequence between functional domain 2 and 3 of the L protein of *Mononegavirales* and has been widely used for the insertion of fluorescent tags (Ruedas and Perrault, 2009; Duprex et al., 2002; Fix et al., 2011; Hoenen et al., 2012). The construction contained an ampicillin resistance gene for specific selection of competent cells containing the plasmid (Figure 4.2B). The recombinant L sequence was under the control of the T7 bacteriophage polymerase promoter. An electrophoresis gel run with the digested products of the construction confirmed both size of the insert and the backbone (Figure 4.2C).

To assess the proper expression of the recombinant L-mCherry protein in cell culture, BSR-T7 cells were transfected with Lipofectamine™ 2000 with different amounts of pL-mCherry ranging from 0.5µg to 2µg per well. The highest expression of the

recombinant viral protein was observed by western blot at the highest transfected amount. In order to investigate whether the recombinant L-mCherry required the other RNP complex proteins to enhance its transcription and translation in cell culture, pNP, pVP35 and pVP30 were also transfected at pL-mCherry amounts 0.5μg and 1μg. L-mCherry did not require the co-expression of the other RNP complex proteins for its appropriate expression and stability (Figure 4.3).

In order to prove the tolerance of the insertion of the reporter gene *mCherry* into the viral RNA polymerase gene and whether it compromised the RNP complex functionality, and EBOV minigenome system was used to characterise the recombinant L protein transcription and replication activities. BSR-T7 cells were transfected with the minigenome system plasmids (500ng pMG, 250ng pNP, 125ng pVP30, 125ng pVP35 and 125ng pL or pUC57) together with 50ng of the control plasmid pRLTK, encoding *Renilla* luciferase, in a 24 well format. In one of the conditions, the support plasmid encoding EBOV L was replaced with the plasmid encoding the recombinant protein L-mCherry at a concentration of 125ng/well, the same plasmid amount that was used for L in the MG control. The relative luciferase activity of L-mCherry compared to L was 78%, confirming a reduction but not the loss of the total replicase and transcriptase activities of the viral RNA polymerase (Table 4.1 and Figure 4.4A). The detection of *Firefly* luciferase and GAPDH expression with specific antibodies by western blotting confirmed the reduced but still functional activity of L-mCherry (Figure 4.4B).

A)

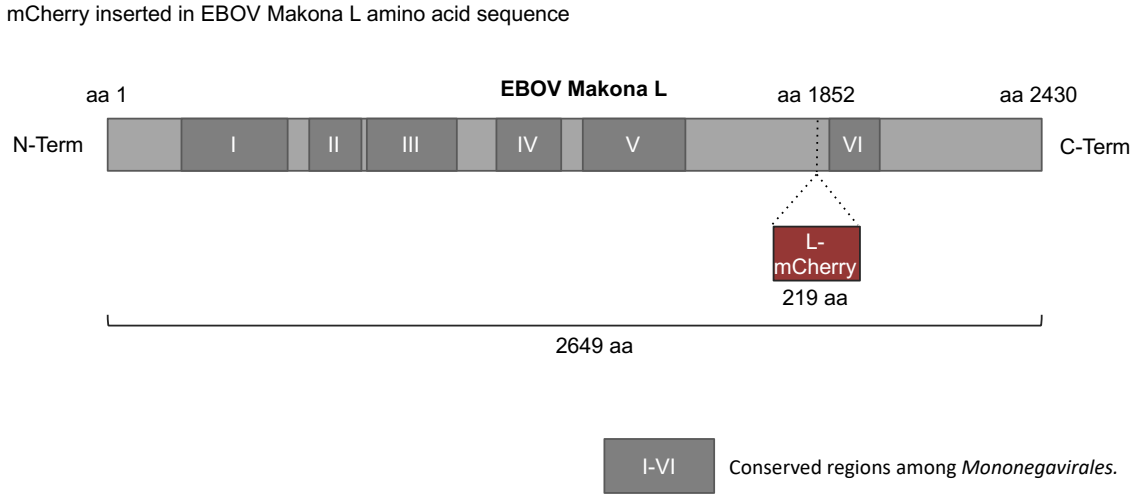
mCherry inserted in EBOV Makona L amino acid sequence
aa 1
EBOV Makona L
aa 1852
aa 2430
N-Term
I
II
III
IV
V
VI
C-Term
L-
mCherry
219 aa
2649 aa
I-VI
Conserved regions among Mononegavirales.

B)

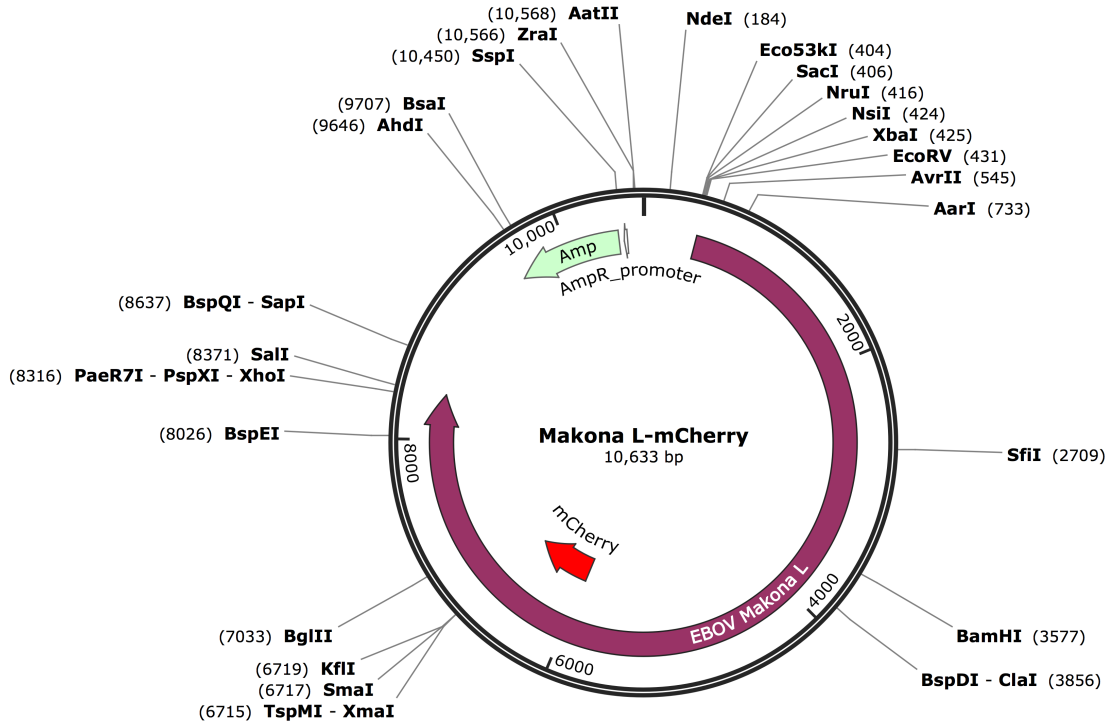
(10,568) AatII
(10,566) ZraI
(10,450) SspI
NdeI (184)
Eco53kI (404)
SacI (406)
NruI (416)
NsiI (424)
XbaI (425)
EcoRV (431)
AvrII (545)
AarI (733)
(9707) BsaI
(9646) AhdI
10,000
Amp
AmpR_promoter
2000
(8637) BspQI - SapI
(8371) SalI
(8316) PaeR7I - PspXI - XhoI
(8026) BspEI
8000
Makona L-mCherry
10,633 bp
SfiI (2709)
mCherry
EBOV Makona L
4000
BamHI (3577)
BspDI - ClaI (3856)
(7033) BglII
(6719) KflI
(6717) SmaI
(6715) TspMI - XmaI
6000

(C)

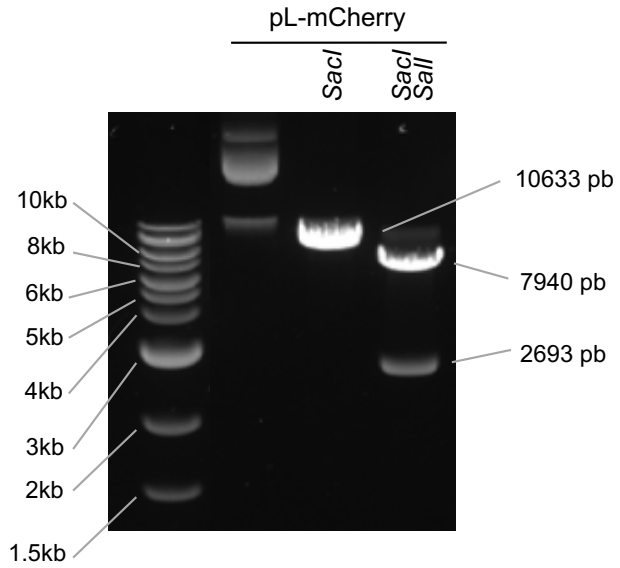

Figure 4.2. Recombinant EBOV L-mCherry construct design. *(A) A reporter mCherry tag was inserted between amino acids 1852 and 1853 for the Makona strain Zaire ebolavirus RNA-dependent RNA polymerase, L. Conserved domains based on a model by Poch et al.* (Poch et al., 1990)*. (B) Map of pUC57 vector encoding the recombinant viral protein with the inserted reporter gene mCherry. An ampicillin resistance gene allowed the selection of the growth of the competent cells when growing the plasmid for production. (C) Endonuclease digestion of plasmid L-mCherry. The vector was cut once by SacI, and twice by SacI and SalI. A 1% agarose gel was loaded with the uncut plasmid and digestion products and an electrophoresis was run to confirm product lengths (pL-mCherry = 10633 pb).*

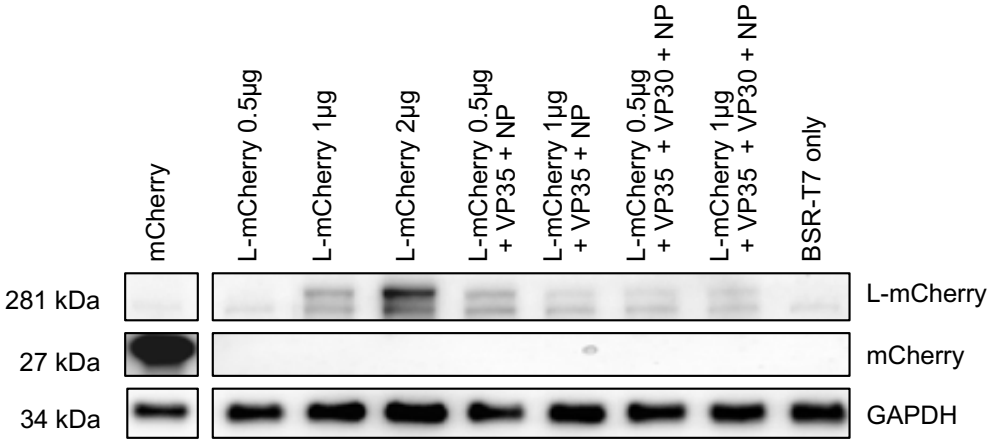

Figure 4.3. Expression of L-mCherry in BSR-T7 cells. *Different amounts of the plasmid encoding the recombinant viral protein were mixed with Lipofectamine™ 2000 and transfected into BSR-T7 cells alone or with vectors encoding the other RNP complex proteins. Into each well of the SDS-PAGE, 2.5µg of total protein was run. Specific antibodies against mCherry and GAPDH assessed protein expression. Detection or GAPDH was used as loading control.*

Table 4.1. Statistical analysis of luciferase activities in BSR-T7 cells transfected with EBOV minigenome system plasmids with either wt L or L-mCherry. *A Dual Luciferase assay (DLA) was performed on BSR-T7 cell lysates. Each condition was performed and measured in triplicate. Measurements of Firefly luciferase were normalised with Renilla luciferase values. A t-test between –L and the other conditions assessed significance. FC, fold change.*

Condition	Normalised FC difference over -L	Relative luciferase activity (%)	Standard deviation (SD)	t-test (p-value)
+ L	1534.72	100	0.09	0.00004
L-mCherry	1198.42	78.09	0.10	0.0002
- L	1	0.07	0.00	1

A)

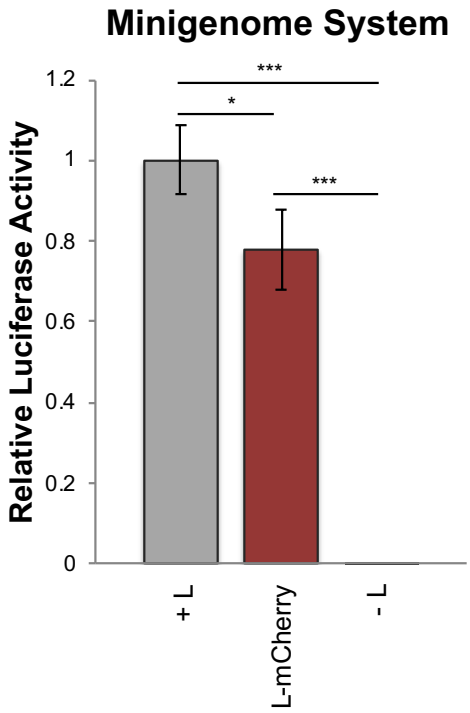

B)

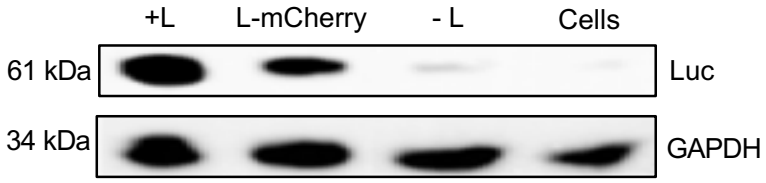

Figure 4.4. Functionality of the recombinant EBOV L-mCherry in BSR-T7 cells. *(A) An EBOV minigenome system assay assessed the functionality of the L-mCherry protein compared to the wt L in BSR-T7 cells. Firefly luciferase activities were normalised with Renilla luciferase values. Each condition was performed in triplicate. A t-test between conditions assessed significance (* p-value < 0.05, ***p-value < 0.001). (B) A western blot was performed to detect and compare the expression of Firefly luciferase in an EBOV minigenome system where either wt L or L-mCherry expressing plasmids were transfected. Assessed by BCA, 2.5µg of total protein was loaded into each well. Specific antibodies against Firefly luciferase were used in BSR-T7 lysates. +L indicates the expression of the minigenome system with the wt L. –L indicates the expression of the minigenome system without the viral polymerase as a negative control for reporter activity. Detection of GAPDH with specific antibodies was used as a loading control.*

4.2.2. Expression of EBOV L-mCherry in rabbit reticulocytes and coIP

The recombinant L-mCherry protein has a size of 281 kDa, which complicated its expression for co-immunoprecipitation and sufficient amounts could not be obtained in mammalian cells (data not shown). Also, as a common feature of *Mononegavirales*, EBOV genes are transcribed in a gradient where the transcripts of genes proximal to the genomic 3' terminus are more abundant than the transcripts of the genes proximal to the 5' end. This characteristic makes the *L* gene the least transcribed of the EBOV genome (Albariño et al., 2018) and high concentrations of this protein in cells result detrimental to virus replication (Shabman et al., 2013).

In order to obtain sufficient amounts of translated L-mCherry for the co-immunoprecipitation (coIP) assays by an RFP-Trap® approach and subsequent LC-MS/MS analyses, a cell-free TnT® Quick Coupled Transcription/Translation System (TnT) was used to study potential EBOV L-interactors (Figure 4.5A). This transcription and translation system is based on cell-free rabbit reticulocytes expressing the protein of interest *in vitro* by using a T7 RNA polymerase. Reticulocytes are immature red blood cells that contain all the translational machinery but lack the nucleus. Cell-free systems allow the expression of toxic proteins and allow fast production in a simple format. They contain all the macromolecules and components needed for transcription, translation and post-translational modification. These components include transcription factors, regulatory protein factors, ribosomes and transporter RNA (tRNA). TnT systems have been widely used to examine and study protein-protein interactions (PPIs), protein-DNA/RNA interactions, and post-translational modifications (PTMs) among others (Arduengo et al., 2007). Although not ideal for the study of cellular interactomes, TnT systems can alternatively help elucidate PPIs as they contain eukaryote and mammalian transcription and translation elements, which can show interaction with the EBOV RNA-dependent RNA polymerase.

Within the *in vitro* TnT system, 2 µg of pL-mCherry were incubated. As a negative control for the LC-MS/MS, distilled water was added to the TnT systems in triplicate. As a positive control for expression, *Firefly* luciferase under the control of a T7

polymerase promoter was added in one of the *in vitro* systems set. Cell lysates from BSR-T7 cells expressing mCherry were run together with the rest of the samples to assess the detection of the reporter protein by specific antibodies in all the samples. The expressed L-mCherry was co-immunoprecipitated by RFP-Trap® beads and protein-protein complexes were eluted. A western blot was conducted to confirm the presence of L-mCherry in the eluted fraction of the co-immunoprecipitations (Figure 4.5B).

A)

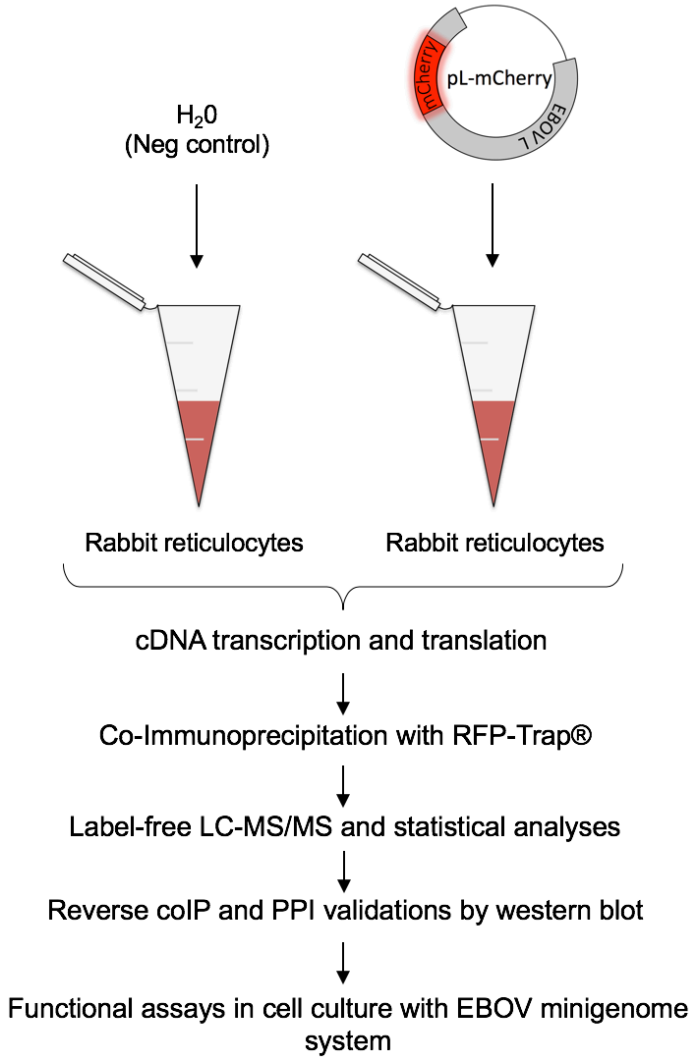

B)

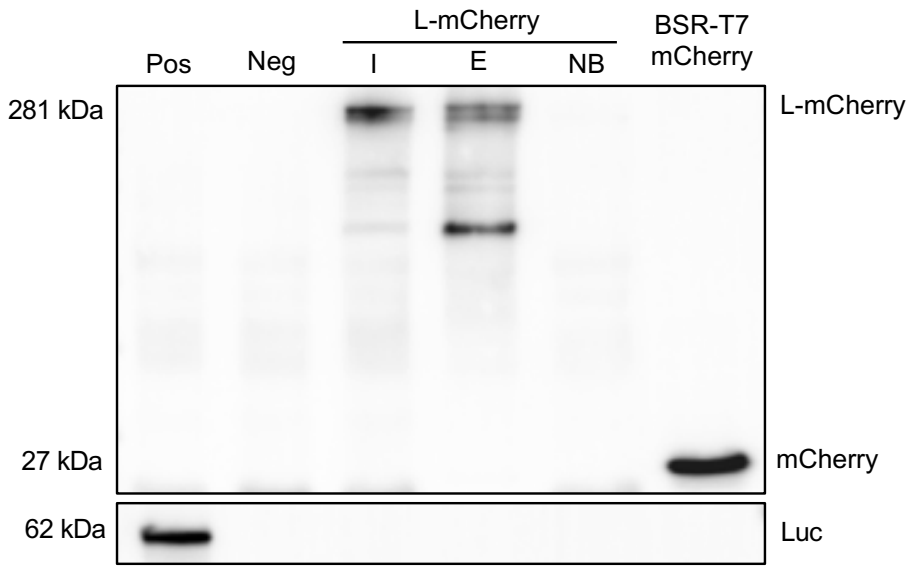

Figure 4.5. Co-immunoprecipitation (coIP) of L-mCherry expressed in a cell-free rabbit reticulocyte transcription and translation (TnT) system. *(A) Methodology used for the analysis of L-mCherry-host protein-protein interactions (PPIs). The vector encoding L-mCherry was added to rabbit reticulocytes, whereas distilled water was used as mock. Conditions were performed in triplicate. The expressed recombinant protein with their host interactors were pulled-down with RFP-Trap® beads and analyzed by LC-MS/MS. PPIs were validated by western blot with specific antibodies and further validated by reverse coIP. Functional assays for specific PPIs were performed with small molecule inhibitors. (B) Western blot assessing the confirmation of L-mCherry expression and coIP. In cell-free rabbit reticulocytes, 2µg of pL-mCherry were transcribed and transfected under the control of the T7 promoter. Co-immunoprecipitation (coIP) with RFP-Trap beads of L-mCherry and detection of the pull-down product by western blot with a specific antibody against mCherry confirmed L-mCherry presence. A vector encoding Firefly luciferase was used as a transcription/translation control of the expression system. mCherry-transfected BSR-T7 lysates were used as a positive control for the specificity of the antibody against mCherry in the whole rabbit reticulocyte (I, input), the coIP product (E, eluate) and the non-binding fraction (NB).*

4.2.3. Label-free LC-MS/MS results

A peptide coverage of the pulled-down L-mCherry identified by mass spectrometry was assessed to confirm that the recombinant protein was expressed and identified along its whole length. Peptides from both the reporter mCherry insert and from EBOV L (N-terminal and C-terminal ends) were identified (Figure 4.6). RFP-Trap® co-IP were performed in triplicate on EBOV L-mCherry-expressing TnT systems and on non-protein expressing TnT systems as negative controls to distinguish any non-specific binding to the bead matrix. The eluted fractions were digested and analysed by label-free mass spectrometry in triplicate to investigate host proteins that were susceptible of associating with L in the eluted fraction of the pulled down TnT systems. Label-free quantitation was performed using MaxQuant (MQ) software (version 1.6.1.0) with its internal search engine Andromeda. The significance of the identified proteins LFQ intensity values were analysed using a t-test to distinguish between significant and specific, and non-specific L partners. A volcano plot was generated, showing the logarithmic p-values for confidence in peptide identification (y-axis) vs. fold change difference in binding proteins (x-axis) between L-mCherry and the mock (Figure 4.7A). Dots in the top right side of the volcano plots represent the statistically significant identified cellular partners of L. The proteins that interacted specifically with L-mCherry were expected to show a higher binding ratio that the ones that interacted with the control. Proteins that bound equally to the control and test samples were predicted to have a fold change of 1. Therefore, interacting partners with a binding ratio equal or less than 1.9 were removed. Using these criteria, 4 TnT system proteins were found to potentially interact with L-mCherry (Table 4.2). A novel significant interaction, the nuclease-sensitive element-binding protein 1 (YBX1) was found to potentially associate with L-mCherry. YBX1 is a splicing regulator that binds to splice-sites in pre-mRNA, contributing to the regulation of translation. It also binds and stabilises cytoplasmic mRNA (Eliseeva et al., 2011).

Presence of most of the cellular partners in the L-mCherry pull-downs were not found to be statistically significant. Nevertheless, bearing in mind the limitations of the expression system, a heatmap was generated in order to have a further insight into

the potential L-host PPIs, even though they were not statistically significant. Several potential interactions were observed to occur in each biological replicate, differing between them. However, as shown in the heatmap in Figure 4.7B, EBOV L was present at high intensity in all the TnT systems that expressed the recombinant protein and in none of the negative TnT ones. The database, configured for human proteins (Uniprot release-2017_11), identified all the rabbit proteins that had homologous human proteins showing potential association with L-mCherry. Of particular interest were those host proteins that were detected and identified in L-mCherry but not in negative TnT pulldowns, meaning that they potentially associated with the recombinant viral protein and not with the RFP-bead instead. For instance, one of them is the heat shock cognate 71 protein (HSPA8), a constitutive chaperone that belongs to the HSC70 family, is critical for cell surviving during stress situations and assists mis-folded polypeptide chains to become functional proteins (Stricher et al., 2013). A co-chaperone of the HSC70 family, BAG family molecular chaperone regulator 2 (BAG2), was also only present in the 3 pull-downs of L-mCherry. It acts as a nucleotide-exchange factor promoting the release of ADP from the HSC70 family proteins (Rauch et al., 2014). Peroxiredoxin-1 (PRDX1), calmodulin-1 (CALM) and calmodulin-like protein 5 (CALML5), were other host associations found only in the co-immunoprecipitation eluates of the TnT that expressed the recombinant L-mCherry. Interestingly, BAG2 and PRDX1 were also seen to interact with EBOV L previously, giving more confidence in the observed interactions by using a cell-free system to express the recombinant viral protein (Takahashi et al., 2013). Keratins were considered contaminants, as they are found in the outer layer of human skin, epithelial cells or hair and are due to human contamination by manipulation of the samples.

Nevertheless, the potential association between EBOV L and CALM in one of the three replicates was of interest. Besides, the protein sequence homology between rabbit (Uniprot entry num. P0DP23) and human (Uniprot entry num. P62160) calmodulin is 100%, giving confidence that the interaction observed between L and CALM in rabbit reticulocytes can be extrapolated to occur between the viral protein and the human protein homolog. CALM has a 149 amino acid length and is a calcium-

modulated protein that is found in the cytoplasm of all eukaryotic cells. CALM gets activated by sensing Ca^{2+} and acts as an intermediary protein that regulates and modulates the function of other enzymes, like a number of phosphatases and kinases, ion channels and structural proteins (Villalobo et al., 2018).

matqhtqypdarlsspivldqcdlvtrACGLYSSYSLNPQLRNCKLPKHIYRLKYDVTVTKFLSDVPVATLPIDFIVPIL
LKALSGNGFCPVEPRCQQFLDEIIKYTMQDALFLKYYLKnvgaqedcvddhfqekILSSIQGNEFLHQMFFWY
DLAILTRRGRLNRGNSRSTWFVHDDLIDILGYGDYVFWKIPISLLPLNTQGIPHAAMDWYQTSVFKEAVQG
HTHIVSVSTADVLIMCKDLITCRFNTTLISKIAEVEDPVCSDYPNFKIVSMLYQSGDYLLSILGSDGYKIIKFLEP
LCLAKIQLCSKYTERKGRFLTQMHLAVNHTLEEITEIRALKPSQAHKIREFHRTLIRLEMTPQQLCELFSIQKH
WGHPVLHSETAIQKVKKHATVLKALRPIVIFETYCVFKYSIAKHYFDSQGSWYSVTSDRNLTPGLNSYIKRN
QFPPLPMIKELLWEFYHLDHPPLFSTKIISDLSIFIKDRATAVERTCWDAVFEPNVLGYNPPHKFSTKRVPEQ
FLEQENFSIENVLSYAQKLEYLLPQYRNFSFSLKekelnvgrtfgklpyptrnvqtlcealladglakAFPSNMMVVTER
EQKESLLHQASWHHTSDDFGEHATVRGSSFVTDLEKYNLAFRYEFTAPFIEYCNRCYGVKNVFNWMHYTI
PQCYMHVSDYYNPPHNLTLENRNNPPEGPSSYRGHMGGIEGLQQKLWTSISCAQISLVEIKTGFKLRSAV
MGDNQCITVLSVFPLETDADEQEQSAEDNAARVAASLAKVTSACGIFLKPDETFVHSGFIYFGKKQYLNGV
QLPQSLKTATRMAPLSDAIFDDLQGTLASIGTAFERSISETRHIFPCRITAAFHTFFSVRILQYHHLGFNKGFD
LGQLTLGKPLDFGTISLALAVPQVLGGLSFLNPEKCFYRNLGDPVTSGLFQLKTYLRMIEMDDLFLPLIAKNP
GNCTAIDFVLNPSGLNVPGSQDLTSFLRQIVRRTITLSAKNKLINTLFHASADFEDEMVCKWLLSSTPVMSR
FAADIFSRTPSGKRLQILGYLEGTRTLLASKIINNNTETPVLDRLRKITLQRWSLWFSYLDHCDNILAEALTQIT
CTVDLAQILREYSWAHILEGRPLIGATLPCMIEQFKVVWLKPYEQCPQCSNAKQPGGKPFVSVAVKKhivsa
wpnasrISWTIGDGIPYIGSRtedkigqpaikpkCPSAALREAIELASRLTWVTQGSSNSDLLIKPFLEARVNLSV
QEILQMTPSHYSGNIVHRYNDQYSPHSFMANRMSNSATRLIVSTNTLGEFSGGGQSARDSNIIFQNVINY
AVALFDIKFRNTEATDIQYNRAHLHLTKCCTREVPAQYLTYTSTLDLDLTRYRENELIYDNNPLKGGLNCNIS
FDNPFFQGKQLNIIEDDLIRLPHLSGWELAKTIMQSIISDSNNSSTDPISSGETRSFTTHFLTYPKIGLLYSFGA
FVSYYLGNTILRTKKLTLDNFLYYLTTQIHNLPHRSLRILKPTFKHASVMSRLMSIDPHFSIYIGGAAGDRGLS
DAARLFLRTSISSFLTFVKEWIINRGTIVPLWIVYPLEGQNPTPVNNFLHQIVELLVHDSSRHQAFKTTINDH
VHPHDNLVYTCKSTASNFFHASLAYWRSRHRNSNRKDLTRNSSTGMVSKGEEDNMAIIKEFMRFKVHME
GSVNGHEFEIEGEGEGRPYEGTQTAKLKVTKGGPLPFAWDILSPQFMYGSKAYVKHPADIPDYLKLSFPEG
FKWERVMNFEDGGVVTVTQDSSLQDGEFIYKVKLRGTNFPSDGPVMQKKTmgweasserMYPEDGALK
GEIKQRLKlkdgghydaevkTTYKAKKPVQLPGAYNVNIKLDITSHNEDYTIVEQYERAEGRhstggmdelykSST
NNSDGHIKRsqeqttrdphdgterslvlqmsheikrTTIPQENTHQGPSFQSFLSDSACGTANPKLNFDRSRHNV
KSQDHNSASKREGHQIISHRlvlpfftlsqgtrqltssnesqtqdeiskYLRQLRsvidttvycrFTGIVSSMHYKLDEVL
WEIENFKSAVTLAEGEGAGALLLIQKYQVKTLFFNTLATESSIESEIVSGMTTPRMLLPVMSKFHNDQIEIIL
NNSASQITDITNPTWFKDQRARLPRQVEVITMDAETTENINRSKLYEAVHKLILHHVDPSVLKAVVLKVFLS
DTEGMLWLNDNLAPFFATGYLIKPITSSARSSEWYLCLTNFLSTTRKMPHQNHLSCKQVILTALQLQIQRSP
YWLSHLTQYADCDLHLSYIRLGFPSLEKVLYHRYNLVDSKRGPLVSVTQHLAHLRAEIRELTNDYNQQRQSR
TQTYHFIRTAKGRITKLVNDYLKFFLIVQALKHNGTWQAEFKKLPELISVCNRFYHIRDCNCEERFLVQTLYL
HRMQDSEVKLIERLTGLLSLFPDGLYRFD

KLILHH → EBOV L amino acid sequence
LRGTN → inserted mCherry amino acid sequence
Lqmshe → Peptides identified by MS

Figure 4.6. Peptide coverage of L-mCherry identified by label-free mass spectrometry. *Amino acid sequence of the recombinant protein L-mCherry. Highlighted in red, the reporter mCherry insertion. Highlighted in grey, peptides that were identified in a single replicate.*

A)

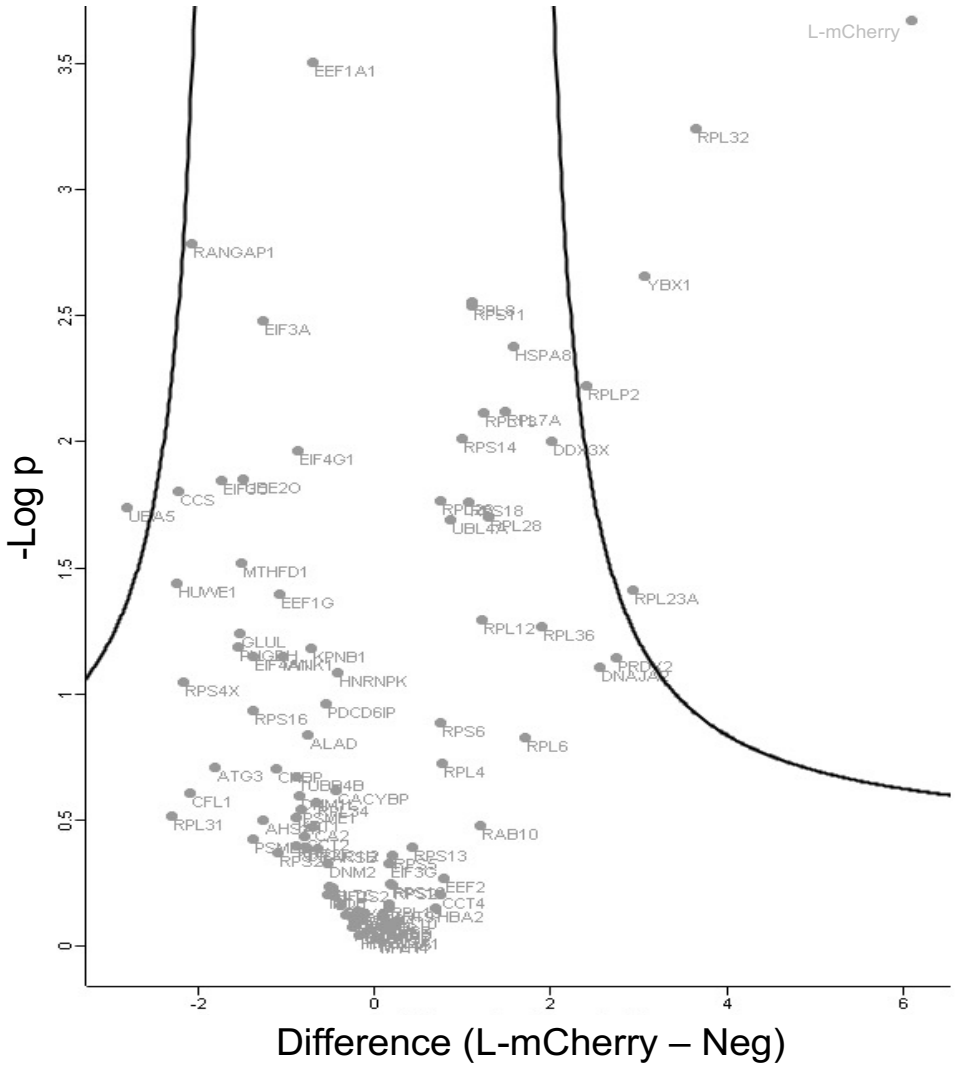
L-mCherry
EEF1A1
RPL32
RANGAP1
YBX1
EIF3A
HSPA8
RPLP2
EIF4G1
RPS14
DDX3X
CCS
UBA5
MTHFD1
HUWE1
EEF1G
RPL23A
RPL12
RPL36
GLUL
KPNB1
HNRNPK
RPS4X
RPS16
PDCD6IP
RPS6
ALAD
RPL6
ATG3
RPL4
CFL1
RPL31
RAB10
RPS13
DNM2
EIF3G
EEF2
CCT4
HBA2
-Log p
Difference (L-mCherry – Neg)

B)

Acc.	Description
P04264	Keratin, type Ⅱ cytoskeletal 1 OS=Homo sapiens GN=KRT1 PE=1 SV=6
P06702	Protein S100-A9 OS=Homo sapiens GN=S100A9 PE=1 SV=1
O75821	Eukaryotic translation initiation factor 3 subunit G OS=Homo sapiens GN=EIF3G PE=1 SV=2
P35908	Keratin, type Ⅱ cytoskeletal 2 epidermal OS=Homo sapiens GN=KRT2 PE=1 SV=2
P02787	Serotransferrin OS=Homo sapiens GN=TF PE=1 SV=3
P01763	Immunoglobulin heavy variable 3-48 OS=Homo sapiens GN=IGHV3-48 PE=1 SV=2
Q5D862	Filaggrin-2 OS=Homo sapiens GN=FLG2 PE=1 SV=1
P62857	40S ribosomal protein S28 OS=Homo sapiens GN=RPS28 PE=1 SV=1
Q9H0E2	Toll-interacting protein OS=Homo sapiens GN=TOLLIP PE=1 SV=1
Q15370	Transcription elongation factor B polypeptide 2 OS=Homo sapiens GN=TCEB2 PE=1 SV=1
P68871	Hemoglobin subunit beta OS=Homo sapiens GN=HBB PE=1 SV=2
P02042	Hemoglobin subunit delta OS=Homo sapiens GN=HBD PE=1 SV=2
P39019	40S ribosomal protein S19 OS=Homo sapiens GN=RPS19 PE=1 SV=2
P32119	Peroxiredoxin-2 OS=Homo sapiens GN=PRDX2 PE=1 SV=5
P63220	40S ribosomal protein S21 OS=Homo sapiens GN=RPS21 PE=1 SV=1
P69905	Hemoglobin subunit alpha OS=Homo sapiens GN=HBA1 PE=1 SV=2
P11441	Ubiquitin-like protein 4A OS=Homo sapiens GN=UBL4A PE=1 SV=1
P04040	Catalase OS=Homo sapiens GN=CAT PE=1 SV=3
Q06323	Proteasome activator complex subunit 1 OS=Homo sapiens GN=PSME1 PE=1 SV=1
P62750	60S ribosomal protein L23a OS=Homo sapiens GN=RPL23A PE=1 SV=1
P16949	Stathmin OS=Homo sapiens GN=STMN1 PE=1 SV=3
P24534	Elongation factor 1-beta OS=Homo sapiens GN=EEF1B2 PE=1 SV=3
P49773	Histidine triad nucleotide-binding protein 1 OS=Homo sapiens GN=HINT1 PE=1 SV=2
P02100	Hemoglobin subunit epsilon OS=Homo sapiens GN=HBE1 PE=1 SV=2
P09651	Heterogeneous nuclear ribonucleoprotein A1 OS=Homo sapiens GN=HNRNPA1 PE=1 SV=5
P62273	40S ribosomal protein S29 OS=Homo sapiens GN=RPS29 PE=1 SV=2
Q99497	Protein deglycase DJ-1 OS=Homo sapiens GN=PARK7 PE=1 SV=2
P02788	Lactotransferrin OS=Homo sapiens GN=LTF PE=1 SV=6
P81605	Dermcidin OS=Homo sapiens GN=DCD PE=1 SV=2
P60709	Actin, cytoplasmic 1 OS=Homo sapiens GN=ACTB PE=1 SV=1
Q86YZ3	Hornerin OS=Homo sapiens GN=HRNR PE=1 SV=2
P67809	Nuclease-sensitive element-binding protein 1 OS=Homo sapiens GN=YBX1 PE=1 SV=3
P01764	Immunoglobulin heavy variable 3-23 OS=Homo sapiens GN=IGHV3-23 PE=1 SV=2
P55036	26S proteasome non-ATPase regulatory subunit 4 OS=Homo sapiens GN=PSMD4 PE=1 SV=1
P35754	Glutaredoxin-1 OS=Homo sapiens GN=GLRX PE=1 SV=2
P62937	Peptidyl-prolyl cis-trans isomerase A OS=Homo sapiens GN=PPIA PE=1 SV=2
P62861	40S ribosomal protein S30 OS=Homo sapiens GN=FAU PE=1 SV=1
Q9NZT1	Calmodulin-like protein 5 OS=Homo sapiens GN=CALML5 PE=1 SV=2
P11142	Heat shock cognate 71 kDa protein OS=Homo sapiens GN=HSPA8 PE=1 SV=1
O95816	BAG family molecular chaperone regulator 2 OS=Homo sapiens GN=BAG2 PE=1 SV=1
EBOV	Makona Polymerase (L protein) with the inserted mCherry amino acid sequence
Q15365	Poly(rC)-binding protein 1 OS=Homo sapiens GN=PCBP1 PE=1 SV=2
Q9UL46	Proteasome activator complex subunit 2 OS=Homo sapiens GN=PSME2 PE=1 SV=4
P25398	40S ribosomal protein S12 OS=Homo sapiens GN=RPS12 PE=1 SV=3
P30050	60S ribosomal protein L12 OS=Homo sapiens GN=RPL12 PE=1 SV=1
P30043	Flavin reductase (NADPH) OS=Homo sapiens GN=BLVRB PE=1 SV=3
P69891	Hemoglobin subunit gamma-1 OS=Homo sapiens GN=HBG1 PE=1 SV=2
P05387	60S acidic ribosomal protein P2 OS=Homo sapiens GN=RPLP2 PE=1 SV=1
P02008	Hemoglobin subunit zeta OS=Homo sapiens GN=HBZ PE=1 SV=2
Q06830	Peroxiredoxin-1 OS=Homo sapiens GN=PRDX1 PE=1 SV=1
P62158	Calmodulin OS=Homo sapiens GN=CALM1 PE=1 SV=2
P33316	Deoxyuridine 5'-triphosphate nucleotidohydrolase, mitochondrial OS=Homo sapiens GN=DUT PE=1 SV=4
P37840	Alpha-synuclein OS=Homo sapiens GN=SNCA PE=1 SV=1
P31948	Stress-induced-phosphoprotein 1 OS=Homo sapiens GN=STIP1 PE=1 SV=1
P60174	Triosephosphate isomerase OS=Homo sapiens GN=TPI1 PE=1 SV=3
P13645	Keratin, type Ⅰ cytoskeletal 10 OS=Homo sapiens GN=KRT10 PE=1 SV=6
P13647	Keratin, type Ⅱ cytoskeletal 5 OS=Homo sapiens GN=KRT5 PE=1 SV=3
P02538	Keratin, type Ⅱ cytoskeletal 6A OS=Homo sapiens GN=KRT6A PE=1 SV=3
P02533	Keratin, type Ⅰ cytoskeletal 14 OS=Homo sapiens GN=KRT14 PE=1 SV=4
Q15366	Poly(rC)-binding protein 2 OS=Homo sapiens GN=PCBP2 PE=1 SV=1
P08779	Keratin, type Ⅰ cytoskeletal 16 OS=Homo sapiens GN=KRT16 PE=1 SV=4
P35527	Keratin, type Ⅰ cytoskeletal 9 OS=Homo sapiens GN=KRT9 PE=1 SV=3
P04259	Keratin, type Ⅱ cytoskeletal 6B OS=Homo sapiens GN=KRT6B PE=1 SV=5

Figure 4.7. Protein-protein interactors between EBOV L-mCherry and rabbit reticulocytes protein components identified by LC-MS/MS. *(A) Analysis of the potentially significant cellular proteins that interact with EBOV VP35. A volcano plot shows the cellular proteins found to potentially interact with L-mCherry in a cell-free rabbit reticulocyte transcription and translation (TnT) system. The logarithmic p-value for confidence in peptide identification is plotted against the fold change difference in binding protein between L-mCherry and a negative (≥ 2 FC). (B) Triplicates of rabbit reticulocytes-expressed L-mCherry were co-immunoprecipitated and protein-protein complexes were quantified and identified by label-free LC-MS/MS and compared with mock rabbit reticulocyte triplicates. A heatmap was generated showing the LFQ intensities of the proteins identified in each replicate.*

Table 4.2. Significant protein-protein interactions between EBOV L and rabbit reticulocytes TnT system proteins elucidated by LC-MS/MS. *Contaminants and proteins identified by only one unique peptide were removed. The false discovery rate (FDR) was set at 1% or below. LFQ intensity values of the identified proteins were analysed using a t-test. The proteins that interact specifically with L-mCherry would be expected to show a higher binding ratio that the ones that interact with the control, which show a FC close to 1. The binding ratio between the negative TnT system and L-mCherry interactors was set to 2.*

Protein ID	Protein name	Gene name	(-) LOG (P-value)	FC difference	Score	Unique peptides	Function	Localisation
P62910	60S ribosomal protein L32	RPL32	3.24	3.65	44.96	3	Belongs to the ribosomal protein L32e family.	Cytosol, cytoskeleton, mitochondrion, nucleus.
P67809	Nuclease-sensitive element-binding protein 1	YBX1	2.66	3.07	97.75	8	Mediates pre-mRNA alternative splicing regulation.	Nucleus, cytosol, cytoskeleton.
P62750	60S ribosomal protein L23a	RPL23A	1.42	2.93	18.30	3	Component of the ribosome.	Nucleus, cytosol.
P05387	60S acidic ribosomal protein P2	RPLP2	2.22	2.42	13.10	2	Plays an important role in the elongation step of protein synthesis.	Cytosol, mitochondrion, nucleus, plasma membrane, peroxisome.

4.2.4. Validation of cellular interactions with EBOV L-mCherry

To validate the potential EBOV L partners observed by LC-MS/MS, the co-IP products were separated by SDS-PAGE and western blotting assessed the presence of selected host proteins by using specific antibodies to CALM, to BAG2 and to YBX1 (Figure 4.8A). The observed statistically significant L interactor YBX1 and also CALM were selected to be further validated by reverse coIP. The negative and the L-mCherry expressing TnT products were incubated with 3 µg/ml of specific antibody against either YBX1 or CALM. Protein-antibody complexes were reverse pulled-down with protein G sepharose beads and an SDS-PAGE and western blotting were carried out with reverse co-IP products to detect L-mCherry with a specific antibody against mCherry. L-mCherry was detected in the eluates, confirming the interaction of L with CALM and YBX1 (Figure 4.8B). The L protein is part of the RNP complex and can bind RNA with different affinities. Therefore, to investigate whether the PPIs observed were either direct between proteins or due to an RNA intermediate, TnT products were treated with RNase A followed by forward co-IP. Detection of the selected proteins in the co-IP products only showed presence of BAG2 in the co-IP eluate sample, suggesting that CALM and YBX1 require RNA to interact with L (Figure 4.8C and Figure 4.8D).

To investigate if the L-CALM interaction also take place in human cells, 12-well dishes seeded with 293T cells at a cell density of 10^5 cells were transfected with 720ng of pL-mCherry and 360ng of pT7-Pol. Presence and expression of L-mCherry and CALM were confirmed by immunofluorescence microscopy. The merged expression of L-CALM (Figure 4.9A) suggested co-localisation of the viral and the host factor and reinforced their potential interaction.

A)

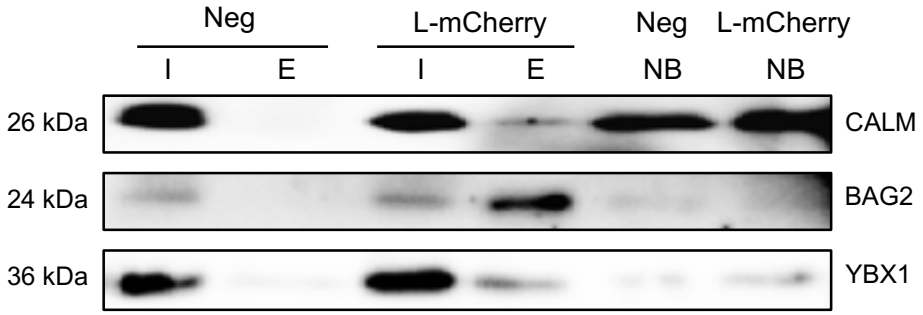
Neg
L-mCherry
Neg
L-mCherry
I
E
I
E
NB
NB
26 kDa
CALM
24 kDa
BAG2
36 kDa
YBX1

B)

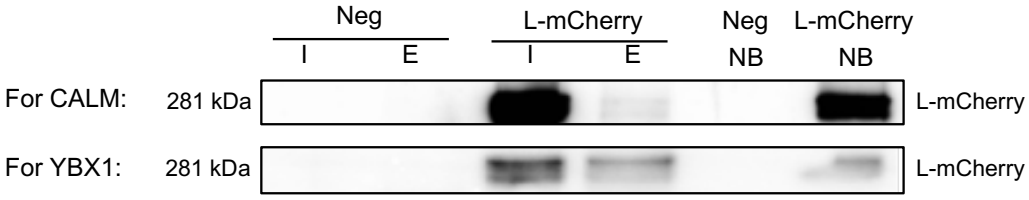
Neg
L-mCherry
Neg
L-mCherry
I
E
I
E
NB
NB
For CALM:
281 kDa
L-mCherry
For YBX1:
281 kDa
L-mCherry

C)

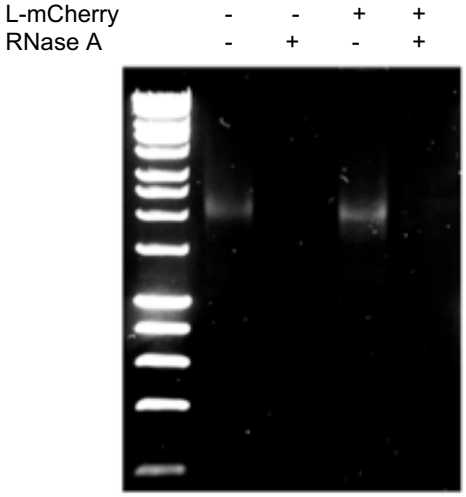
L-mCherry - - + +
RNase A - + - +

D)

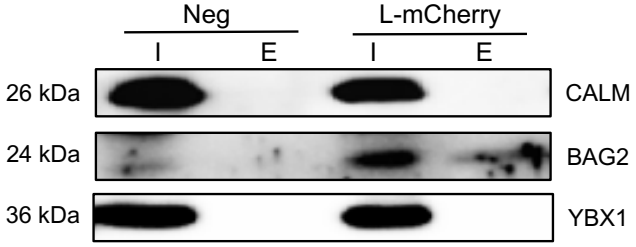
Neg
L-mCherry
I
E
I
E
26 kDa
CALM
24 kDa
BAG2
36 kDa
YBX1

Figure 4.8. Validation of PPIs between L-mCherry and TnT cellular proteins. *(A) Western blot showing the presence of CALM, BAG2 and YBX1 in the negative TnT and the L-mCherry expressed TnT systems. (B) Western blot performed for the detection of CALM and YBX1 in the reverse co-IP products of TnT systems. Rabbit reticulocytes were incubated with 3μg of a specific antibody against mCherry for 2 hours and incubated again with protein G sepharose beads overnight. Specific antibodies against L-mCherry confirmed its interaction with both CALM and YBX1. (C) Determination of the RNA intermediate dependency on PPIs between L-mCherry and host proteins. Western blotting assessed the presence of CALM, BAG2 and YBX1 in RNase A treated negative TnT and the L-mCherry expressed TnT systems. (D) Confirmation of RNA absence in the RNase A treated input samples for co-immunoprecipitation. I, input; E, eluate; RNase A treated (+) and non-treated (-).*

A)

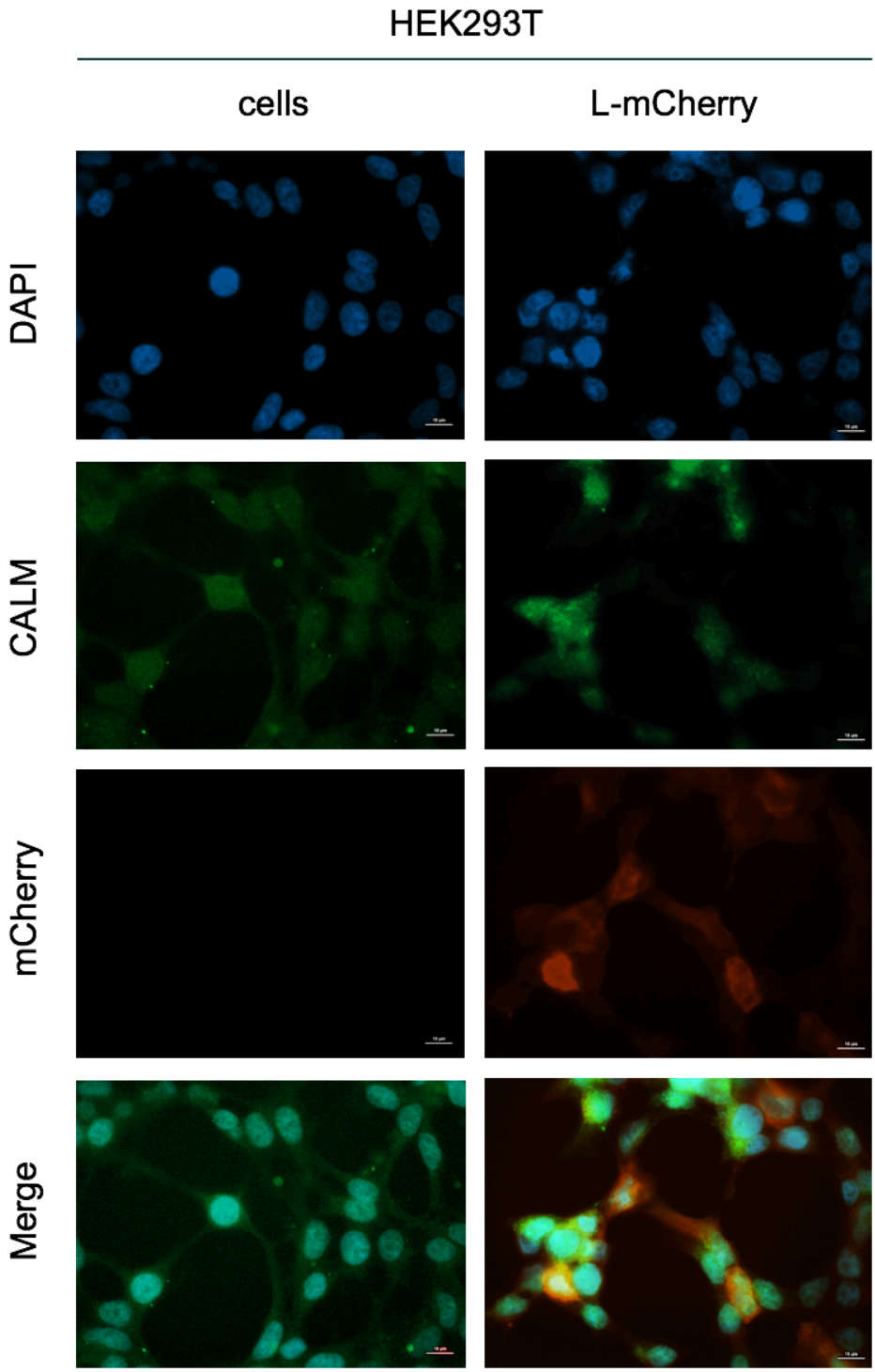

Figure 4.9. Potential co-localisation of CALM with EBOV L-mCherry in 293T cells. *Immunofluorescence microscopy image of 293T cells transfected with EBOV L-mCherry and mock cells. In blue, DAPI-stained nuclei; in red, EBOV L-mCherry; in green, CALM. Scale bars indicate 10µm.*

4.2.5. The antagonism of CALM negatively affects the transcription and replication of EBOV

CALM is an intermediary protein that senses calcium levels and relays signals to various calcium-sensitive enzymes. CALM is abundant in the cytoplasm, a critical component in eukaryotic cells and transduces Ca^{2+} signals into biological responses through its modulation of the structure and function of aquaporins, ion channels, and enzymes like kinases and phosphatases (Walsh, 1983). CALM has been observed to functionally associate with other viruses proteins (Chattopadhyay et al., 2013; Bautista-Carbajal et al., 2017) and also with the EBOV matrix protein VP40 (Han et al., 2007). Although its interaction with EBOV L in the performed label-free mass spectrometry analysis did not show significance, its association with L-mCherry was confirmed by forward and reverse pulldowns in the cell-free system followed by western botting, so its hypothesised role on EBOV transcription and replication was addressed.

To gain confidence in the L-CALM interaction, the protein sequence L-mCherry was uploaded to the web-based database "Calmodulin Target Database" (http://calcium.uhnres.utoronto.ca/ctdb) to predict putative CALM-binding motifs within the viral protein. Potential calmodulin recruitment signalling (CRS) motifs on the protein of interest were predicted by searching for homology to the database and by numerous criteria such as distribution of hydrophobicity and basic charge, presence of proline residues and similarity to typical database parameters (Yap et al., 2000). According to the results obtained, a putative CALM-binding motif close to the N-terminal end of the L-mCherry protein sequence was found to have a high score in consonance with the database algorithm criteria (Figure 4.10). The putative motif, AKGRITKLVNDY, did not overlap with the mCherry insert sequence an it was found close to the C-terminal end of the viral protein. As reported in Chapter 3, the LC-MS/MS analysis did not identify CALM as a potential interactor of VP35. Therefore, the amino acid sequence of EBOV VP35 was also uploaded to the database as a negative control and the scoring for a potential CALM-binding domain in this viral protein was zero.

The repurposed drug W-7 (N-(6-aminohexyl)-5-chloro-1- naphthalenesulfonamide hydrochloride) antagonises CALM by binding to its calcium-binding domains and blocks the interaction of calmodulin with its target proteins. The cytotoxicity of W-7 on BSR-T7 cells treated for 24 hours was assessed with an MTT assay. Concentrations ranging up to 40µM did not result significantly cytotoxic to cells, but concentrations of 50µM and above resulted in cell death, showing >90% reduction on cell viability (Figure 4.11A). Therefore, BSR-T7 cells were treated with W-7 concentrations of 10µM and below to ensure optimal cell viability and that any observed effects on virus biology were down to specific virus effects and not off target effects. To investigate the repercussion of the CALM antagonism with W-7 on EBOV transcription and replication, an EBOV minigenome system was used. BSR-T7 cells were seeded at 10^5 cells/well in a 24-well dish format 24 hours prior to transfection. 500ng of pMG, 250ng of pNP, 125ng of pVP30, 125ng of pVP35, 125ng of pL or empty vector pUC57 and 50ng of pRLTK were transfected with Lipofectamine® 2000 and cell media was replaced with fresh media with non-cytotoxic concentrations of W-7 four hours post-transfection. After 24 hours, BSR-T7 cells were harvested and lysed. Each condition was performed in triplicate for statistical significance. Results indicated that BSR-T7 cells treated with 2.5µM, 5µM and 10µM of W-7 had their minigenome normalised luciferase abundance reduced up to 55.6%, 42.3% and 27%, respectively. Reporter activity of minigenome system-transfected BSR-T7 cells was significantly decreased in a dose-dependent manner when treated with the CALM antagonist W-7 (Figure 4.11B and Table 4.3). An SDS-PAGE was performed on cell lysates to further confirm the drop of reporter activity of the minigenome system, where a decrease of EBOV L detection in W-7-treated cells was also seen, suggesting that the viral RNA polymerase may lose stability in the host cell when CALM is antagonised. The abundance of NP remained stable even if cells were treated with W-7, indicating that the effect of the drug on the viral RNA synthesis was not due to a disruption in the expression or stability of the support proteins (Figure 4.11B). The observed reduction of the minigenome system activity was not due to non-specific cytotoxicity effects, as the W-7 concentrations selected for the functional assay had no significant effect on cell viability according to the cell viability assay previously performed.

Figure 4.10. EBOV L has a putative CALM-binding motif at the C-terminal end. *Putative CALM-binding site was predicted by "CaM Target Database" (http://calcium.uhnres.utoronto.ca/ctdb/ctdb/home.html) by using the protein sequence of EBOV L-mCherry. Normalised scores (0-9) are shown below the amino acid sequence. A consecutive string of high values indicates a putative CALM-binding site, 0 representing null chance and 9 representing high chance of CALM interaction. In this case, AKGRITKLVNDY (in blue) at amino acid positions 2356-2367, constitute a putative CALM-binding motif. In red, sequence of the inserted mCherry. Only the C-terminal end of the protein sequence is shown in the figure, from amino acid 1651 to 2449.*

A)

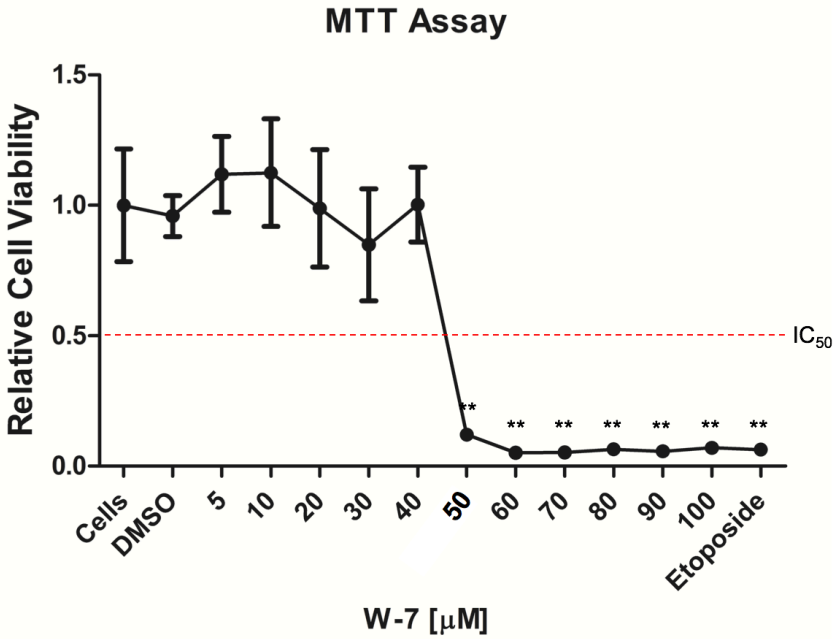
MTT Assay
Relative Cell Viability
1.5
1.0
0.5
0.0
IC50
**
Cells
DMSO
5
10
20
30
40
50
60
70
80
90
100
Etoposide
W-7 [µM]

B)

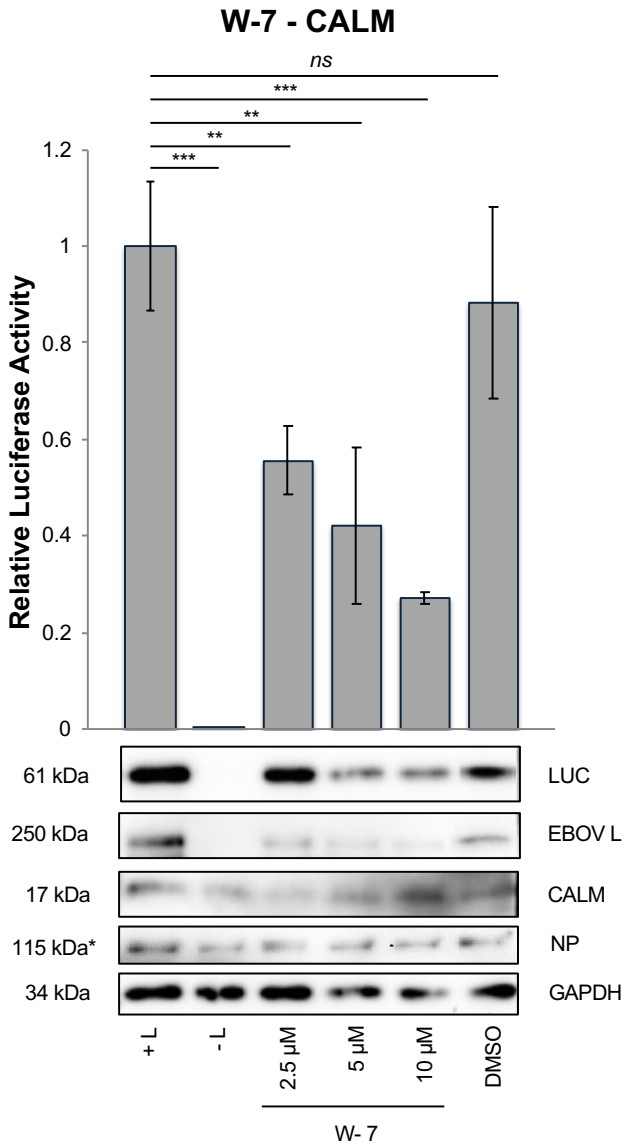
W-7 - CALM
ns
***
**
**
***
Relative Luciferase Activity
1.2
1
0.8
0.6
0.4
0.2
0
61 kDa
LUC
250 kDa
EBOV L
17 kDa
CALM
115 kDa*
NP
34 kDa
GAPDH
+ L
- L
2.5 µM
5 µM
10 µM
DMSO
W- 7

Figure 4.11. Effect of the calmodulin inhibitor W-7 on the reporter activity of an EBOV minigenome system in BRS-T7 cells. *(A) Cell viability assay (MTT) of BSR-T7 cells treated for 24 hours with the small molecule inhibitor W-7, a calmodulin (CALM) antagonist. A concentration range between 5µM and 100µM of W-7 was used to treat BSR-T7 cells for 24h. DMSO as vehicle control. Etoposide 10nM was used as a positive control for the induction of apoptosis. (B) DLA to assess the effect of W-7 on the viral RNA synthesis of an EBOV minigenome system in BSR-T7 cells. Each condition was performed in triplicate. Firefly luciferase activities were normalised with Renilla luciferase measurements. Each condition was performed in triplicate. A t-test between conditions assessed significance (ns non-significant, **p-value<0.01, ***p-value<0.001). Western blot showing levels of Firefly luciferase (LUC), CALM, NP (*actual protein size = 84 kDa; seen at 115 kDa due to protein phosphorylation) and EBOV L in the cell lysates 24 hours post-transfection and 20 hours post-treatment with W-7. GAPDH used as loading control. Assessed by a BCA assay, 2.5µg of total protein were loaded in each well. – L indicates the expression of the minigenome system without the vector expressing the viral polymerase. DMSO-treated cells were used as vehicle control.*

Table 4.3. Statistical analysis of luciferase activities in BSR-T7 cells transfected with EBOV minigenome system plasmids and treated with different concentrations of the CALM antagonist W-7. *A dual luciferase assay (DLA) was performed on BSR-T7 cell lysates treated with different concentrations of W-7. Each condition was performed and measured in triplicate. Measurements of Firefly luciferase were normalised with Renilla luciferase values. A t-test between –L and the other conditions assessed significance. Significance of the DMSO condition was compared to +L. FC, fold change.*

Condition	Normalised FC difference over -L	Relative luciferase activity (%)	Standard deviation (SD)	t-test (p-value)
+ L	1358.4147	100	0.13	0.0002
- L	1	0.07	0.00	1
W-7 2.5µM	755.7764	55.64	0.07	0.0069
W-7 5µM	573.6931	42.23	0.16	0.0087
W-7 10µM	366.7664	27.00	0.01	0.0007
DMSO	1198.1217	88.20	0.1980	0.4233

4.2.6. Depletion of intracellular free calcium ions is detrimental for EBOV replication

Viral infection alters calcium homeostasis within the infected cell. Several viruses have been shown to induce calcium release with a subsequent enhanced intracellular calcium concentration during their infection cycle (reviewed in Zhou et al., 2009). Free calcium ions promote Ebola virus virion egress. Han and Harty demonstrated that calcium chelation affects the amount of VP40 released from transfected cells, resulting in a reduction of viral-like particles (VLP) budding (Han and Harty, 2007). In order to investigate whether the disruption of free intracellular calcium levels affects EBOV replication independently of the L-CALM interaction, BSR-T7 cells transfected with the minigenome system were treated with the calcium chelator acetoxymethyl ester (BAPTA-AM) and its activity was examined.

To assess if the cell permeable Ca^{2+} chelator BAPTA-AM caused non-specific cytotoxic effects on BSR-T7, an MTT assay was performed with concentrations of the drug ranging from 5 μM to 200μM (Figure 4.12A). No significant cell viability reduction was observed. In cells transfected with the EBOV minigenome system, Ca^{2+} chelation resulted in significant reduction of EBOV replication activity in a dose-dependent manner, with concentration 50 μM showing 47% reporter activity and going down to 30% when treated with a BAPTA-AM concentration ≥100μM (Figure 4.12B and Table 4.4). Treatment with BAPTA-AM resulted in an alteration of the stable expression of EBOV L (Figure 4.12B). However, it did not affect the abundance of another RNP complex protein, EBOV NP, suggesting that the reduced activity of the minigenome system was not due to a disruption of the viral ribonucleoprotein complex. Protein abundance of CALM also resulted intact, according to the western blotting performed with cell lysates. These results suggest that the disruption of intracellular calcium homeostasis by decreasing the level of free Ca^{2+} ions is detrimental for EBOV replication.

A)

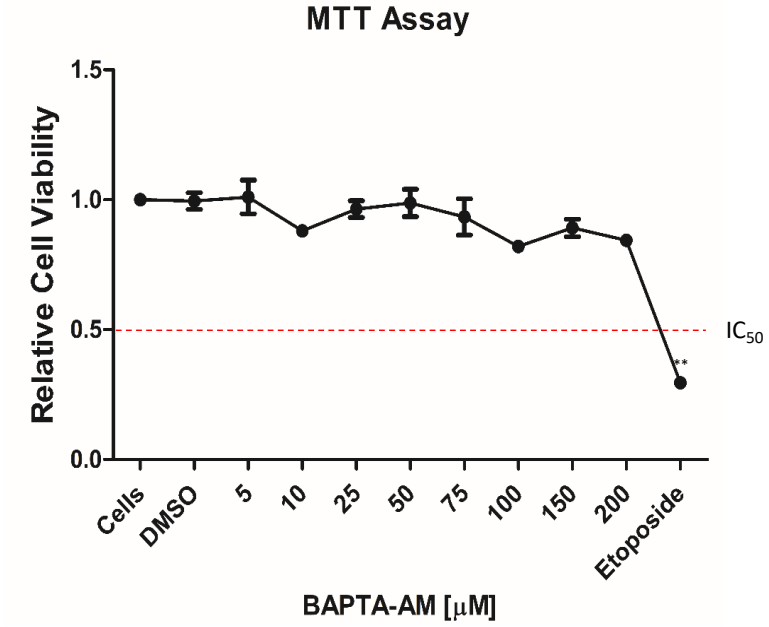
MTT Assay
Relative Cell Viability
1.5
1.0
0.5
0.0
IC50
**
Cells
DMSO
5
10
25
50
75
100
150
200
Etoposide
BAPTA-AM [μM]

B)

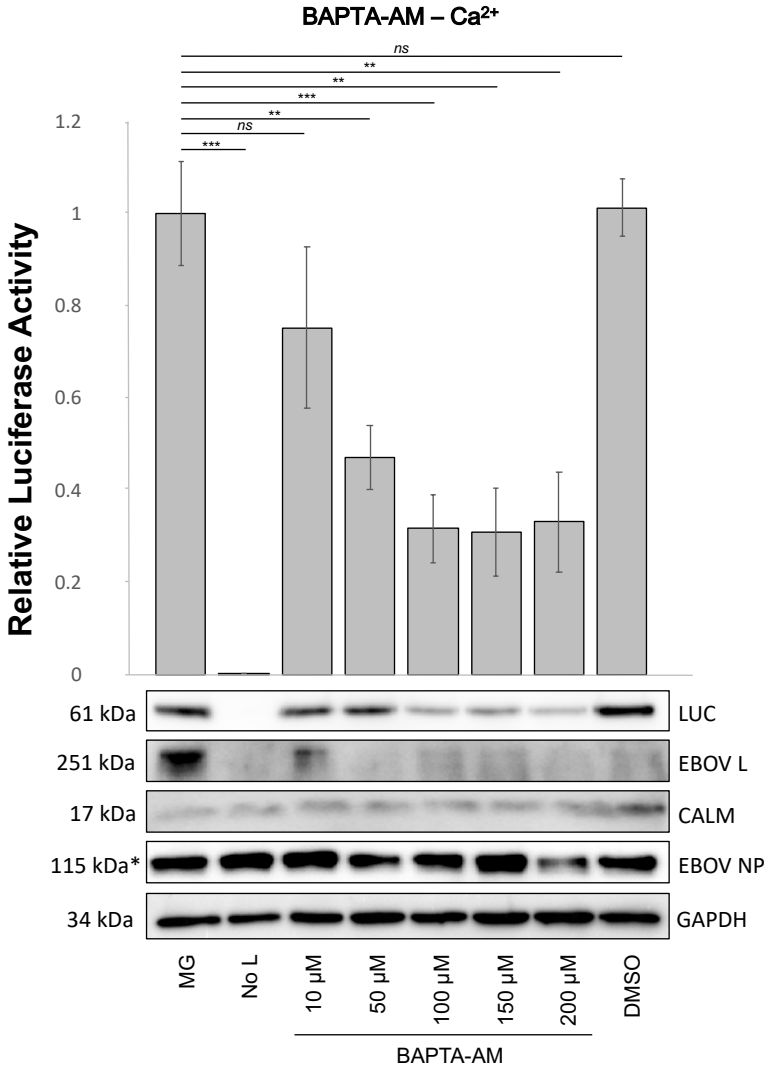
BAPTA-AM – Ca2+
ns
**
**
***
**
ns
***
Relative Luciferase Activity
1.2
1
0.8
0.6
0.4
0.2
0
61 kDa
LUC
251 kDa
EBOV L
17 kDa
CALM
115 kDa*
EBOV NP
34 kDa
GAPDH
MG
No L
10 μM
50 μM
100 μM
150 μM
200 μM
DMSO
BAPTA-AM

Figure 4.12. Effect of the depletion of intracellular Ca^{2+} on the replication of the EBOV minigenome system in BSR-T7 cells. *(A) An MTT assay was performed on BSR-T7 cells treated with BAPTA-AM, a membrane permeable intracellular Ca^{2+} chelator. A concentration range between 5µM and 200µM of BAPTA-AM was used to treat BSR-T7 cells for 2 hours, followed by a replacement of fresh media. DMSO was used as vehicle control and Etoposide 10nM was used as a control for the induction of apoptosis. (B) DLA to assess the effect of calcium chelation on viral RNA synthesis in BSR-T7 cells transfected with an EBOV minigenome system plasmids. Each condition was performed in triplicate. Firefly luciferase activities were normalised with Renilla luciferase measurements. Each condition was performed in triplicate. A t-test between conditions assessed significance (ns non-significant, **p-value<0.01, ***p-value<0.001). Western blot showing abundance of Firefly luciferase (LUC), CALM, NP (*actual protein size = 84 kDa; seen at 115 kDa due to protein phosphorylation) and EBOV L in the cell lysates 24 hours post-transfection and treated with BAPTA-AM. GAPDH used as loading control. Assessed by BCA, 2.5µg of total protein was loaded in each well. DMSO-treated cells were used as vehicle control.*

Table 4.4. Statistical analysis of luciferase activities in BSR-T7 cells transfected with EBOV minigenome system plasmids and treated with different concentrations of BAPTA-AM. *A DLA was performed on BSR-T7 cell lysates treated with different concentrations of Ca^{2+} chelator. Each condition was performed and measured in triplicate. Measurements of Firefly luciferase were normalised with Renilla luciferase values. A t-test between –L and the other conditions assessed significance. Significance of the DMSO condition was compared to +L. FC, fold change.*

Condition	Normalised FC difference over -L	Relative luciferase activity (%)	Standard deviation (SD)	t-test (p-value)
+ L	364.56	100	0.11	0.0001
- L	1	0.27	0.00	1
BAPTA-AM 10µM	274.12	75.21	0.17	0.1083
BAPTA-AM 50µM	171.52	47.06	0.07	0.0023
BAPTA-AM 100µM	115.36	31.65	0.07	0.0009
BAPTA-AM 150µM	112.38	30.84	0.10	0.0013
BAPTA-AM 200µM	120.80	33.14	0.11	0.0018
DMSO	369.13	101.28	0.06	0.8723

4.3. Discussion

Since Ebola virus RNA-dependent RNA protein (L) is the catalytic subunit of the RNP complex, and transcription and replication processes are an interesting alternative target for antiviral exploitation, the main aim of this study was the investigation of novel interactions between L and host proteins to characterise their functionality in the EBOV biological cycle. To our knowledge, only a few studies have investigated EBOV L due to its complexity (Tchesnokov et al., 2018). Nevertheless, only one study has been able to determine EBOV L host partners in cell culture by co-immunoprecipitating the viral protein and analysing protein-protein associations by mass spectrometry. Takahashi et al. developed a Flag-EBOV L. By pulling-down and analysing the protein complexes by LC-MS/MS, DNA topoisomerase 1 (TOP1) was identified as a significant L partner with an important role in the transcription and replication of the virus (Takahashi et al., 2013). As tags can affect the viral protein conformation and, therefore, the interactions that it can stablish with cellular factors, in this study an EBOV L protein was engineered with the reporter gene mCherry inserted at the second hinge, which constitutes a variable region located between conserved domains V and VI. The insertion of a reporter gene in this region has been previously demonstrated not to disrupt the viral RNA polymerase activity of Ebola virus and other members of the order *Mononegavirales,* like human respiratory syncytial virus (HRSV), vesicular stomatitis virus (VSV) and rabies virus (RABV) (Hoenen et al., 2012; Fix et al., 2011; Ruedas et al., 2014; Duprex et al., 2002). Hence, by changing the location of the EBOV L tag, the observation of both similar and different PPIs to the ones observed by Takahashi et al. was expected. In the work performed in this chapter, cellular factors BAG2 and PRDX-1 were found to potentially interact with EBOV L, and they coincide with the mass spectrometry results obtained by Takahashi et al., giving confidence in the outcome of the study described in this chapter.

The reason why L-mCherry could not be detected by LC-MS/MS when expressed in cell culture in this study is not clear. At first glance, it was hypothesised that

recombinant L-mCherry might have not been functional or stable in cell culture but a western blotting with minigenome and L-mCherry expressing cell lysates proved that was not the case. Little amounts of the recombinant protein could be detected by western blot in coIP eluates from cell lysates expressing L-mCherry (data not shown), but the required amounts for LC-MS/MS analysis could never be obtained in cellular culture. To overcome this hindrance, a TnT system was used instead to overexpress the recombinant viral protein. Although TnT systems cannot be employed to elucidate cellular interactomes, they can help investigate virus-host protein-protein interactions related to the transcription and translation processes, and these can later be extrapolated and validated in mammalian cells (reviwed in Arduengo et al., 2007). Potential novel interactions between the host and EBOV L proteins were found out in this piece of work, such as YBX1 and CALM. Giving more confidence to mass spectrometry analysis on rabbit reticulocytes expressing L-mCherry, CALM and YBX1 had been previously elucidated by mass spectrometry as components of human reticulocytes (Chu et al., 2018).

YBX1 is a nuclear/cytoplasmic protein involved in the regulation of cellular transcription and translation in the cytoplasm. It regulates the translation of mRNA (Matsumoto et al., 1998) and has been observed to interact with other viruses and to have a role in their biological cycle. YBX1 translocates to the nucleus of Influenza-infected cells and facilitates the association of the RNP complex to the cellular microtubules, facilitating the egress of the virus to the vesicular trafficking system. Overexpression of YBX1 has been seen to stimulate the production of influenza virus virions progeny (Kawaguchi et al., 2012). In hepatitis C virus (HCV), phosphorylated YBX1 stabilises viral non-structural protein 5A (NS5A) and regulates HCV propagation (Chatel-Caix et al., 2013; Wang et al., 2015). Another example of viral YBX1 interaction occurs with Dengue virus (DENV), where the cellular protein binds to the viral 3' untranslated region (UTR) and represses translation, suggesting that in this case YBX1 may have an antiviral role within the viral infection (Paranjape et al., 2007). Further work on the role of YBX1 in the biological cycle of Ebola virus will need to be addressed, but these preliminary results could shed light on a new and exploitable host-directed antiviral target.

Other interesting potential EBOV L associations elucidated by mass spectrometry were chaperones HSPA8 and BAG2. Chaperones are thought to be needed for the stability and for the RNP complex formation (Noton et al., 2012; Tchesnokov et al., 2018). A mutational analysis performed by Sztuba-Solinska et al. proved that the first 50 nucleotides of the Ebola virus trailer region constitute an interacting HSPA8 motif that conforms a small-stem loop, which is essential for sustaining viral replication. Mutational analysis on this region showed that the HSPA8 interaction is key for EBOV minigenome system replication (Sztuba-Solinska et al., 2016). HSPA8 co-chaperone, BAG2, shows to be enriched in the elute fraction of the pull-downs performed in this piece of work and has also been previously revealed to interact with EBOV L and NP (Takahashi et al., 2013; García-Dorival et al., 2016), suggesting that this cellular factor may play a role in the stability of the RNP complex and its functionality on the viral transcription and replication.

CALM was the chosen host factor for further functional analysis on the Ebola virus RNA synthesis. CALM is a calcium-modulated protein that is found in the cytoplasm of all eukaryotic cells. It gets activated by sensing Ca^{2+} and acts as an intermediary protein that regulates and modulates the function of other enzymes, like a number of phosphatases and kinases, ion channels and structural proteins (Villalobo et al., 2018). Homeostasis of intracellular calcium gets compromised during viral infections as viruses can create a tailored environment for their own demands (Zhou et al., 2009). A previous study in our lab conducted by Wu et al. (data not published) showed that CALM interacted with porcine reproductive and respiratory syndrome virus (PRRSV) RNA-dependent RNA polymerase (RdRp or nsp9) and had a role in the transcription and replication of the RNA virus. Moreover, the importance of CALM and calcium free ions has been previously reported to play a pivotal role in EBOV budding process by interacting with VP40 (Han and Harty, 2007). Therefore, in this study it is hypothesised that CALM and intracellular Ca^{2+}, indirectly, may also have a role in the transcription and replication of EBOV and CALM was present in one of the three TnT system replicas expressing L-mCherry pulldowns.

In this study, the interaction EBOV L-CALM and the performance of EBOV replication when free intracellular Ca^{2+} levels are decreased, were addressed. Evidence was provided regarding the role of the host protein and the importance of calcium on viral transcription and replication in an Ebola virus minigenome system. When minigenome-transfected BSR-T7 cells are treated with either the CALM antagonist small molecule W-7 or the Ca^{2+} chelator BAPTA-AM at non-cytotoxic concentrations, the system's reporter activity diminished down to 27% and 30% relative luciferase abundance, respectively. Both effects on the minigenome RNA synthesis were dose-dependent. Detection by specific antibodies in a western blot of *Firefly* luciferase proved the reduction on its expression in CALM antagonist and BAPTA-AM drug-treated cells. Abundance of EBOV L was also affected by the presence of both drugs, suggesting that the viral polymerase requires available and functional CALM not only to carry out viral transcription and replication but also to stabilise its expression in cellular culture. As W-7 binds to the calcium domains of calmodulin in a competitive manner and disrupts its interaction with other enzymes (Osawa et al., 1998), it was expected that CALM abundance in treated and non-treated cells remained the same. EBOV NP expression and stability in treated and non-treated cell lysates was also assessed by western blot, showing no difference in its abundance along all the conditions tested and indicating that the disruption on CALM activity or the free intracellular Ca^{2+} levels may not affect the support proteins abundance, thus having an antiviral effect due to the loss of Ebola virus L stability. W-7 had also been used in other studies to antagonise CALM, showing to have an antiviral effect against dengue virus, rotavirus and human immunodeficiency virus type 1 (HIV-1), for instance (Bautista-Carbajal et al., 2017; Chattopadhyay et al., 2013; Taylor et al., 2012). Moreover, CALM is implicated in the virion budding process of Ebola virus by interacting with VP40, and W-7 had been observed to inhibit this process in a dose-dependent manner (Han et al., 2007). These studies all together, suggested that CALM and calcium, indirectly, may be involved in the biological cycle of RNA viruses at different stages of their biological cycle and that the host protein and the calcium pathway could represent attractive host-directed antiviral targets for a broad range of viral infections.

This piece of work provides evidence that cell-free systems can be considered to help elucidate protein-protein interactions in those cases where the protein under study results difficult to be expressed in cell culture. The novel interactions between CALM, YBX1 and BAG2 and L-mCherry observed to occur in rabbit reticulocytes by LC-MS/MS were further validated by co-immunoprecipitation. Replication of an EBOV minigenome system was shown to be reduced in a dose-dependent manner when cells were treated with the CALM antagonist W-7 and calcium chelator BAPTA-AM, demonstrating that CALM/Ca^{2+} played a pivotal role in these viral processes.

Chapter 5: Functional characterisation of non-synonymous mutations in EBOV VP35 that occurred at the start of the 2013-2016 West Africa Ebola virus outbreak

5.1. Introduction

Ebola virus was first identified in 1976 and, since then, small outbreaks have been occurring in rural areas of the Central African belt countries. The largest EBOV outbreak until now occurred in West Africa between 2013 to 2016. This resulted in more than 28,000 cases and 11,000 deaths (Mendoza et al., 2016). Nevertheless, the rapid response of the international community helped with diagnostics, spreading prevention measures and supportive care of patients in order to control transmission. The 2013-2016 EBOV outbreak surpassed both cases and fatalities of all the previous Ebola virus outbreaks combined (Kaner and Schaack, 2016). This unprecedented magnitude together with the fact that, to date, there are no licensed therapeutics for human use against Ebola virus disease (EVD), speeded up the investigation of human, environmental and host factors that might have played a role in the scale and impact of the outbreak. Due to the high error rate of the EBOV RNA-dependent RNA polymerase replicase (Hanada et al., 2004; Hoenen et al., 2015; Sanjuan et al., 2010), non-synonymous variations in the amino acid sequence of EBOV proteins can be frequently found (Deng et al., 2015; Tong et al., 2015; Pappalardo et al., 2017), with the potential to enhance viral fitness or adaptation to new hosts (Dowall et al., 2014; Wong et al., 2019). Deep sequencing approaches helped gain insight into the evolution of EBOV and identified several mutations in all of the viral proteins during the outbreak (Carroll et al., 2015; Dietzel et al., 2017a; Wong et al., 2019). The importance of studying non-synonymous mutations lay in the fact that these can have an impact on viral virulence, host tropism and the design of antiviral approaches (Alfson et al., 2016; Pappalardo et al., 2017; Ueda et al., 2017; Wong et al., 2019).

This study was focused on VP35 and the importance of observed naturally occurring mutations in this protein during the largest EBOV outbreak to date. VP35 is a multifunctional protein essential for viral transcription and replication as it is one of the constituents of the viral ribonucleoprotein (RNP) complex. VP35 has several known functions. The viral protein is a structural element required for viral genome packaging (Johnson et al., 2006), assembly (Kirchdoerfer et al., 2015), and the viral

RNA polymerase co-factor. VP35 is also an RNAi silencing suppressor (Haasnoot et al., 2007) and facilitates the immune evasion by antagonising the type-I interferon (IFN-α/β) responses by binding to dsRNA and supressing the retinoic acid-inducible gene 1 (RIG-1) helicase signalling cascade (Cardenas et al., 2006; Chang et al., 2009; Prins et al., 2010). The structure of VP35 comprises two main domains; a coiled-coil domain (CCD) is located at the N-terminal end of the protein. This region is required for the oligomerisation of the protein (Reid et al., 2005). The oligomerisation domain has a critical role in the nucleoprotein (NP) and VP40 binding as well as RNP complex formation (Johnson et al., 2006; Kirchdoerfer et al., 2015). At the C-terminal end there is the IFN inhibitory domain (IID), which binds to dsRNA and blocks several signalling components that trigger the type-I IFN response of the host (Edwards et al., 2016; Leung et al., 2009). The VP35 IID has been demonstrated to be critical for full virulence of EBOV (Leung et al., 2009; Schumann et al., 2009). Mutations in any of these domains or close to them could represent a change on the protein configuration and/or the way it interacts with other viral and host proteins (Binning, et al., 2010).

In the present study, the effect of naturally occurring substitutions in the EBOV VP35 from Makona gene sequence analysis and whether they affect function in terms of viral RNA synthesis and interferon antagonism was investigated.

5.1.1. Objectives

In this study, the available VP35 sequence data from EBOV Makona strain genomes sampled during years 2014-2015 in West Africa were compared between them and to a Mayinga sequence sampled in 1976 to elucidate non-synonymous mutations in the viral RNA dependent RNA polymerase co-factor. The goal of the study was the characterisation of the most frequent residue substitutions in VP35 early during the West African outbreak. For that, the effect of the selected mutations in VP35 on EBOV viral RNA synthesis function was assessed by using an EBOV minigenome system that faithfully recapitulated viral RNA synthesis. Moreover, the effect of those mutations on the IFN-β response suppression was investigated by using an IFN-β reporter assay in cell culture.

5.2. Results

5.2.1. Analysis of EBOV VP35 sequences

In order to investigate whether non-synonymous mutations had occurred in VP35 during the West African Outbreak, all the available *Zaire ebolavirus* (EBOV) Makona strain VP35 sequences from samples taken in 2014-15 that had a complete protein sequence were identified in the GenBank database on the date 6th of March 2017 (http://www.ncbi. nlm.nih.gov/GenBank/).

A total of 950 EBOV VP35 sequences were included in the alignment (see Appendix). From them, 947 of the downloaded sequences were sampled in 2014 in Liberia, Guinea, Nigeria, Sierra Leone, Switzerland, Great Britain, Mali and Democratic Republic of Congo. Three of the 950 sequences were sampled in 2015 in Liberia. To examine the year of appearance of the observed mutations, 18 sequences from outbreaks that occurred prior 2013 were also included in the analysis. Those were sampled in 1976, 1977, 1995, 1996, 2002 and 2007 and were from Gabon and Democratic Republic of Congo (Table 5.1). The 950 sequences of VP35 protein sampled during 2014 and 2015 were aligned and compared to a reference EBOV Makona strain from 2014 [KJ660347.2], the same VP35 sequence used in the EBOV minigenome in this thesis, in search for non-synonymous mutations.

In total, 45 non-synonymous mutations were detected. From these, five mutations had an occurrence frequency higher than 1.5%. These were V12A (1.68% of the sequences), N41S (2.53%), L144F (2%), L249F (4.75%) and L330F (2.83%). From the 950 VP35 amino acid sequences analysed, 46 contained the non-synonymous mutation L249F; 45 of them belonged to strains sampled in Liberia in 2014, and 1 belonged to a strain sampled in Sierra Leone in 2014. The non-synonymous mutation L330F was present in 25 out of the 950 VP35 amino acid sequences analysed, all of them belonging to viral genomes sampled in Guinea in 2014 (Table 5.1). Interestingly, the reference sequence (AGB56837.1, 1976, Democratic Republic of Congo) had a threonine (T) at the position 68, whereas all except for 6 of the sequences from the

samples taken in 2014-15 had a methionine (M). According to the alignment of the 18 VP35 sequences sampled prior 2014, the residue change T > M at position 68 occurred in 2002 in Gabon and was maintained through the viral progeny onwards. Therefore, the reverse mutation M68T on VP35 was included in this study. L249F and L330F are located in the interferon inhibitory domain (IID, position 221-340). L249F is between residues K248 and K251, which are amino acids with polymerase cofactor activity in VP35 together with positions 240, 282-3, 298 and 300. M68T is located at the N-terminal of the protein sequence, close to the coiled-coil domain (CCD) (Dunham et al., 2015). This region is thought to interact with the viral RNA polymerase L (Cardenas et al., 2006) and to be responsible for the oligomerisation of the region (St Patrick Reid et al., 2005) (Figure 5.2). No combination of any of these three mutations was found in the same EBOV genome.

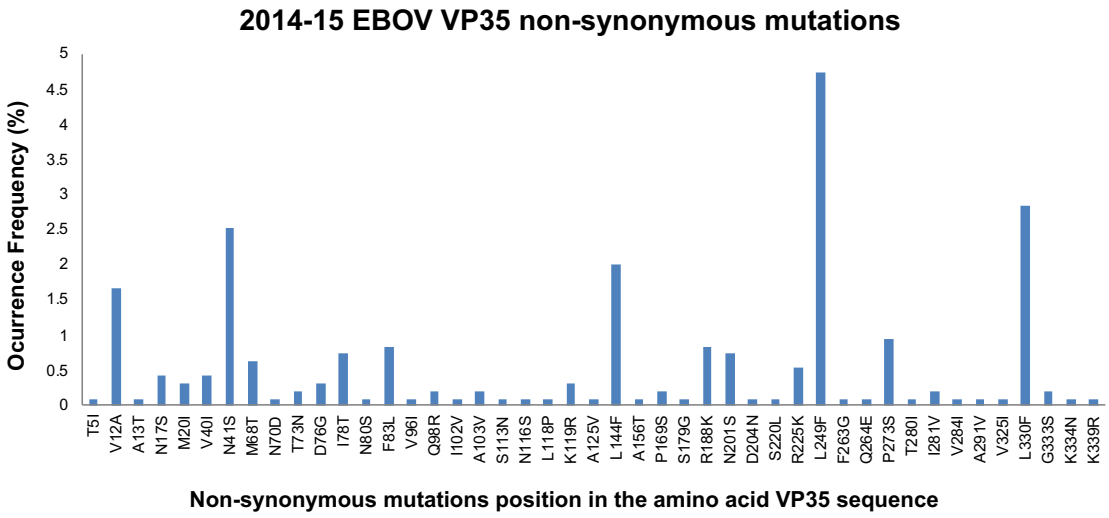

Figure 5.1. Occurrence frequency and amino acid position of non-synonymous mutations in EBOV VP35 sequences. *Alignments were performed by using the software MEGA6 (Version 6.06). Compared to the reference sequence [GenBank acc. num.* KJ660347.2*], 45 non-synonymous mutations were found in the EBOV VP35 protein analysis from 950 EBOV genome samples between 2014-15 in West Africa,.*

Table 5.1. Non-synonymous mutations at amino acid positions 68, 249 and 330 of the EBOV VP35. *Rows indicate year of first appearance of these mutations in VP35, frequency of occurrence during years 2014-2015 and countries where they were observed to occur.*

Amino acid mutation	Year of appearance	Frequency of occurrence in 2014-15	Countries of appearance in 2014-15
T68M	2002	944/950 (99.37%)	LBR, GIN, NGA, SLE, CHE, GBR, COD
L249F	2014	46/950 (4.84%)	SLE, LBR
L330F	2014	25/950 (2.63%)	GIN

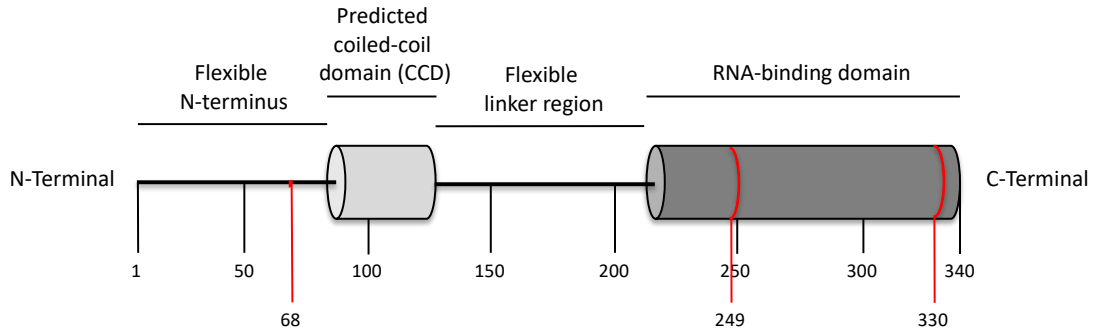

Figure 5.2. Schematic representation of the protein structure of EBOV VP35. *VP35 is 340 amino acids in length and has two functional domains. CCD, coiled-coil domain (aa 82-118) at the N-terminus of the protein sequence. IID, interferon inhibitory domain (aa 221-340) at the C-terminal end of the protein. The numbers indicate the amino acid position. In red, selected residue substitutions to be further studied. VP35 functional domains are based on models by Kimberlin et al., 2010, Reid et al., 2005 and Dunham et al., 2015.*

5.3.2. Construction of mutated EBOV VP35 and expression in 293T cells

In order to characterise the functional effect of M68T and the observed L249F and L330F mutations found in EBOV VP35 sequences during 2014-2015 in the West African outbreak, 3 plasmids were designed. Each vector encoded EBOV VP35 with each of these single non-synonymous mutations. Being VP35 a multifunctional viral protein, their effect on transcription and replication, and their IFN-β antagonism functions were studied by using an EBOV minigenome system and an IFN-β reporter assay, respectively (Figure 5.3). The synthetic genes encoding EBOV VP35 with the specific mutations were designed by using the online tool GeneArt (https://www.thermofisher.com/uk/en/home/life-science/cloning/gene-synthesis/geneart-gene-synthesis.html). The inserts had a size of 1624 bp and were cloned into pUC57 vectors between restriction enzymes SacI and SalI. Initial mRNA transcription was under the control of a phage T7 polymerase promoter. An encephalomyocarditis virus internal ribosome entry site (EMCV IRES) was located downstream to facilitate translation. Like the pVP35 support plasmid of the mini-genome system, called "pwtVP35" in this chapter, the mutated EBOV VP35 inserts (Figure 5.4) were codon-optimised for human translation. Three different EBOV VP35 genes with single non-synonymous mutations were constructed. One of them encoded EBOV VP35 with a leucine (L) to phenylalanine (F) replacement at the amino acid position 249 ($pVP35_{L249F}$). A second vector was designed to encode EBOV VP35 with an F instead of an L at the amino acid position 330 ($pVP35_{L330F}$). A third vector was constructed to encode VP35 with the amino acid change methionine (M) to threonine (T) at position 68 ($pVP35_{M68T}$).

To assess the presence of the inserts in the backbone after plasmid transformation, production and purification, an agarose gel loaded with undigested, digested once and digested twice mutated VP35 cDNA constructions confirmed both insert and backbone vector lengths (Figure 5.5).

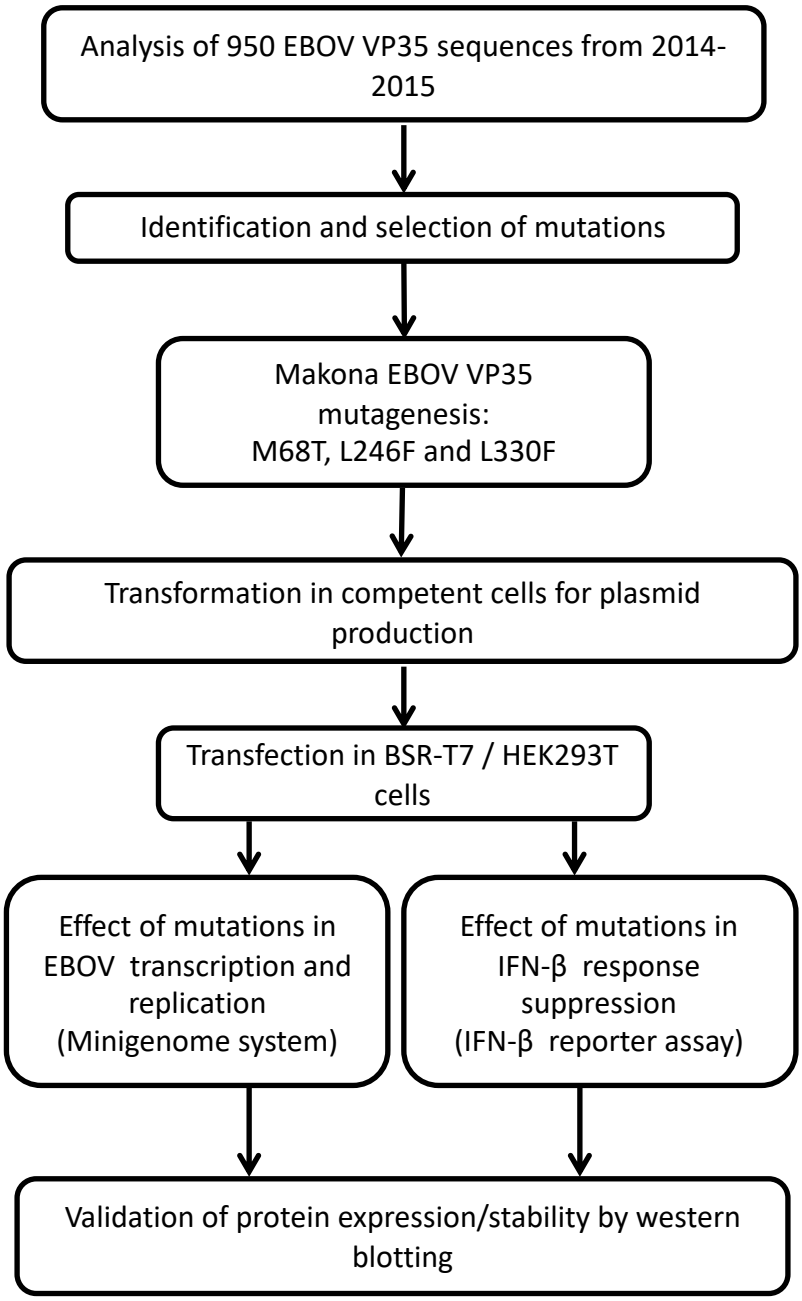

Figure 5.3. Diagram of the methodology used in this study.

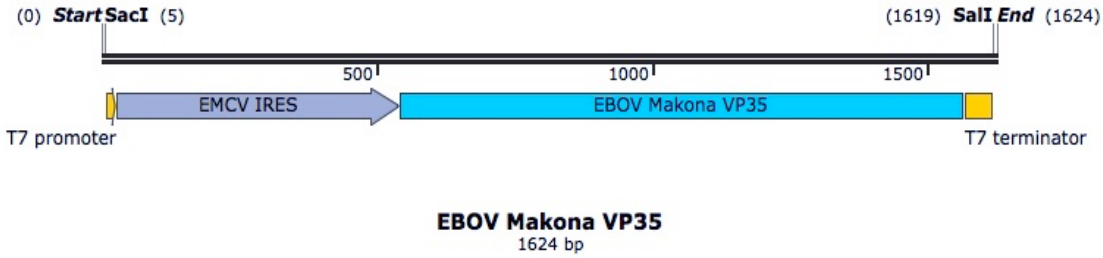

Figure 5.4. Insert construct utilised for the study of the mutated Ebola virus VP35. *Graphic representation of the insert encoding the Ebola virus Makona VP35 protein where non-synonymous mutations were introduced. The insert comprises a T7 polymerase promoter, followed by an EMCV IRES, the EBOV VP35 open reading frame (ORF) and the T7 polymerase terminator. The backbone used was pUC57. Nucleotide changes that led to single amino acid changes were inserted at the positions equivalent to amino acids 68 (M to T), 249 (L to F) or 330 (L to F).*

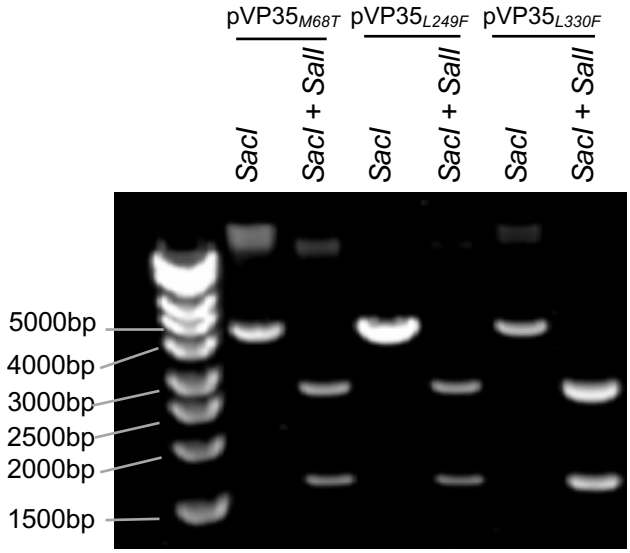

Figure 5.5. Endonuclease digestion of vectors encoding mutated EBOV VP35. *Vectors were cut once by SacI, and twice by SacI and SalI. Digestion products were run in a 1% agarose gel electrophoresis to confirm product lengths. The insert lengths were 1624pb, the backbone length was 2658bp and the total plasmid lengths were 4282bp.*

5.3.3. Effect of VP35 mutations on the EBOV viral RNA synthesis

In order to characterise the potential effect of the observed non-synonymous VP35 mutations on the viral transcription and replication, an EBOV Makona minigenome system was used in BSR-T7 cells. Each mutated VP35 was used individually and the amount of luciferase was compared to the one obtained by a minigenome system with the *wt*VP35. The minigenome plasmid of the system encodes *Firefly* luciferase, under the control of EBOV transcription/replication signals and therefore is dependent on the viral RNP complex proteins. BSR-T7 cells were harvested and lysed 24 hours post-transfection of the minigenome and support plasmids and a dual luciferase assay (DLA) was performed for each condition. *Firefly* luciferase values were normalised with measurements of *Renilla* luciferase, encoded in the co-transfected plasmid pRLTK in the system. No significant differences in the reporter activity of the system were observed between *wt*VP35 and $VP35_{M68T}$, suggesting that the change that occurred in 2002 onwards from T to M at the position 68 constituted a neutral mutation and results suggested that this mutation did not constitute an advantage to the virus fitness/adaptation in terms of transcription and replication (Table 5.2 and Figure 5.6A). However, to our knowledge, the substitution at position 68 was conserved through time. In contrast, VP35 mutations L to F at positions 249 and 330 individually conferred a replication advantage with a significantly higher fold change difference of 1.64 (p-value = 0.003) and 1.33 (p-value = 0.05), respectively, compared to the *wt*VP35 functionality. Each condition was performed in triplicate, assuring the minimum number of replicas to have a robust statistical test for significance.

Western blotting was performed to confirm the protein abundance of the reporter protein *Firefly* luciferase, EBOV VP35 and the housekeeping protein GAPDH, which was used as loading control. Specific antibodies against EBOV NP were used in order to see if the mutations studied on VP35 affected somehow the structure of the RNP complex. Abundance of NP was enriched in cells expressing the minigenome system proteins with $VP35_{L330F}$. Although further studies would need to be addressed, these

results suggest that the interaction between VP35 and NP could be affected by residue changes at position 330 in VP35 (Figure 5.6B).

Table 5.2. Statistical analysis of luciferase activities in BSR-T7 cells transfected with EBOV minigenome system plasmids with either wt VP35, VP35$_{M68T}$, VP35$_{L249F}$ or VP35$_{L330F}$. *A Dual Luciferase assay (DLA) was performed on BSR-T7 cell lysates. Each condition was performed and measured in triplicate. Measurements of Firefly luciferase were normalised with Renilla luciferase values. A T-test between wt VP35 and the other conditions assessed significance on the luciferase activity differences observed. FC, fold change.*

Condition	FC difference over -L	Relative luciferase activity (%)	Standard deviation (SD)	t-test (p-value)
***wt* VP35**	1534.72	100	0.09	0.00004
- L	1	0.065	0.00	1
VP35$_{M68T}$	1660.53	108.18	0.28	0.66
VP35$_{L249F}$	2514.95	163.87	0.15	0.003
VP35$_{L330F}$	2039.83	132.91	0.19	0.05

A)

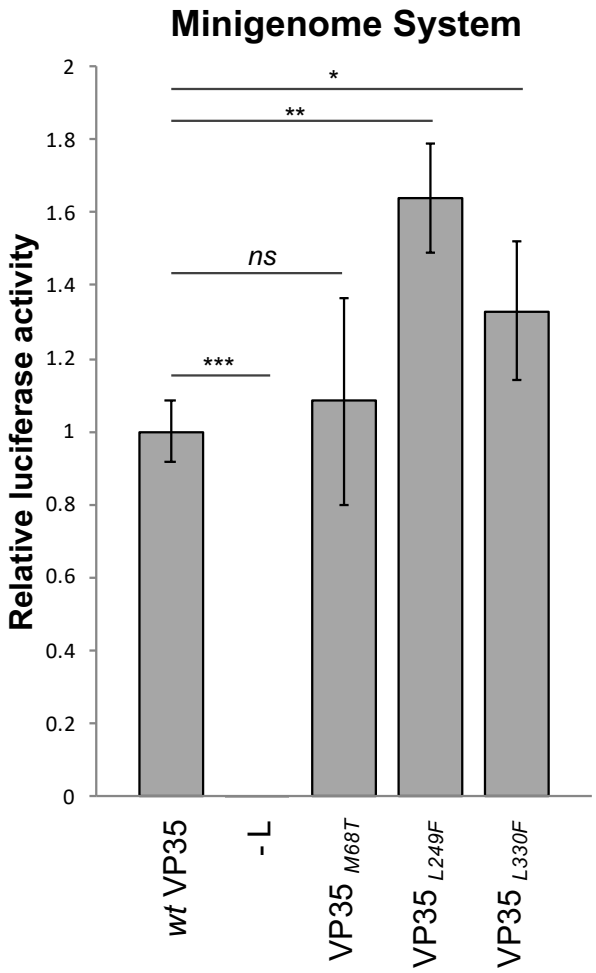
Minigenome System
Relative luciferase activity
2
1.8
1.6
1.4
1.2
1
0.8
0.6
0.4
0.2
0
*
**
ns
***
wt VP35
- L
VP35 M68T
VP35 L249F
VP35 L330F

B)

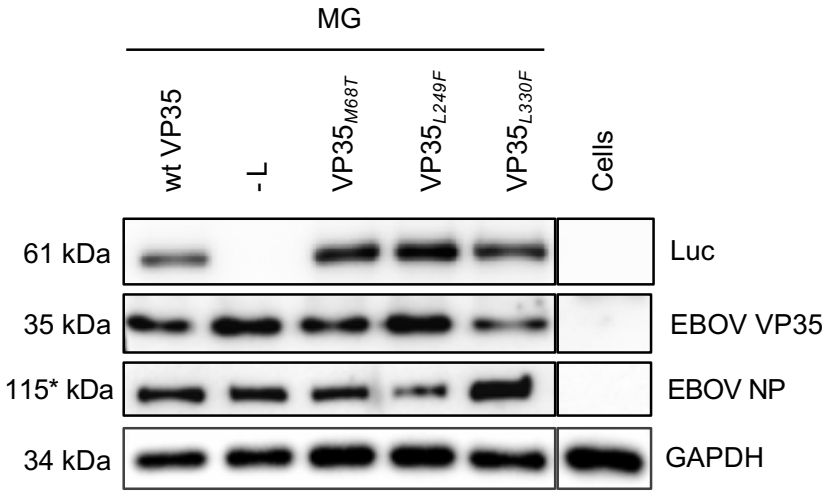
MG
wt VP35
- L
VP35M68T
VP35L249F
VP35L330F
Cells
61 kDa
Luc
35 kDa
EBOV VP35
115* kDa
EBOV NP
34 kDa
GAPDH

Figure 5.6. Functionality of mutated VP35. *(A) An EBOV minigenome system assay assessed the reporter gene activity of* $VP35_{M68T}$*,* $VP35_{L249F}$ *and* $VP35_{L330}$ *proteins compared to wt VP35 in BSR-T7 cells. Firefly luciferase activities were normalised with Renilla luciferase values. A minigenome system lacking the support plasmid encoding L was used as a negative control. Each condition was performed in triplicate. A t-test between conditions assessed significance (n/s non-significant, *p-value<0.05, **p-value<0.01, ***p-value>0.001). (B) Firefly luciferase (LUC), EBOV VP35, EBOV NP and GAPDH proteins expression and stability were confirmed by western blotting. Assessed by BCA, 2.5 µg of total protein from the lysed cells were loaded in each well. *EBOV NP has a predicted molecular weight of 85 kDa, but an actual weight of 115 kDa when run through an SDS-PAGE* (Shi et al., 2008).

5.3.4. Effect of VP35 mutations on the IFN-β antagonism

5.3.4.1. Standardisation of IFN-β reporter assay in 293T cells

EBOV VP35 is a multifunctional protein (Leung et al., 2010). Apart from being a component of the RNP complex and the viral RNA polymerase co-factor, it also plays a key role in shutting down the induction of the anti-viral immune response of the host by inactivating the RIG-I signalling pathway by recognition of dsRNA (Basler et al., 2000; Cardenas et al., 2006) (Figure 5.7A). In order to measure the IFN-β response of the host in cell culture, an IFN-β reporter assay was established in 293T cells. Primary transfection of plasmids encoding EBOV VP35 were co-transfected with pT7-Pol for the transcription of the viral mRNA. pIFN-β_GL3 was a gift from Nicolas Manel (Addgene plasmid # 102597) (Gentili et al., 2015) and encoded the *Firefly* luciferase reporter gene under the control of an IFN-β promoter. A pRLTK plasmid, encoding a *Renilla* luciferase protein, was also transfected for the normalisation of the *Firefly* values. 24 hours after primary transfection, a secondary transfection was carried out with the low molecular weight synthetic mismatched analog of dsRNA polyinosinic-polycytidylic acid (poly(I:C)). Poly(I:C) is a pathogen associated molecular pattern (PAMP) that is recognised by antiviral receptors TLR-3, RIG-1/MDA5 and PKR. Therefore, it induces inflammatory pathways and the expression of type-I interferons. EBOV VP35, already expressed in the transfected cell, was expected to block the IFN-β induction of the host (Figure 5.7B).

The reporter activity of the system showed a dose-response curve with saturation when more than 2.5μg of poly(I:C) was transfected in cells (Figure 5.8A). Therefore, the optimal amount of the dsRNA analog IFN-β inducer poly(I:C) was determined to be 2.5μg/well in a 24-well plate format. The antagonism effect at different amounts of *wt* VP35 on the IFN-β induced reporter activity of the system was also tested. 250ng, 1000ng, and 2000ng of p*wt*VP35 were transfected in BSR-T7 cells in a 24-well plate format and then IFN-β was induced by transfecting 2.5μg of poly(I:C) per well. As seen in Figure 5.8B, the more the amount of plasmid expressing VP35 transfected, the fewer the luciferase reporter activity of the IFN-β assay. The amounts of VP35

used and the corresponding suppression of reporter activity were in accordance with other IFN-β assays in the literature (Cannas et al., 2015; Cardenas et al., 2006).

A)

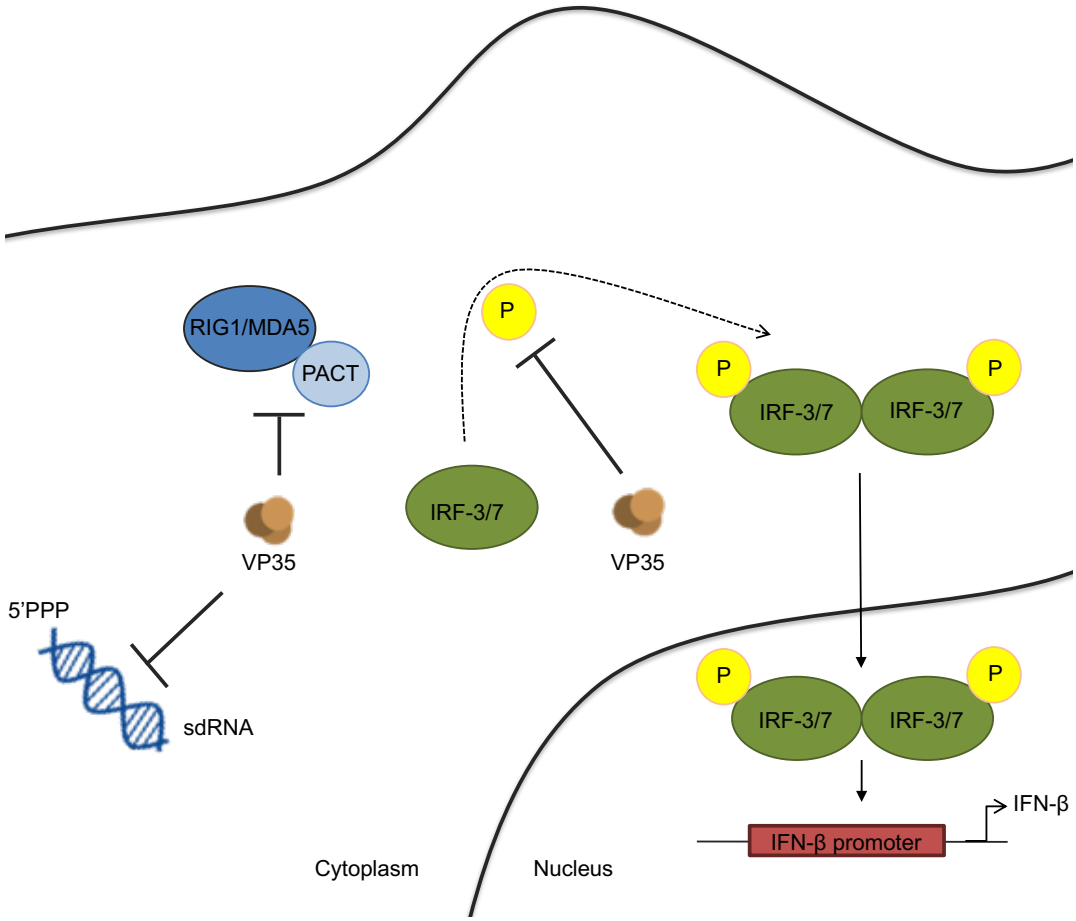

B)

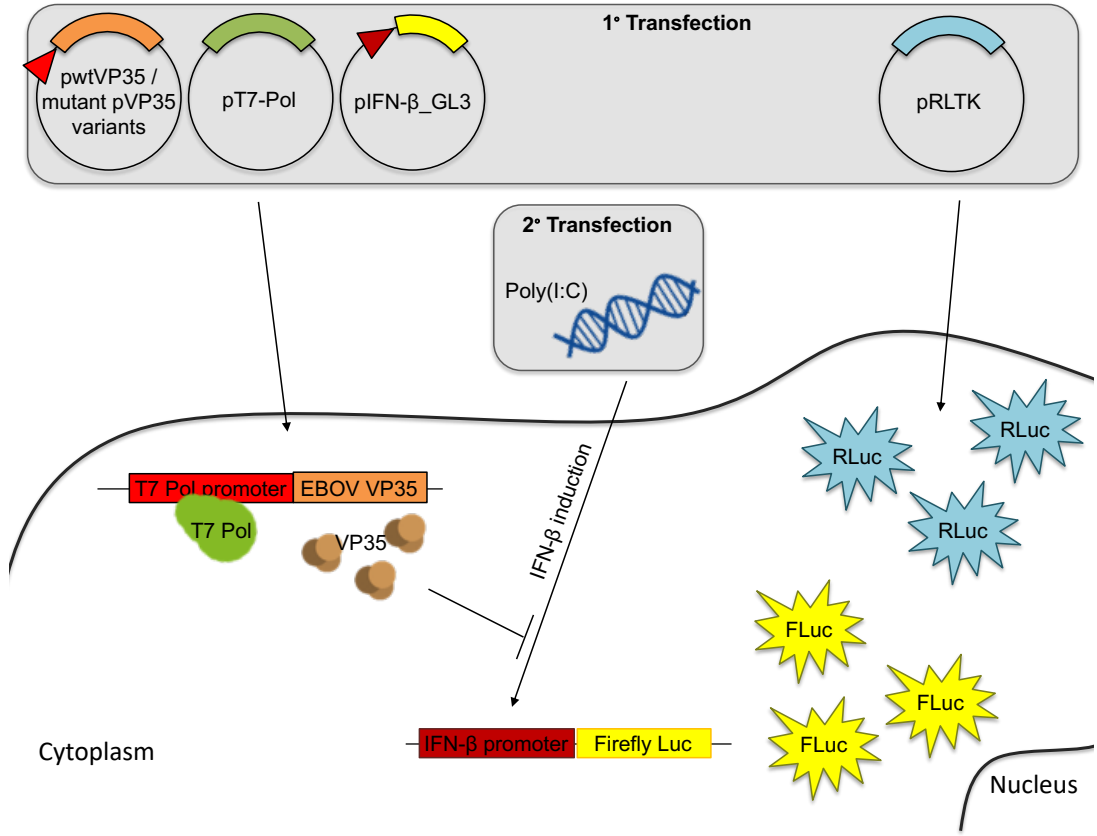

Figure 5.7. Schematic representation of IFN-β induction repression by EBOV VP35. *A) EBOV VP35 blocks the detection of viral RNA by cytosolic helicases RIG-1/MDA5 and impedes the phosphorylation and nuclear translocation of the transcription factor IRF-3/7. B) IFN-β reporter assay in 293T cells. 24 hours after 293T cells are plated in 24 well dishes, pwtVP35 or mutated VP35 proteins, pIFN-β_GL3, pT7-Pol and pRLTK are transfected with Lipofectamine™ 3000 and incubated at 37℃, 5% CO_2. Media is replaced with fresh DMEM and 2.5μg of poly(I:C) is transfected with Lipofectamine™ 2000 and incubated for 24 hours before cells are lysed. The synthetic double-stranded analog Poly(I:C) is recognised by TRL-3, RIG-1/MDA5 and PKR and induces signalling via multiple inflammatory pathways and the expression of IFN-β. pIFN-β_GL3 encodes the reporter gene Firefly luciferase, which is transcribed if IFN-β is present due to its IFN-β promoter. Therefore, detection of Firefly luciferase (FLuc) in cell lysates is indicative of IFN-β expression. pRLTK encodes Renilla luciferase and its expression (RLuc) is used as a control for normalisation of the Firefly measurements. The expression of VP35 is under the control of a T7 polymerase promoter, and its presence antagonises the induction of IFN-β.*

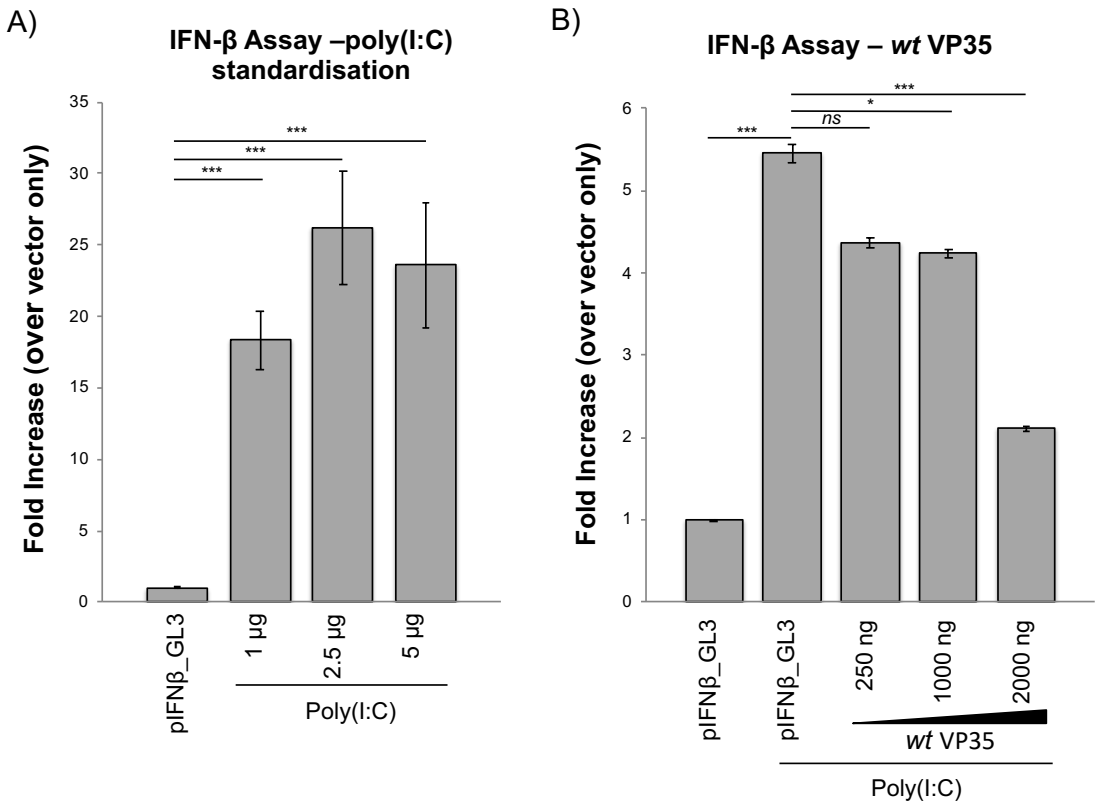

Figure 5.8. Standardisation of the IFN-β reporter assay in 293T cells. *DLA on 293T cells transfected with the IFN-β assay plasmids. (A) Different poly(I:C) concentrations were tested to assess the maximum IFN-β expression; and (B) different quantities of transfected wild-type EBOV VP35 encoding vectors were tested to assess the amounts required to observe increasing levels of IFN-β antagonism. Assays were performed in 24-well plates and each condition was done in triplicate. To assess significance, a t-test was applied between conditions (n/s non-significant, *p-value<0.05, **p-value<0.01, ***p-value<0.001).*

5.3.4.2. Comparison of the effects on the IFN-β induction inhibition between wild-type VP35 and single mutated VP35 proteins.

Once the IFN-β reporter assay was optimised, the effect of each single mutation in EBOV VP35 on the IFN-β induction and antagonism in 293T cells was determined. As shown in Table 5.3, cells transfected with pIFN-β_GL3, pRLTK, pT7-Pol and the empty vector pUC57 were used as negative and positive controls for the IFN-β induction, with a secondary transfection with poly(I:C) in the case of the positive one. The amounts 250ng, 1000ng and 2000ng of each mutated EBOV VP35-encoding plasmid were compared to the same amounts of *wt* VP35 and its effect on IFN-β antagonism when inflammatory pathways were induced with poly(I:C). The empty vector pUC57 was added to each well to have a 2000ng total amount of pVP35+pUC57. Amounts of pT7-Pol were adjusted to amounts of pVP35. Each condition was performed in triplicate for statistical analysis, at once and with the same 293T cell passage number to reduce experimental variation. A DLA was performed 24 hours after IFN-β induced cells were lysed. *Firefly* luciferase values were normalised with *Renilla* luciferase measurements. The functionality of $VP35_{M68T}$, $VP35_{F249L}$ and $VP35_{F330L}$ was intact and a dose-response curve was observed in all the different expression levels tested. The more the VP35 expressed, the higher the suppression of IFN-β and, therefore, the less *Firefly* luciferase activity measured in the system (Figure 5.9A). The only exception was $VP35_{F330L}$, whose antagonism function seemed to be saturated at a transfected amount of 1000ng onwards.

If comparisons are made between VP35 variants at the level of 250ng of transfected cDNA condition (Figure 5.9B), the three mutated viral proteins seemed to have a significantly better performance at blocking the induction of IFN-β compared to *wt* VP35. However, *wt* VP35 at 1000ng displayed a higher IFN-β antagonism than $VP35_{M68T}$ and $VP35_{F249L}$ when 1000ng and 2000ng of viral protein-encoding plasmids were transfected. These results may suggest that at low concentrations of VP35, variants $VP35_{M68T}$, $VP35_{F249L}$ and $VP35_{F330L}$ have a faster immune evasion regarding the IFN-β cellular induction. Nevertheless, at higher protein amounts, they do not display an advantage for the cellular IFN-β expression compared to *wt* VP35.

A western blotting was performed with the cell lysates in order to validate the expression of each variant of EBOV VP35. The reporter activity of the system was detected by specific antibodies against *Firefly* luciferase (LUC), and the housekeeping protein GAPDH was detected as loading control of the total protein amounts run in each well during the SDS-PAGE procedure (Figure 5.9C). At equal total protein amounts loaded, western blots showed differences between the abundance of the different VP35 protein variants. EBOV *wt* VP35 and $VP35_{L249F}$ seemed to be more efficient at being expressed or more stable, making intrinsic protein processing or stability determinants the cause of such differences at their IFN-β antagonism function.

Table 5.3. Plasmids and amount of cDNA used in the IFN-β reporter assay. *Different amounts of wtVP35 and vectors encoding single non-synonymous mutations $VP35_{M68T}$, $VP35_{L249F}$ or $VP35_{L330F}$ were co-transfected with the reporter plasmid pIFN-β_GL3, the Renilla luciferase-encoding plasmid pRLTK for normalisation, pT7-Pol and the empty vector pUC57. The amounts in the table are given in microliters (μl) from plasmid stocks at 500ng/μl except for pRLTK (*100ng/μl). 24 hours post primary transfection, cells were transfected again with the IFN-β inducer poly(I:C). Primary transfection was performed with 1μl of Lipofectamine3000™ and 1.5μl P3000 reagent per well. Secondary transfection was performed with 2μl of Lipofectamine2000™ per well. Amounts of plasmids given reflect that each condition was performed in triplicate and in a 24-well plate format.*

	IFN-β_Luc		***wt* VP35**			**$VP35_{M68T}$**			**$VP35_{L249F}$**			**$VP35_{F330L}$**		
(μl)	**-**	**+**	**250ng**	**1ug**	**2ug**	**250ng**	**1ug**	**2ug**	**250ng**	**1ug**	**2ug**	**250ng**	**1ug**	**2ug**
pIFN-β_GL3	3	3	3	3	3	3	3	3	3	3	3	3	3	3
***pRLTK**	1.5	1.5	1.5	1.5	1.5	1.5	1.5	1.5	1.5	1.5	1.5	1.5	1.5	1.5
pT7-Pol	6	6	1.5	6	12	1.5	6	12	1.5	6	12	1.5	6	12
pVP35		-	1.5	6	12	-	-	-	-	-	-	-	-	-
$pVP35_{M68T}$		-	-	-	-	1.5	6	12	-	-	-	-	-	-
$pVP35_{L249F}$		-	-	-	-	-	-	-	1.5	6	12	-	-	-
$pVP35_{L330F}$		-	-	-	-	-	-	-	-	-	-	1.5	6	12
pUC57	12	12	10.5	6	-	10.5	6	-	10.5	6	-	10.5	6	-
Poly(I:C)	-	7.5	7.5	7.5	7.5	7.5	7.5	7.5	7.5	7.5	7.5	7.5	7.5	7.5

A)

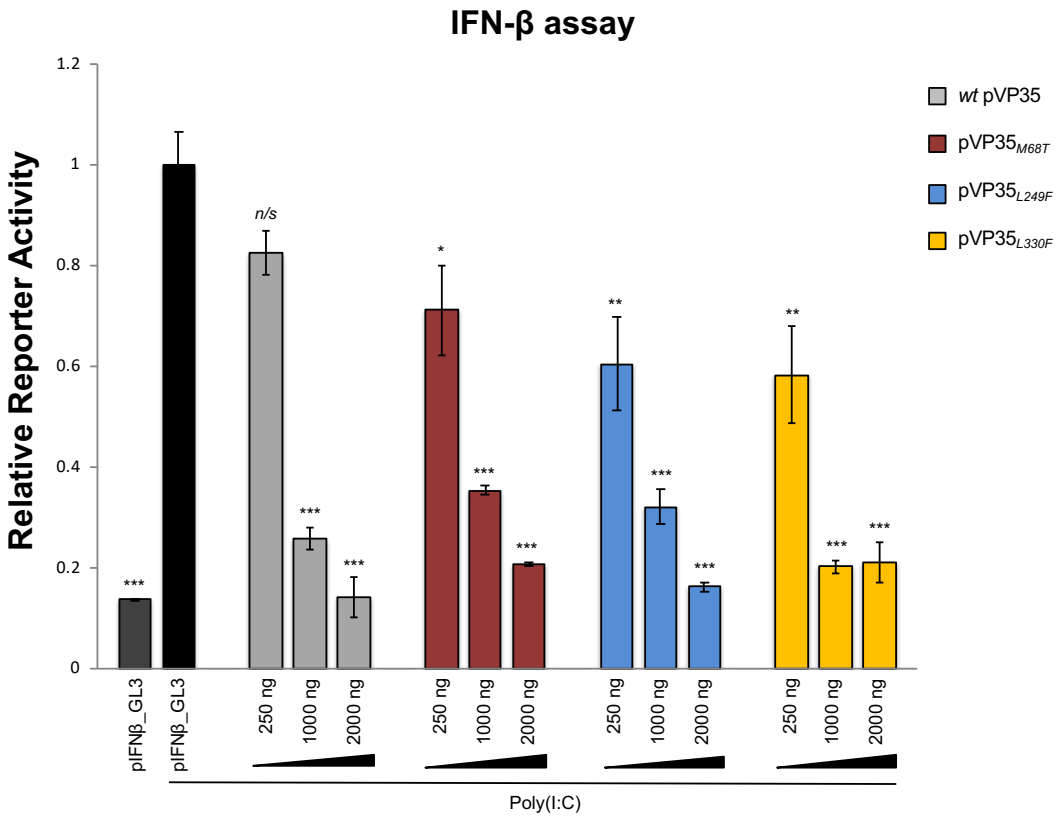
IFN-β assay
Relative Reporter Activity
1.2
1
0.8
0.6
0.4
0.2
0
wt pVP35
pVP35M68T
pVP35L249F
pVP35L330F
n/s
*
**
***
pIFNβ_GL3
pIFNβ_GL3
250 ng
1000 ng
2000 ng
Poly(I:C)

B)

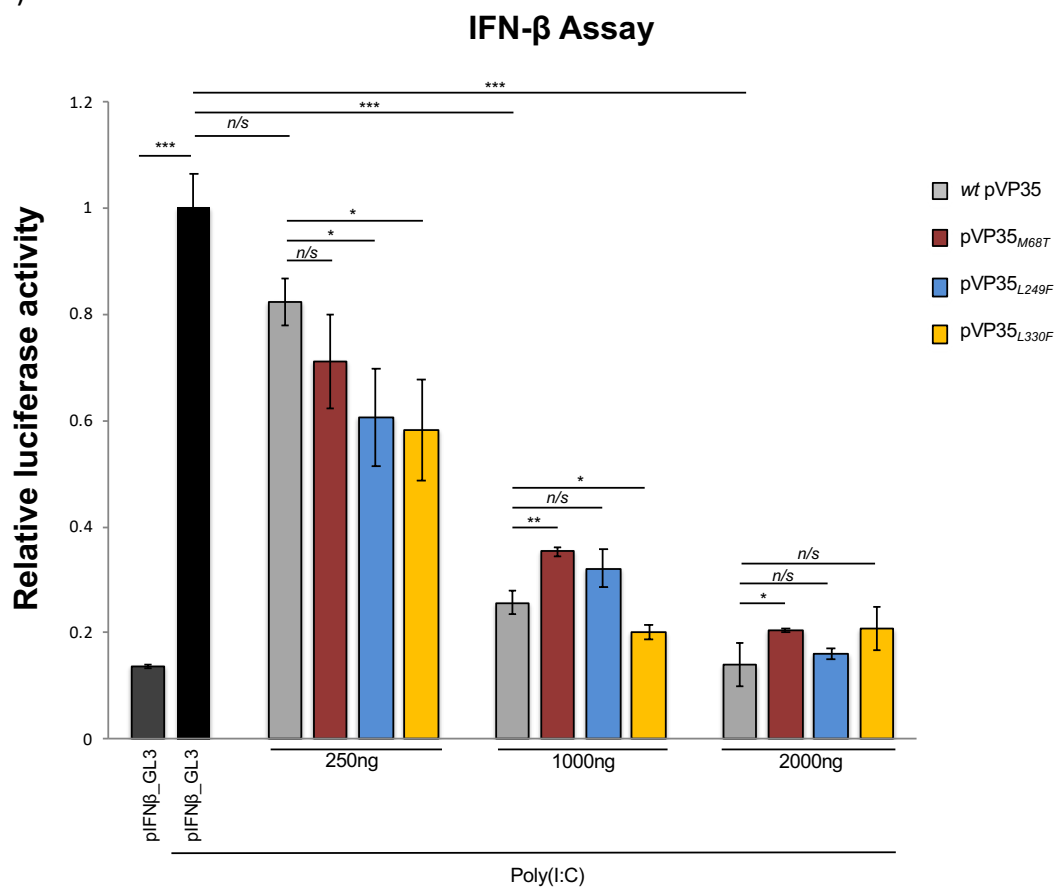
IFN-β Assay
Relative luciferase activity
1.2
1
0.8
0.6
0.4
0.2
0
wt pVP35
pVP35M68T
pVP35L249F
pVP35L330F
n/s
*
**
***
pIFNβ_GL3
pIFNβ_GL3
250ng
1000ng
2000ng
Poly(I:C)

C)

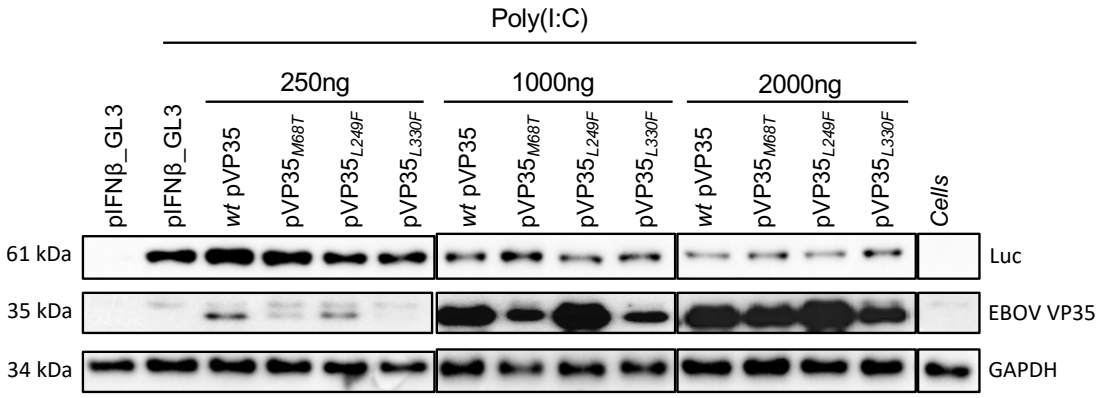

Figure 5.9. IFN-β antagonism at different amounts of transfected plasmids encoding EBOV wt VP35, VP35$_{M68T}$, VP35$_{L249F}$ and VP35$_{L330F}$ encoding plasmids in cells. *293T cells were seeded at 1.6x10^5 cells per well in a 24-well dish format. pVP35, pIFN-β_GL3, pRLTK, pUC57 and pT7-Pol were transfected with Lipofectamine™3000. Poly(I:C) was transfected with Lipofectamine™ 2000 and cells were incubated for 24 hours. Significance between conditions was assessed with a t-test (n/s non-significant, *p-value<0.05, **p-value<0.01, ***p-value<0.001). A) Comparison between different amounts of each EBOV VP35 variant. Significance was assessed between each condition and the positive control. B) Comparison between EBOV VP35 variants at each plasmid amount transfection (250ng, 1000ng and 2000ng). T-tests for significance were assessed between wt VP35 and VP35 variants at each transfected plasmid amount. C) Detection of Firefly luciferase (LUC), EBOV VP35 and GAPDH proteins with specific antibodies on a western blot membrane. For each condition, 2.5ug of total protein was loaded in a polyacrylamide gel for SDS-PAGE.*

5.4. Discussion

Virulence of a pathogen is multifactorial in nature. The study of viral mutations during the course of an epidemic is essential to monitor the evolution of circulating virus populations. Non-synonymous mutations can have relevant effects on viral virulence (Dietzel et al., 2017b), antiviral therapy efficiency (Kugelman et al., 2015) or virus adaptation to novel species (Dowall et al., 2014; Pappalardo et al., 2017). The 2013-2016 West African EBOV outbreak was the largest on record and unprecedented in terms of cases and fatalities (Holmes et al., 2016). Since EBOV discovery in 1976, sporadic outbreaks have occurred in Central and West Africa (Breman et al., 2016). Due to the shortness and relatively few cases of previous outbreaks, consistent changes in the viral genome sequence had been observed but not studied before the West African outbreak, to our knowledge (Leroy et al., 2002; Rodriguez et al., 1999). Next-generation sequencing of clinical samples from the 2013-2016 West African EBOV outbreak allowed the rapid elucidation of naturally occurring single nucleotide polymorphisms (SNPs) that led to discover non-synonymous mutations in the viral protein sequences of the EBOV Makona strain (Carroll et al., 2015; Dietzel et al., 2017b; Dowall et al., 2014; Wong et al., 2019). Nevertheless, a complete characterisation of the impact of dominant non-synonymous mutations is lacking and can help understand the virus enhanced fitness, its mechanisms of virulence across its evolution and its adaptation to novel hosts.

Studies made early in the outbreak claim no gain in virulence from a genetic point of view of the virus since its discovery in 1976 to 2014 (Dunham et al., 2015; Olabode et al., 2015). Nevertheless, later studies proved that naturally occurring mutations like NP_{R111C} or L_{D759G} improved viral infectivity and replication during the West African outbreak, conferring an advantage to the virus during the epidemic (Bedford and Malik, 2016; Wong et al., 2019). For instance, GP_{A82V} is believed to be the cause of the rapid spread of EBOV pandemic early in 2014. Located at the interaction interface of the viral glycoprotein, it made the mammal cell receptor Niemann Pick C1 (NPC1) more susceptible to binding and entry from the endosome to the cytoplasm by EBOV

(Carroll et al., 2015; Diehl et al., 2016). Controversially, Marzi et al. found that Makona EBOV isolates from late 2014 displayed decreased growth kinetics compared to Makona EBOV isolates from early 2014 and to Mayinga EBOV isolates in animal models and tissue culture. Therefore, they concluded that the naturally occurring mutations observed during the 2013-2016 outbreak did not increase viral pathogenicity in animal models (Marzi et al., 2018).

In this study, reverse genetics were used to study the effect of identified naturally occurring mutations in VP35 on the protein functionality in isolation. 950 available Makona EBOV VP35 sequences on GenBank from genomes sampled in 2014 and 2015 were analysed. Several amino acid changes were observed compared to a Mayinga isolate from 1976. Changes from leucine to phenylalanine (L > F) at positions 249 and 330, both substitutions located at the functional IID, were the most abundant. This functional domain of VP35 carries out at least two different functions, involving interaction with binding partners for viral replication and host IFN responses suppression. VP35 IID needs to interact with NP for viral RNA polymerase function and also requires binding to dsRNA to suppress type-I IFN responses (Leung et al., 2010). According to the results presented in this chapter, stability of NP in an EBOV minigenome system seemed to be slightly compromised when $VP35_{L249F}$ was present but enriched when $VP35_{L330F}$ was added instead. Previous studies demonstrated that some residues in the IID are essential for the viral RNA polymerase co-factor function of VP35 but are not critical for the IFN response suppression, and that not all residues involved in viral RNA synthesis require a strong binding to NP. Point mutations R305, K309, R312, K319 and R322 in the IID of EBOV VP35 have been demonstrated to be critical for type-I IFN response inhibition and dsRNA binding and, curiously, are conserved in VP35 of Lloviu virus (LLOV), a member of the *Filoviridae* family that has not been found to infect humans to date (Feagins and Basler, 2015; Hartman et al., 2004; Leung et al., 2010). Regarding the viral RNA polymerase co-factor function, Prins et al. observed that residues R225, K248 and K251 in the CCD are essential for transcription and replication of an EBOV minigenome system (Prins et al., 2010). None of these punctual residues were found to be substituted in the Makona EBOV VP35 sequences from 2014 and 2015 analysed in this study except for R225K, which

had only a 0.53% occurrence frequency. These observations reinforce that these residues are key for VP35 functionality and any substitution at the above-mentioned amino acid positions could have been detrimental for EBOV virulence, as negative mutations affecting vital functions tend to be eliminated.

The effect of mutations at protein residues 68, 249 and 330 on different functions of VP35 and whether they could have been determinant for the course of the largest EBOV outbreak were investigated in this chapter. With the exception of the residue substitution at position 68, mutations occurred early during the West African outbreak and were not found simultaneously in the same genomes. Therefore, their effect on the protein functionality was characterised in isolation. Results proved that these naturally occurring amino acid changes individually enhanced the viral genome transcription and replication function *in vitro* in a minigenome system compared to a *wild type* VP35. Moreover, their IFN-β antagonism function was also evaluated, showing mutation L330F to heighten this immune response evasion mechanism and L249F to do so at lower amounts compared to *wild type* Makona VP35. These findings suggest both mutations could have contributed to disease severity early in the EVD epidemic. Amino acid change at position 68, on the contrary, constituted a neutral mutation that neither enhanced or suppressed the viral RNA polymerase co-factor function, also in accordance with findings by Dunham et al. (Dunham et al., 2015). Nevertheless, residue replacement methionine to threonine (M > T) at position 68 constituted a discrete disadvantage in terms of IFN-β suppression, suggesting that it was the reason why T > M substitution observed in 2002 onwards was favoured and maintained through time.

This study provides evidence that single mutations in a multifunctional viral protein can affect different functions and modulate viral features between virus populations, and that outbreaks should be stopped as soon as possible to avoid the emergence of naturally occurring mutations that confer more virulence to EBOV. Further work should include the characterisation of the combination of these two mutations on both viral replicase activity and IFN-β antagonism performances, as in an *in vivo* EBOV infection there are multiple RNA virus populations infecting a host, having either a

synergic or an antagonistic effect on the infected cells. Moreover, virus-like particles would be an attractive tool to study whether substitutions L249F and L330F get neutralised by compensatory mutations in *VP35* or other viral genes. Nevertheless, EVD severity depends not only on virus genome mutations, but also on other parameters like comorbidities, infection dose, patient health state or quality of the treatment (Hartley et al., 2017). Another limitation of the study is that mutations were studied in cell culture, which is not representative of the complex environment an organism constitutes. To better understand the impact of $VP35_{T68M}$, $VP35_{L249F}$ and $VP35L_{330F}$ or any other mutation observed on the viral performance, suitable animal models should be considered.

Chapter 6: General discussion, conclusions and future perspectives

6.1. General discussion

Ebola virus disease caused more than 28,000 cases and 11,000 deaths during the 2013-2016 West African outbreak and is currently striking again in the Democratic Republic of Congo with a total of 1367 confirmed and probable EVD cases, of which 885 died (case-fatality rate 65%), as of 23rd of April 2019 ("WHO | Ebola virus disease – Democratic Republic of the Congo," 2019). The broad cell tropism the virus has (Geisbert et al., 2003), together with the diverse manifestations that EVD presents, make Ebola virus pathogenicity not completely unveiled and urges for a better understanding of the mechanisms underlying the virus biology in order to guide the development of therapeutics against the disease. Although determinants of patient survival are poorly understood, viral load has been reported to peak 3 to 7 days after the onset of symptoms in patients, being 10 to 100 fold higher in fatal cases than in survivors (Lanini et al., 2015). Thus, viral transcription and replication, conducted by the viral RNP complex, are very attractive viral stages of the virus life cycle to be further studied and targeted by antivirals in order to prevent and revert the outcome of patients presenting a high level of viremia (Martin et al., 2017). Since the viral RNA-dependent polymerase (L) and its co-factor (VP35) are the main players of the above-mentioned processes, this thesis intended to tackle three main themes. Chapter 3 and 4 explored novel and essential interactions between VP35, L and the host cell. In them, the effect of antagonising with small molecule inhibitors two potential host-virus interactions with roles in EBOV transcription and replication in cell culture - DYNLL1 and CALM/calcium – were also examined. Finally, chapter 5 focused on the virus genetics, characterising three non-synonymous mutations in VP35 occurring early in the West African EBOV outbreak. Their effect on VP35's functionality on both viral replication and interferon beta suppression in the host cell were assessed in order to characterise the consequences of having circulating viral populations carrying these mutations.

Co-immunoprecipitation of protein-protein complexes and LC-MS/MS analyses are reliable tools for the elucidation of novel cellular factors that play a key role in viral processes (Pichlmair et al., 2012). This approach helps gaining knowledge on viral

biology and on cellular response to infection, and has been widely used to determine protein-protein interactions between viruses and their hosts, leading to the discovery of promising antiviral cellular targets (Dong et al., 2016; Emmott et al., 2013; García-Dorival et al., 2016, 2014; Martinez-Gil et al., 2017; Munday et al., 2015; Wang et al., 2017; Wu et al., 2011).

6.1.1. Elucidation of the cellular interactome of EBOV VP35 – Chapter 3

In the case of EBOV VP35, this thesis presents the first study of the Makona strain VP35 cellular interactome. Results showed 28 statistically significant host proteins that potentially associate with VP35. Following forward and reverse co-immunoprecipitations, protein-protein complexes were validated by western blot and novel VP35-host interactions were described for the first time. These were CIRBP, PAI1, SDF2L1 and ATP5I. EBOV VP35 interactome also showed a cluster of ribosomal proteins to potentially associate with VP35, suggesting a putative role on modulation of the host translational machinery or the stability of mRNA (Batra et al., 2018). Host chaperones from the TIMM family were also observed in the LC-MS/MS analysis, as well as proteins involved in intracellular transport and cellular motility. These were proteins from the TUBB family and DYNLL1, which had been reported previously to interact with VP35 and to have a role in Ebola virus replication (Kubota et al., 2009; Luthra et al., 2015). Finding DYNLL1 to be one of the top hits in our analysis gave confidence in the outcome of this study. To our knowledge, only Batra et al. did previously elucidate the interactome of EBOV VP35 by using a label-free LC-MS/MS approach in 293T cells, but they expressed Mayinga strain *Zaire ebolavirus* VP35 (GenBank Ref. Number NC_002549.1) (Batra et al., 2018). Although using a very similar approach, when the Makona and Mayinga VP35 cellular interactomes in 293T cells are compared, the only significant PPI that could found in both was DYNLL1. Further studies should be addressed to examine whether the differences observed in both interactomes were due to the affinity tags used or whether Mayinga and Makona strains do associate with the host proteins dissimilarly, as the protein sequences used in the two studies differed in 4 amino acid residues.

6.1.2. Using rabbit reticulocytes to determine protein-protein interactions between EBOV L and the host - Chapter 4

In chapter 4, expression of L-mCherry was challenging in cell culture and a cell-free rabbit reticulocyte system was used alternatively, not making possible to study the cellular interactome of the viral RNA polymerase in mammalian cells. Similar issues with the expression of steady-state amounts of recombinant protein to further proceed with LC-MS/MS were encountered by Batra et al. when they attempted to elucidate EBOV L's cellular interactome (Batra et al., 2018). L-mCherry, being large in size and having the reporter gene inserted in a variable region between functional domains, proved to be functional at replicating the Ebola minigenome system, as expected from similar constructions used previously in other studies for EBOV and other members of the order *Mononegaviridae* (Duprex et al., 2002a; Fix et al., 2011; Hoenen et al., 2012; Ruedas and Perrault, 2009a). Takahashi et al. constructed a FLAG-tagged EBOV L and elucidated viral-host protein associations by LC-MS/MS. They did not validate those interactions but focussed on the functionality of the L cellular partner DNA topoisomerase 1 (TOP1) (Takahashi et al., 2013). This particular association was not found in the analyses showed in this thesis, but other PPIs found by Takahashi et al. were present in our study. These were BAG2 and PRDX1. Validation by western blot of the association between EBOV L and BAG2 gave confidence in the cell-free-EBOV L protein associations observed by LC-MS/MS in this piece of work. Nevertheless, some interactions between the recombinant protein and host factors were unrevealed for the first time and further validated, like CALM and YBX1. Although not all of them were found statistically significant due to the complexity to express EBOV L, they might guide towards future approaches to better understand the interactions between the viral RNA polymerase and the host. Further optimisation of the cellular expression of L-mCherry should be addressed to better understand the cellular associations involved in the viral RNA polymerase functionality.

6.1.3. Antagonism of host proteins DYNLL1 and CALM by using repurposed drugs Ciliobrevin D and W-7, respectively, reduce the EBOV viral RNA synthesis in cell culture – Chapter 3 and 4

Huge efforts are currently being made in order to find effective therapeutics against Ebola virus disease, being host-directed antivirals arising as an alternative to virus-specific drugs (Mohr et al., 2015; Wilde et al., 2014; Zeisel et al., 2015). Virus biology often requires host factors. For instance, endosomal membrane fusion requires cathepsin L and B for GP proteolytic cleavage and Niemann-Pick C1 cholesterol transporter for entry; viral protein progeny needs the host translation machinery; and virion assembly and budding rely on the host cytoskeleton and ubiquitin ligases (Carette et al., 2011; Chandranet al., 2005; Côté et al., 2011; Gordon, et al., 2019). Cellular factor-directed targets are often perceived as non-beneficial for the host as they are not specific and may lead to target-related cytotoxicity (Lin et al., 2013). Knocking-down a host gene or protein expression to basal levels may be sufficient for a virus to have their replication affected. Cells, on the contrary, have redundant pathways that can make up for the suppression of a specific cellular factor, so such risk can be mitigated. Moreover, cellular proteins are less likely to show drug resistance within time. Another advantage of using host-directed therapies is that they represent an alternative to combat quasispecies populations. In this thesis, host factors DYNLL1 (Chapter 3) and CALM (Chapter 4) were antagonised with repurposed small molecule drugs in order to assess their potential as antiviral targets. The use of an EBOV minigenome system (García-Dorival et al., 2016) allowed the study of the effect of Ciliobrevin D and W-7, antagonist drugs targeting DYNLL1 and CALM respectively, on the viral RNA synthesis. In this piece of work, the use of the above-mentioned drugs was demonstrated to be detrimental for EBOV replication in cellular culture at non-cytotoxic concentrations. Findings in chapter 3 reinforced the role of DYNLL1 in the biological cycle of Ebola virus by associating with VP35 (Luthra et al., 2015) and demonstrated that the use of the repurposed drug Ciliobrevin D affects detrimentally viral replication in a minigenome system. Results in chapter 4 demonstrated that CALM interacts with the Ebola virus RNA polymerase and that the host protein antagonism by W-7 diminishes the reporter activity of the previously

mentioned EBOV minigenome. Moreover, cell culture pre-treated with W-7 had previously shown ton inhibit budding of EBOV virus-like particles (Han and Harty, 2007). Additionally, literature shows that both DYNLL1 and CALM are host factors widely used by viruses to carry out different stages of their viral lifecycles (Alonso et al., 2001; Bauer et al., 2015; Bautista-Carbajal et al., 2017; Chattopadhyay et al., 2013; Jacobet al., 2000; Jayappa et al., 2015; Osseman et al., 2018). Although further experiments should be addressed, these findings suggest that Ciliobrevin D and W-7 could constitute broad range host-directed antiviral repurposed drugs.

6.1.4. Chelation of free intracellular ions of calcium correlates to a decrease in EBOV RNA synthesis – Chapter 4

The dependency of EBOV RNA synthesis on free intracellular calcium levels was also demonstrated, potentially through the functionality of Ca^{2+}-dependent enzymes such as CALM, which was previously shown to interact with EBOV L in chapter 4. The ability of some viruses to appropriate or interrupt the calcium signalling pathways and other calcium-dependent cellular processes to their own benefit has been observed in the literature, such as HIV-I, enterovirus, HCV or rotavirus (reviewed in Zhou et al., 2009). Cellular pre-treatment with the intracellular calcium chelator BAPTA-AM proves that an alteration of the calcium homeostasis in the cytoplasm disturbs the EBOV vRNA synthesis. Calcium ions play important roles in the lifecycle of many viruses. Some viral proteins such as Tat and gp120 in HIV-I are able to disturb calcium homeostasis inside the host cell (Lannuzel et al., 1995), some others bind to intracellular calcium ions for structural integrity or functionality, like NSP4 in rotavirus (Bowman et al., 2000) and some virus-host interactions depend on cellular calcium-regulated proteins such as CALM and the HIV-I protein MA (Taylor et al., 2012). Whether a drop in the intracellular free calcium ions level causes a weaker interaction between EBOV L and CALM or whether it affects other calcium-dependent enzymes required for viral replication, disrupting EBOV vRNA synthesis, needs to be further studied.

6.1.5. Naturally occurring mutations in EBOV VP35 during the West African outbreak can potentially enhance viral virulence – Chapter 5

Due to the nature of RNA viruses, they encode RNA polymerases lacking proofreading, allowing viral populations to rapidly adapt to new environments and to develop resistance to antiviral therapeutics. RNA viruses exist as "clouds" of similar variants generated by continuous mutations during genomic replication and limit the prediction of the outcome of an infection (Lauring and Andino, 2010). The examination of the effect of naturally occurring phenotypic changes in EBOV viral proteins during the 2013-2016 West African outbreak could help understand the viral evolutionary dynamics and its relationship to virulence. Although changes in the amino acid sequence of Ebola virus proteins have been reported early during the largest west African EBOV outbreak (Carroll et al., 2015; Deng et al., 2015; Gire et al., 2014; Tong et al., 2015), not many studies have undertaken the investigation of the effect of these naturally occurring mutations on the virus biology up to date. In harmony with the lack of genetic variation reported in 1995 during the EBOV outbreak in Kikwit (Rodriguez et al., 1999), Dunham et al. and Olabode et al. claimed no gain in virulence of EBOV at the beginning of the West African outbreak in 2013 (Dunham et al., 2015; Olabode et al., 2015a). However, naturally occurring mutations in NP, L and GP were found later to enhance viral fitness during the course of the epidemic (Dietzel et al., 2017b; Wong et al., 2019). Currently, there is a lack of a complete definition of the impact of the observed mutations in the viral proteins and their functionality. In chapter 5, it was hypothesised that genomic changes observed in VP35 early in the 2013-2016 EBOV outbreak led to an enhanced viral virulence. Amino acid variation in the EBOV VP35 protein sequence from 950 samples taken at the start of the outbreak, from different countries and available in GenBank, was examined. The effect of mutations L249F and L330F on EBOV VP35 functionality in cell culture was examined in isolation for the first time, as they represented the most occurring non-synonymous amino acid changes among the sequences included in the analysis (4.75% and 2.83%, respectively). Mutation T68M was observed for the first time in an EBOV genome from Gabon sampled in 2002. Methionine was maintained as the major variant from that year on, representing a neutral mutation in viral

transcription and replication terms. L249F and L330F, on the contrary, showed enhanced activity in an EBOV minigenome system compared to the wild type RNP complex proteins. The IFN-β induction antagonism of the mentioned mutations was also examined, as residues 249 and 330 are located within the interferon inhibitory domain of VP35. Amino acid changes M68T, L249F and L330F keep VP35 functional at repressing the IFN-β expression and show significant differences in the IFN-β induction compared to the wild type VP35, enhancing the inhibition of the IFN- β induction when mutated VP35s were added individually at lower amounts. These findings give evidence of the necessity of characterising naturally occurring phenotypic changes in the viral protein sequences, as they can modulate their functionality and enhance virulence in a specific viral population.

6.2. Conclusion

Overall, this thesis presents the cellular interactome of EBOV Makona strain VP35 and the interactome of EBOV Makona strain L in a cell-free expression system for the first time. Moreover, it gives insight into novel virus-host interactions and host factors with potential to be used as antiviral targets to disrupt the Ebola virus replication. DYNLL1 and CALM proved to have a role in the virus replication and repurposed drugs Ciliobrevin D and W-7 showed to have detrimental effects for the virus biological cycle. Also, it is demonstrated that free intracellular Ca^{2+} levels are determinant for EBOV to carry out replication. The characterisation of naturally occurring mutations in VP35 during the largest EBOV outbreak to date in this thesis points out the need of isolating dominant amino acid changes for the study of the consequences in the protein functionality and the study of viral populations.

6.3. Future perspectives

Future perspectives regarding the work done in this thesis involve the examination of EBOV VP35-CIRBP and EBOV L-YBX1 interactions role on the virus replication. A further characterisation of the interaction between EBOV L and CALM may also be of interest, since the host protein is a calcium-dependent modulator of a wide range of enzymes and has been reported to have diverse roles in the biology of other viruses. For instance, the role of the putative CALM-binding domain in EBOV L predicted in Chapter 4 could be further studied by site-directed mutagenesis. Ebola virus is currently a concern in the Democratic Republic of Congo, and it is in the RNA virus nature to present high mutation rates. Continuing with the work done in chapter 5, it would certainly be interesting to keep tracking non-synonymous mutations occurring in the viral proteins and characterising them to examine the virus evolution and implications of such changes on the viral fitness and the effectiveness of antiviral therapeutics. Investigating the effect of non-synonymous mutations in VP35 and extending the work to L's mutations between survivor and deceased patients is quite attractive since these viral proteins are the main players of the viral transcription and replication. Moreover, VP35 in particular, has multiple roles within the virus infectious cycle. Also, there is no evidence whether the amino acid changes observed in this piece of work translate to differences in protein functionality *in vivo* and studies in animal models could help elucidate their real significance during infection.

Chapter 7: References

Albariño, C. G., Guerrero, L. W., Chakrabarti, A. K., & Nichol, S. T. (2018). Transcriptional analysis of viral mRNAs reveals common transcription patterns in cells infected by five different filoviruses. *PLOS ONE*, *13*(8), 1–13. https://doi.org/10.1371/journal.pone.0201827

Alfson, K. J., Worwa, G., Carrion, R., & Griffiths, A. (2016). Determination and Therapeutic Exploitation of Ebola Virus Spontaneous Mutation Frequency. *Journal of Virology*, *90*(5), 2345–2355. https://doi.org/10.1128/JVI.02701-15.Editor

Alonso, C., Miskin, J., Hernaez, B., Fernandez-Zapatero, P., Soto, L., Canto, C., … Escribano, J. M. (2001). African Swine Fever Virus Protein p54 Interacts with the Microtubular Motor Complex through Direct Binding to Light-Chain Dynein. *Journal of Virology*, *75*(20), 9819–9827. https://doi.org/10.1128/JVI.75.20.9819-9827.2001

Amarasinghe, G. K., Bejerman, N., Kim Blasdell, B. R., Alisa Bochnowski, B., Thomas Briese, B., Alexander Bukreyev, B., … Kuhn, J. H. (2017). Taxonomy of the order Mononegavirales: update 2017. *Archives of Virology*, *162*, 2493–2504. https://doi.org/10.1007/s00705-017-3311-7

Arduengo, M., Schenborn, E., & Hurst, R. (2007). *The Role of Cell-Free Rabbit Reticulocyte Expression Systems in Functional Proteomics*. *Cell-free Expression*. Retrieved from https://worldwide.promega.com/-/media/files/resources/product-guides/rabbit-reticulocyte-expression-systems/rrl_expression.pdf?la=en

Audet, J., & Kobinger, G. P. (2015). Immune Evasion in Ebolavirus Infections. *Viral Immunology*, *28*(1), 10–18. https://doi.org/10.1089/vim.2014.0066

Bai, C. Q., Mu, J. S., Kargbo, D., Song, Y. Bin, Niu, W. K., Nie, W. M., … Jiang, J. F. (2016). Clinical and Virological Characteristics of Ebola Virus Disease Patients Treated with Favipiravir (T-705) - Sierra Leone, 2014. *Clinical Infectious Diseases*, *63*(10), 1288–1294. https://doi.org/10.1093/cid/ciw571

Baillie, J. K., & Digard, P. (2013). Influenza — Time to Target the Host ? *The New England Journal of Medicine*, *369*(2), 191–193.

Baize, S., Leroy, E. M., Georges, A. J., Capron, M., & Bedjabaga, I. (2002). Inflammatory responses in Ebola virus-infected patients. *Clnical and*

Expermiental Immunology, *128*(1), 163–168. https://doi.org/https://doi.org/10.1046/j.1365-2249.2002.01800.x

Banadyga, L., Hoenen, T., Ambroggio, X., Dunham, E., Groseth, A., & Ebihara, H. (2017). Ebola virus VP24 interacts with NP to facilitate nucleocapsid assembly and genome packaging. *Scientific Reports*, *7*(1), 1–14. https://doi.org/10.1038/s41598-017-08167-8

Baseler, L., Chertow, D. S., Johnson, K. M., Feldmann, H., & Morens, D. M. (2017). The Pathogenesis of Ebola Virus Disease. *Annual Review of Pathology*, *12*(15), 387–418. https://doi.org/10.1146/annurev-pathol-052016-100506

Basler, C. F., Mikulasova, A., Martinez-Sobrido, L., Paragas, J., Mühlberger, E., Bray, M., … García-Sastre, A. (2003). The Ebola virus VP35 protein inhibits activation of interferon regulatory factor 3. *Journal of Virology*, *77*(14), 7945–7956. https://doi.org/10.1128/JVI.77.14.7945

Basler, C. F., Wang, X., Mühlberger, E., Volchkov, V., Paragas, J., Klenk, H., & Palese, P. (2000). The Ebola virus VP35 protein functions as a type I IFN antagonist. *PNAS*, *97*(22), 12289–12294. https://doi.org/10.1073/pnas.220398297

Batra, J., Hultquist, J. F., Liu, D., Shtanko, O., Von Dollen, J., Satkamp, L., … Krogan, N. J. (2018). Protein Interaction Mapping Identifies RBBP6 as a Negative Regulator of Ebola Virus Replication. *Cell*, *175*(7), 1917-1930.e13. https://doi.org/10.1016/j.cell.2018.08.044

Bauer, A., Nolden, T., Nemitz, S., Perlson, E., & Finke, S. (2015). A Dynein Light Chain 1 Binding Motif in Rabies Virus Polymerase L Protein Plays a Role in Microtubule Reorganization and Viral Primary Transcription. *Journal of Virology*, *89*(18), 9591–9600. https://doi.org/10.1128/JVI.01298-15

Bautista-Carbajal, P., Soto-Acosta, R., Angel-Ambrocio, A. H., Cervantes-Salazar, M., Loranca-Vega, C. I., Herrera-Martínez, M., & del Angel, R. M. (2017). The calmodulin antagonist W-7 (N-(6-aminohexyl)-5-chloro-1-naphthalenesulfonamide hydrochloride) inhibits DENV infection in Huh-7 cells. *Virology*, *501*(December 2016), 188–198. https://doi.org/10.1016/j.virol.2016.12.004

Bedford, T., & Malik, H. S. (2016). Did a Single Amino Acid Change Make Ebola Virus More Virulent? *Cell*, *167*(4), 892–894.

https://doi.org/10.1016/j.cell.2016.10.032

Biedenkopf, N., Lier, C., & Becker, S. (2016). Dynamic Phosphorylation of VP30 Is Essential for Ebola Virus Life, *90*(10), 4914–4925. https://doi.org/10.1128/JVI.03257-15.Editor

Binning, J. M., Wang, T., Luthra, P., Shabman, R. S., Borek, D. M., Liu, G., … Amarasinghe, G. K. (2013). Development of RNA aptamers targeting Ebola virus VP35. *Biochemistry*. https://doi.org/10.1021/bi400704d

Blondot, M. L., Dubosclard, V., Fix, J., Lassoued, S., Aumont-Nicaise, M., Bontems, F., … Sizun, C. (2012). Structure and functional analysis of the RNA- and viral phosphoprotein-binding domain of respiratory syncytial virus M2-1 protein. *PLoS Pathogens*, *8*(5), 1–13. https://doi.org/10.1371/journal.ppat.1002734

Bornholdt, Z. A., Noda, T., Abelson, D. M., Halfmann, P., Wood, M. R., Kawaoka, Y., & Saphire, E. O. (2013). Structural rearrangement of ebola virus vp40 begets multiple functions in the virus life cycle. *Cell*, *154*(4), 763–774. https://doi.org/10.1016/j.cell.2013.07.015

Bowman, G. D., Nodelman, I. M., Levy, O., Lin, S. L., Tian, P., Zamb, T. J., … Schutt, C. E. (2000). Crystal Structure of the Oligomerization Domain of NSP4 from Rotavirus Reveals a Core Metal-binding Site. *Journal of Molecular Biology*, *304*, 861–871. https://doi.org/10.1006/jmbi.2000.4250

Bradfute, S. B., Swanson, P. E., Smith, M. a, Watanabe, E., McDunn, J. E., Hotchkiss, R. S., & Bavari, S. (2010). Mechanisms and consequences of ebolavirus-induced lymphocyte apoptosis. *Journal of Immunology (Baltimore, Md. : 1950)*, *184*(1), 327–335. https://doi.org/10.4049/jimmunol.0901231

Brauburger, K., Boehmann, Y., Krähling, V., & Mühlberger, E. (2016). Transcriptional Regulation in Ebola Virus: Effects of Gene Border Structure and Regulatory Elements on Gene Expression and Polymerase Scanning Behavior. *Journal Fo Virology*, *90*(4), 1898–1909. https://doi.org/10.1128/JVI.02341-15

Breman, J. G., Heymann, D. L., Lloyd, G., McCormick, J. B., Miatudila, M., Murphy, F. A., … Johnson, K. M. (2016). Discovery and Description of Ebola Zaire Virus in 1976 and Relevance to the West African Epidemic during 2013-2016. *Journal of Infectious Diseases*, *214*, S93–S101. https://doi.org/10.1093/infdis/jiw207

Brzózka, K., Finke, S., & Conzelmann, K. (2005). Identification of the Rabies Virus

Alpha / Beta Interferon Antagonist : Phosphoprotein P Interferes with Phosphorylation of Interferon Regulatory Factor 3. *Journal of Virology*, *79*(12), 7673–7681. https://doi.org/10.1128/JVI.79.12.7673

Burke, J., Ghysebrechts, G., Pattyn, S. R., Piot, P., Ruppol, J. F., Thonon, D., … Colbourne, G. (1978). *Ebola haemorrhagic fever in Zaire , 1976*. *Bulletin of the World Health Organization* (Vol. 56).

Calain, P., Monroe, M. C., & Nichol, S. T. (1999). Ebola Virus Defective Interfering Particles and Persistent Infection. *Vilology*, *262*(1), 114–128. https://doi.org/https://doi.org/10.1006/viro.1999.9915

Cannas, V., Daino, G. L., Corona, A., Esposito, F., & Tramontano, E. (2015). A Luciferase Reporter Gene Assay to Measure Ebola Virus Viral Protein 35-Associated Inhibition of Double-Stranded RNA-Stimulated, Retinoic Acid-Inducible Gene 1-Mediated Induction of Interferon β. *Journal of Infectious Diseases*, *212*(Suppl 2), S277–S281. https://doi.org/10.1093/infdis/jiv214

Cantoni, D., & Rossman, J. S. (2018). Ebolaviruses : New roles for old proteins. *PLoS Neglected Tropical Diseases*, *12*(5), 1–17. https://doi.org/10.1371/journal.pntd.0006349

Cardenas, W. B., Loo, Y.-M., Gale, M., Hartman, A. L., Kimberlin, C. R., Martinez-Sobrido, L., … Basler, C. F. (2006). Ebola Virus VP35 Protein Binds Double-Stranded RNA and Inhibits Alpha/Beta Interferon Production Induced by RIG-I Signaling. *Journal of Virology*, *80*(11), 5168–5178. https://doi.org/10.1128/JVI.02199-05

Carette, J. E., Raaben, M., Wong, A. C., Herbert, A. S., Obernosterer, G., Mulherkar, N., … Whelan, S. P. (2011). Ebola virus entry requires the cholesterol transporter Niemann-Pick C1. *Nature*, *477*(7364), 340–343. https://doi.org/10.1038/nature10348

Carroll, M. W., Matthews, D. A., Hiscox, J. A., Elmore, M. J., Pollakis, G., Rambaut, A., … Günther, S. (2015). Temporal and spatial analysis of the 2014-2015 Ebola virus outbreak in West Africa. *Nature*, *524*(7563), 97–101. https://doi.org/10.1038/nature14594

Cesari, M., Pahor, M., & Incalzi, R. A. (2010). Plasminogen activator inhibitor-1 (PAI-1): A key factor linking fibrinolysis and age-related subclinical and clinical

conditions. *Cardiovascular Therapeutics*, *28*(5), 72–91. https://doi.org/10.1111/j.1755-5922.2010.00171.x

Chandran, K., Sullivan, N. J., Felbor, U., Whelan, S. P., & Cunningham, J. M. (2005). Endosomal Proteolysis of the Ebola Virus Glycoprotein Is Necessary for Infection. *Science*, *308*, 1643–1646.

Chang, J. (2017). Pathogenesis of Ebola Viral Haemorrhagic Fever: TTP-like Syndrome Associated with Hepatic Coagulopathy based on "Two Activation Theory of the Endothelium." *Journal of Prevention and Infection Control*, *3*(1), 1–7. https://doi.org/10.21767/2471-9668.100029

Chang, T. H., Kubota, T., Matsuoka, M., Jones, S., Bradfute, S. B., Bray, M., & Ozato, K. (2009). Ebola Zaire virus blocks type I interferon production by exploiting the host SUMO modification machinery. *PLoS Pathogens*. https://doi.org/10.1371/journal.ppat.1000493

Chatel-Caix, L., Germain, Ma.-A., Motorina, A., Bonneil, E., Thibault, P., Baril, M., & Lammarre, D. (2013). A Host YB-1 Ribonucleoprotein Complex Is Hijacked by Hepatitis C Virus for the Control of NS3-Dependent Particle Production. *Journal of Virology*, *87*(21), 11704–11720. https://doi.org/10.1128/JVI.01474-13

Chattopadhyay, S., Basak, T., Nayak, M. K., Bhardwaj, G., Mukherjee, A., Bhowmick, R., … Chawla-Sarkar, M. (2013). Identification of Cellular Calcium Binding Protein Calmodulin as a Regulator of Rotavirus A Infection during Comparative Proteomic Study. *PLoS ONE*, *8*(2), 1–15. https://doi.org/10.1371/journal.pone.0056655

Chu, T. T. T., Sinha, A., Malleret, B., Suwa-, R., Park, J. E., Naidu, R., … Sze, S. K. (2018). Quantitative mass spectrometry of human reticulocytes reveal proteome-wide modifications during maturation. *British Journal of Haematolgy*, *180*, 118–133. https://doi.org/10.1111/bjh.14976

Cilloniz, C., Ebihara, H., Ni, C., Neumann, G., Korth, M. J., Kelly, S. M., … Katze, M. G. (2011). Functional Genomics Reveals the Induction of Inflammatory Response and Metalloproteinase Gene Expression during Lethal Ebola Virus Infection. *Journal of Virology*, *85*(17), 9060–9068. https://doi.org/10.1128/JVI.00659-11

Collins, P. L., Mink, M. A., Hill, M. G., Camargo, E., Grosfeld, H., & Stec, D. S. (1993). Rescue of a 7502-nucleotide (49.3% of full-length) synthetic analog of

respiratory syncytial virus genomic rna. *Virology*. https://doi.org/10.1006/viro.1993.1368

Conzelmann, K. K. (2004). *Reverse genetics of Mononegavirales* (Vol. 283). https://doi.org/10.1007/978-3-662-06099-5

Côté, M., Misasi, J., Ren, T., Bruchez, A., Lee, K., Filone, C. M., … Cunningham, J. (2011). Small molecule inhibitors reveal Niemann–Pick C1 is essential for Ebola virus infection. *Nature*, *477*, 344–350. https://doi.org/10.1038/nature10380

Davey, R. T., Dodd, L., Proschan, M. A., Neaton, J., Neuhaus Nordwall, L., Koopmeiners, J. S., … Malvy, D. (2016). A Randomized, Controlled Trial of ZMapp for Ebola Virus Infection. *New England Journal of Medicine*, *375*(15), 1448–1456. https://doi.org/10.1056/nejmoa1604330

de La Vega, M. A., Stein, D., & Kobinger, G. P. (2015). Ebolavirus Evolution: Past and Present. *PLoS Pathogens*. https://doi.org/10.1371/journal.ppat.1005221

Deng, L., Liu, M., HUa, S., Peng, Y., Wu, A., Qin, F. X.-F., … Jiang, T. (2015). Network of co-mutations in Ebola virus genome predicts the disease lethality. *Cell Research*, *25*, 753–756. https://doi.org/10.1038/cr.2015.54

Diehl, W. E., Lin, A. E., Grubaugh, N. D., Andersen, K. G., Sabeti, P. C., Diehl, W. E., … Kyawe, P. P. (2016). Ebola Virus Glycoprotein with Increased Infectivity Article Ebola Virus Glycoprotein with Increased Infectivity Dominated the 2013 – 2016 Epidemic. *Cell*, *167*(4), 1088-1097.e6. https://doi.org/10.1016/j.cell.2016.10.014

Dietzel, E., Schudt, G., Krähling, V., Matrosovich, M., & Becker, S. (2017a). Functional Characterization of Adaptive Mutations during the West African Ebola Virus Outbreak. *Journal of Virology*, *91*(2), e01913-16. https://doi.org/10.1128/JVI.01913-16

Dietzel, E., Schudt, G., Krähling, V., Matrosovich, M., & Becker, S. (2017b). Functional Characterization of Adaptive Mutations during the West African Ebola Virus Outbreak. *Journal of Virology*, *91*(2), e01913-16. https://doi.org/10.1128/JVI.01913-16

Dimmock, N. J., & Easton, A. J. (2014). Defective Interfering Influenza Virus RNAs: Time To Reevaluate Their Clinical Potential as Broad-Spectrum Antivirals? *Journal of Virology*, *88*(10), 5217–5227. https://doi.org/10.1128/jvi.03193-13

Dodding, M. P., & Way, M. (2011). Coupling viruses to dynein and kinesin-1. *EMBO Journal*, *30*(17), 3527–3539. https://doi.org/10.1038/emboj.2011.283

Dohner, K., Wolfstein, A., Prank, U., Echevarri, C., Dujardin, D., Vallee, R., & Sodeik, B. (2002). Function of dynein and dynactin in herpes simplex virus capsid transport. *Molecular Biology of the Cell*, *13*, 2795–2809. https://doi.org/10.1091/mbc.01

Dolnik, O., Stevermann, L., Kolesnikova, L., & Becker, S. (2015). Marburg virus inclusions: A virus-induced microcompartment and interface to multivesicular bodies and the late endosomal compartment. *European Journal of Cell Biology*, *94*(7–9), 323–331. https://doi.org/10.1016/j.ejcb.2015.05.006

Dong, S., Liu, L., Wu, W., Armstrong, S. D., Xia, D., Nan, H., … Chen, H. (2016). Determination of the interactome of non-structural protein12 from highly pathogenic porcine reproductive and RSV with host cellular proteins using HTP proteomics and identification of HSP70 as a cellular factor for virus replication. *Journal of Proteomics*, *146*, 58–69. https://doi.org/http://dx.doi.org/10.1016/j.jprot.2016.06.019

Dong, X., Armstrong, S. D., Xia, D., Makepeace, B. L., Darby, A. C., & Kadowaki, T. (2017). Draft genome of the honey bee ectoparasitic mite, Tropilaelaps mercedesae, is shaped by the parasitic life history. *GigaScience*, *6*(3), 1–17. https://doi.org/10.1093/gigascience/gix008

Dowall, S. D., Matthews, D. A., García-Dorival, I., Taylor, I., Kenny, J., Hertz-Fowler, C., … Hiscox, J. A. (2014). Elucidating variations in the nucleotide sequence of Ebola virus associated with increasing pathogenicity. *Genome Biology*, *15*(11), 540. https://doi.org/10.1186/s13059-014-0540-x

Dunham, E. C., Banadyga, L., Groseth, A., Chiramel, A. I., Best, S. M., Ebihara, H., … Hoenen, T. (2015). Assessing the contribution of interferon antagonism to the virulence of West African Ebola viruses. *Nature Communications*, *6*(8000), 1–6. https://doi.org/10.1038/ncomms9000

Duprex, W. P., Collins, F. M., & Rima, B. K. (2002a). Modulating the function of the measles virus RNA-dependent RNA polymerase by insertion of green fluorescent protein into the open reading frame. *Journal of Virology*, *76*(14), 7322–7328. https://doi.org/Doi 10.1128/Jvi.76.14.7322-7328.2002

Duprex, W. P., Collins, F. M., & Rima, B. K. (2002b). Modulating the Function of the Measles Virus RNA-Dependent RNA Polymerase by Insertion of Green Fluorescent Protein into the Open Reading Frame Modulating the Function of the Measles Virus RNA-Dependent RNA Polymerase by Insertion of Green Fluorescent Pro. *Journal of Virology*, *76*(14), 7322–7328. https://doi.org/10.1128/JVI.76.14.7322

Ebola Situation Report - 4 November 2015 | Ebola. (2015). Retrieved March 17, 2019, from http://apps.who.int/ebola/current-situation/ebola-situation-report-4-november-2015

Ebola Virus Disease Distribution Map: Cases of Ebola Virus Disease in Africa Since 1976 | 2014-2016 Outbreak West Africa | History | Ebola (Ebola Virus Disease) | CDC. (2018). Retrieved March 17, 2019, from https://www.cdc.gov/vhf/ebola/history/distribution-map.html

Edwards, M. R., Liu, G., Mire, C. E., Sureshchandra, S., Luthra, P., Yen, B., … Basler, C. F. (2016). Differential Regulation of Interferon Responses by Ebola and Marburg Virus VP35 Proteins. *Cell Reports*. https://doi.org/10.1016/j.celrep.2016.01.049

Eliseeva, I. A., Kim, E. R., Guryanov, S. G., Ovchinnikov, L. P., & Lyabin, D. N. (2011). Y-Box-Binding Protein 1 (YB-1) and Its Functions. *Biochemistry*, *76*(13), 1402–1433.

Elshabrawy, H. A., Erickson, T. B., & Prabhakar, B. S. (2015). Ebola virus outbreak, updates on current therapeutic strategies. *Reviews in Medical Virology*. https://doi.org/10.1002/rmv.1841

Emmott, E., Munday, D., Bickerton, E., Britton, P., Rodgers, M. A., Whitehouse, A., … Hiscox, J. A. (2013). The Cellular Interactome of the Coronavirus Infectious Bronchitis Virus Nucleocapsid Protein and Functional Implications for Virus Biology. *Journal of Virology*, *87*(17), 9486–9500. https://doi.org/10.1128/JVI.00321-13

Espeland, E. M., Tsai, C. W., Larsen, J., & Disbrow, G. L. (2018). Safeguarding against Ebola: Vaccines and therapeutics to be stockpiled for future outbreaks. *PLoS Neglected Tropical Diseases*, *12*(4), 2013–2016. https://doi.org/10.1371/journal.pntd.0006275

Evans, D. K., Goldstein, M., & Popova, A. (2015). Health-care worker mortality and the legacy of the Ebola epidemic. *The Lancet Global Health*, *3*(8), e439–e440. https://doi.org/10.1016/S2214-109X(15)00065-0

Feagins, A. R., & Basler, C. F. (2015). Lloviu virus VP24 and VP35 proteins function as innate immune antagonists in human and bat cells. *Virology*, *485*, 145–152. https://doi.org/10.1016/j.virol.2015.07.010

Feldmann, H., & Geisbert, T. W. (2011). Ebola haemorrhagic fever. *The Lancet*, *377*(9768), 849–862. https://doi.org/10.1016/S0140-6736(10)60667-8

Firestone, A. J., Weinger, J. S., Maldonado, M., Barlan, K., Langston, L. D., O'Donnell, M., … Chen, J. K. (2012). Small-molecule inhibitors of the AAA+ ATPase motor cytoplasmic dynein. *Nature*, *484*(7392), 125–129. https://doi.org/10.1038/nature10936

Fitzpatrick, G., Vogt, F., Gbabai, O. B. M., Decroo, T., Keane, M., De Clerck, H., … Van Herp, M. (2015). The Contribution of Ebola Viral Load at Admission and Other Patient Characteristics to Mortality in a Médecins Sans Frontières Ebola Case Management Centre, Kailahun, Sierra Leone, June-October 2014. *Journal of Infectious Diseases*, *212*(10), 1752–1758. https://doi.org/10.1093/infdis/jiv304

Fix, J., Galloux, M., Blondot, M.-L., & Eléouët, J.-F. (2011). The Insertion of Fluorescent Proteins in a Variable Region of Respiratory Syncytial Virus L Polymerase Results in Fluorescent and Functional Enzymes But with Reduced Activities. *The Open Virology Journal*, *5*, 103–108. https://doi.org/10.2174/1874357901105010103

Francica, J. R., Varela-Rohena, A., Medvec, A., Plesa, G., Riley, J. L., & Bates, P. (2010). Steric shielding of surface epitopes and impaired immune recognition induced by the Ebola virus glycoprotein. *PLoS Pathogens*, *6*(9). https://doi.org/10.1371/journal.ppat.1001098

Freiberg, A., Dolores, L. K., Enterlein, S., & Flick, R. (2008). Establishment and characterization of plasmid-driven minigenome rescue systems for Nipah virus: RNA polymerase I- and T7-catalyzed generation of functional paramyxoviral RNA. *Virology*, *370*(1), 33–44. https://doi.org/10.1016/j.virol.2007.08.008

Fuentes, S. M., Sun, D., Schmitt, A. P., & He, B. (2010). Phosphorylation of paramyxovirus phosphoprotein and its role in viral gene expression. *Future*

Microbiology, *5*(1), 9–13. https://doi.org/10.2217/fmb.09.93

Furuta, Y., Komeno, T., & Nakamura, T. (2017). Favipiravir (T-705), a broad spectrum inhibitor of viral RNA polymerase. *Procedings of the Japan Academy Series B*, *93*(7), 449–463. https://doi.org/10.2183/pjab.93.027

Galet, H., Hallett, D., & Prevec, L. (1976). Analysis of In Vitro Transcription Products of Intracellular Vesicular Stomatitis Virus RNA Polymerase. *Journal of Virology*, *19*(2), 467–474.

García-Dorival, I., Wu, W., Armstrong, S. D., Barr, J. N., Carroll, M. W., Hewson, R., & Hiscox, J. A. (2016). Elucidation of the Cellular Interactome of Ebola Virus Nucleoprotein and Identification of Therapeutic Targets. *Journal of Proteome Research*, *15*(12), 4290–4303. https://doi.org/10.1021/acs.jproteome.6b00337

García-Dorival, I., Wu, W., Dowall, S., Armstrong, S., Touzelet, O., Wastling, J., … Hiscox, J. A. (2014). Elucidation of the ebola virus VP24 cellular interactome and disruption of virus biology through targeted inhibition of host-cell protein function. *Journal of Proteome Research*, *13*(11), 5120–5135. https://doi.org/10.1021/pr500556d

García-Mayoral, M. F., Rodríguez-Crespo, I., & Bruix, M. (2011). Structural models of DYNLL1 with interacting partners: African swine fever virus protein p54 and postsynaptic scaffolding protein gephyrin. *FEBS Letters*, *585*(1), 53–57. https://doi.org/10.1016/j.febslet.2010.11.027

García, M., Cooper, A., Shi, W., Bornmann, W., Carrion, R., Kalman, D., & Nabel, G. J. (2012). Productive replication of ebola virus is regulated by the c-Abl1 tyrosine kinase. *Science Translational Medicine*, *4*(123), 1–11. https://doi.org/10.1126/scitranslmed.3003500

GC, J. B., Gerstman, B. S., & Chapagain, P. P. (2017). Membrane association and localization dynamics of the Ebola virus matrix protein VP40. *Biochimica et Biophysica Acta - Biomembranes*, *1859*(10), 2012–2020. https://doi.org/10.1016/j.bbamem.2017.07.007

Geisbert, T. W., Young, H. A., Jahrling, P. B., Davis, K. J., Kagan, E., & Hensley, L. E. (2003). Mechanisms Underlying Coagulation Abnormalities in Ebola Hemorrhagic Fever: Overexpression of Tissue Factor in Primate Monocytes/Macrophages Is a Key Event. *The Journal of Infectious Diseases*,

188(11), 1618–1629. https://doi.org/10.1086/379724

Geisbert, T. W., Young, H. A., Jahrling, P. B., Davis, K. J., Larsen, T., Kagan, E., & Hensley, L. E. (2003). Pathogenesis of Ebola hemorrhagic fever in primate models: evidence that hemorrhage is not a direct effect of virus-induced cytolysis of endothelial cells. *The American Journal of Pathology*, *163*(6), 2371–2382. https://doi.org/10.1016/S0002-9440(10)63592-4

Geller, R., Taguwa, S., & Frydman, J. (2012). Broad action of Hsp90 as a host chaperone required for viral replication. *Biochimica et Biophysica Acta - Molecular Cell Research*, *1823*(3), 698–706. https://doi.org/10.1016/j.bbamcr.2011.11.007

Gentili, M., Kowal, J., Tkach, M., Satoh, T., Lahaye, X., Conrad, C., … Manel, N. (2015). Transmission of innate immue signaling by packaging of cGAMP in viral particles. *Science*, *349*(6253), 1232–1236. https://doi.org/10.1126/science.aab3628

Gire, S. K., Goba, A., Andersen, K. G., Sealfon, R. S. G., Park, D. J., Kanneh, L., … Sabeti, P. C. (2014). Genomic surveillance elucidates Ebola virus origin and transmission during the 2014 outbreak. *Science*, *345*(6202), 1369–1372.

Goldstein, T., Anthony, S. J., Gbakima, A., Bird, B. H., Bangura, J., Tremeau-Bravard, A., … Mazet, J. A. K. (2018). The discovery of Bombali virus adds further support for bats as hosts of ebolaviruses. *Nature Microbiology*, 1. https://doi.org/10.1038/s41564-018-0227-2

Gordon, T. B., Hayward, J. A., Marsh, G. A., Baker, M. L., & Tachedjian, G. (2019). Host and Viral Proteins Modulating Ebola and Marburg Virus Egress. *Viruses*, *11*(25), 1–24. https://doi.org/10.3390/v11010025

Greer, L. F., & Szalay, A. A. (2002). Imaging of light emission fron the expression of liciferases in living cells and organisms: a review. *Luminescence*, *17*(1), 43–74. https://doi.org/doi:10.1002/bio.676.

Groseth, A., Charton, J. E., Sauerborn, M., Feldmann, F., Jones, S. M., Hoenen, T., & Feldmann, H. (2009). The Ebola virus ribonucleoprotein complex: A novel VP30-L interaction identified. *Virus Research*, *140*(1–2), 8–14. https://doi.org/10.1016/j.virusres.2008.10.017

Haasnoot, J., De Vries, W., Geutjes, E. J., Prins, M., De Haan, P., & Berkhout, B.

(2007). The ebola virus VP35 protein is a suppressor of RNA silencing. *PLoS Pathogens*, *3*(6), 0794–0803. https://doi.org/10.1371/journal.ppat.0030086

Han, Z., Boshra, H., Sunyer, J. O., Zwiers, S. H., Paragas, J., & Harty, R. N. (2003). Biochemical and Functional Characterization of the EbolaVirus VP24 Protein: Implications for a Role in Virus Assembly and Budding. *Journal of Virology*, *77*(3), 1793–1800. https://doi.org/10.1128/JVI.77.3.1793

Han, Z., & Harty, R. N. (2007). Influence of calcium/calmodulin on budding of Ebola VLPs: Implications for the involvement of the Ras/Raf/MEK/ERK pathway. *Virus Genes*, *35*(3), 511–520. https://doi.org/10.1007/s11262-007-0125-9

Hanada, K., Suzuki, Y., & Gojobori, T. (2004). A large variation in the rates of synonymous substitution for RNA viruses and its relationship to a diversity of viral infection and transmission modes. *Molecular Biology and Evolution*, *21*(6), 1074–1080. https://doi.org/10.1093/molbev/msh109

Hartley, M. A., Young, A., Tran, A. M., Okoni-Williams, H. H., Suma, M., Mancuso, B., … Faouzi, M. (2017). Predicting Ebola Severity: A Clinical Prioritization Score for Ebola Virus Disease. *PLoS Neglected Tropical Diseases*, *11*(2), 1–20. https://doi.org/10.1371/journal.pntd.0005265

Hartman, A. L., Towner, J. S., & Nichol, S. T. (2004). A C-terminal basic amino acid motif of Zaire ebolavirus VP35 is essential for type I interferon antagonism and displays high identity with the RNA-binding domain of another interferon antagonist, the NS1 protein of influenza a virus. *Virology*, *328*(2), 177–184. https://doi.org/10.1016/j.virol.2004.07.006

Henao-Restrepo, A. M., Camacho, A., Longini, I. M., Watson, C. H., Edmunds, W. J., Egger, M., … Kieny, M. P. (2017). Efficacy and effectiveness of an rVSV-vectored vaccine in preventing Ebola virus disease: final results from the Guinea ring vaccination, open-label, cluster-randomised trial (Ebola Ça Suffit!). *The Lancet*, *389*(10068), 505–518. https://doi.org/10.1016/S0140-6736(16)32621-6

Hoenen, T, Safronetz, D., Groseth, A., Wollenberg, K., Koita, B., Fall, I., … Sow, S. (2015). Mutation rate and genotype variation of Ebola virus from Mali case sequences, *348*(6230), 117–119.

Hoenen, Thomas, Shabman, R. S., Groseth, A., Herwig, A., Weber, M., Schudt, G., … Feldmann, H. (2012). Inclusion Bodies Are a Site of Ebolavirus Replication.

American Society for Microbiology, *8*(21), 11779–11788. https://doi.org/10.1128/JVI.01525-12

Holmes, E. C., Dudas, G., Rambaut, A., & Andersen, K. G. (2016). The evolution of Ebola virus: Insights from the 2013-2016 epidemic. *Nature*, *538*(7624), 193–200. https://doi.org/10.1038/nature19790

Hook, P., & Vallee, R. B. (2006). The dynein family at a glance. *Journal of Cell Science*, *119*(21), 4369–4371. https://doi.org/10.1242/jcs.03176

Huang, Y., Xu, L., Sun, Y., & Nabel, G. J. (2002). The assembly of Ebola virus nucleocapsid requires virion-associated proteins 35 and 24 and posttranslational modification of nucleoprotein. *Molecular Cell*, *10*(2), 307–316. https://doi.org/10.1016/S1097-2765(02)00588-9

Ikegami, T., Peters, C. J., & Makino, S. (2005). Rift Valley Fever Virus Nonstructural Protein NSs Promotes Viral RNA Replication and Transcription in a Minigenome System. *Journal of Virology*, *79*(9), 5606–5615. https://doi.org/10.1128/jvi.79.9.5606-5615.2005

Jacob, Y., Badrane, H., Ceccaldi, P. E., Tordo, N., & Lyssavirus, L. (2000). Cytoplasmic dynein LC8 interacts with lyssavirus phosphoprotein. *Journal of Virology*, *74*(21), 10217–10222. https://doi.org/10.1128/JVI.74.21.10217-10222.2000

Jasenosky, L. D., Neumann, G., & Kawaoka, Y. (2010). Minigenome-based reporter system suitable for high-throughput screening of compounds able to inhibit Ebolavirus replication and/or transcription. *Antimicrobial Agents and Chemotherapy*, *54*(7), 3007–3010. https://doi.org/10.1128/AAC.00138-10

Jayappa, K. D., Ao, Z., Wang, X., Mouland, A. J., Shekhar, S., Yang, X., & Yao, X. (2015). Human Immunodeficiency Virus Type 1 Employs the Cellular Dynein Light Chain 1 Protein for Reverse Transcription through Interaction with Its Integrase Protein. *Journal of Virology*, *89*(7), 3497–3511. https://doi.org/10.1128/JVI.03347-14

Jenkins, G. M., Rambaut, A., Pybus, O. G., & Holmes, E. C. (2002). Rates of molecular evolution in RNA viruses: A quantitative phylogenetic analysis. *Journal of Molecular Evolution*, *54*(2), 156–165. https://doi.org/10.1007/s00239-001-0064-3

Johnson, R. F., McCarthy, S. E., Godlewski, P. J., & Harty, R. N. (2006). Ebola Virus

VP35-VP40 Interaction Is Sufficient for Packaging 3E-5E Minigenome RNA into Virus-Like Particles. *Journal of Virology*, *80*(11), 5135–5144. https://doi.org/10.1128/JVI.01857-05

Jun, S.-R., Leuze, M. R., Nookaew, I., Uberbacher, E. C., Land, M., Zhang, Q., … Ussery, D. W. (2015). Ebolavirus comparative genomics. *FEMS Microbiology Reviews*. https://doi.org/10.1093/femsre/fuv031

Kaletsky, R. L., Francica, J. R., Agrawal-Gamse, C., & Bates, P. (2009). Tetherin-mediated restriction of filovirus budding is antagonized by the Ebola glycoprotein. *Proceedings of the National Academy of Sciences*, *106*(8), 2886–2891. https://doi.org/10.1073/pnas.0811014106

Kaner, J., & Schaack, S. (2016). Understanding Ebola: the 2014 epidemic. *Globalization and Health*, *12*(57), 1–7. https://doi.org/10.1186/s12992-016-0194-4

Kawaguchi, A., Matsumoto, K., & Nagata, K. (2012). YB-1 Functions as a Porter To Lead Influenza Virus Ribonucleoprotein Complexes to Microtubules. *Journal of Virology*, *86*(20), 11086–11095. https://doi.org/10.1128/JVI.00453-12

Kerber, R., Krumkamp, R., DIallo, B., Jaeger, A., Rudolf, M., Lanini, S., … DI Caro, A. (2016). Analysis of Diagnostic Findings from the European Mobile Laboratory in Guéckédou, Guinea, March 2014 Through March 2015. *Journal of Infectious Diseases*, *214*(March 2015), S250–S257. https://doi.org/10.1093/infdis/jiw269

Kimberlin, C. R., Bornholdt, Z. A., Li, S., Woods, V. L., MacRae, I. J., & Saphire, E. O. (2010). Ebolavirus VP35 uses a bimodal strategy to bind dsRNA for innate immune suppression. *Proceedings of the National Academy of Sciences*, *107*(1), 314–319. https://doi.org/10.1073/pnas.0910547107

King, S. M. (2008). Dynein-independent functions of DYNLL1/LC8: Redox state sensing and transcriptional control. *Science Signaling*, *1*(47), 1–4. https://doi.org/10.1126/scisignal.147pe51

Kirchdoerfer, R. N., Abelson, D. M., Li, S., Wood, M. R., & Saphire, E. O. (2015). Assembly of the Ebola Virus Nucleoprotein from a Chaperoned VP35 Complex. *Cell Reports*, *12*(1), 140–149. https://doi.org/10.1016/j.celrep.2015.06.003

Ksiazek, T. G., Rollin, P. E., Williams, A. J., Bressler, D. S., Martin, M. L., Swanepoel, R., … Peters, C. J. (1999). Clinical Virology of Ebola Hemorrhagic Fever (EHF):

Virus , Virus Antigen , and IgG and IgM Antibody Findings among EHF Patients in Kikwit , Democratic Republic of the Congo , 1995. *The Journal of Infectious Disease*, *179*(Suppl 1), 177–187.

Kubota, T., Matsuoka, M., Chang, T.-H., Bray, M., Jones, S., Tashiro, M., … Ozato, K. (2009). Ebolavirus VP35 Interacts with the Cytoplasmic Dynein Light Chain 8. *Journal of Virology*, *83*(13), 6952–6956. https://doi.org/10.1128/JVI.00480-09

Kugelman, J. R., Sanchez-lockhart, M., Andersen, K. G., Gire, S., Park, D. J., Sealfon, R., … Palacios, F. (2015). Evaluation of the Potential Impact of Ebola Virus Genomic Drift on the Efficacy of Sequence-Based Candidate Therapeutics. *MBio*, *6*(1), 2013–2016. https://doi.org/10.1128/mBio.02227-14.Editor

Lanini, S., Portella, G., Vairo, F., Kobinger, G. P., Pesenti, A., Langer, M., … Ippolito, G. (2015). Blood kinetics of Ebola virus in survivors and nonsurvivors. *The Journal of Clinical Investigation*, *125*(12), 4692–4698. https://doi.org/10.1172/JCI83111.who

Lauring, A. S., & Andino, R. (2010). Quasispecies Theory and the Behavior of RNA Viruses. *PLoS Pathogens*, *6*(7), 1–8. https://doi.org/10.1371/journal.ppat.1001005

Lee, J. E., & Saphire, E. O. (2009). Ebolavirus glycoprotein structure and mechanism of entry. *Future Virology*, *4*(6), 621–635. https://doi.org/10.2217/FVL.09.56

Leroy, E. m., Baize, S., Mavoungou, E., & Apetei, C. (2002). Sequence analysis of the GP, NP, VP40 and VP24 genes of Ebola virus isolated from deceased, surviving and asymptomatically infected individuals during the 1996 outbreak in Gabon: Comparative studies and phylogenetic characterization. *Journal of General Virology*, *83*(1), 67–73. https://doi.org/10.1099/0022-1317-83-1-67

Leroy, E. M., Kumulungui, B., Pourrut, X., Rouquet, P., Hassanin, A., Yaba, P., … Swanepoel, R. (2005). Fruit Bats as reservoir of Ebola virus. *Nature*, *438*(7068), 575–576. https://doi.org/10.1038/438575a

Leung, D. W., Ginder, N. D., Fulton, D. B., Nix, J., Basler, C. F., Honzatko, R. B., & Amarasinghe, G. K. (2009). Structure of the Ebola VP35 interferon inhibitory domain. *Proceedings of the National Academy of Sciences*, *106*(2), 411–416. https://doi.org/10.1073/pnas.0807854106

Leung, D. W., Prins, K. C., Basler, C. F., & Amarasinghe, G. K. (2010). Ebolavirus VP35

is a multifunctional virulence factor. *Virulence*, *1*(6), 526–531. https://doi.org/10.4161/viru.1.6.12984

Leung, D. W., Prins, K. C., Borek, D. M., Farahbakhsh, M., M, J., Ramanan, P., … Amarasinghe, G. K. (2010). Structural basis for dsRNA recognition and interferon antagonism by Ebola VP35. *Nature Structural & Molecular Biology*, *17*(2), 165–172. https://doi.org/10.1038/nsmb.1765

Lévy, Y., Lane, C., Piot, P., Beavogui, A. H., Kieh, M., Leigh, B., … Yazdanpanah, Y. (2018). Prevention of Ebola virus disease through vaccination: where we are in 2018. *The Lancet*, *392*(1), 787–790. https://doi.org/10.1016/S0140-6736(18)31710-0

Li, Y., Lu, J., Han, Y., Fan, X., & Ding, S. (2013). RNA Interference Functions as an Antiviral Immunity Mechanism in Mammals. *Science*, *342*(October), 231–234. https://doi.org/10.1126/science.1241911

Lin, K., & Gallay, P. (2013). Curing a viral infection by targeting the host: The example of cyclophilin inhibitors. *Antiviral Research*, *99*(1), 68–77. https://doi.org/10.1016/j.antiviral.2013.03.020

Liu, X., Speranza, E., Muñoz-Fontela, C., Haldenby, S., Rickett, N. Y., Garcia-Dorival, I., … Hiscox, J. A. (2017). Transcriptomic signatures differentiate survival from fatal outcomes in humans infected with Ebola virus. *Genome Biology*, *18*(4). https://doi.org/10.1186/s13059-016-1137-3

LLeonart, M. E. (2010). A new generation of proto-oncogenes: Cold-inducible RNA binding proteins. *Biochimica et Biophysica Acta - Reviews on Cancer*, *1805*(1), 43–52. https://doi.org/10.1016/j.bbcan.2009.11.001

Luthra, P., Jordan, D. S., Leung, D. W., Amarasinghe, G. K., & Basler, C. F. (2015). Ebola Virus VP35 Interaction with Dynein LC8 Regulates Viral RNA Synthesis. *Journal of Virology*, *89*(9), 5148–5153. https://doi.org/10.1128/JVI.03652-14

Luytjes, W., Krystal, M., Enami, M., Parvin, J. D., & Palese, P. (1989). Amplification, expression, and packaging of a foreign gene by influenza virus. *Cell*, *59*(6), 1107–1113. https://doi.org/10.1016/0092-8674(89)90766-6

Ma-Lauer, Y., Lei, J., Hilgenfeld, R., & Von Brunn, A. (2012). Virus-host interactomes - Antiviral drug discovery. *Current Opinion in Virology*, *2*(5), 614–621. https://doi.org/10.1016/j.coviro.2012.09.003

Martin, B., Canard, B., & Decroly, E. (2017). Filovirus proteins for antiviral drug discovery: Structure/function bases of the replication cycle. *Antiviral Research*, *141*, 48–61. https://doi.org/10.1016/j.antiviral.2017.02.004

Martinez-Gil, L., Vera-velasco, N. M., & Mingarro, I. (2017). Exploring the Human-Nipah Virus Protein-Protein Interactome. *Journal of Virology*, *91*(23), 1–18.

Martinez, M. J., Biedenkopf, N., Volchkova, V., Hartlieb, B., Alazard-Dany, N., Reynard, O., … Volchkov, V. (2008). Role of Ebola Virus VP30 in Transcription Reinitiation. *Journal of Virology*, *82*(24), 12569–12573. https://doi.org/10.1128/JVI.01395-08

Marzi, A., Chadinah, S., Haddock, E., Feldmann, F., Arndt, N., Martellaro, C., … Feldmann, H. (2018). Recently Identified Mutations in the Ebola Virus-Makona Genome Do Not Alter Pathogenicity in Animal Models. *Cell Reports*, *23*(6), 1806–1816. https://doi.org/10.1016/j.celrep.2018.04.027

Mateo, M., Carbonnelle, C., Martinez, M. J., Reynard, O., Page, A., Volchkova, V. A., & Volchkov, V. E. (2011). Knockdown of Ebola virus VP24 impairs viral nucleocapsid assembly and prevents virus replication. *Journal of Infectious Diseases*, *204*(SUPPL. 3). https://doi.org/10.1093/infdis/jir311

Matsumoto, K., & Wolffe, A. P. (1998). Gene regulation by Y-box proteins : coupling control of transcription and translation. *Cell Biology*, *8*, 318–323.

Mehedi, M., Falzarano, D., Seebach, J., Hu, X., Carpenter, M. S., Schnittler, H.-J., & Feldmann, H. (2011). A New Ebola Virus Nonstructural Glycoprotein Expressed through RNA Editing. *Journal of Virology*, *85*(11), 5406–5414. https://doi.org/10.1128/JVI.02190-10

Mendoza, E. J., Qiu, X., & Kobinger, G. P. (2016). Progression of Ebola therapeutics during the 2014-2015 outbreak. *Trends in Molecular Medicine*, *22*(2), 164–173. https://doi.org/10.1016/j.molmed.2015.12.005

Meyniel-Schicklin, L., de Chassey, B., André, P., & Lotteau, V. (2012). Viruses and Interactomes in Translation. *Molecular & Cellular Proteomics*, *11*(7), 1–12. https://doi.org/10.1074/mcp.M111.014738

Modrof, J., Becker, S., & Mühlberger, E. (2003). Ebola Virus Transcription Activator VP30 Is a Zinc-Binding Protein. *Journal of Virology*, *77*(5), 3334–3338. https://doi.org/10.1128/JVI.77.5.3334–3338.2003

Modrof, J., Mühlberger, E., Klenk, H. D., & Becker, S. (2002). Phosphorylation of VP30 impairs Ebola virus transcription. *Journal of Biological Chemistry*, *277*(36), 33099–33104. https://doi.org/10.1074/jbc.M203775200

Moghadam, S. R. J., Omidi, N., Bayrami, S., Moghadam, S. J., & SeyedAlinaghi, S. A. (2015). Ebola viral disease: A review literature. *Asian Pacific Journal of Tropical Biomedicine*, *5*(4), 260–267. https://doi.org/10.1016/S2221-1691(15)30341-5

Mohamadzadeh, M., Chen, L., & Schmaljohn, A. L. (2007). How Ebola and Marburg viruses battle the immune system. *Nature Reviews Immunology*, *7*(7), 556–567. https://doi.org/10.1038/nri2098

Mohan, G. S., Li, W., Ye, L., Compans, R. W., & Yang, C. (2012). Antigenic Subversion: A Novel Mechanism of Host Immune Evasion by Ebola Virus. *PLoS Pathogens*, *8*(12). https://doi.org/10.1371/journal.ppat.1003065

Mohan, P. M. K., Barve, M., Chatterjee, A., & Hosur, R. V. (2006). pH driven conformational dynamics and dimer-to-monomer transition in DLC8. *Protein Science : A Publication of the Protein Society*, *15*(2), 335–342. https://doi.org/10.1110/ps.051854906

Mohr, E. L., McMullan, L. K., Lo, M. K., Spengler, J. R., Bergeron, É., Albariño, C. G., … Flint, M. (2015). Inhibitors of cellular kinases with broad-spectrum antiviral activity for hemorrhagic fever viruses. *Antiviral Research*, *120*, 40–47. https://doi.org/10.1016/j.antiviral.2015.05.003

Mühlberger, E. (2007). Filovirus replication and transcription. *Future Virology*, *2*(2), 205–215. https://doi.org/10.2217/17460794.2.2.205

Muhlberger, E. M., Weik, M., Volchkov, V. E., Klenk, H.-D., & Becker, S. (1999). Comparison of the Transcription and Replication Strategies of Marburg Virus and Ebola Virus by Using Artificial Replication Systems. *Journal of Virology*, *73*(3), 2333–2342.

Muhlberger, E., Tfering, B. L., Klenk, H.-D., & Becker, S. (1998). Three of the Four Nucleocapsid Proteins of Marburg Virus, NP, VP35, and L, Are Sufficient To Mediate Replication and Transcription of Marburg Virus-Specific Monocistronic Minigenomes. *Journal of Virology*, *72*(11), 8756–8764.

Munday, D. C., Wu, W., Smith, N., Fix, J., Noton, S. L., Galloux, M., … Hiscox, J. A. (2015). Interactome Analysis of the Human Respiratory Syncytial Virus RNA

Polymerase Complex Identifies Protein Chaperones as Important Cofactors That Promote L-Protein Stability and RNA Synthesis. *Journal of Virology*, *89*(2), 917–930. https://doi.org/10.1128/JVI.01783-14

Neumann, G., Feldmann, H., Watanabe, S., Lukashevich, I., & Kawaoka, Y. (2002). Reverse Genetics Demonstrates that Proteolytic Processing of the Ebola Virus Glycoprotein Is Not Essential for Replication in Cell Culture. *JOURNAL OF VIROLOGY*, *76*(1), 406–410. https://doi.org/10.1128/JVI.76.1.406–410.2002

Neumann, G., Watanabe, S., & Kawaoka, Y. (2009). Characterization of Ebolavirus regulatory genomic regions. *Virus Research*, *144*(1–2), 1–7. https://doi.org/10.1016/j.virusres.2009.02.005

Ng, L., & Hiscox, J. A. (2018). Viperin Poisons Viral Replication. *Cell Host and Microbe*, *24*(2), 181–183. https://doi.org/10.1016/j.chom.2018.07.014

Noda, T., Ebihara, H., Muramoto, Y., Fujii, K., Takada, A., Sagara, H., … Kawaoka, Y. (2006). Assembly and budding of Ebolavirus. *PLoS Pathogens*, *2*(9), 0864–0872. https://doi.org/10.1371/journal.ppat.0020099

Noton, S. L., Deflube, L. R., Tremaglio, C. Z., & Fearns, R. (2012). The Respiratory Syncytial Virus Polymerase Has Multiple RNA Synthesis Activities at the Promoter. *PLOS Pathogens*, *8*(10), 1–13. https://doi.org/10.1371/journal.ppat.1002980

Noyori, O., Nakayama, E., Maruyama, J., Yoshida, R., & Takada, A. (2013). Suppression of Fas-mediated apoptosis via steric shielding by filovirus glycoproteins. *Biochemical and Biophysical Research Communications*, *441*(4), 994–998. https://doi.org/10.1016/j.bbrc.2013.11.018

Olabode, A. S., Jiang, X., Robertson, D. L., & Lovell, S. C. (2015a). Ebolavirus is evolving but not changing : No evidence for functional change in EBOV from 1976 to the 2014 outbreak. *Virology*, *482*, 202–207. https://doi.org/10.1016/j.virol.2015.03.029

Olabode, A. S., Jiang, X., Robertson, D. L., & Lovell, S. C. (2015b). Ebolavirus is evolving but not changing: No evidence for functional change in EBOV from 1976 to the 2014 outbreak. *Virology*, *482*, 202–207. https://doi.org/10.1016/j.virol.2015.03.029

Olival, K., & Hayman, D. (2014). Filoviruses in Bats: Current Knowledge and Future

Directions. *Viruses*, *6*(4), 1759–1788. https://doi.org/10.3390/v6041759

Ortín, J., & Martín-Benito, J. (2015). The RNA synthesis machinery of negative-stranded RNA viruses. *Virology*. https://doi.org/10.1016/j.virol.2015.03.018

Osawa, M., Swindells, M. B., Tanikawa, J., Tanaka, T., Mase, T., Furuya, T., & Ikura, M. (1998). Solution Structure of Calmodulin ± W-7 Complex : The Basis of Diversity in Molecular Recognition. *Journal of Molecular Biology*, *276*, 165–176.

Osseman, Q., Gallucci, L., Au, S., Cazenave, C., Berdance, E., Blondot, M. L., … Kann, M. (2018). The chaperone dynein LL1 mediates cytoplasmic transport of empty and mature hepatitis B virus capsids. *Journal of Hepatology*, *68*(3), 441–448. https://doi.org/10.1016/j.jhep.2017.10.032

Osterholm, M. T., Moore, K. a, Kelley, N. S., Brosseau, L. M., Wong, G., Murphy, F. a, … Kobinger, G. P. (2015). Transmission of Ebola Viruses: What We Know and What We Do Not Know. *MBio*, *6*(2), 1–9. https://doi.org/10.1128/mBio.00137-15

Pappalardo, M., Reddin, I. G., Cantoni, D., Jeremy, S., Michaelis, M., & Wass, M. N. (2017). Changes associated with Ebola virus adaptation to novel species. *Bioinformatics*, *33*(13), 1911–1915. https://doi.org/10.1093/bioinformatics/btx065

Paranjape, S. M., & Harris, E. (2007). Y box-binding protein-1 binds to the dengue virus 3???-untranslated region and mediates antiviral effects. *Journal of Biological Chemistry*, *282*(42), 30497–30508. https://doi.org/10.1074/jbc.M705755200

Park, K. H., Huang, T., Correia, F. F., & Krystal, M. (1991). Rescue of a foreign gene by Sendai virus. *Proceedings of the National Academy of Sciences of the United States of America*, *88*(13), 5537–5541. https://doi.org/10.1073/pnas.88.13.5537

Pathak, K. B., & Nagy, P. D. (2009). Defective interfering RNAs: Foes of viruses and friends of virologists. *Viruses*. https://doi.org/10.3390/v1030895

Pattnaik, A. K., Andrew Ball, L., LeGrone, A. W., & Wertz, G. W. (1992). Infectious defective interfering particles of VSV from transcripts of a cDNA clone. *Cell*, *69*(6), 1011–1020. https://doi.org/10.1016/0092-8674(92)90619-N

Pattnaik, A. K., & Wertz, G. W. (1991). Cells that express all five proteins of vesicular

stomatitis virus from cloned cDNAs support replication, assembly, and budding of defective interfering particles. *Proc Natl Acad Sci U S A*, *88*(4), 1379–1383. https://doi.org/10.1073/pnas.88.4.1379

Pichlmair, A., Kandasamy, K., Alvisi, G., Mulhen, O., Sacco, R., Jabjan, M., … Superti-Furga, G. (2012). Viral immune modulators perturb the human molecular network by common and unique strategies. *Nature*, *487*(26), 486–492. https://doi.org/10.1038/nature11289

Pigott, D. M., Millear, A. I., Earl, L., Morozoff, C., Han, B. A., Shearer, F. M., … Hay, S. I. (2016). Updates to the zoonotic niche map of Ebola virus disease in Africa. *ELife*, *5*(2016JULY), 1–13. https://doi.org/10.7554/eLife.16412

Poch, O., Blumberg, B. M., Bougueleret, L., & Tordo, N. (1990). Sequence comparison of five polymerases (L proteins) of unsegmented negative-strand RNA viruses: theoretical assignment of functional domains. *Journal of General Virology*, *71*(5), 1153–1162. https://doi.org/10.1099/0022-1317-71-5-1153

Prins, K. C., Binning, J. M., Shabman, R. S., Leung, D. W., Amarasinghe, G. K., & Basler, C. F. (2010). Basic Residues within the Ebolavirus VP35 Protein Are Required for Its Viral Polymerase Cofactor Function. *Journal of Virology*, *84*(20), 10581–10591. https://doi.org/10.1128/JVI.00925-10

Prins, K. C., Delpeut, S., Leung, D. W., Reynard, O., Volchkova, V. A., Reid, S. P., … Basler, C. F. (2010). Mutations Abrogating VP35 Interaction with Double-Stranded RNA Render Ebola Virus Avirulent in Guinea Pigs. *Journal of Virology*, *84*(6), 3004–3015. https://doi.org/10.1128/JVI.02459-09

Racaniello, V. R., & Baltimore, D. (1981). Molecular cloning of poliovirus cDNA and determination of the complete nucleotide sequence of the viral genome. *Proceedings of the National Academy of Sciences of the United States of America*, *78*(8), 4887–4891. https://doi.org/10.1073/pnas.78.8.4887

Rauch, J. N., & Gestwicki, J. E. (2014). Binding of Human Nucleotide Exchange Factors to Heat Shock Protein 70 (Hsp70) Generates Functionally Distinct Complexes in Vitro. *The Journal of Biological Chemistry*, *289*(3), 1402–1414. https://doi.org/10.1074/jbc.M113.521997

Reid, St. P., Leung, L. W., Hartman, A. L., Martinez, O., Shaw, M. L., Carbonnelle, C., … Basler, C. F. (2006). Ebola Virus VP24 Binds Karyopherin 1 and Blocks STAT1

Nuclear Accumulation. *Journal of Virology*, *80*(11), 5156–5167. https://doi.org/10.1128/JVI.02349-05

Reid, St Patrick, Cárdenas, W. B., Basler, C. F., & Basler, C. F. (2005). Homo-Oligomerization Facilitates the Interferon-Antagonist Activity of the Ebolavirus VP35 Protein. *Virology*, *341*(2), 179–189. https://doi.org/10.1016/j.virol.2005.06.044.Homo-Oligomerization

Rodriguez, L. L., De Roo, A., Guimard, Y., Trappier, S. G., Sanchez, A., Bressler, D., … Nichol, S. T. (1999). Persistence and Genetic Stability of Ebola Virus during the Outbreak in Kikwit, Democratic Republic of the Congo, 1995. *The Journal of Infectious Diseases*, *179*(s1), S170–S176. https://doi.org/10.1086/514291

Roossien, D. H., Miller, K. E., & Gallo, G. (2015). Ciliobrevins as tools for studying dynein motor function. *Frontiers in Cellular Neuroscience*, *9*(252), 1–10. https://doi.org/10.3389/fncel.2015.00252

Ruedas, J. B., & Perrault, J. (2009a). Insertion of Enhanced Green Fluorescent Protein in a Hinge Region of Vesicular Stomatitis Virus L Polymerase Protein Creates a Temperature-Sensitive Virus That Displays No Virion-Associated Polymerase Activity In Vitro. *Journal of Virology*, *83*(23), 12241–12252. https://doi.org/10.1128/JVI.01273-09

Ruedas, J. B., & Perrault, J. (2009b). Insertion of Enhanced Green Fluorescent Protein in a Hinge Region of Vesicular Stomatitis Virus L Polymerase Protein Creates a Temperature-Sensitive Virus That Displays No Virion-Associated Polymerase Activity In Vitro □. *Journal of Virology*, *83*(23), 12241–12252. https://doi.org/10.1128/JVI.01273-09

Ruedas, J. B., & Perrault, J. (2014). Putative Domain-Domain Interactions in the Vesicular Stomatitis Virus L Polymerase Protein Appendage Region. *Journal of Virology*, *88*(24), 14458–14466. https://doi.org/10.1128/JVI.02267-14

Ruibal, P., Oestereich, L., Ludtke, A., Becker-Ziaja, B., Wozniak, D. M., Kerber, R., … Munoz-Fontela, C. (2016). Unique human immune signature of Ebola virus disease in Guinea. *Nature*, *533*(7601), 100–104. https://doi.org/10.1038/nature17949

Ruigrok, R. W. H., Schoehn, G., Dessen, A., Forest, E., Volchkov, V., Dolnik, O., … Weissenhorn, W. (2000). Structural characterization and membrane binding

properties of the matrix protein VP40 of Ebola virus. *Journal of Molecular Biology*, *300*(1), 103–112. https://doi.org/10.1006/jmbi.2000.3822

Saeed, M. F., Kolokoltsov, A. A., Albrecht, T., & Davey, R. A. (2010). Cellular entry of ebola virus involves uptake by a macropinocytosis-like mechanism and subsequent trafficking through early and late endosomes. *PLoS Pathogens*, *6*(9). https://doi.org/10.1371/journal.ppat.1001110

Sakurai, Y., Kolokoltsov, A. A., Chen, C., Tidwell, M. W., Bauta, W. E., Klugbauer, N., … Davey, R. A. (2015). Targets for Disease Treatment. *Science*, *347*(6225), 995–998. https://doi.org/10.1126/science.1258758.Two

Sanchez, A., Kiley, M. P., Holloway, B. P., & Auperin, D. D. (1993). Sequence analysis of the Ebola virus genome: organization, genetic elements, and comparison with the genome of Marburg virus. *Virus Research*, *29*(3), 215–240. https://doi.org/10.1016/0168-1702(93)90063-S

Sanjuán, R., & Domingo-Calap, P. (2016). Mechanisms of viral mutation. *Cellular and Molecular Life Sciences*, *73*(23), 4433–4448. https://doi.org/10.1007/s00018-016-2299-6

Sanjuan, R., Nebot, M. R., Chirico, N., Mansky, L. M., & Belshaw, R. (2010). Viral Mutation Rates. *Journal of Virology*, *84*(19), 9733–9748. https://doi.org/10.1128/JVI.00694-10

Schlereth, J., Grünweller, A., Biedenkopf, N., Becker, S., & Hartmann, R. K. (2016). RNA binding specificity of Ebola virus transcription factor VP30. *RNA Biology*, *13*(9), 783–798. https://doi.org/10.1080/15476286.2016.1194160

Schneider, M. A., Spoden, G. A., Florin, L., & Lambert, C. (2011). Identification of the dynein light chains required for human papillomavirus infection. *Cellular Microbiology*, *13*(1), 32–46. https://doi.org/10.1111/j.1462-5822.2010.01515.x

Schnell, M. J., Mebatsion, T., & Conzelmann1, K.-K. (1994). Infectious rabies viruses from cloned cDNA. *The EMBO Journal*, *13*(18), 4195–4203.

Schumann, Mi., Gantke, T., & Muhlberger, E. (2009). Ebola Virus VP35 Antagonizes PKR Activity through Its C-Terminal Interferon Inhibitory Domain. *Journal of Virology*, *83*(17), 8993–8997. https://doi.org/10.1128/JVI.00523-09

Shabman, R. S., Hoenen, T., Groseth, A., Jabado, O., Binning, J. M., Amarasinghe, G. K., … Basler, C. F. (2013). An Upstream Open Reading Frame Modulates Ebola

Virus Polymerase Translation and Virus Replication. *PLoS Pathogens*, *9*(1). https://doi.org/10.1371/journal.ppat.1003147

Shabman, R. S., Leung, D. W., Johnson, J., Glennon, N., Gulcicek, E. E., Stone, K. L., … Basler, C. F. (2011). DRBP76 associates with Ebola virus VP35 and suppresses viral polymerase function. *Journal of Infectious Diseases*, *204*(SUPPL. 3), 911–918. https://doi.org/10.1093/infdis/jir343

Shah, P. S., Wojcechowskyj, J. A., Eckhardt, M., & Krogan, N. J. (2015). Comparative mapping of host-pathogen protein-protein interactions. *Current Opinion in Microbiology*, *27*, 62–68. https://doi.org/10.1016/j.mib.2015.07.008

Shi, W., Huang, Y., Sutton-Smith, M., Tissot, B., Panico, M., Morris, H. R., … Nabel, G. J. (2008). A Filovirus-Unique Region of Ebola Virus Nucleoprotein Confers Aberrant Migration and Mediates Its Incorporation into Virions. *Journal of Virology*, *82*(13), 6190–6199. https://doi.org/10.1128/JVI.02731-07

Simmons, G., Reeves, J. D., Grogan, C. C., Vandenberghe, L. H., Baribaud, F., Whitbeck, J. C., … Pöhlmann, S. (2003). DC-SIGN and DC-SIGNR bind Ebola glycoproteins and enhance infection of macrophages and endothelial cells. *Virology*, *305*(1), 115–123. https://doi.org/10.1006/viro.2002.1730

Sissoko, D., Laouenan, C., Folkesson, E., M'Lebing, A. B., Beavogui, A. H., Baize, S., … Malvy, D. (2016). Experimental Treatment with Favipiravir for Ebola Virus Disease (the JIKI Trial): A Historically Controlled, Single-Arm Proof-of-Concept Trial in Guinea. *PLoS Medicine*, *13*(3), 1–36. https://doi.org/10.1371/journal.pmed.1001967

Smith, D. R., McCarthy, S., Chrovian, A., Olinger, G., Stossel, A., Geisbert, T. W., … Connor, J. H. (2010). Inhibition of heat-shock protein 90 reduces Ebola virus replication. *Antiviral Res*, *87*(2), 187–194. https://doi.org/S0166-3542(10)00604-2 [pii]\r10.1016/j.antiviral.2010.04.015

Smith, L. M., Hensley, L. E., Geisbert, T. W., Johnson, J., Stossel, A., Honko, A., … Karp, C. L. (2013). Interferon- therapy prolongs survival in rhesus macaque models of ebola and marburg hemorrhagic fever. *Journal of Infectious Diseases*, *208*(2), 310–318. https://doi.org/10.1093/infdis/jis921

Snapp, E. (2005). Design and use of fluorescent fusion proteins in cell biology. *Current Protocols in Cell Biology*, *21*(4), 1–13.

https://doi.org/10.1002/0471143030.cb2104s27.Design

Sodeik, B., Ebersold, M. W., & Helenius, A. (1997). Microtubule-mediated transport of incoming herpes simplex virus 1 capsid to the nucleous. *The Journal of Cell Biology*, *136*(5), 1007–1021.

Stricher, F., Macri, C., Ruff, M., & Muller, S. (2013). HSPA8 / HSC70 chaperone protein Structure , function , and chemical targeting. *Autophagy*, *9*(12), 1937–1954. https://doi.org/10.4161/auto.26448

Sullivan, N. J., Peterson, M., Yang, Z., Duckers, H., Nabel, E., Gary, J., … Nabel, G. J. (2005). Ebola Virus Glycoprotein Toxicity Is Mediated by a Dynamin-Dependent Protein-Trafficking Pathway Ebola Virus Glycoprotein Toxicity Is Mediated by a Dynamin-Dependent Protein-Trafficking Pathway. *Journal of Virology*, *79*(1), 547–553. https://doi.org/10.1128/JVI.79.1.547

Sztuba-solinska, J., Diaz, L., Kumar, M. R., Wiley, M. R., Jozwick, L., Kuhn, J. H., … Johnson, R. F. (2016). A small stem-loop structure of the Ebola virus trailer is essential for replication and interacts with heat-shock protein A8. *Nucleic Acids Research*, *44*(20), 9831–9846. https://doi.org/10.1093/nar/gkw825

Takahashi, K., Halfmann, P., Oyama, M., Kozuka-Hata, H., Noda, T., & Kawaoka, Y. (2013). DNA Topoisomerase 1 Facilitates the Transcription and Replication of the Ebola Virus Genome. *Journal of Virology*, *87*(16), 8862–8869. https://doi.org/10.1128/JVI.03544-12

Takamatsu, Y., Kolesnikova, L., & Becker, S. (2018). Ebola virus proteins NP, VP35, and VP24 are essential and sufficient to mediate nucleocapsid transport. *Proceedings of the National Academy of Sciences*, *115*(5), 1075–1080. https://doi.org/10.1073/pnas.1712263115

Taylor, J. E., Chow, J. Y. H., Jeffries, C. M., Kwan, A. H., Duff, A. P., Hamilton, W. A., & Trewhella, J. (2012). Calmodulin Binds a Highly Extended HIV-1 MA Protein That Refolds Upon Its Release. *Biophysical Journal*, *103*(3), 541–549. https://doi.org/10.1016/j.bpj.2012.06.042

Tchesnokov, E. P., Raeisimakiani, P., Ngure, M., Marchant, D., & Götte, M. (2018). Recombinant RNA-Dependent RNA Polymerase Complex of Ebola Virus. *Scientific Reports*, *8*(1), 1–9. https://doi.org/10.1038/s41598-018-22328-3

Timmins, J., Schoehn, G., Kohlhaas, C., Klenk, H. D., Ruigrok, R. W. H., &

Weissenhorn, W. (2003). Oligomerization and polymerization of the filovirus matrix protein VP40. *Virology*, *312*(2), 359–368. https://doi.org/10.1016/S0042-6822(03)00260-5

Tong, Y., Shi, W., Liu, D., Qian, J., Liang, L., Bo, X., … Fan, H. (2015). Genetic diversity and evolutionary dynamics of Ebola virus in Sierra Leone. *Nature*, *524*(302), 93–96. https://doi.org/10.1038/nature14490

Tran, E. E. H., Nelson, E. A., Bonagiri, P., Simmons, J. A., Shoemaker, C. J., Schmaljohn, C. S., … White, J. M. (2016). Mapping of Ebolavirus Neutralization by Monoclonal Antibodies in the ZMapp Cocktail Using Cryo-Electron Tomography and Studies of Cellular Entry. *Journal of Virology*, *90*(17), 7618–7627. https://doi.org/10.1128/jvi.00406-16

Ueda, M. T., Kurosaki, Y., Izumi, T., Nakano, Y., Oloniniyi, O. K., Yasuda, J., … Nakagawa, S. (2017). Functional muations in spike glycoprotein of Zaire ebolavirus associated with an increase in infection efficency. *Genes to Cells*, *22*, 148–159. https://doi.org/10.1111/gtc.12463

UN. (2015). *Socio-Economic Impact of Ebola Virus Disease in West African Countries. A call for national and regional containment*. *United Nations Development Group - Western and Central Africa*.

Vetter, P., Kaiser, L., Schibler, M., Ciglenecki, I., & Bausch, D. G. (2016). Sequelae of Ebola virus disease: the emergency within the emergency. *The Lancet Infectious Diseases*, *16*(6), e82–e91. https://doi.org/10.1016/S1473-3099(16)00077-3

Villalobo, A., Ishida, H., Vogel, H. J., & Berchtold, M. W. (2018). Calmodulin as a protein linker and a regulator of adaptor/scaffold proteins. *Biochimica et Biophysica Acta - Molecular Cell Research*, *1865*(3), 507–521. https://doi.org/10.1016/j.bbamcr.2017.12.004

Volchkov, V. E., Volchkova, V. A., Chepurnov, A. A., Blinov, V. M., Dolnik, O., Netesov, S. V., & Feldmann, H. (1999a). Characterization of the L gene and 5’ trailer region of Ebola virus. *Journal of General Virology*, *80*(2), 355–362. https://doi.org/10.1099/0022-1317-80-2-355

Volchkov, V. E., Volchkova, V. A., Chepurnov, A. A., Blinov, V. M., Dolnik, O., Netesov, S. V, & Feldmann, H. (1999b). Characterization of the L gene and 5’

trailer region of Ebola virus. *Journal of General Virology*, *80*(2), 355–362. https://doi.org/10.1099/0022-1317-80-2-355

Volchkov, V., Volchova, V., Muhlberger, E. M., Kolesnikova, L., Weik, M., Dolnik, O., & Klenk, H.-D. (2001). Recovery of Infectious Ebola Virus from Complementary DNA: RNA Editing of the GP Gene and Viral Cytotoxicity, *291*(March), 1965–1970. https://doi.org/10.1126/science.1057269

von Magnus, P. (1954). Incomplete Forms of Influenza Virus. *Advances in Virus Research*, *2*, 59–79. https://doi.org/10.1016/S0065-3527(08)60529-1

Wahl-jensen, V., Kurz, S. K., Hazelton, P. R., Schnittler, H., Ströher, U., & Burton, D. R. (2005). Role of Ebola Virus Secreted Glycoproteins and Virus-Like Particles in Activation of Human Macrophages Role of Ebola Virus Secreted Glycoproteins and Virus-Like Particles in Activation of Human Macrophages. *Society*, *79*(4), 2413–2419. https://doi.org/10.1128/JVI.79.4.2413

Walsh, M. P. (1983). Calmodulin and its roles in skeletal muscle function. *Canadian Anaesthetists' Society Journal*, *30*(4), 390–398. https://doi.org/10.1007/BF03007862

Wan, W., Kolesnikova, L., Clarke, M., Koehler, A., Noda, T., Becker, S., & Briggs, J. A. G. (2017). Structure and assembly of the Ebola virus nucleocapsid. *Nature*, *551*(7680), 394–397. https://doi.org/10.1038/nature24490

Wang, H., Shi, Y., Song, J., Qi, J., Lu, G., Yan, J., & Gao, G. F. (2016). Ebola Viral Glycoprotein Bound to Its Endosomal Receptor Niemann-Pick C1. *Cell*, *164*(1–2), 258–268. https://doi.org/10.1016/j.cell.2015.12.044

Wang, L., Fu, B., Li, W., Patil, G., Liu, L., Dorf, M. E., & Li, S. (2017). Comparative influenza protein interactomes identify the role of plakophilin 2 in virus restriction. *Nature Communications*, *8*(May 2016), 1–12. https://doi.org/10.1038/ncomms13876

Wang, W.-T., Tsai, T.-Y., Chao, C.-H., Lai, B.-Y., & Wu Lee, Y.-H. (2015). Y-Box Binding Protein 1 Stabilizes Hepatitis C Virus NS5A via Phosphorylation-Mediated Interaction with NS5A To Regulate Viral Propagation. *Journal of Virology*, *89*(22), 11584–11602. https://doi.org/10.1128/JVI.01513-15

Warfield, K. L., Bosio, C. M., Welcher, B. C., Deal, E. M., Mohamadzadeh, M., Schmaljohn, A., … Bavari, S. (2003). Ebola virus-like particles protect from

lethal Ebola virus infection. *Proceedings of the National Academy of Sciences*, *100*(26), 15889–15894. https://doi.org/10.1073/pnas.2237038100

Watanabe, S., Watanabe, T., Noda, T., Feldmann, H., Jasenosky, L. D., Takada, A., & Kawaoka, Y. (2004). Production of Novel Ebola Virus-Like Particles from cDNAs : an Alternative to Ebola Virus Generation by Reverse Genetics Production of Novel Ebola Virus-Like Particles from cDNAs : an Alternative to Ebola Virus Generation by Reverse Genetics. *JOURNAL OF VIROLOGY*, *78*(2), 999–1005. https://doi.org/10.1128/JVI.78.2.999

Weik, M., Modrof, J., Klenk, H.-D., Becker, S., & Mühlberger, E. (2002). Ebola Virus VP30-Mediated Transcription Is Regulated by RNA Secondary Structure Formation. *JOURNAL OF VIROLOGY*, *76*(17), 8532–8539. https://doi.org/10.1128/JVI.76.17.8532–8539.2002

Weyer, J., Grobbelaar, A., & Blumberg, L. (2015). Ebola Virus Disease: History, Epidemiology and Outbreaks. *Current Infectious Disease Reports*. https://doi.org/10.1007/s11908-015-0480-y

Whelan, S. P. J., Barr, J. N., & Wertz, G. W. (2004). *Transcription and replication of nonsegmented negative-strand RNA viruses.*

WHO | Ebola virus disease – Democratic Republic of the Congo. (2019). Retrieved March 17, 2019, from https://www.who.int/csr/don/21-february-2019-ebola-drc/en/

Wilde, A. H. de, Jochmans, D., Posthuma, C. C., Zevenhoven-Dobbe, J. C., Nieuwkoop, S. Van, Bestebroer, T. M., … Snijder, E. J. (2014). Screening of an FDA-Approved Compound Library Identifies Four Small-Molecule Inhibitors of Middle East Respiratory Syndrome Coronavirus Replication in Cell Culture. *Antimicrobial Agents and Chemotherapy*, *58*(8), 4875–4884. https://doi.org/10.1128/AAC.03011-14

Wong, G., He, S., Leung, A., Cao, W., Bi, Y., Zhang, Z., … Qiu, X. (2019). Naturally Occurring Single Mutations in Ebola Virus Observably Impact Infectivity. *Journal of Virolo*, *93*(1), 1–12. https://doi.org/doi.org/10.1128/JVI .01098-18.

Wu, W., Munday, D. C., Howell, G., Platt, G., Barr, J. N., & Hiscox, J. A. (2011). Characterization of the Interaction between Human Respiratory Syncytial Virus and the Cell Cycle in Continuous Cell Culture and Primary Human Airway

Epithelial Cells. *JOURNAL OF VIROLOGY*, *85*(19), 10300–10309. https://doi.org/10.1128/JVI.05164-11

Yap, K. L., Kim, J., Truong, K., Sherman, M., & Yuan, T. (2000). Calmodulin Target Database. *Journal of Structural and Functional Genomics*, *14*(1), 8–14.

Yen, B., Mulder, L. C. F., Martinez, O., & Basler, C. F. (2014). Molecular Basis for Ebolavirus VP35 Suppression of Human Dendritic Cell Maturation. *Journal of Virology*, *88*(21), 12500–12510. https://doi.org/10.1128/JVI.02163-14

Yu, D.-S., Weng, T.-H., Wu, X.-X., Wang, F. X. C., Lu, X.-Y., Wu, H.-B., … Yao, H.-P. (2017). The lifecycle of the Ebola virus in host cells. *Oncotarget*, *8*(33), 55750–55759. https://doi.org/10.18632/oncotarget.18498

Zeisel, M. B., Crouchet, E., Baumert, T. F., & Schuster, C. (2015). Host-Targeting Agents to Prevent and Cure Hepatitis C Virus Infection. *Viruses*, *7*, 5659–5685. https://doi.org/10.3390/v7112898

Zhou, Y., Frey, T. K., & Yang, J. J. (2009). Viral calciomics: Interplays between Ca2+and virus. *Cell Calcium*, *46*(1), 1–17. https://doi.org/10.1016/j.ceca.2009.05.005

Zhu, F. C., Wurie, A. H., Hou, L. H., Liang, Q., Li, Y. H., Russell, J. B. W., … Chen, W. (2017). Safety and immunogenicity of a recombinant adenovirus type-5 vector-based Ebola vaccine in healthy adults in Sierra Leone: a single-centre, randomised, double-blind, placebo-controlled, phase 2 trial. *The Lancet*, *389*(10069), 621–628. https://doi.org/10.1016/S0140-6736(16)32617-4

Zinzula, L., Esposito, F., Pala, D., & Tramontano, E. (2012). DsRNA binding characterization of full length recombinant wild type and mutants Zaire ebolavirus VP35. *Antiviral Research*, *93*(3), 354–363. https://doi.org/10.1016/j.antiviral.2012.01.005

Appendix

8.1. Sequence reference numbers of EBOV Makona VP35 from 2014-15

AQS26739.1	AMT75726.1	ALX34108.1	ALX31874.1
AQS26730.1	AMT75717.1	ALX34096.1	ALX31724.1
AQS26721.1	AMT75708.1	ALX34068.1	ALX31681.1
AQS26712.1	AMT75699.1	ALX34014.1	ALX31630.1
AQS26703.1	AMT75690.1	ALX34009.1	ALX31500.1
APT69713.1	AMT75681.1	ALX33855.1	ALX31465.1
APT69686.1	AMT75672.1	ALX33838.1	ALX31430.1
APT69677.1	AMT75663.1	ALX33785.1	ALX31241.1
APT69646.1	AMT75654.1	ALX33732.1	ALX31215.1
APT69637.1	AMT75645.1	ALX33724.1	ALX31197.1
APT69619.1	AMT75636.1	ALX33676.1	ALX31118.1
APT69561.1	AMT75627.1	ALX33650.1	ALT66783.1
AND81204.1	AMT75618.1	ALX33561.1	ALT66774.1
AND81195.1	AMT75609.1	ALX33451.1	ALT66765.1
AND81186.1	AMT75600.1	ALX33370.1	ALT66756.1
AMY60352.1	AMT75591.1	ALX33145.1	ALT66747.1
AMY60343.1	AMT75582.1	ALX33133.1	ALT66738.1
AMY60334.1	AMT75573.1	ALX33088.1	ALT66729.1
AMY60325.1	AMT75564.1	ALX32988.1	ALP30064.1
AMY60316.1	AMT75555.1	ALX32655.1	ALP30056.1
AMY60307.1	AMT75546.1	ALX32633.1	ALN12277.1
AMY60298.1	ALX34556.1	ALX32589.1	ALH21461.1
AMY60289.1	ALX34480.1	ALX32350.1	ALH21452.1
AMY60280.1	ALX34420.1	ALX32271.1	ALG02123.1
AMY60271.1	ALX34414.1	ALX32171.1	ALG02114.1
AMY60262.1	ALX34389.1	ALX32150.1	ALG02105.1
AMT75753.1	ALX34348.1	ALX32064.1	ALG02078.1
AMT75744.1	ALX34337.1	ALX31986.1	ALG02069.1
AMT75735.1	ALX34122.1	ALX31954.1	ALG02060.1
ALG02051.1	ALG01745.1	ALG01412.1	ALG01115.1
ALG02042.1	ALG01736.1	ALG01403.1	ALG01097.1
ALG02033.1	ALG01727.1	ALG01394.1	ALG01088.1

ALG02024.1	ALG01718.1	ALG01385.1	ALG01079.1
ALG02015.1	ALG01709.1	ALG01376.1	ALG01070.1
ALG02006.1	ALG01682.1	ALG01358.1	ALG01061.1
ALG01997.1	ALG01673.1	ALG01349.1	ALG01052.1
ALG01988.1	ALG01664.1	ALG01340.1	ALG01043.1
ALG01979.1	ALG01655.1	ALG01331.1	ALG01034.1
ALG01961.1	ALG01646.1	ALG01322.1	ALG01016.1
ALG01952.1	ALG01619.1	ALG01313.1	ALG01007.1
ALG01943.1	ALG01610.1	ALG01304.1	ALG00998.1
ALG01934.1	ALG01601.1	ALG01295.1	ALG00980.1
ALG01925.1	ALG01592.1	ALG01286.1	ALG00971.1
ALG01916.1	ALG01583.1	ALG01277.1	ALG00962.1
ALG01907.1	ALG01565.1	ALG01268.1	ALG00953.1
ALG01898.1	ALG01556.1	ALG01259.1	ALG00944.1
ALG01889.1	ALG01547.1	ALG01250.1	ALG00935.1
ALG01880.1	ALG01538.1	ALG01241.1	ALG00926.1
ALG01871.1	ALG01529.1	ALG01232.1	ALG00917.1
ALG01862.1	ALG01520.1	ALG01223.1	ALG00908.1
ALG01853.1	ALG01511.1	ALG01205.1	ALG00899.1
ALG01844.1	ALG01502.1	ALG01196.1	ALG00890.1
ALG01826.1	ALG01493.1	ALG01187.1	ALG00881.1
ALG01817.1	ALG01484.1	ALG01178.1	ALG00872.1
ALG01808.1	ALG01466.1	ALG01169.1	ALF04599.1
ALG01790.1	ALG01457.1	ALG01160.1	ALF04590.1
ALG01781.1	ALG01448.1	ALG01151.1	ALF04581.1
ALG01772.1	ALG01439.1	ALG01142.1	ALF04549.1
ALG01763.1	ALG01430.1	ALG01133.1	ALF04540.1
ALG01754.1	ALG01421.1	ALG01124.1	ALB07142.1
ALB07133.1	AKI84038.1	AKI84038.1	AKI83759.1
AKL91131.1	AKI84029.1	AKI84029.1	AKI83750.1
AKL91122.1	AKI84020.1	AKI84020.1	AKI83741.1
AKL91113.1	AKI84011.1	AKI84011.1	AKI83732.1
AKL91104.1	AKI84002.1	AKI84002.1	AKI83723.1
AKL91095.1	AKI83993.1	AKI83993.1	AKI83714.1

AKL91086.1	AKI83984.1	AKI83984.1	AKI83705.1
AKI84254.1	AKI83975.1	AKI83975.1	AKI83696.1
AKI84251.1	AKI83966.1	AKI83966.1	AKI83687.1
AKI84236.1	AKI83957.1	AKI83957.1	AKI83678.1
AKI84227.1	AKI83948.1	AKI83948.1	AKI83669.1
AKI84218.1	AKI83939.1	AKI83939.1	AKI83660.1
AKI84209.1	AKI83930.1	AKI83930.1	AKI83651.1
AKI84200.1	AKI83921.1	AKI83921.1	AKI83642.1
AKI84191.1	AKI83912.1	AKI83912.1	AKI83624.1
AKI84182.1	AKI83903.1	AKI83903.1	AKI83615.1
AKI84173.1	AKI83894.1	AKI83894.1	AKI83606.1
AKI84164.1	AKI83885.1	AKI83885.1	AKI83597.1
AKI84155.1	AKI83876.1	AKI83876.1	AKI83588.1
AKI84146.1	AKI83867.1	AKI83867.1	AKI83579.1
AKI84137.1	AKI83858.1	AKI83858.1	AKI83570.1
AKI84128.1	AKI83849.1	AKI83849.1	AKI83561.1
AKI84119.1	AKI83840.1	AKI83840.1	AKI83552.1
AKI84110.1	AKI83831.1	AKI83831.1	AKI83543.1
AKI84101.1	AKI83822.1	AKI83822.1	AKI83534.1
AKI84092.1	AKI83813.1	AKI83813.1	AKI83525.1
AKI84083.1	AKI83804.1	AKI83804.1	AKI83516.1
AKI84074.1	AKI83795.1	AKI83795.1	AKI83507.1
AKI84065.1	AKI83786.1	AKI83786.1	AKI83498.1
AKI84056.1	AKI83777.1	AKI83777.1	AKI83489.1
AKI84047.1	AKI83768.1	AKI83768.1	AKI83480.1
AKI83471.1	AKI83183.1	AKI82904.1	AKI82626.1
AKI83462.1	AKI83174.1	AKI82895.1	AKI82618.1
AKI83453.1	AKI83165.1	AKI82886.1	AKG96269.1
AKI83444.1	AKI83156.1	AKI82877.1	AKG96260.1
AKI83435.1	AKI83147.1	AKI82868.1	AKG96251.1
AKI83426.1	AKI83138.1	AKI82859.1	AKG96242.1
AKI83408.1	AKI83129.1	AKI82850.1	AKG96233.1
AKI83399.1	AKI83120.1	AKI82841.1	AKG96224.1
AKI83390.1	AKI83111.1	AKI82832.1	AKG96215.1

AKI83381.1	AKI83102.1	AKI82823.1	AKG96206.1
AKI83372.1	AKI83093.1	AKI82814.1	AKG96197.1
AKI83363.1	AKI83084.1	AKI82805.1	AKG96188.1
AKI83354.1	AKI83075.1	AKI82796.1	AKG96179.1
AKI83345.1	AKI83066.1	AKI82787.1	AKG96170.1
AKI83336.1	AKI83057.1	AKI82778.1	AKG96161.1
AKI83327.1	AKI83048.1	AKI82769.1	AKG96152.1
AKI83318.1	AKI83039.1	AKI82760.1	AKG96143.1
AKI83309.1	AKI83030.1	AKI82751.1	AKG96134.1
AKI83300.1	AKI83021.1	AKI82742.1	AKG96125.1
AKI83291.1	AKI83012.1	AKI82733.1	AKG96116.1
AKI83282.1	AKI83003.1	AKI82724.1	AKG96107.1
AKI83273.1	AKI82994.1	AKI82715.1	AKG96098.1
AKI83264.1	AKI82985.1	AKI82706.1	AKG96089.1
AKI83255.1	AKI82976.1	AKI82697.1	AKG96080.1
AKI83246.1	AKI82967.1	AKI82688.1	AKG96071.1
AKI83237.1	AKI82958.1	AKI82679.1	AKG96062.1
AKI83228.1	AKI82949.1	AKI82670.1	AKG96053.1
AKI83219.1	AKI82940.1	AKI82661.1	AKG96044.1
AKI83210.1	AKI82931.1	AKI82652.1	AKG96035.1
AKI83201.1	AKI82922.1	AKI82643.1	AKG96026.1
AKI83192.1	AKI82913.1	AKI82634.1	AKG96017.1
AKG96008.1	AKG95729.1	AKC37181.1	AKC36902.1
AKG95999.1	AKG95720.1	AKC37172.1	AKC36893.1
AKG95990.1	AKG95711.1	AKC37163.1	AKC36884.1
AKG95981.1	AKG95702.1	AKC37154.1	AKC36875.1
AKG95972.1	AKG95693.1	AKC37145.1	AKC36866.1
AKG95963.1	AKG95684.1	AKC37136.1	AKC36857.1
AKG95954.1	AKG95675.1	AKC37127.1	AKC36848.1
AKG95945.1	AKG95666.1	AKC37118.1	AKC36839.1
AKG95936.1	AKG95657.1	AKC37109.1	AKC36830.1
AKG95927.1	AKG95648.1	AKC37100.1	AKC36821.1
AKG95918.1	AKG95639.1	AKC37091.1	AKC36812.1
AKG95909.1	AKG95630.1	AKC37082.1	AKC36803.1

AKG95900.1	AKG95621.1	AKC37073.1	AKC36794.1
AKG95891.1	AKG95612.1	AKC37064.1	AKC36776.1
AKG95882.1	AKG95603.1	AKC37055.1	AKC36767.1
AKG95873.1	AKG95594.1	AKC37046.1	AKC36758.1
AKG95864.1	AKG95585.1	AKC37037.1	AKC36749.1
AKG95855.1	AKG95576.1	AKC37028.1	AKC36740.1
AKG95846.1	AKG95567.1	AKC37019.1	AKC36731.1
AKG95837.1	AKG95558.1	AKC37010.1	AKC36722.1
AKG95828.1	AKG95549.1	AKC37001.1	AKC36713.1
AKG95819.1	AKG95540.1	AKC36992.1	AKC36704.1
AKG95810.1	AKC37262.1	AKC36983.1	AKC36695.1
AKG95801.1	AKC37253.1	AKC36974.1	AKC36686.1
AKG95792.1	AKC37244.1	AKC36965.1	AKC36677.1
AKG95783.1	AKC37235.1	AKC36956.1	AKC36668.1
AKG95774.1	AKC37226.1	AKC36947.1	AKC36659.1
AKG95765.1	AKC37217.1	AKC36938.1	AKC36650.1
AKG95756.1	AKC37208.1	AKC36929.1	AKC36641.1
AKG95747.1	AKC37199.1	AKC36920.1	AKC36632.1
AKG95738.1	AKC37190.1	AKC36911.1	AKC36623.1
AKC36614.1	AKC36327.1	AKC36048.1	AKC36048.1
AKC36605.1	AKC36318.1	AKC36039.1	AKC36039.1
AKC36596.1	AKC36309.1	AKC36030.1	AKC36030.1
AKC36587.1	AKC36300.1	AKC36021.1	AKC36021.1
AKC36578.1	AKC36291.1	AKC36012.1	AKC36012.1
AKC36570.1	AKC36282.1	AKC36003.1	AKC36003.1
AKC36561.1	AKC36273.1	AKC35994.1	AKC35994.1
AKC36552.1	AKC36264.1	AKC35985.1	AKC35985.1
AKC36543.1	AKC36255.1	AKC35976.1	AKC35976.1
AKC36534.1	AKC36246.1	AKC35967.1	AKC35967.1
AKC36525.1	AKC36237.1	AKC35958.1	AKC35958.1
AKC36516.1	AKC36228.1	AKC35940.1	AKC35940.1
AKC36507.1	AKC36219.1	AKC35931.1	AKC35931.1
AKC36498.1	AKC36210.1	AKC35922.1	AKC35922.1
AKC36489.1	AKC36201.1	AKC01490.1	AKC01490.1

AKC36480.1	AKC36192.1	AKC01482.1	AKC01482.1
AKC36471.1	AKC36183.1	AKC01474.1	AKC01474.1
AKC36462.1	AKC36174.1	AKC01434.1	AKC01434.1
AKC36453.1	AKC36165.1	AKA43778.1	AKA43778.1
AKC36444.1	AKC36156.1	AJZ74727.1	AJZ74727.1
AKC36435.1	AKC36147.1	AJZ74657.1	AJZ74657.1
AKC36426.1	AKC36138.1	AJZ74623.1	AJZ74623.1
AKC36417.1	AKC36129.1	AJZ74589.1	AJZ74589.1
AKC36399.1	AKC36120.1	AJZ74580.1	AJZ74580.1
AKC36390.1	AKC36111.1	AJZ74553.1	AJZ74553.1
AKC36381.1	AKC36102.1	AJP15502.1	AJP15502.1
AKC36372.1	AKC36093.1	AJP15493.1	AJP15493.1
AKC36363.1	AKC36084.1	AJP15484.1	AJP15484.1
AKC36354.1	AKC36075.1	AJP15475.1	AJP15475.1
AKC36345.1	AKC36066.1	AJP15466.1	AJP15466.1
AKC36336.1	AKC36057.1	AJP15457.1	AJP15457.1
AJP15449.1	AJP15170.1	AJP14891.1	AJP14612.1
AJP15440.1	AJP15161.1	AJP14882.1	AJP14603.1
AJP15431.1	AJP15152.1	AJP14873.1	AJP14594.1
AJP15422.1	AJP15143.1	AJP14864.1	AJP14585.1
AJP15413.1	AJP15133.1	AJP14855.1	AJP14576.1
AJP15404.1	AJP15125.1	AJP14846.1	AJP14567.1
AJP15395.1	AJP15116.1	AJP14837.1	AJP14558.1
AJP15386.1	AJP15107.1	AJP14828.1	AJP14549.1
AJP15377.1	AJP15098.1	AJP14819.1	AJP14540.1
AJP15368.1	AJP15089.1	AJP14810.1	AJP14531.1
AJP15359.1	AJP15080.1	AJP14801.1	AJP14522.1
AJP15350.1	AJP15071.1	AJP14792.1	AJP14513.1
AJP15341.1	AJP15062.1	AJP14783.1	AJP14504.1
AJP15332.1	AJP15053.1	AJP14774.1	AJP14495.1
AJP15323.1	AJP15044.1	AJP14765.1	AJP14486.1
AJP15314.1	AJP15035.1	AJP14756.1	AJP14477.1
AJP15305.1	AJP15026.1	AJP14747.1	AJP14468.1
AJP15296.1	AJP15017.1	AJP14738.1	AJP14459.1

AJP15287.1	AJP15008.1	AJP14729.1	AJP14450.1
AJP15278.1	AJP14999.1	AJP14720.1	AJP14441.1
AJP15269.1	AJP14990.1	AJP14711.1	AJP14432.1
AJP15260.1	AJP14981.1	AJP14702.1	AJP14423.1
AJP15251.1	AJP14972.1	AJP14693.1	AJP14414.1
AJP15242.1	AJP14963.1	AJP14684.1	AJP14405.1
AJP15233.1	AJP14954.1	AJP14675.1	AJP14397.1
AJP15224.1	AJP14945.1	AJP14666.1	AJP14388.1
AJP15215.1	AJP14936.1	AJP14657.1	AJP14379.1
AJP15206.1	AJP14927.1	AJP14648.1	AJP14370.1
AJP15197.1	AJP14918.1	AJP14639.1	AJP14361.1
AJP15188.1	AJP14909.1	AJP14630.1	AJP14352.1
AJP15179.1	AJP14900.1	AJP14621.1	AJP14343.1
AJP14334.1	AJP14055.1	AIW47459.1	AIG96380.1
AJP14325.1	AJP14046.1	AIW47451.1	AIG96371.1
AJP14316.1	AJP14037.1	AIO11748.1	AIG96362.1
AJP14307.1	AJP14028.1	AIG96632.1	AIG96353.1
AJP14298.1	AJP14019.1	AIG96623.1	AIG96344.1
AJP14289.1	AJP14010.1	AIG96614.1	AIG96335.1
AJP14280.1	AJP14001.1	AIG96605.1	AIG96326.1
AJP14271.1	AJP13992.1	AIG96596.1	AIG96317.1
AJP14262.1	AJP13983.1	AIG96587.1	AIG96308.1
AJP14253.1	AJP13974.1	AIG96578.1	AIG96299.1
AJP14244.1	AJP13965.1	AIG96569.1	AIG96290.1
AJP14235.1	AJP13956.1	AIG96560.1	AIG96281.1
AJP14226.1	AJP13947.1	AIG96551.1	AIG96272.1
AJP14217.1	AJP13938.1	AIG96542.1	AIG96263.1
AJP14208.1	AJG44190.1	AIG96533.1	AIG96254.1
AJP14199.1	AJE60742.1	AIG96524.1	AIG96245.1
AJP14190.1	AJA04406.1	AIG96515.1	AIG96236.1
AJP14181.1	AJA04388.1	AIG96506.1	AIG96227.1
AJP14172.1	AIZ68630.1	AIG96497.1	AIG96218.1
AJP14163.1	AIZ68622.1	AIG96488.1	AIG96209.1
AJP14154.1	AIZ68614.1	AIG96479.1	AIG96200.1

AJP14145.1	AIZ68606.1	AIG96470.1	AIG96191.1
AJP14136.1	AIZ50425.1	AIG96461.1	AIG96182.1
AJP14127.1	AIZ50416.1	AIG96452.1	AIG96173.1
AJP14118.1	AIZ50407.1	AIG96443.1	AIG96164.1
AJP14109.1	AIZ50398.1	AIG96434.1	AIG96155.1
AJP14100.1	AIZ50389.1	AIG96425.1	AIG96146.1
AJP14091.1	AIY29180.1	AIG96416.1	AIG96137.1
AJP14082.1	AIY27574.1	AIG96407.1	AIG96128.1
AJP14073.1	AIW65948.1	AIG96398.1	AIG96119.1
AJP14064.1	AIW47467.1	AIG96389.1	AIG96110.1
AIG96101.1	AGB56810.1	AIG96002.1	AGB56711.1
AIG96092.1	AGB56801.1	AIG95993.1	AGB56702.1
AIG96083.1	AGB56792.1	AIG95984.1	AGB56693.1
AIG96074.1	AGB56783.1	AIG95975.1	AGB56684.1
AIG96065.1	AGB56774.1	AIG95966.1	AIG95885.1
AIG96056.1	AGB56765.1	AIG95957.1	AHX24665.1
AIG96047.1	AGB56756.1	AIG95948.1	AHX24656.1
AIG96038.1	AGB56747.1	AIG95939.1	AHX24647.1
AIG96029.1	AGB56738.1	AIG95930.1	AGB56837.1
AIG96020.1	AGB56729.1	AIG95921.1	AGB56828.1
AIG96011.1	AGB56720.1	AIG95912.1	AGB56819.1
AIG95894.1	AIG95903.1		